Ruthenium(II)-1,8-Naphthalimide Conjugates as DNA Probes and Photoreagents

Gary J. Ryan

May 2008

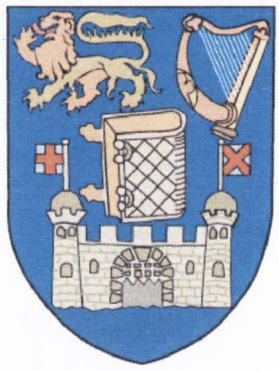

University of Dublin

Trinity College

Based on research carried out under the direction of

Prof. Thorfinnur Gunnlaugsson and Dr. Susan Quinn

A thesis submitted to the School of Chemistry, University of Dublin, Trinity College in fulfilment of the requirements for the degree of Doctor of Philosophy

Declaration

This thesis is being submitted for the degree of Doctor of Philosophy in the University of Dublin, Trinity College and has not been submitted before for any degree or examination in this or any other University. Except where acknowledgement is given, all work described is original and carried out by the author alone. Permission is granted so that the library may lend or copy this thesis upon request. This permission covers only single copies made for study purposes, subject to normal conditions of acknowledgement.

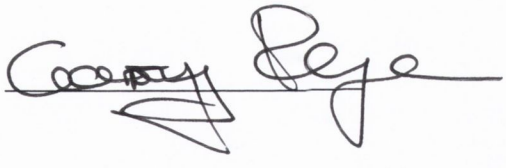

Gary Ryan

Summary

This thesis entitled "Ru(II)-1,8-Naphthalimide Conjugates as DNA Probes and Photoreagents" is divided into seven chapters. *Chapter 1*, the introduction, details the structure of DNA and the different modes by which small molecules interact with it. This is followed by a description of the photophysical and DNA binding properties of polypyridyl Ru(II) complexes from the literature, and the various means that have been employed, to improve their properties for application as DNA probes and photocleavers. Finally, the properties of 1,8-naphthalimide based compounds as anti-cancer agents and DNA photocleavers are discussed. This chapter also describes the aims of the research detailed in each of the subsequent chapters.

Chapter 2 describes the interaction of a series of flexibly linked Ru(II)-4-nitro-1,8-naphthalimide conjugates with DNA. All of the systems described in this chapter were weakly emissive in aqueous solution, but displayed substantial enhancements in the MLCT based emission in the presence of DNA. The nature and magnitude of the enhancement was shown to be sensitive to the length of the linker moiety, and the presence of one or two 1,8-naphthalimide chromophores. Furthermore, a modification to the design, in incorporating a 3-nitro vs. a 4-nitro substituent on the 1,8-naphthalimide ring system, was shown to result in substantially improved response to added DNA.

Chapter 3 describes another family of flexibly linked bifunctional complexes, containing Ru(II) and 1,8-naphthalimide functionality. In this case the 1,8-naphthalimide was shown to sensitize that MLCT emission, a process that was interrupted upon binding to DNA. Significantly different responses to different DNA sequences were displayed by the complexes discussed in this chapter.

Chapter 4 describes systems comprising a more rigid arrangement of the Ru(II) and 1,8-naphthalimide subunits, in which their orientation was shown to be more precisely controlled. Effects were observed on both the solution photophysical properties of the resulting conjugates, and their response upon DNA binding. A wedged or meta arrangement around the connecting ring was shown to result in greater affinity for DNA, and greater change in spectroscopic properties, due to greater complementarity in the shape of the complex and that of the DNA. Furthermore, it was demonstrated that systems incorporating 4-nitro vs. 4-amino 1,8-naphthalimide functionality possessed contrasting photophysical properties.

Chapter 5 describes a series of compounds comprising 1,8-naphthalimide and diquat functionality. Similar to the systems described in *Chapter 4*, it was shown that the

orientation of the components, by virtue of their arrangement around the connecting aromatic ring, had consequences on the DNA binding behaviour of the resulting conjugates. The components performed similar functions to those in the metal complex counterparts, the 1,8-naphthalimide binding DNA through intercalation and the charged diquat binding electrostatically to the backbone, and in the grooves, with a wedged arrangement again resulting in the most efficient interaction.

Chapter 6 details the results of biological studies carried out on the complexes described in *Chapter 2 – 4*. It was demonstrated that the systems from *Chapter 2* and *3* were relatively inefficient at photocleaving DNA, but those described in *Chapter 4* displayed quite promising photocleavage abilty, dependent on the substituents on the complex. These promising candidates were chosen for more detailed study to investigate the possible reactive species involved in the cleavage process. The ability of the complexes described in *Chapter 2 – 4* to enter HeLa cells was then investigated, with all of the conjugates showing excellent cellular uptake properties. The complexes from *Chapter 4* were chosen for confocal laser scanning microscopy study, from which it was shown that each complex was within the cell interior, and more significantly in the nucleus.

Chapter 7 provides an overall summary of the results and observations from this thesis and details future work that will be undertaken in the research group.

Chapter 8, the final chapter details experimental procedures, which were employed for the synthesis and photophysical evaluation of the compounds described in the previous five chapters. Finally literature references are provided.

The appendix provides crystallographic data, in addition to spectroscopic and titration data relevant to each of the preceding chapters.

Acknowledgements

I would firstly like to thank all of the technical staff of the School of Chemistry. In particular Dr. Martin Feeney for assistance with gel electrophoresis, SPC, and mass spectrometry, Dr. Tom McCabe for X-Ray crystallography, and Drs. John O'Brien and Manuel Ruether for NMR.

Also to David McGovern and Pauric Keane of the Kelly group for help with my many queries regarding fluorescence lifetime determination, and the members of the Rozas group whom I have worked beside for the last few years.

I count myself very lucky to have worked with such a fantastic group of people over the last three and a half or so years. To the many past members of the group; Andrew, Ann-Marie, Celine, Flo, Joe, Julien, Lin, Lisa, thank you for making the lab such an enjoyable working environment and for patiently answering all the questions I had when starting my PhD. A special acknowledgement of a few former group members. Eoin, for all those "just the one" pints and many informative conversations on chemistry and food, and the chemistry of food. Debbie, who could always be relied on for a good cup of tea or a bout of hysterical laughter whenever needed. Finally, Sally, for being a great friend and frequent travel companion.

The current members of the group. My former fellow postgrads Cidalia and Emma, now postdocs, its been a pleasure working with both of you, as it has been with our newer postdocs Celia and Aline. My "huge friend" Cristophe and co-second year Jen, its been terrific working with you the last year and a bit. Rebecca for making us laugh on numerous occasions with stories worthy of any soap opera, Doireann for your constant cheeriness, and Claire although you have finished you still get counted with these two, its been wonderful working with all of you. Niamh for sharing my fanaticism about food and for all the South Africa stories that we like to tell so often. Danni, for being a fantastic friend over the last few years, and for your patience when showing me how to work with cells. Also yourself and Una for accommodating me on my trips back to Dublin the past few months, and always making me feel so welcome. Finally, the new members of the group, Sam, Brien and Rob, who have integrated in to the group so easily, the best of luck over the next few years. Everyone has helped in some manner over the past few months, but particular thanks to those of you who proofread parts of the thesis for me.

I have been very fortunate to have two supervisors whose advice, encouragement and endless enthusiasm for chemistry has made my project and my PhD experience as a whole most enjoyable. Thorri and Susan thank you both for everything.

To my "second family" in Dublin, Rosie and John, and finally my own family for putting up with my occasional bad moods and periods of walking around the house muttering to myself the past few months. Thank you for the constant support and encouragement during this time, and indeed during the last almost eight years that I have spent in Trinity. I dedicate this thesis to all of you.

Abbreviations

br s	broad singlet
Boc	*tert*-butoxycarbonyl
Bpy	bipyridine
CD	circular dichroism
d	doublet
DABCO	1,4-diazabicyclo(2,2,2)octane
dd	double doublet
δ	chemical shift
DMF	dimethylformamide
DNA	deoxyribonucleic acid
EnT	energy transfer
ϵ	molar extinction coefficient
Eq.	equivalents
ET	electron transfer
Hz	hertz
IR	infrared
ISC	inter system crossing
J	coupling constant
λ	wavelength
m	multiplet
MeOH	methanol
m.p.	melting point
m/z	mass charge ratio
NMR	nuclear magnetic resonance
Pd/C	palladium on carbon catalyst
ppm	parts per million
q	quartet
s	singlet
t	triplet
TFA	trifluoroacetic acid
THF	tetrahydrofuran
TLC	thin layer chromatography
UV	ultraviolet

Chapter 1

Introduction

1.1 Introduction

The ability to prepare molecules that selectively bind DNA, and that exhibit photophysical properties that are sensitive to the binding event, continues to be the focus of a significant amount of research.[1-4] Such species have become highly desirable for use as nucleic acid probes, whose potential applications as highly sensitive diagnostic agents are vast.[5] In addition, molecules that can bind particular regions of DNA or particular genes, may allow one to precisely control the expression of specific genes.[4] This would provide novel therapies through the regulation of expression of proteins involved in a particular disease being targeted.[4] Another potential application of such molecules is as nucleic acid cleavage agents, whose development has been driven by the shortcomings of natural agents such as restriction enzymes.[6] Synthetic cleavage agents may allow one to cleave nucleic acids non-specifically at any region, or alternatively with a high degree of sequence selectivity, and have the added advantage that they may be activated photochemically. This thesis focuses on the interaction and reaction of small spectroscopically active molecules with DNA. The introduction, however, begins with a short description of DNA structure and the factors governing its recognition, followed by a discussion of some relevant examples of small molecules that bind DNA from the literature.

1.2 DNA Structure and Recognition

DNA (deoxyribonucleic acid) is regarded as the central icon of molecular biology, being found in each of the 10 trillion cells that comprise a human body. It is a class of nucleic acid which plays a central role in the transmission, expression and conservation of genetic information. DNA molecules may be enormous; the entire human genome for example contains 3.2 giga bases of information. This information encodes the instructions on how to construct an entire living organism and directs the function of that organism throughout its lifetime.

The molecule itself is a biological polymer consisting of two strands arranged in an anti-parallel helix. This orientation gives rise to the formation of a chiral molecule, which has both a major and minor groove on its surface. The strands are formed by a number of heterocyclic bases linked by a negatively charged sugar phosphate backbone. There are two types of bases; the purines - *adenine* and *guanine*, and the pyrimidines – *thymine* and *cytosine*. The oxygen and nitrogen atoms of each base act as hydrogen bond donors or acceptors, as illustrated in Figure 1.1. This allows for two types of specific interaction. The first is Watson-Crick base pairing which consists of hydrogen bonding between bases

on different chains, with *adenine* always bonding to *thymine* and *guanine* always bonding to *cytosine*, through complementary interactions. This arrangement is vital to maintaining the specificity of base pairing in DNA, and also forms the basis of the mechanism by which DNA is replicated, and thus the way in which all genetic information is propagated.[7] The second type of specific interaction is Hoogsteen base pairing, which occurs with the functional groups that protrude into the major groove. This type of base pairing is important in the formation of triple helices as will be discussed in a later section.

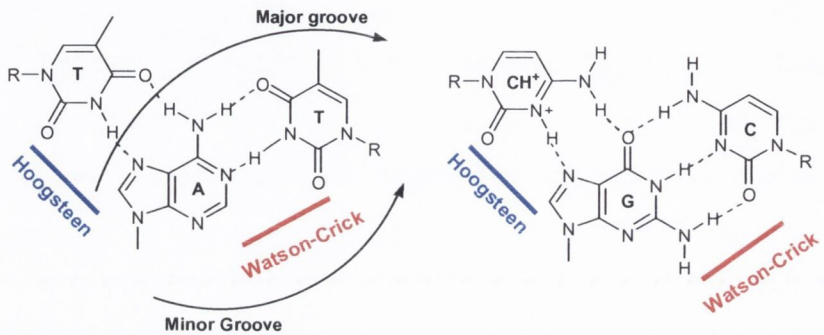

Figure 1.1 *Structures of the DNA bases showing the Watson-Crick and Hoogsteen base pairs and position of the grooves.*

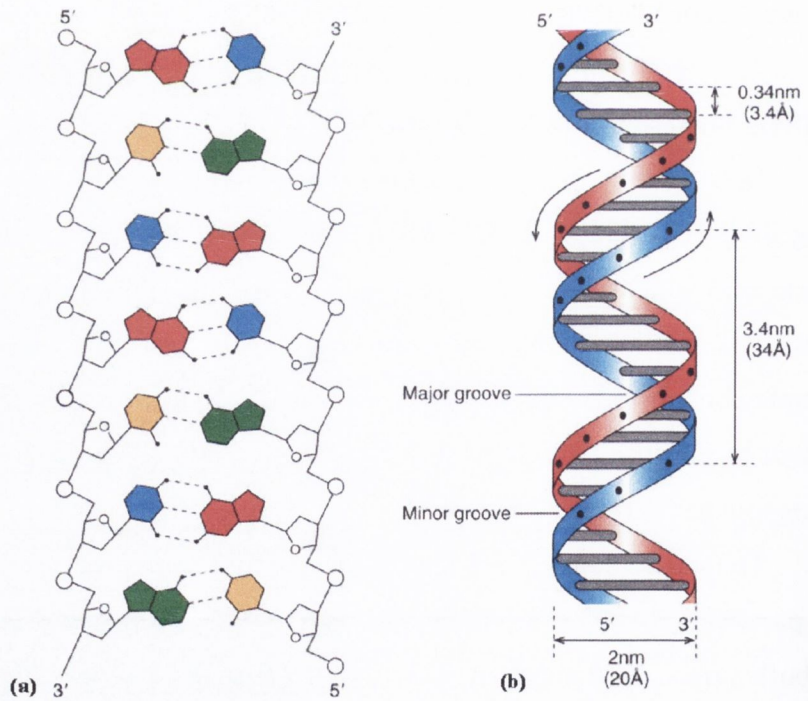

Figure 1.2 *Schematic representation of DNA structure showing; (a) the Watson-Crick base pairs between adenine (●), cytosine (●), guanine (●) and thymine (●), and (b) the double helical structure.*[8]

Hydrogen bonds govern specific interactions with and within the DNA helix but actually contribute little to its overall stability. However, the DNA bases exhibit extensive stacking interactions and hydrophobic forces that result from this are the primary means by which the helix is stabilized.[9]

The configuration of DNA remains constant. However, the conformation is dynamic and depends very much on environmental conditions such as humidity, temperature, pH, and salt concentration. The classical B-DNA structure, which was elucidated by the work of Watson and Crick is observed when the counter-ion is an alkali metal such as Na^+ and the relative humidity is 92 %.[9] The main structural features are:

- the helix is right handed.
- the glycosidic bonds (bonds linking the base and sugar) are in the *anti*-conformation.
- the ribose sugar units are C2'-endo puckered.[10,11]

This gives a structure with 10 base pairs per helix turn, a pitch of 3.4 nm, and the formation of two types of grooves, as depicted in Figure 1.2. The major groove is wide and the minor groove is narrow, but both are of similar depth. These structural features are summarised in Table 1.1.

Table 1.1. *Structural features of different DNA conformations.*[9]

	A	B	Z
Helical sense	Right handed	Right handed	Left handed
Diameter	~26 Å	~20 Å	~18 Å
Base pairs per helical turn	11	10	12 (6 dimers)
Helical twist per base pair	33°	36°	60° (per dimer)
Helix pitch	28 Å	34 Å	45 Å
Helix rise per base pair	2.6 Å	3.4 Å	3.7 Å
Base tilt to the helix axis	20°	6°	7°
Major groove	Narrow and deep	Wide and deep	Flat
Minor groove	Wide and shallow	Narrow and deep	Narrow and deep
Sugar pucker	C3'-endo	C2'-endo	C2'-endo for pyrimidines, C3'-endo for purines
Glycosidic bond	Anti	Anti	Anti for pyrimidines, syn for purines

When the relative humidity is reduced to 75 %, the B-DNA may undergo a reversible conformational change to the A form.[9] This structure is again a right handed helix but is somewhat wider and flatter than for B-DNA. The most obvious structural differences are the presence of an axial hole through the centre of the helix and the much increased tilt of the bases with respect to the helix axis. This results in there being a deep major groove and a very shallow minor groove. These structural features are summarized in Table 1.1 and depicted in Figure 1.3.

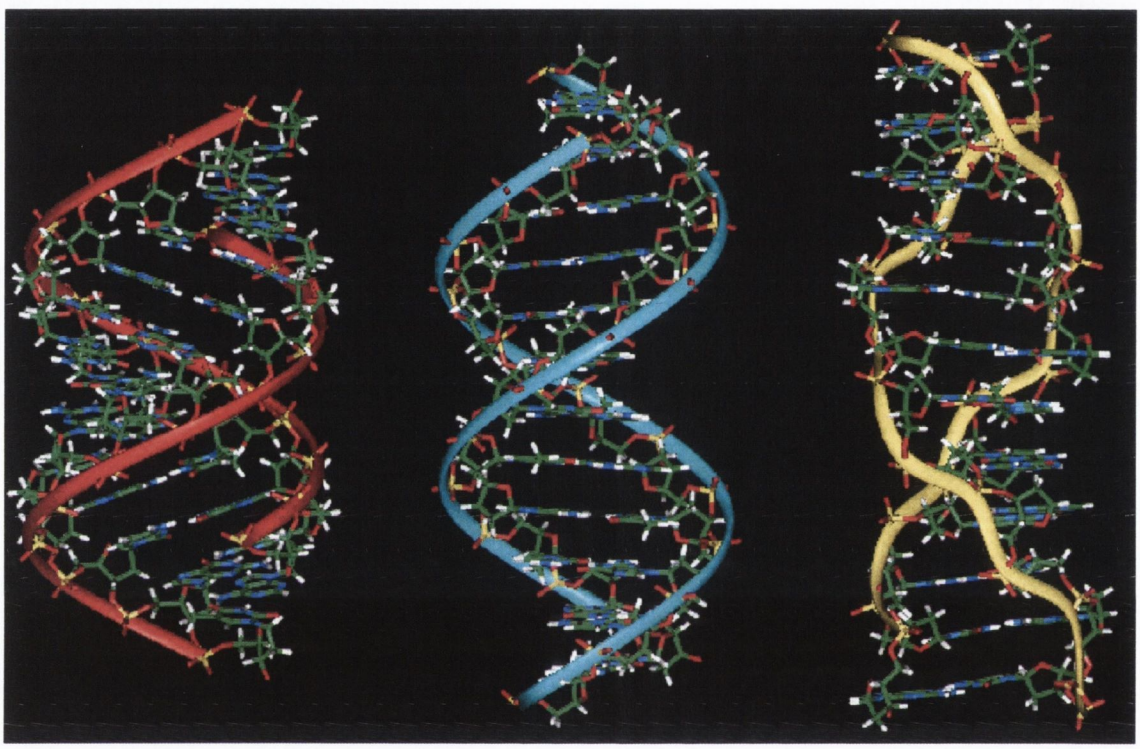

Figure 1.3 *Representation of possible structural forms of DNA. Left to right; A-DNA, B-DNA and Z-DNA.*

A third conformation is the left handed double helix Z-DNA, which forms with complementary polynucleotides with alternating purines and pyrimidines, at high concentration of counterion such as Na^+ or Mg^{2+}.[9] In this structure the pyrimidines display a C2'-endo sugar pucker and *anti* glycosidic bond, whereas the purines display a C3'-endo sugar pucker and a *syn* conformation around the glycosidic bond. These features give rise to the left-handed structure, where the phosphate backbone has a zig-zag appearance, with the constituent bases protruding into the groove. Here, the minor groove is narrow and deep, but the major groove has become so shallow that normally inaccessible parts of the G and C bases are exposed. The exact biological role of Z-DNA remains elusive although it

is suggested to be involved in the regulation of gene expression.[12] Current research aims to produce chiral molecules, which may distinguish between right and left handed DNA duplexes, and different types of duplex of the same sense.

The presence of DNA in living cells had led to it being recognized as a valuable target for the development of novel therapies. In particular a considerable amount of research has focused on the development of small molecules that may bind DNA and interrupt its normal function. When considering the interaction of a particular species with DNA, five general modes of binding may be considered; **(1)** minor groove binding, **(2)** major groove binding, **(3)** intercalation, **(4)** electrostatic binding, and **(5)** covalent attachment, as represented in Figure 1.4. Each mode places certain requirements on the structure of the molecule under examination. Investigation of the predominance of each mode of interaction for different structural motifs will allow us to build up an understanding of the features of small molecules that contribute to each, and in turn enable more elegant and controlled targeting of DNA in the future. This thesis will primarily focus on the interaction of metal complexes with nucleic acids, and the structural features within these complexes that lead to favorable binding to DNA.

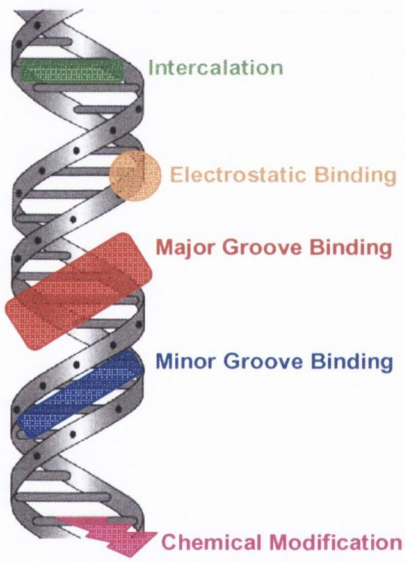

Figure 1.4 *Representation of the possible modes of binding to DNA.*

1.2.1 Minor Groove Binding

The grooves are a very important aspect of DNA structure. In the grooves the edges of the bases are exposed to the environment, thus providing functional groups that are accessible to species in solution. Molecules may be designed to bind in either the major or the minor grooves, making use of the particular H-bonding groups in each groove

to bind specifically. The naturally occurring antibiotic netropsin, is a classical example of a polyamide structure that binds in the minor groove at AT-rich sequences, a schematic representation of its interaction being shown in Figure 1.5.[13] The presence of specific hydrogen bond donor and acceptor groups and complementary shape were shown to govern recognition of the binding site. Studies on this class of compounds have led to the development of synthetic polyamides containing pyrrole and imidazole heterocycles, whose recognition of DNA in a sequence specific manner may be controlled through appropriate design.[14,15] Groove binding interactions have been shown to be primarily entropically driven, as ordered solvent molecules are expelled from the grooves upon binding.

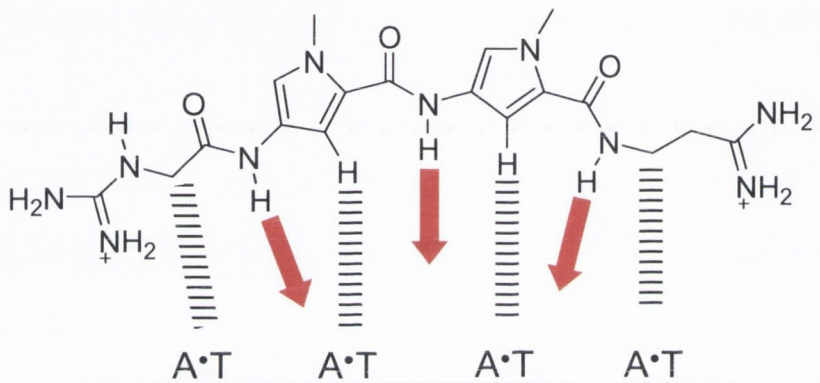

Figure 1.5 *Binding of netropsin to four successive base pairs. Arrows represent hydrogen bonds between drug and DNA,* IIIIIIII *are van der Waals interactions between drug and and adenine C_2-H atoms.*

1.2.2 Major Groove Binding

The major groove is, in general, more difficult to target specifically, due to its larger size. It is, however, rich in functional groups and in living cells is the site of binding of proteins that control gene expression *i.e.* promoters and repressors.[13] Synthetic oligonucleotides and peptide nucleic acids (PNAs) may be designed to bind in the major groove, which in doing so give rise to triple helix (triplex) formation.[13] Hoogsteen base pairing is important in forming such structures, and may occur when the third strand runs both parallel and anti-parallel to the duplex purine strand. Triplex forming molecules have been widely studied because of their possible anti-gene applications. If targeted to the control regions of genes, triplex forming agents may prevent the attachment of RNA polymerase, and thus prevent the transcription process. Triplexes form with exquisite specificity but are often less stable than their duplex counterparts. One means of

overcoming this is to add a compound which selectively binds to triplex DNA, thereby drawing the equilibrium in the direction of triplex formation. Examples of such compounds include benzo[e]pyridoindole, [16] **1** and the berbine alkaloid coralyne,[17] **2**.

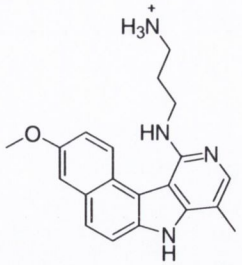

1

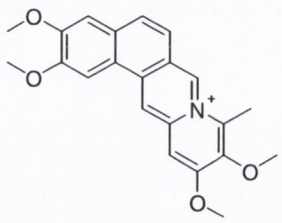

2

1.2.3 Intercalation

Another important mode of DNA binding is intercalation. This binding mode involves the insertion of flat polyaromatic ligands between the DNA base pairs and was first described for the acridine proflavine. The driving force for this mode of binding is primarily stacking between the intercalator and the base pairs, with positive entropy changes due to dislodgement of ordered water also playing a significant role. Fused two-ring systems are generally regarded as being the minimum requirement for intercalative binding.[18] In practice intercalators are usually of more extended planar character, are electron deficient, and often have appended groups which aid in binding. Such groups include positively charged side chains, which bind electrostatically to the negatively charged phosphate backbone of DNA. Intercalator-groove binder hybrid molecules have also been explored in efforts to design novel therapies.[19] Intercalators display useful cytotoxic properties with many such as amsacrine, **3** and mitoxantrone, **4** currently in clinical use for the treatment of cancer.[18] The primary mechanism of these intercalating agents is the production of DNA double-strand breaks through interference with the normal functioning of the DNA enzyme topoisomerase II (Topo II).

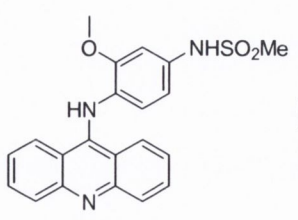

3

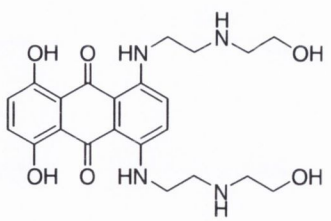

4

1.2.4 Electrostatic Binding

The sugar-phosphate backbone is another potential binding site on the DNA helix. As it is a hard oxygen-rich polyanion surface, interactions with group I and II metal cations

is observed.[4] Such electrostatic interactions with the cationic residues of proteins is also common, although these occur in conjunction with groove binding processes. Binding of the trinuclear platinum(II) complex **5**, has recently been reported, and shown to involve both tracking of the complex along the backbone and stretching across the minor groove contacting phosphates on either side.[20] More extensively studied in the context of DNA interaction are a range of spectroscopically active transition metal complexes, a detailed discussion of which will be given in Section 1.2.

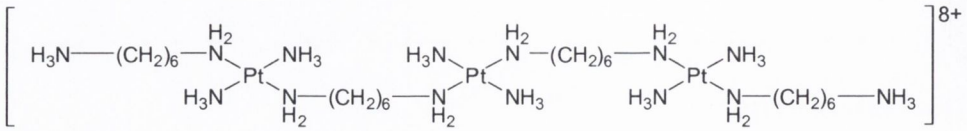

5

1.2.5 Covalent Attachment

The final mode of DNA binding and one that has been widely exploited in chemotherapy involves covalent attachment to nucleophilic sites on the DNA bases, namely the N7 atoms of adenine and guanine. Agents that bind in this manner such as the nitrogen mustard chlorambucil, **6**, are known as alkylating agents.[21] Cisplatin, **7**, which is one of the leading metal based anti-cancer drugs also falls into this category, its toxicity arising from the formation of covalent strand cross-links.[22] Such cross-links interfere with the normal function of DNA within cells, and ultimately result in cell death.

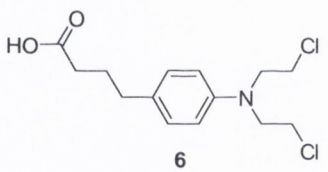

6

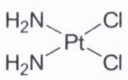

7

The binding of small molecules to DNA may occur by the combination of several of the modes of interaction discussed above. The targeting of DNA has been shown to be a successful strategy in the design of novel drugs but the ability to precisely control particular genes remains elusive. This therefore remains an active area of research with many different types of small molecule systems currently being explored. Transition metal complexes, in particular the polypyridyl ruthenium(II) complexes, are at the forefront of these efforts, as will be discussed in the following section.

1.3 Polypyridyl Ru(II) Complexes

Polypyridyl Ru(II) complexes have been extensively studied as both spectroscopic probes and photoreactive reagents for DNA.[5,23] They possess a number of excellent

tuneable photophysical, photochemical and redox properties, which may be exploited to probe their local binding environment. They are generally photostable and inert to ligand substitution, and are often water soluble. They have a defined geometry and can bind in the grooves of DNA, or by intercalation between the DNA base pairs, depending on the ligands employed. In addition polypyridyl Ru(II) complexes are chiral, and display varying degrees of specificity for nucleic acids of right or left handed configuration. Their synthesis, photophysics, electrochemistry, and use in areas such as materials science have been widely described in the literature.[24]

1.3.1 Photophysical and Redox Properties

In order to understand how tris(polypyridyl) Ru(II) complexes both interact and photoreact with DNA, an explanation of their photophysics is necessary. The photophysical scheme for $Ru(bpy)_3^{2+}$, the most extensively studied complex of this type is described in Figure 1.6. This scheme is applicable to complexes of other polypyridyl ligands.

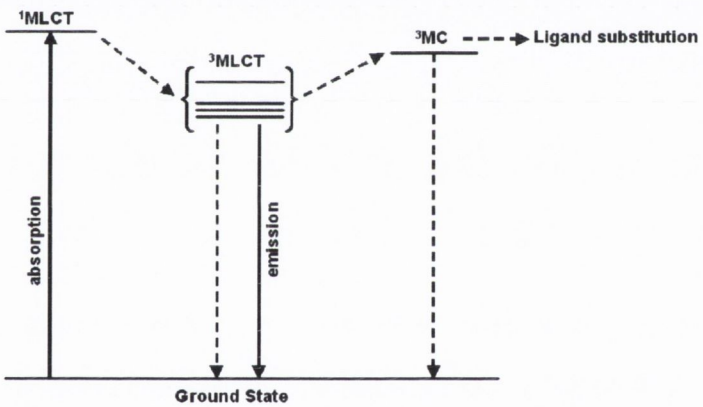

Figure 1.6 *Energy level diagram for the lowest excited states of* $Ru(bpy)_3^{2+}$. *Radiative processes are denoted by solid arrows and non-radiative by dashed.*

Absorption in the visible leads to population of the singlet metal to ligand charge transfer (MLCT) excited state.[23,25] This deactivates rapidly (< 1ps) by intersystem crossing (ISC) to the lowest lying triplet MLCT excited state, with a quantum yield (Φ) of nearly unity. Emission from this state is relatively long lived, and has been measured as 0.6 μs in degassed H_2O with $\Phi = 0.042$. The energy gap between the lowest ^{1}MLCT and ^{3}MLCT states has been estimated to be about 5000 cm^{-1}.[25] The ^{3}MLCT state has been shown to consist of three closely spaced levels ($\Delta E \approx 100$ cm^{-1}) which have similar but not identical properties, and a fourth state at about 600 cm^{-1} above the lowest of these states. Regarding

the three lower states, as the energy spacings are small, the photophysical properties are considered to arise from a single state having the averaged properties of all of the three states. Theoretical studies have shown that the singlet character of these three states is less than 11%.[26] The fourth state, is somewhat different and has a shorter lifetime because of its greater singlet state character. In terms of a detailed description of the overall excited state, two models have been proposed; (a) the delocalised orbital picture in which the excited electron is shared by the three ligands, and (b) the localised orbital picture whereby the electron resides on a single ligand for a certain period of time.[25] The predominance of neither has been proved conclusively. However, in solution evidence seems to point more towards a localised orbital model. The most convincing evidence has come from resonance Raman experiments, where upon laser excitation Raman bands corresponding to reduced ligand anion radicals were observed.[27]

There are three major pathways available for deactivation of the ^{3}MLCT. These are (1) radiative and (2) non-radiative decay to the ground state, and (3) cross over into thermally accessible *d-d* or metal centred (^{3}MC) triplet states located about 3600 cm^{-1} above the emitting level.[25] The two types of excited state display distinct reactivities. Reactivity of ^{3}MLCT generally involves redox processes undergoing both oxidation and reduction depending on the conditions, whereas ^{3}MC is strongly distorted with respect to the ground state as it involves promotion of a largely non-bonding electron to an antibonding σ orbital and may undergo ligand substitution reactions.[28] The relative population of these two states is of particular relevance when dealing with the photoreactivity of Ru(II) polypyridyl complexes with nucleic acids, as will be discussed in a later section.

1.3.2 Structurally Simple Ru(II) Complexes

The first studies involving Ru(II) polypyridyl complexes as DNA binders and photocleavers employed bipyridine and phenanthroline groups as ligands. The binding mode of $Ru(bpy)_3^{2+}$ was established to be electrostatic in nature, where the positively charged complex associated externally with the negative charges on the DNA backbone.[29,30] This was ascribed from changes in the thermal denaturation of DNA, showing similar behaviour to Mg^{2+}, which is known to bind purely by electrostatic means.[31] Moderate hypochromicity in the absorption maximum of the complex was also observed in the presence of DNA at low ionic strength, as was a 1.5 fold increase in Φ_F of the MLCT state, due to protection of the complex from solvent molecules and quenchers.

The binding of $Ru(phen)_3^{2+}$, shown in Figure 1.7, to DNA was first described in the 1980's. Studies by Barton and co-workers suggested this complex to bind DNA through intercalation of one of the ligands, with electrostatic interaction also playing a role.[32,33] The system displayed a binding constant of 6.2×10^3 M^{-1} in a buffer comprising 5 mM Tris and 50 mM NaCl.[32] Stereospecificity in the binding interaction was also observed, the Δ-isomer displaying higher affinity for B-DNA.[34] This was proposed to occur as with one of the phenanthroline ligands intercalated, the two non-intercalated ligands of the Δ-isomer fit closely along the right handed helical groove. In contrast, the non-intercalated ligands of the Λ-enantiomer are repelled sterically by the phosphate backbone of the duplex. These observations were in agreement with a previous study on the electric dichroism of the enantiomers of the complex in the presence of DNA, where stereospecific binding was also observed.[35]

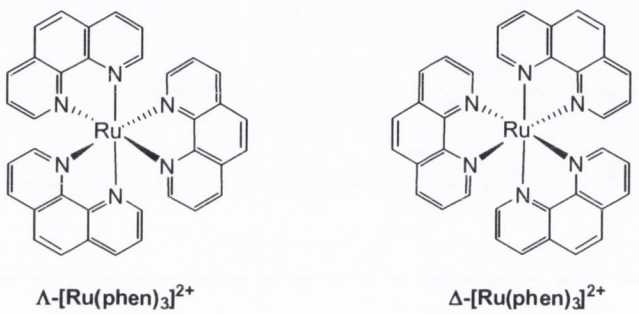

Figure 1.7 *Structure of $Ru(phen)_3^{2+}$ showing the enantiomeric forms.*

Further investigation by Barton and co-workers revealed the binding to be more complex involving two binding modes: (1) intercalation and (2) surface binding involving ligand interactions along the major groove.[36] This was ascribed from changes in the steady-state emission polarisation upon interaction with DNA. The binding was again shown to be dependent on ionic strength, thus electrostatic interactions still playing a role. The enantiomers of this complex were proposed to favour one mode over the other, the Δ-enantiomer favouring intercalation and the Λ-enantiomer favouring the surface binding mode. An extension of this work involving ^1H NMR studies of complexes bound to oligonucleotides provided some evidence for intercalation from the major groove side, and strong evidence of surface binding in the minor groove.[37] More recent two-dimensional NMR and NOE studies supported binding of $Ru(phen)_3^{2+}$ in the minor groove, but argued against an intercalative binding mode.[38,39] The absence of intercalative binding had previously been proposed by Hiort *et al.* from the results of linear dichroism and circular dichroism studies.[40] This matter of intercalation *vs.* non-intercalation was further resolved

in favour of the latter, by Satyanarayana *et al.* through viscosity studies.[41] They suggested that previous observations of unwinding of the helix caused by metal complex binding was not a definite indication of intercalation, data for irehidiamine A, **8** and crystal violet, **9** having in fact previously shown that the DNA may be unwound without intercalation. They observed a slight decrease in the viscosity of a DNA solution upon metal complex binding, which was attributed to partial non-classical intercalation, resulting in a kink in the helix. This conclusion was further supported by a later study using scanning force microscopy.[42]

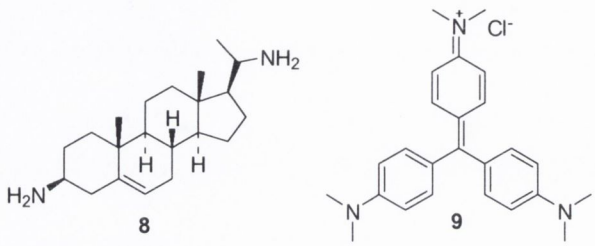

From the above discussion it is apparent that the assignment of the binding mode of this seemingly simple system has been much debated to date. This debate is possibly due to the different techniques used to probe the binding of these metal complexes, as they may detect certain modes more effectively than others, the different DNA sequences used, and also the DNA:metal complex concentration (P/D) ratio.[43] Despite all of this, these studies provided a basis for conceptualising how octahedral metal complexes might be used to probe DNA, and also provided much useful information on the application of various spectroscopic techniques to such an endeavour.[5]

1.3.3 Ruthenium (II) Polypyridyl Complexes Incorporating Extended Heteroaromatic Ligands

The main drawbacks associated with the two systems discussed in the previous section, with regards to their DNA binding properties, were low affinity and relatively small changes in photophysical properties. One means of increasing the affinity of such metal complexes for DNA, is to increase the surface area for intercalative stacking, through the use of extended aromatic heterocyclic ligands. An example of such a ligand is dipyrido[3,2-α:2',3'-c]phenazine (dppz). The first complex studied in this regard was $Ru(bpy)_2(dppz)^{2+}$, **9**, whose synthesis and photophysical properties had been described previously by Sauvage and co-workers.[44] Barton and co-workers showed the complex to bind DNA with very high affinity and more significantly act as a true molecular "*light switch*" for DNA.[45] In other words, the complex displayed no luminescence in aqueous solution at room temperature, but the luminescence was significantly increased in the

presence of double stranded DNA. The metal to ligand charge transfer transition had been shown to be directed to the phenazine ring, and the resulting excited state subject to efficient non-radiative deactivation by hydrogen bond formation between the phenazine nitrogens of the dppz and solvent molecules.[44] Thus shielding of the *dppz* moiety from quenching upon intercalation of the complex to DNA was regarded as being responsible for the observed emission enhancement.

Further investigation into the nature of this light switch effect, revealed the process to be more complex.[46] It was established that there were actually two MLCT states on the *dppz* ligand, which exist in equilibrium; a bright, luminescent state associated with the bipyridine fragment, and a dark, non-luminescent state localised on the phenazine portion of the molecule.[46-48] It was proposed that the molecule was non-luminescent in aqueous solution, as the second state corresponding to localisation on the phenazine portion, was stabilised to a greater degree by hydrogen bonding to the solvent. As a result the dark state was lower in energy than the bright state, and hence populated to a greater extent. The light switch effect was proposed to be a result of a state reversal upon binding to DNA, in which the dark state was no longer stabilised relative to the bright state. An alternative explanation was offered by Papanikolas and co-workers.[49] From temperature dependent studies that were carried out in both protic and aprotic solvents, they proposed that the dark state was always lowest in energy, and that the light switch behaviour was not driven by a state reversal but rather was due to a competition between energetic factors that favour the dark state and entropic factors that favour the bright state.[49,50] This explanation was supported by a second study in glycerol where the photophysical properties were assigned as being due to two MLCT states in equilibrium.[51] Recent theoretical studies have calculated that the lowest energy state is a dppz centered 3π-π^* state, and that this actually corresponds to the dark state.[52] A slightly different model has been proposed by Lincoln and co-workers from studies in hydroxylic solvents, which represents a refinement of the model of Papanikolas and co-workers.[53,54] The model involves an equilibrium between three states; (a) a non-hydrogen bonded emissive state, (b) a second emissive state lower in energy, in which there is one hydrogen bond between the solvent and one nitrogen on the phenazine ring, and (c) a non-emissive state with two hydrogen bonds to the phenazine nitrogens. Complete assignment of the photophysical mechanism that gives rise to the light switch effect in complexes such as **10** is still somewhat debated but certainly may be regarded to involve bright and dark states in equilibrium with each other, whose relative population depends on the local environment.

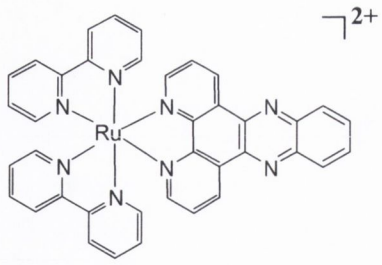

10

Further study by the Barton group showed that the ancillary bipyridine ligands on the complex could be changed to *phen* without affecting the light switch behaviour, but that changes to the *dppz* ligand itself gave complexes which luminesce in aqueous solution to some extent.[55] The same report presents a more extensive evaluation of the photophysical properties of such complexes in the presence of DNA, a biexponential decay of luminescence suggesting two modes of binding. Two intercalative binding modes were also proposed, one perpendicular mode where the ligand intercalates such that the metal-phenazine axis lies along the dyad axis, and a second side-on mode where the metal-phenazine axis lies along the axis of the base pairs. Differential solvent accessibilities to the phenazine nitrogens in each mode would explain the different lifetimes observed. Additionally, no quenching of MLCT emission of bound complex with $Fe(CN)_6^{4-}$ was observed implying that both binding modes, and hence both lifetimes correspond to modes where the complex was embedded deep or intercalated in the helix.[56] An intercalative binding mode has been futher supported by other research groups through the use of linear dichroism,[57,58] and viscosity and fluorescence energy transfer studies.[59]

The issue of the groove position of such complexes was first addressed through NMR studies, where intermolecular NOE's to DNA major groove protons were observed, indicating that the complex binds through the major groove.[60] These results were disputed, when another study showed that the complex emitted strongly when bound to T4-DNA, or DNA which is glucosylated in the major groove.[61] Longer lifetimes with AT and [poly(dI-dC)]$_2$, which resembles GC but that the exocyclic amino of guanine has been removed, further supporting the proposal that the complex intercalates from the minor groove. Bi-exponential emission was proposed to occur as a result of a dye distribution effect. The original assignment of binding from the major groove side was later supported by competition binding studies using known major and minor groove binders.[62] A decrease in emission from bound $Ru(phen)_2(dppz)^{2+}$ was observed upon addition of Δ-α-[Rh[(R,R)-Me_2trien]phi]$^{3+}$, **11**, a well characterised major groove binder, which is consistant with binding from the major groove side. Similar experiments with distamycin demonstrated

that the complex was not in the minor groove, a slight increase in emission from the metal complex actually being observed which was attributed to a stiffening of the helix upon distamycin binding. A lack of power dependence to the excited state decay was given as an argument against biexponential decay resulting from distribution of metal complex.[62] The consensus now seems to be that intercalation occurs from the major groove side, with two main orientations leading to biexponential decay of luminescence.

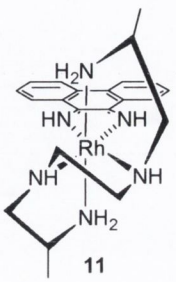

11

The extended polyazaaromatic system of dppz has been shown to generate Ru(II) complexes with high binding affinity for DNA that are particularly useful as probes. However, Ru(II) polypyridyl complexes also display interesting photochemistry and as such their excited state reactivity with DNA has been explored extensively, this being the subject of a number of recent reviews.[23,63] Photosensitized cleavage of DNA was reported early on for $Ru(bpy)_3^{2+}$ and $Ru(phen)_3^{2+}$, but the efficiency for these systems was quite low and shown to originate primarily from singlet oxygen formation.[29,64] More strongly π-accepting ligands such as those shown in Figure 1.8 are necessary if the complex is to react directly and abstract an electron from the bases in DNA.[23] Complexes such as $Ru(TAP)_3^{2+}$ have low lying molecular orbitals on the ligands and have been shown to be strongly oxidizing in their ^{3}MLCT excited state.[65,66]

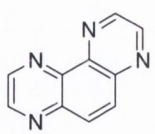

1,4,5,8-tetraazaphenanthrene (TAP)

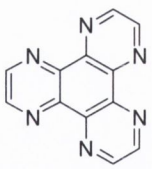

1,4,5,8,9,12-hexaazatriphenylene (HAT)

Figure 1.8 *Strongly π-accepting ligands incorporated in photooxidizing complexes.*

$Ru(TAP)_3^{2+}$ was shown to induce strand breaks in DNA with a much higher efficiency than $Ru(bpy)_3^{2+}$ or $Ru(phen)_3^{2+}$.[67,68] Emission from the complex was also shown to be strongly quenched by guanine rich DNA, and thus the cleavage was proposed to be due to an electron transfer from guanine to the metal complex, and subsequent reaction of

the radical cation formed. Direct evidence of electron transfer from guanine was provided by Lecomte *et al.* using flash photolysis studies of complex in the presence of mononucletides and DNA.[69] Transients were observed corresponding to the reduced complex, the extent of which was greater in the presence of GMP than ct-DNA. Electrophoretic experiments with $Ru(TAP)_3^{2+}$ illuminated in the presence of ^{32}P-labeled oligonucleotides surprisingly showed the appearance of bands of lower mobility than the starting oligomer.[70] These bands were attributed to the formation of covalent adducts between the metal complex and the DNA. A subsequent study involving spectroscopic and dialysis experiments showed that light induced addition of the metal complex to both double and single stranded DNA involved direct reaction of the complex rather than dechelation.[71] Changes in the absorption spectrum at around 500 nm that were consistent with dechelation were not observed. However, a hypsochromic shift in conjunction with a hyperchroism in the 350 – 400 nm region was observed, in accordance with the formation of a substituted metal complex. Comparative experiments with $[poly(dA\text{-}dT)]_2$ and $[poly(dG\text{-}dC)]_2$ showed that formation of this type of adduct is particular to reaction with guanine.[71] In fact, the formation of a different type of adduct was demonstrated for the photoreaction of $Ru(TAP)_3^{2+}$ with AMP, that involved substitution of one of the TAP ligands.[72] This process can be related to the photophysical properties of the complex which had previously been shown to undergo photodechelation due to efficient thermal population of its ^3MC state.[66] Thus, reaction would involve photosubstitution of one of the TAP ligands by adenine and another monodentate ligand.

In comparison with the substitution with AMP, structural identification of the adduct with GMP was not intuitive. Both ^1H NMR and ESMS analysis of the resulting photoadduct was necessary and showed that the linkage occurred *via* bonding of the N-2 of guanine to C-2 of one of the TAP ligands, as shown in Figure 1.9.[73] Furthermore formation of the photoadduct was proposed to proceed by initial oxidation of guanine by the metal complex excited state, subsequent proton transfer, and finally coupling of the radicals so formed.

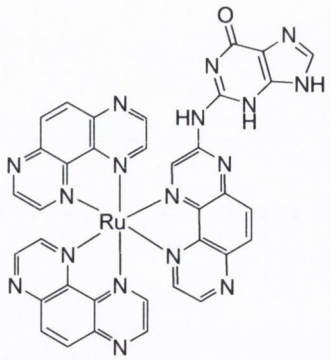

Figure 1.9 *Structure of the adduct formed between* $Ru(TAP)_3^{2+}$ *and guanine.*

Similar structural identification has been conducted for the photoaddition of mixed ligand complexes such as $Ru(TAP)_2(bpy)^{2+}$ and $Ru(HAT)_2(phen)^{2+}$ to DNA.[74,75] Addition was shown to occur to the TAP and HAT ligands exclusively, the ancillary bipyridine or phenanthroline ligands not participating in the process. Such mixed ligand complexes were also studied as part of a series which possessed modulated redox properties by virtue of the number of TAP or HAT ligands. The yield of strand breaks was shown to be strongly influenced by the number of TAP or HAT ligands and was actually shown to be higher when two such ligands were incorporated in a single metal complex.[76] This was attributed to the occurance of side reactions with the tris complex $Ru(TAP)_3^{2+}$, which reduced the overall efficiency in this system.

By increasing the heteroaromaticity of the ligands incorporated into Ru(II) polypyridyl complexes, species which bind to DNA with extremely high affinity or efficiently react with it in the excited state, may be generated. The PHEHAT ligand present in complex **12** was designed with the purpose of achieving this, by combining these two properties *i.e.* the strong intercalative binding of dppz type complexes with the excited state reactivity of HAT type complexes.

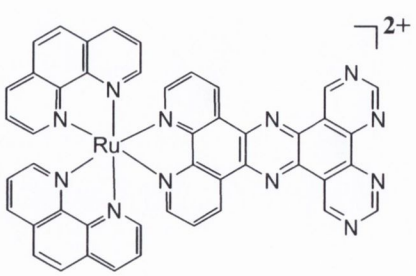

12

Changes in the UV/Visible spectrum of $Ru(phen)_2(PHEHAT)^{2+}$, **12** upon addition of DNA were consistent with high affinity intercalative binding, two distribution modes of the complex on DNA also being apparent, similar to the results from studies on the *dppz*

complexes discussed earlier.[77] Significantly, a luminescent light switch effect was also observed, where no emission was detected in aqueous solution, but upon addition of DNA, the complex luminesced due to intercalation of the PHEHAT ligand within the helix. The light switch mechanism for this complex was proposed to occur by a similar mechanism to that of the dppz complexes, involving changes in the population of bright and dark states, that exist in equilibrium with each other.[78] As expected, the complex was oxidizing in the excited state, the excited state reduction potential being of the same order as that of the Ru(II) complexes containing two π-deficient TAP or HAT ligands.[77] Flash photolysis studies using GMP showed the presence of reduced complex and oxidized guanine, verifying that the complex was oxidizing enough to abstract an electron from guanine. The traces, however, were rather weak and no photoadduct was detected after continuous illumination in the presence of GMP, indicating that the efficiency of electron transfer was rather poor.[77] The authors did note that the absence of a photoadduct could be attributed to the lack of reactivity of the resulting radical ion pair formed by the electron transfer. There was no evidence of electron transfer with DNA, which may be due to the fact that the complex was not sufficiently oxidizing to undergo efficient electron transfer with DNA. Alternatively, the transients may be very short lived, and hence not detectable on the instrument used. Incorporation of a PHEHAT ligand into a Ru(II) complex did result in enhanced affinity for DNA, but the excited state reactivity with DNA was modest compared to the previously studied TAP and HAT complexes. Further research is necessary to generate systems with the correct balance of DNA binding affinity and reactivity.

A strategy that has proven successful in yielding systems that possess high binding affinity for DNA, while at the same time displaying good excited state reactivity, is the preparation of mixed ligand complexes, where one of the ligands confers high affinity and the other two photonuclease activity. As such, $Ru(bpz)_2(dppz)^{2+}$, **13a** was studied by Paillous and co-workers, [79] in which the dppz ligand was expected to confer high binding affinity towards DNA, and the ancillary bpz ligands to confer good excited state reactivity.[80,81] No binding constant was reported for these systems to DNA, but it was assumed to be of the same order as that for the reference complex **11**. Significant differences in cleavage efficiencies were observed between the bpy and bpz complexes. Cleavage for the bpy complex was shown to proceed *via* a singlet oxygen mechanism but cleavage induced by the bpz complex was proposed to be due to electron transfer from guanine residues, and subsequent reaction of the guanine radical cation formed. The

occurrence of an electron transfer was ascribed from differences in the luminescence lifetimes of the complex in the absence and in the presence of DNA and polynucleotides.

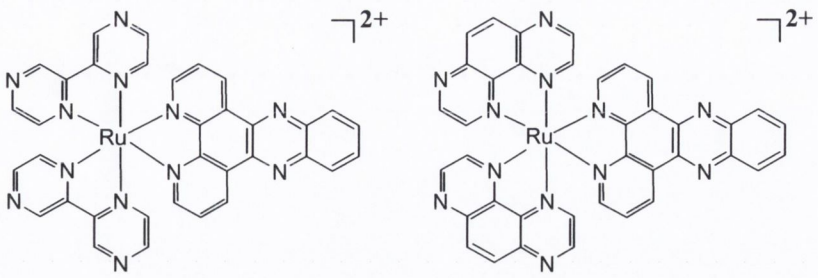

13a **13b**

The same approach was applied in the design of $Ru(TAP)_2(dppz)^{2+}$, **13b** in which the ancillary ligands have been changed for TAP. UV/Visible studies with ct-DNA showed this complex to possess similar affinity as seen for the reference bis-phen complex.[82] The lowest excited ^{3}MLCT state was shown to correspond to a charge transfer to one of the TAP ligands, and as such the complex was strongly emissive in water. Luminescent quenching by GMP or polynucleotides containing guanine was also observed, which in conjunction with flash photolysis experiments demonstrated the occurrence of electron transfer from guanine. An observed isotope effect also led the authors to propose that the electron transfer was in fact proton-coupled.

By extending the heteroaromaticity of the ligands incorporated into Ru(II) polypyridyl complexes, systems with a range of useful properties may be obtained. These include complexes which display significant spectral responses upon DNA binding such as the $Ru(bpy)_2(dppz)^{2+}$ "light switch" and those which exhibit excellent photosensitized cleavage of DNA such as $Ru(TAP)_3^{2+}$. The next important step anticipated with systems such as these will be to modify them such that they can effectively enter cells, thus allowing their application as intracellular probes or reactive agents.

1.3.4 Bimetallic Ru(II) Complexes

Another approach to enhancing the DNA binding properties of Ru(II) polypyridyl complexes has been the covalent linkage of two metal centres together to give bifunctional or bimetallic complexes. This approach had previously been applied to purely organic systems such as the bis-intercalating diacridines where increased affinity for DNA was observed over their mono-functional counterparts.[83,84] One of the first examples of metal complexes of this type was developed by Kelly and co-workers, and was based on the

weakly interacting 2,2'-bipyridine ligand, and comprised two metal centres linked by an aliphatic chain as shown in Figure 1.10.[85]

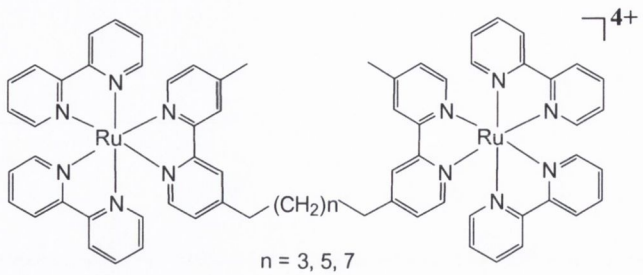

Figure 1.10 *Bimetallic complexes comprising* $Ru(bpy)_3^{2+}$ *like units.*

These systems were shown to possess much higher binding affinity for DNA than their monometallic analogue, display binding that was less sensitive to ionic strength, and photocleave DNA more efficiently. A more extensive photophysical study on these complexes verified that they bind to DNA at least 100 times stronger than their monometallic analogues, thereby displaying a cooperative effect in interaction with the helix.[86] Furthermore, the binding was shown to be dominated by electrostatic factors, and occur in a manner such that the two centres exhibited two types of site on the DNA, each with a very different environment. The presence of two types of site was inferred from lifetime data where both short and long lived species were observed. The short lived species was shown to be more sensitive to quenching by oxygen, but less than that observed for the complex in the absence of DNA, suggesting that it was bound on the surface of DNA and not intercalated. However, the longer lived species had a reduced oxygen quenching rate constant, which suggested it was buried deep within the groove of DNA. The authors did note that due to the salt dependence of the binding constants, intercalation, or partial intercalation was unlikely even for the longer lived species. An interesting observation in this study was the occurrence of a strong hypochromism in the UV/Visible absorption spectrum at low P/D ratios. This was attributed to DNA promoted interaction between the different metal centres, and it was speculated that both intra- and inter-molecular processes were occurring. However, the interaction did not lead to any quenching of the metal based emission.

Other structurally related systems having ancillary phen ligands were also studied, and these displayed similar affinity for DNA.[87] A hypochromism in absorbance was observed along with a quenching of the Ru(II) MLCT emission. Time resolved emission data indicated the presence of three components bound to DNA, including species with a

lifetime significantly shorter than that of the free complex in solution. This was attributed to a DNA induced stacking conformation of the complexes which facilitated a partial quenching process. It was assumed that the less extended aromatic character of the bimetallic bipyridine complexes was the reason for the absence of quenching in these systems.

A more rigid arrangement of the two metal complex cores in bimetallic species has also recently been explored. Lincoln, Nordén and co-workers investigated the binding of the two enantiomeric forms of **14**, and analogous complexes with ancillary bpy ligands, using linear dichroism (LD), absorption and an assay based on the displacement of DNA bound Δ-$[Ru(phen)_2(dppz)]^{2+}$.[88] All the complexes were shown to bind DNA with extremely high affinity, with binding constants of the order of 10^{12}. However, from the modest hypochromicity in absorbance observed and strong deviation of the bi(dppz) plane from perpendicularity in the LD experiments the mode of binding was concluded to be non-intercalative in nature. Rather, for the two enantiomers of the bpy complex, binding was proposed to occur in a manner in which the concave bi(dppz) ligand embraced the sugar-phosphate backbone of DNA, placing one metal centre in each groove, with the same occurring for the ΛΛ enantiomer of the phen complex. For the ΔΔ enantiomer of the phen complex both metal centres were concluded to be in the same groove. As will be discussed shortly the binding process was actually more complex than this.

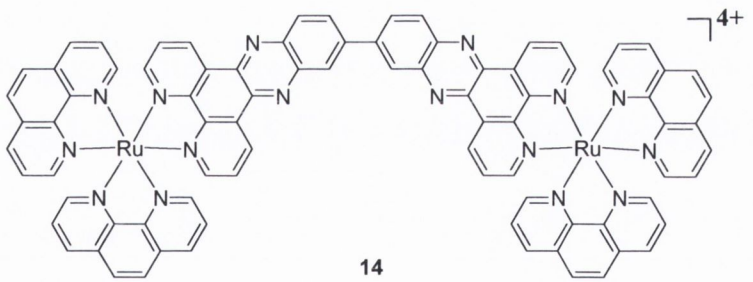

14

Flexible analogues of the semi-rigid complex **14** were also prepared in which two $[Ru(phen)_2(dppz)]^{2+}$ moieties were tethered to each other *via* an aliphatic diamide linker to give **15**.[89] Using LD experiments the ΔΔ and ΛΛ dimers were shown to bind to DNA with orientations similar to their monomers, both complexes bis-intercalating. The LD of the DNA bound *meso* form was actually the mean of the LD of the two opposite enantiomers, which suggested that the binding geometry of each subunit depended only on the absolute configuration. In addition to this, very slow dissociation rates were observed from DNA, upon addition of SDS, which should effectively sequester the complex. This led to the proposal that the complexes were threading bis-intercalators.

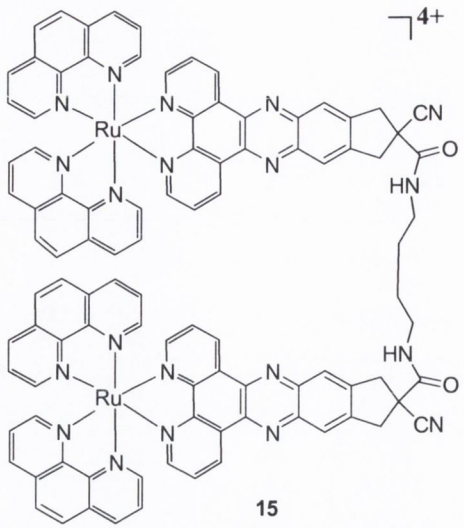

15

A later publication reported a more extensive study of the DNA binding and threading dynamics of these systems.[90] The chirality of the metal centre was shown to be important for the threading mechanism, all three different stereoisomers displaying different dissociation rates. The rates were in the order ΛΛ > ΔΛ > ΔΔ, with that for the meso complex being more like that observed for ΔΔ. In addition to a faster dissociation rate, ΛΛ also displayed a greater ionic strength dependence. In order to accommodate the threading of the bulky parts of the complexes between the strands, a substantial conformational change in the DNA helix was necessary, which was envisaged to involve both opening and unstacking of the base pairs. It was proposed that a smaller conformational change of DNA was associated with unthreading of the ΛΛ enantiomer. Moreover, the rate limiting step of dissociation was suggested to be from a mono-intercalated intermediate which explained the observed similarities in the rates for ΔΔ and ΔΛ.

A serendipitous discovery by the same group showed that the semi-rigid binuclear complexes previously assigned as being groove bound actually rearranged extremely slowly to an intercalative mode, these molecules therefore being regarded as dynamic binders of DNA.[91] This was inferred from a solution of complex and DNA that had been left for two weeks at room temperature and showed a change of LD signal from positive to negative. The complex was proposed to rearrange itself from groove binding to intercalative geometry by threading of one of the $Ru(phen)_2$ moieties through the duplex. This was consistent with the fact that the complex dissociates almost instantaneously from the initial binding mode upon addition of SDS, whereas it needed several days at 45 °C to dissociate from the final mode. The presence of a final intercalative mode was further supported by luminescence measurements. Here the Φ_F of **14** in its final binding mode to

ct-DNA was approximately 1500 times that observed for the free complex in solution. The threading process in this system was much slower than that for the flexible system **15**, which is most likely due to the greater flexibility of **15** afforded by the aliphatic linker. More extensive study showed that the bridging ligand was intercalated in the *anti* geometry with one Ru(II) in each groove.[92] Furthermore, an increase in the MLCT emission after completion of intercalation was observed due to reorganisation of the intercalated complex to the thermodynamically favoured distribution.[93] This 'shuffling' process was ascribed from changes in fluorescence resonance energy transfer (FRET) between DAPI and the complex on DNA, a process that is sensitive to the spatial separation between the two species.[93] The complexes were shown to move from a "*spread out*" binding during intercalation to the more favoured distribution. An interesting application proposed for this phenomenon of slow rearrangement was the kinetic recognition of AT-rich DNA sequences by **14** and its analogue containing bipyridine ligands in place of phenanthroline.[94] The rate of rearrangement to the intercalative form was shown to be dependent on the nucleobase composition. Both enantiomers of **14**, and its bipyridine analogue, intercalated into $[poly(dA\text{-}dT)]_2$ within a few minutes at 25 °C, while rates into mixed sequence DNA were very low even at 50 °C, and showed greater variation. In particular, the ΛΛ enantiomer of the bipyridine complex was highly selective where the ratio of $t_{1/2}$ for intercalation into ct-DNA compared to $[poly(dA\text{-}dT)]_2$ was estimated to be 2500 at 50 °C. This complex was studied in detail in the presence of hairpin oligonucleotides with central alternating AT tracts of varying length. It was shown that at least one helix turn of AT base pairs was needed for efficient threading intercalation, and thus this phenomenon represented a very sequence selective DNA interaction. A striking feature is that the recognition process goes beyond the classical lock and key model we usually associate with DNA recognition, but represents a novel mechanism of sequence specific DNA interaction.[94]

The strategy of incorporating two metal centres into a single complex has proved to be successful, having afforded systems with enhanced DNA binding affinity and spectral responses than their monomeric forms. A particular feature of many of these dinuclear species is their ability to thread the DNA helix, a binding mode which also results in extremely low dissociation rates. Such properties are highly desirable in the design of new drugs and may also provide insight into the dynamic behaviour of DNA in solution.

1.3.5 Complexes with Appended Organic Chromophores

The bifunctional strategy is not limited to assemblies based on two metal complexes. A novel series of luminescent probes for DNA was reported by Thornton and Schanze in the 1990's.[95,96] These systems were based on a chromophore-quencher assembly consisting of a Re(I) complex tethered *via* a flexible linker to an anthracene moiety, as shown in Figure 1.11. They proposed that a conformational dependence of the efficiency of intramolecular quenching would provide the basis of operation for this novel set of probes. In solution emission from both components was observed but was strongly quenched in comparison to the corresponding monomers. Reduction of the MLCT emission was proposed to be due to a Dexter energy transfer mechanism from the ^{3}MLCT to the ^{3}An (this state not being phosphorescent in fluid solution). Reduction of the anthracence fluorescence was suggested to be due to a Förster energy transfer mechanism from the ^{1}An to the ^{1}MLCT, and subsequent deactivation of this state by radiative and non-radiative processes. Modest variations in the rate of energy transfer from ^{3}MLCT to ^{3}An were observed with different linker lengths. In such systems it would be expected that the rate of energy transfer would fall off exponentially as the distance between the donor and acceptor was increased. Consequently, it was proposed that the linkers adopt conformations such that the through space distance between the Re and An chromophores would be similar in all complexes, or that the rate was controlled by the conformational dynamics of the spacer and not by the intrinsic rate of energy transfer (EnT).

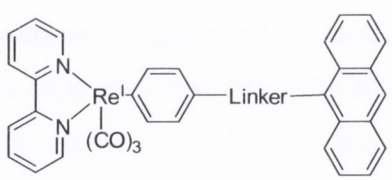

Figure 1.11 *Re(I)-Anthracene based chromophore-quencher DNA probe.*

Upon addition of st-DNA changes in the UV/Visible spectrum were observed that were consistant with intercalation of the anthracence moiety and weak association of the Re(I) complex. Significant enhancement of emission from ^{3}MLCT was also observed but the Φ_{MLCT} did not return to the value observed for the monomer. This was consistent with the results from lifetime experiments, where the longest lifetime component, in the presence of DNA, was still less than that of the unquenched MLCT state. A binding model was proposed in which the An chromophore intercalated into the DNA and the metal complex remained externally bound to the backbone. Such bevaviour restricts the two

chromophores from coming into close proximity to each other, and the increased separation distance reduces the rate of the EnT quenching processes. Interestingly the increase in the emission quantum yield was observed to be approximately the same for all of the systems. The authors concluded that EnT seen in the presence of DNA must occur predominantly through space, but only after the excited Re chromophore "rattles" around on the surface of the helix to attain an optimum geometry for energy transfer.[96] The rate was therefore determined by the dynamics of this process and not by the separation distance.

Kirsch-De Mesmaeker and co-workers developed an assembly based on these same principles, whereby they attached the known DNA intercalctor aminoquinoline *via* a flexible chain to a polypyridyl Ru(II) complex.[97] This gave the bifunctional complexes $[Ru(TAP)_2POQ\text{-}Nmet]^{2+}$, **16a** and $[Ru(Bpy)_2POQ\text{-}Nmet]^{2+}$, **16b** respectively.[97] The initial objective of this work was to increase the DNA binding affinity of the parent metal complex. However, it was also observed that **16a** had a low emission quantum yield in water, which was though to be due to electron transfer (ET) quenching of the Ru(II) centre by the aminoquinoline.[98] This was inferred from theoretical consideration of the process using the Rehm-Weller equation, thermodynamic data indicating that electron transfer would be exergonic, and from transient absorption experiments.

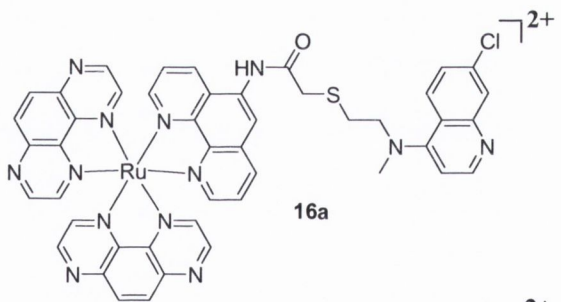

16a

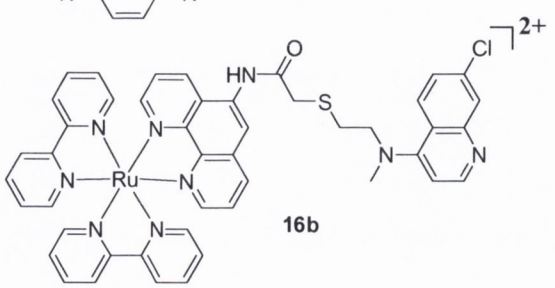

16b

Very weak transient absorption, from which no kinetic data could be obtained was observed, indicating the presence of only small amounts of monoreduced metallic unit. To further investigate this, methylviologen (MV^{2+}) at high concentration was added to **16a** and to $[Ru(TAP)_2(phen)]^{2+}$ + Nmet-quinoline. The MV^{2+} can reoxidize the reduced complex formed from intra- and intermolecular processes and produce the radical cation

($MV^{\bullet+}$), which is detected at 396 and 615 nm respectively. The amount of ($MV^{\bullet+}$) produced with **16a** was approximately twice that produced with the separate components of the complex, indicating that for **16a**, both intra- and intermolecular electron transfer processes occured. The fact that very little transient species could be detected could be due to a fast back electron transfer process, which resulted in the formation of a short lived charge separated state. The quenching process was shown to be pH sensitive, where the emission was restored upon protonation of the quinoline. This was proposed to be due to the diminished reducing ability of the aminoquinoline upon protonation or alternatively electrostatic repulsion of the two charged species that would prevent them from coming into the close proximity needed for electron transfer.[98,99] No quenching of Ru(II) emission was observed for **16b**, which is attributed to the diminished oxidizing power of the metal complex. This system cannot be described as having a chromophore-quencher arrangement and for this reason further discussion will focus on **16a**.

In the presence of DNA, the emission from the metal centre was restored to varying degrees depending on the DNA sequence.[100] This was attributed to a "*switching off*" of the quenching pathway due to partial protonation of the quinoline in the acidic microenvironment of DNA, and also separation of the two components, thereby reducing the rate of electron transfer between the complex and the DNA. Interestingly, the MLCT emission increased by two orders of magnitude in the presence of $[poly(dA\text{-}dT)]_2$, but only by one order of magnitude in the presence of $[poly(dG\text{-}dC)]_2$. In both cases, intramolecular electron transfer was regarded as being switched off by the aforementioned mechanisms. However, in the presence of $[poly(dG\text{-}dC)]_2$ electron transfer from guanine to the metal complex also became an important quenching pathway, thus reducing the overall quantum yield. Studies were also carried out with polynucleotides containing varying percentages of guanine residues and it was shown that the observed enhancement was dependent on the base content, the greater the percentage of AT base pairs, the greater the observed luminescence enhancement. No sequence selectivity in binding affinity was observed, but there was selectivity in the emission response. Hence, this complex can be regarded as a luminescent sensor for base content, acting as a light switch for sequences possessing high AT content.

As discussed in Section 1.2.3, Ru(II) complexes containing TAP ligands are usually excellent photooxidants of DNA, but bind it with relatively poor affinity. One of the reasons for linking such a complex to an organic chromophore such as aminoquinoline was to increase the DNA affinity and consequently the photonuclease ability. However, no

such studies on the photonuclease abilities have been reported thus far. A chromophore-quencher assembly for application as a photonuclease was reported by Turro and co-workers which consisted of a $Ru(bpy)_3^{2+}$ like moiety tethered to an acceptor chain, comprised of two viologens, **17**. No luminescence was observed from the metal centre in aerated aqueous solution, indicating efficient quenching by the viologen moieties by ET. The transient absorption spectrum exhibited peaks at 395 and 605 nm respectively, typical of reduced viologen, and the charge separated state was observed to decay monoexponentially, with a lifetime of 1.7 μs. The long lifetime was consistent with localisation of the transferred electron on the terminal viologen.

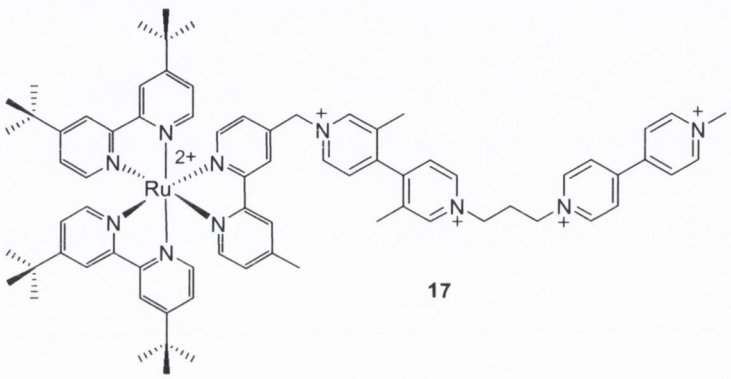

17

The complex was shown to cleave DNA upon irradiation for 20 min with visible light even in the absence of oxygen.[101] This oxygen independent process was proposed to involve oxidation of guanine by the Ru(III) centre of the charge separated state. After oxidation there was a large distance between the oxidized guanine and the reduced terminal viologen, resulting in slower charge recombination, in comparison to the thermal reactions of oxidized guanine, and hence cleavage was observed. Charge hopping along the DNA to GG and GGG sites which are thermodynamically more stable would also increase the distance between the reduced viologen and the oxidized DNA site, and as such may play a role in the efficiency of the process.

Although they have not been explored to a great extent metal complexes with tethered organic functionalities show considerable potential in the development of novel probes and reactive agents for DNA. As discussed the organic component may act as a quencher, the mechanism of quenching depending on its photophysical and redox properties, as well as those of the metal complex. Interruption of these quenching pathways by DNA provides the basis for the development of novel 'light switches' for DNA, whose sequence selectivity may be expanded above that of traditional metal complexes. Such systems may also prove to be highly effective photonucleases due to them potentially having long lived charge separated excited states. Also of significance is

that a large number of potential chromophore-quencher partners exist for such application whose individual interaction and/or reaction with DNA have already been characterised.

Ru(II) polypyridyl complexes possess widely varying properties, binding to DNA *via* a number of different modes depending on the nature of the ligands incorporated in the complex and on any further attached functional groups. Most display limited sequence selectivity in binding although the rigid threading bis-intercalators are very much in contrast to this. Besides DNA binding many complexes display efficient excited state reactivity with DNA, damaging it in the process. These systems offer the possibility of novel light activated therapeutics that may find application in the treatment of diseases of the DNA such as cancer.

1.4 Cancer – A Therapeutic Target

Cancer is a group of more than two hundred diseases usually defined as an uncontrollable growth of cells that originated from normal tissues. It is the second leading cause of death in western countries, just behind cardiovascular disease, and its incidence has increased in recent years due in general to an older population and changes in lifestyle. Cancer is characterised by an increase in cell proliferation and decrease in the rate of apoptosis or programmed cell death. This results in the formation of tumours that interfere with the physiological function of normal cells. The successive accumulation of mutations in DNA drives tumourigenesis or the development of cancer. Mutations may result in altered proteins with anomalous activity, alternated regulatory sequences resulting in abnormally high expression of a particular protein, loss of cellular degradation signals due to abnormally high concentration of particular proteins in the cell, chromosomal rearrangements whereby proteins are inappropriately transcribed when brought under the control of foreign regulatory sequences, gene amplification whereby genes are replicated multiple times, and the loss or inactivation of tumour suppressor genes. These genetic mutations may be driven by a number of physical or chemical agents such as radiation, azo dyes, aflatoxins, and constituents of tobacco. Damage to DNA and the genetic mutations that can result from this are a central theme in carcinogenesis, and thus DNA is an important target in the design and development of novel anti-cancer drugs. Agents that bind DNA may interrupt its function, both in terms of the structural integrity of the helix itself and its interaction with various control proteins in the cell.

1.5 1,8-Naphthalimides as Anti-Cancer Agents

Intercalators are a class of DNA binding agents that possess useful anti-cancer properties, as discussed in Section 1.2.3. Their biological effects are produced primarily by interaction with the Topo II enzyme resulting in inhibition of the replication process or an enhancement of Topo II mediated DNA cleavage.[102] Compounds containing the 1,8-naphthalimide structure were designed for application as intercalators by Braña and co-workers in the 1970's by the combination of the structural components of several anti-tumor compounds into a single molecule; the β-nitronaphthalene of aristolochic acid, the glutarimide rings of cycloheximide and CG-603, and the basic side chain of tilorone and CG-603.[103] The general structure of the 1,8-naphthalimide chromophore along with the possible sites of modification on the ring is shown in Figure 1.12. The use of 1,8-naphthalimides as anti-cancer agents has been discussed in detail in previous theses from this research group including those of Veale, [104] Gillespie,[105] Hussey[106] and Phelan[107] and thus the reader is directed to these for a detailed discussion.

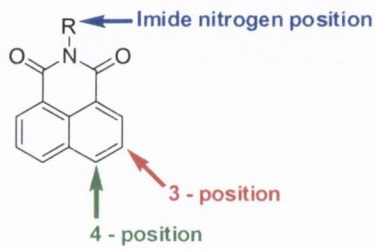

Figure 1.12 *General structure of the naphthalimide chromophore showing the main positions of modification.*

1,8-naphthalimides represent an important group of compounds for potential application as intercalating anti-cancer agents. Currently there are no 1,8-naphthalimide derivatives in the marketplace, but a number such as elinafide, **18**, and amonafide, **19**, (Quinamed®) are currently in clinical trials.

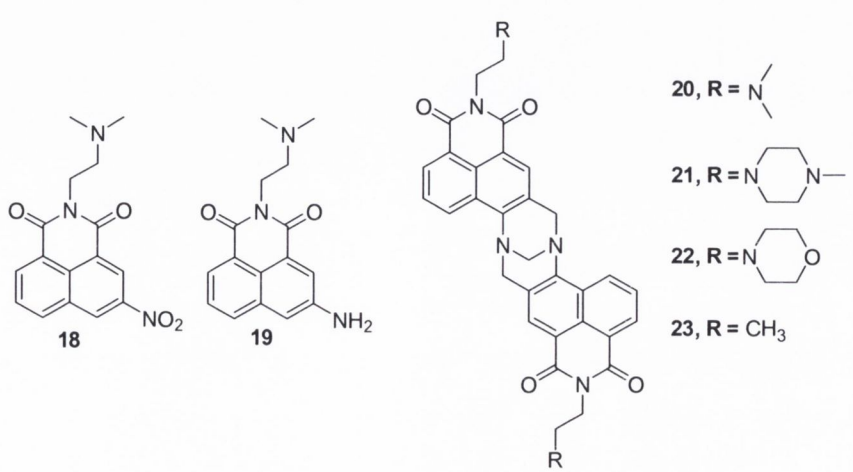

Recent research in this area has focussed on improving the selectivity of such agents and on gaining a more complete understanding of the nature of their interaction with DNA.[108-114] Efforts have also been made in the Gunnlaugsson laboratory to this end, with a number of compounds showing enhanced selectivity over those currently in clinical trials.[107,106] Also of interest are derivatives that have been developed within the group for use as probes. Recent examples are these include the Tröger base derived compounds such as **20** – **23**, discussed in the thesis of Veale.[104]

1.6 1,8-Naphthalimides as DNA Photocleavers

In addition to their "dark" properties in the presence of DNA, 1,8-naphthalimides like the metal complexes discussed in earlier sections may in their excited state react with nucleic acids. Such reactivity was first reported by Saito and co-workers, whereby they demonstrated that the series of *L*-lysine-1,8-naphthalimide derivatives **24** – **26** cleaved both supercoiled DNA and double-stranded oligonucleotides upon irradiation.[115]

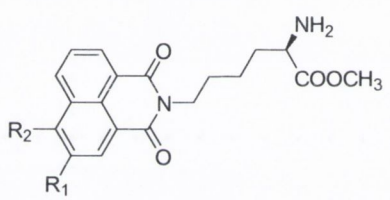

24 $R_1 = R_2 = H$
25 $R_1 = NO_2$, $R_2 = H$
26 $R_1 = H$, $R_2 = NO_2$

Interestingly the site of DNA cleavage was shown to be very much dependent on the substituents on the 1,8-naphthalimide ring system. Derivative **24** induced highly specific cleavage at the 5' side of 5'-GG-3' steps and very weak cleavage at the 5' side of 5'-GA-3' steps after piperidine treatment, with no cleavage observed at other sites. Under the same conditions, 3-nitro derivative **25** was shown to nick DNA preferentially at T residues with very weak cleavage at 5'-GT-3' steps. Finally 4-nitro derivative **26** showed almost equal cleavage at 5'-GG-3' and T sites. The mechanism of T specific cleavage by **25** was shown to involve oxidative transformation of the T methyl into a formyl group by hydrogen abstraction by a photoexcited nitro group. No evidence was found for hydrogen abstraction from the sugar backbone or electron transfer to the bases. The origin of the –GG- selective cleavage by **24** was discussed in a subsequent paper where the 1,8-naphthalimide was irradiated in the presence of various G containing duplex oligomers.[116] Reactivity occurred in the order –GGG- > -GG- > -GA- >> -GC-, -GT-. The lowest ionization potentials of such stacked nucleobases were estimated from *ab initio* calculation and were in good agreement with the observed reactivity. Also of significance was that the HOMO of stacked 5'-GG was calculated to be largely localised on the G at the

5' side, which was in agreement with the observed site of cleavage. Flash photolysis of a solution of **23** in the presence of duplex hexamer revealed production of the imide radical anion concomitant with decay of the imide triplet excited state. It was thus concluded from this study that DNA damage occurs as a result of electron transfer to the imide triplet state, and in addition was shown that the most electron donating sites in duplex DNA are guanine residues located 5' to guanine.

In order to gain a more complete understanding of this redox initiated damage of DNA by 1,8-naphthalimide derivatives Kelly and co-workers carried out photophysical studies on structurally related imide and diimide chromophores, **27** – **29** in the presence of individual nucleotides and polynucleotides. It was noted that naphthalene imide and diimide derivatives had been shown to possess high intersystem crossing efficiencies.[117,118] Charge recombination in the radical ion pairs derived from triplet states is slowed in comparison to those derived from singlet states and therefore would allow the possibility of increased charge separation efficiency. This in turn would lead to enhanced DNA cleavage as the thermal reactions leading to cleavage could occur before disappearance of the reactive intermediates.

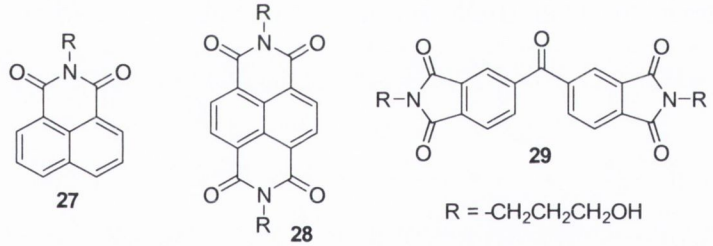

Flash photolysis studies showed that the interaction of the excited triplet states of the 1,8-naphthalimides and diimides with individual nucleotides results exclusively in electron transfer products.[119] The transient absorption spectra observed after nucleotide quenching were identical to those resulting from triplet state quenching by the electron donor 1,4-diazabicyclo(2,2,2)octane (DABCO) pointing to an electron transfer process from the nucleobases. Significantly the site of base oxidation was shown to be very much dependent on the thermodynamic properties of the imide or diimide employed, the rate constants for forward electron transfer varying over two orders of magnitude depending on the donor-acceptor pair. For the 1,8-naphthalimide derivative studied, the excited triplet only resulted in electron transfer from GMP, an observation that may be reconciled with the reduction potential of the triplet excited state.

It must be emphasised that under conditions such as these when the chromophore is not associated with the base, damage initiated by triplet states will predominate due to their

long lifetimes. However, upon association of the chromophore to the target, as would be anticipated in the presence of a DNA polymer, oxidation by the singlet state becomes competitive. A subsequent paper reported the photoprocesses of imide and diimide derivatives, **30** and **31** in aqueous solutions of DNA where particular attention was paid to the relative importance of electron transfer to the singlet versus the triplet excited states.[120]

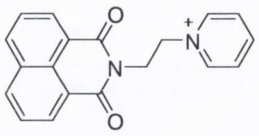

30

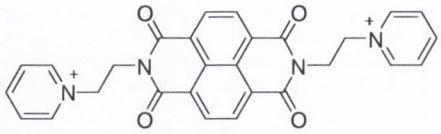

31

In the case of 1,8-naphthalimide **30**, significant fluorescence quenching was observed as DNA was added suggesting the availability of an efficient singlet state quenching pathway. This was assigned as being due to efficient electron transfer to the singlet excited state within the preformed imide/DNA ground state complex. This was in agreement with thermodynamic data where forward electron transfer from all of the nucleotide bases to the singlet excited state of **30** was calculated to be exergonic by at least 1 eV. As electron transfer to the singlet excited state is highly favoured it may compete effectively with intersystem crossing, although the products of electron transfer to the singlet excited state could not be observed on the timescale allowed by the instrumentation employed in this research. In agreement with the studies of Saito and co-workers the formation of radical anion was concomitant with decay of the triplet state. Radical anion was also produced by self-quenching but the amount produced increased in the presence of DNA suggesting that nucleotide oxidation can be facilitated by the triplet state. Within the range of DNA concentrations employed in this study the rate of radical anion production was actually shown to be independent of DNA concentration. This suggested that a dynamic process involving non-associated triplet states and nucleotides was most likely responsible for radical anion formation. Competition between the two pathways of electron transfer to the singlet or triplet excited state is highly relevant to DNA cleavage efficiency as the longer lived triplet derived products can exert damage more efficiently. In this case efficient electron transfer to the singlet excited state of the 1,8-naphthalimide reduced the overall efficiency of cleavage.

In a later paper it was suggested that the contribution to cleavage from direct electron transfer from the triplet state to DNA is actually negligible.[121] It was shown that the major decay pathways for the triplet excited state were self-quenching by ground state 1,8-naphthalimide and quenching by molecular oxygen. Cleavage efficiency was

increased in the absence of oxygen which suggested that the radicals produced from self quenching are more efficient at inducing DNA cleavage. The decay of radical anion from this self-quenching process was considerably slower in the presence of DNA, which was consistent with reaction of DNA with the quenching products. However, no change in decay was observed for the radical anion produced by reductive quenching by DABCO in the presence of DNA, suggesting that the radical cation of 1,8-naphthalimide or radicals derived from it are actually responsible for nicking DNA. At present this mechanism involving electron transfer from the DNA bases to radical species formed by self-quenching in solution is regarded as being responsible for the observed photocleavage by 1,8-naphthalimides with no ring substitution.

One of the most well known DNA cleavage agents is the hydroxyl radical, which acts by abstracting a hydrogen atom from deoxyribose.[122] This produces a carbon based radical that may rearrange, resulting in cleavage of the nucleic acid strand. A variety of methods exist for generating hydroxyl radicals such as Fenton type reactions or photolysis with ionising radiation.[122] A more recent means are the so called "photo-Fenton reagents" which may generate hydroxyl radical by low energy irradiation in a controlled manner. Qian and co-workers synthesised 1,8-naphthalimide peroxides **32** and **33** for such application and showed using ESR that they could efficiently generate hydroxyl radical.[123] In addition they showed that the compounds could convert Form I DNA into Form II and III and do so more efficiently than the reference phthalimide compound **34**, that had previously been studied.[124] Fluorescence quenching studies pointed to a strong association of **32** and **33** with DNA, and thus the enhanced cleavage was proposed to be due to the formation of hydroxyl radicals to some degree in the DNA matrix, by photolysis of the DNA bound naphthalimide hydroperoxides.

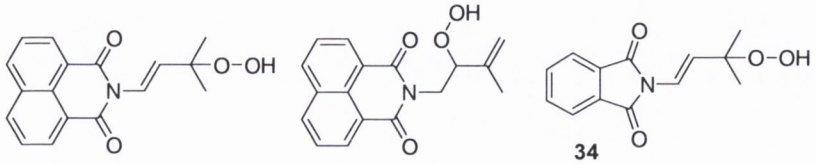

32 **33** **34**

The same group subsequently studied analogues **35** and **36** bearing a conjugated oxazole ring, as the extended planarity was expected to confer greater affinity for DNA.[125] This was indeed found to be the case and the compounds also displayed greater cleavage efficiency than their non-extended counterparts. This was again attributed to the extended planarity and greater DNA affinity in these systems. However, a factor that the authors did not consider was that a photochemical reaction between DNA and the photocleavage agent

could precede hydroperoxide degradation. A previous study on a bis(hydroperoxy)naphthaldiimide as a photocleavage agent showed the compound to effectively photonick supercoiled plasmid DNA.[126] When the cleavage selectivity was studied damage was found to occur with high selectivity at the 5' side of 5'-GG-3' steps after piperidine treatment. This was suggested to be a consequence of selective binding but is more likely due to an electron transfer process as was observed for the simple 1,8-naphthalimide derivatives discussed at the beginning of this section. Selectivity studies with hydroperoxides **32** – **36** would therefore be necessary to more fully understand the nature of their observed cleavage of DNA.

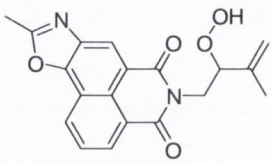

35

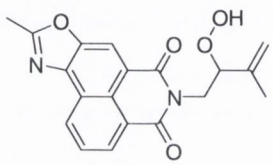

36

Compounds based on the 1,8-naphthalimide structure show potential as novel structural probes or sequencing agents for DNA that may be activated in a controlled manner by irradiation. They have been shown to be capable of generating a number of reactive intermediates, and display differing photochemical reactivity with DNA depending on their structure and functionality. Future research will most likely focus on gaining a more complete understanding of the photochemical processes giving rise to cleavage and the preparation of systems with greater sequence recognition capabilities. Furthermore, 1,8-naphthalimides have been shown to behave as DNA intercalators and display changes in their photophysical properties upon interaction. Agents based on this structure may therefore show potential as DNA probes, as has been demonstrated with the Troger base derived compounds discussed earlier.

1.7 Work Described in this Thesis

This research project is concerned with the development of a range of novel Ru(II)-1,8-naphthalimide conjugates as probes and photoreactive reagents for DNA. These conjugate systems are comprised of structural units with known affinity for DNA, and well characterised photophysical properties that are sensitive to the surrounding environment. Such properties have been discussed in detail in the preceding sections of this chapter. The strategy adopted in the design of these systems is based on that discussed in Section 1.2.5, where the properties of a number of systems comprising a metal complex with a tethered

organic chromophore were discussed. The general structure of the target complexes is presented in Figure 1.13.

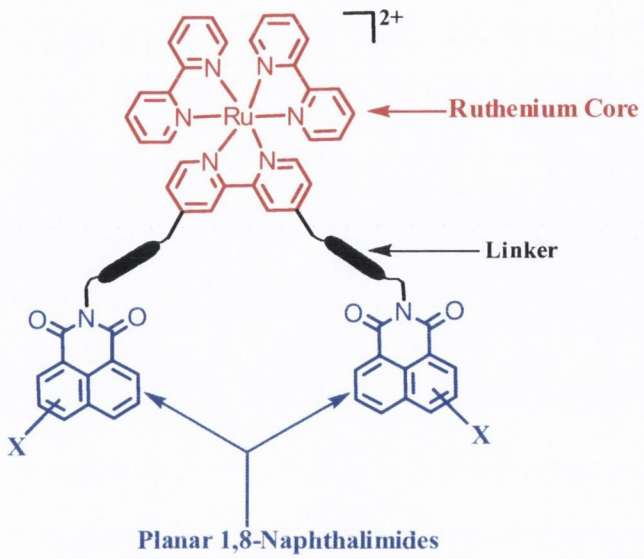

Figure 1.13 *General structure of target complexes.*

The overall aim of this research project was to investigate the effect of variations on the basic structure shown in Figure 1.13. The Ru(II) core was maintained throughout, however, different linker moieties and 1,8-naphthalimide chromophores were incorporated, and the effect that these modifications had on the photophysical and DNA binding properties of the resulting conjugate were investigated. It was hoped that by systematically varying these components, an understanding of the important structural features of the conjugates that leads to excellent DNA probing ability could be identified.

In *Chapter 2*, a series of flexibly linked Ru(II)-nitro-1,8-naphthalimide systems are described. These complexes were designed to possess a chromophore – quencher arrangement. It was anticipated that the 1,8-napthalimide moiety would quench the MLCT excited state by ET, leading to complexes that were weakly emissive in solution. The synthesis of each derivative is discussed, in addition to their photophysical and DNA binding properties.

In *Chapter 3*, flexibly linked Ru(II) conjugates incorporating unsubsitituted 1,8-naphthalimides are detailed. These complexes were designed to display an antenna effect in which the 1,8-naphthalimides would sensitize the Ru(II) MLCT emission. The synthesis of these systems, and their properties in solution and in the presence of DNA will be discussed.

In *Chapter 4*, conjugates with a more rigid arrangement of the Ru(II) and 1,8-naphthalimide subunits will be discussed. The effect that such an arrangement has on the photophysical and DNA binding properties will be explored, and these systems compared to their more flexible analogues.

In *Chapter 5*, a series of purely organic compounds comprising 1,8-naphthalimide and diquat functionality will be investigated. These were designed as a comparison to determine if a Ru(II) complex could be replaced by a charged organic unit, while still retaining strong binding and spectroscopic response to DNA.

In *Chapter 6*, the ability of each of the complexes discussed in *Chapter 2 – 4* to photocleave DNA will be investigated. Furthermore, their cellular uptake properties will be established using flow cytometry, and promising derivatives chosen for application as PDT agents.

In *Chapter 7*, some general conclusions are provided, in addition to future work that will be undertaken as part of this research programme. Finally, in *Chapter 8*, general experimental procedures are outlined and the synthesis of each of the compounds discussed in this thesis given.

Chapter 2

Flexible Ru(II)-nitro-1,8-naphthalimide Conjugates

2.1 Introduction

As discussed in *Chapter 1*, there has been significant interest in the development of bifunctional molecules as efficient binders and probes of DNA. It was shown that the strategy of combining two DNA binding components in a single molecule has been widely applied, particularly to systems containing two metal complex or organic subunits. In these studies, besides the properties of the subunits themselves, the nature of the linking moiety was shown to be very important as it defines the geometric arrangement of the subunits. This has important consequences on the nature of the interaction with DNA and the binding modes available. If considering a system with two linked intercalators three binding modes may be envisaged, as depicted in Figure 2.1.[127] Binding mode **A** represents bis-intercalation in which the neighbour exclusion principle is adhered to and is only possible when the linker is of sufficient length and allows enough flexibility to occlude two base pairs between the intercalating groups. It has been proposed that the linker length must be greater than 10.2 Å for this to occur.[83] Binding mode **B** represents mono-intercalation and will occur when the linker is rigid or too short to span two base pairs,[128] whereas binding mode **C** represents bis-intercalation with violation of the neighbour exclusion principle. This latter binding mode has been reported for relatively few systems.[84]

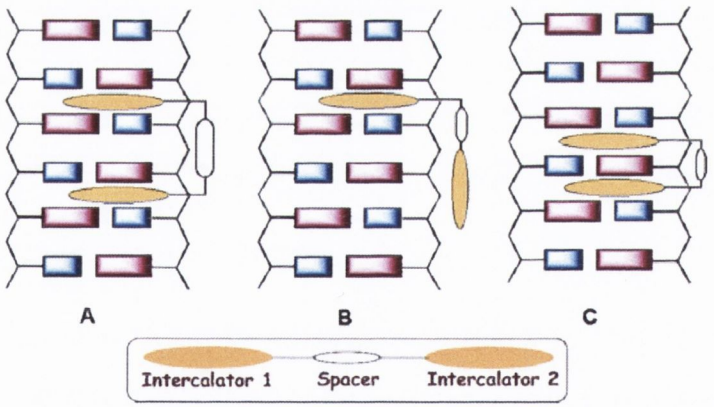

Figure 2.1 *Schematic representation of the DNA binding modes of a molecule bearing two linked intercalators.*[127] ***(A)*** *and* ***(C)*** *Bis-intercalation,* ***(B)*** *Mono-intercalation.*

From the above analysis, it would appear that a flexible linker of sufficient length would be the best choice if a bis-intercalator is desired. However, it is also known that a flexible linker would allow for self-association of the subunits; a process that decreases the overall affinity for DNA as it must be perturbed before intercalation can take place.[129] Waring and co-workers designed derivatives which comprised a rigid polynorbornane backbone with two appended acridine moieties such as the system depicted in Figure

2.2.[130] Self association between the two acridine moieties was possible in this case due to the rigid linker but bis-intercalation was shown to occur when the backbone was of an appropriate length.

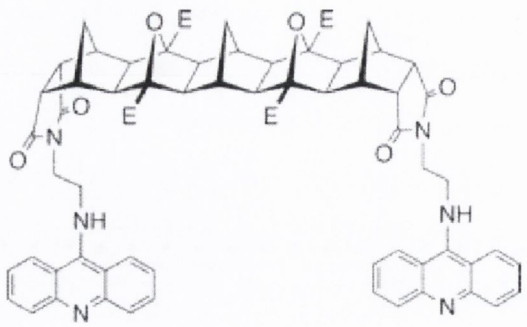

Figure 2.2 *Polynorbornane linked diacridine. E = CO_2Me.*

The objective of the research presented in this Chapter was the development of chromophore-quencher assemblies based on 1,8-naphthalimide and Ru(II) polypyridyl chromophores as novel probes for DNA. As detailed in *Chapter 1* a flexible linker that allows for a range of donor-accceptor distances is necessary in such systems as rates of energy or electron transfer are strongly distance dependent.[96,97] However, in solution the tether may adopt conformations that give a small separation between the chromophore and the quencher and as a result efficient energy/electron transfer. In the presence of DNA one or both of the partners interact with the helix, with the separation distance between them being modulated, and as a result the efficiency of transfer is altered. With this in mind, systems comprising a $Ru(bpy)_3^{2+}$ like core (the chromophore) linked *via* flexible alkyl linkers to 4/3-nitro-1,8-naphthalimides (the quencher) were designed. Nitroaromatics are known electron accepting quenchers,[131-133] this property having recently been suggested as a means of detecting many explosives which contain nitroaromatic functionality.[134] Consequently it is expected that nitro substituted 1,8-naphthalimides will quench the emission from the Ru (II) centre in addition to binding DNA with high affinity. Linkers containing three and five carbon units were employed to investigate the effect of distance between the units, and mono- and bis-substituted complexes were studied to determine if a second 1,8-naphthalimide unit would lead to cooperative binding. The target compounds identified, **45** – **48** are shown below along with a reference compound, **49** that was prepared for quantum yield comparison. This would enable us to determine how efficiently the nitro-1,8-naphthalimides quench the Ru(II) emission and also to evaluate the contribution the metal centre makes to the overall DNA binding process.

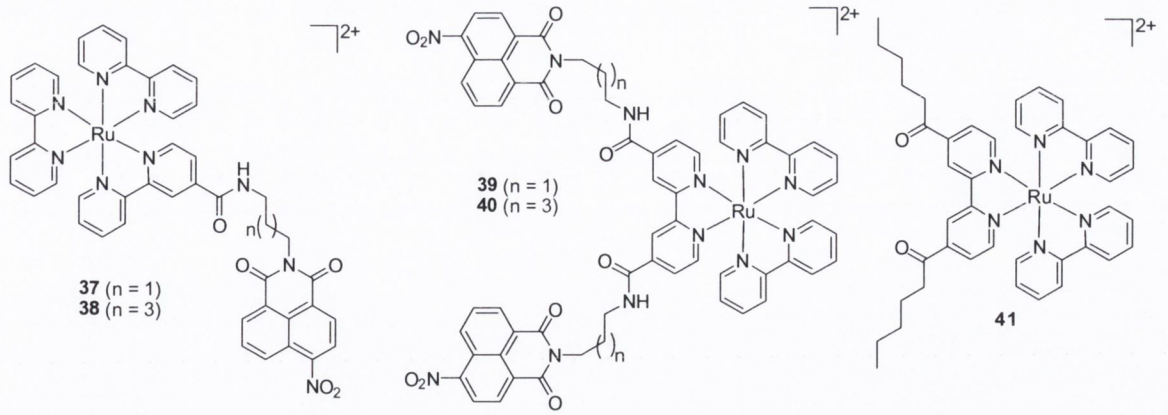

The possible binding modes of **37** – **40** may be related to those presented in Figure 2.1. The Ru(II) complex component in each is expected to act as a scaffold that binds to DNA by electrostatic interactions, and in doing so places the 1,8-naphthalimide chromophores in close proximity to the helix, whereby they may interact. These possible intercalating units should control the overall DNA affinity of each system through strong stacking interactions. For the bis-1,8-naphthalimide derivatives **39** and **40**, each of modes **A** – **C** is possible, depending on the degree of flexibility permitted by the relevant linker. In practice, the modes presented in Figure 2.1 may be an over-simplification, with numerous other modes of binding being possible in which one or both of the 1,8-naphthalimides partially intercalate, or bind within the grooves. Fewer variations are possible with compounds **37** and **38**, which are also expected to bind through intercalation or groove binding of the 1,8-naphthalimides, in addition to external association of the metal centre. As indicated above **41** was prepared to establish the binding properties of the metal centre itself and would only be expected to interact with DNA through electrostatic association. The nature of the interaction of each complex will be established using a number of spectroscopic techniques.

The overall aim of this particular work is to establish the effect that slight variations in linker length and incorporation of one versus two 1,8-naphthalimide quenchers has on the DNA binding affinity and spectroscopic response of these chromophore – quencher assemblies. Firstly, a description of the synthesis and characterisation of each of the conjugate systems **37** – **40** is given. This is followed by a discussion of the photophysical properties of each complex and a proposed photophysical mechanism to account for the observed properties. The DNA binding behaviour of each conjugate will then be established using a range of spectroscopic techniques.

2.2 Synthesis

The target bichromophore complexes **37** – **40** were prepared in a five step synthesis from easily available starting materials. The synthesis of the mono- and bis-4-nitro-1,8-naphthalimide propyl linked complexes **37** and **39** are discussed in detail the following sections. The same procedure was applied to the synthesis of the analogous pentyl linked derivatives **38** and **40**, full details of which are provided in *Chapter 7*.

2.2.1 Synthesis of *N*-alkyl amino Functionalised 1,8-naphthalimides 49 and 50

The 1,8-naphthalimide portion of each of the target complexes was synthesised as outlined in Scheme 2.1. The first step involved mono Boc-protection of the desired diamine. This was achieved by slow dropwise addition of a solution of *tert*-Butyl Dicarbonate (Boc_2O) in $CHCl_3$ to an excess of diamine at 0 °C followed by stirring overnight at room temperature. The solvent was then removed under reduced pressure, the resulting residue was re-dissolved in water and filtered to remove any di-Boc protected amine. Extraction into CH_2Cl_2, followed by drying over $MgSO_4$ and removal of the combined organic layers under reduced pressure afforded the desired product **42**, as a yellow oil in 80 % yield. Following this the mono-protected amine **42** was condensed with 4-nitro-1,8-naphthalic anhydride by addition of both reagents to anhydrous toluene in the presence of freshly distilled Et_3N, followed by overnight reflux under an argon atmosphere. Un-reacted anhydride was removed by hot filtration through celite after which the solvent was removed under vacuum. Any un-reacted amine was removed by dissolution of the product in $CHCl_3$, followed by washing with 0.1 M HCl and water. This gave a brown product that was recrystallised from acetone/ether to give **47** as a pale brown solid in 93% yield. Recrystallisation was not necessary for the analogue of **47** with a five methylene unit linker, **48**. This derivative was obtained in sufficient purity after workup according to ^{1}H NMR analysis. Having obtained **47** the protecting group was removed by stirring it in a 1:1 mixture of TFA/CH_2Cl_2 for 1 hour, affording the de-protected compound **49** as an orange solid in quantative yield. These 1,8-naphthalimide compounds gave characteristic ^{1}H NMR signals in the aromatic region, the spectrum and assignment for **47** being shown in Figure 2.3. All compounds synthesised were also characterised by ^{13}C NMR, melting point and ESMS. Aditionally, accurate mass, elemental analysis and Infrared spectra were obtained for novel compounds. Full characterisation for each of these compounds are presented in *Chapter 7*. The yields for each step in the synthesis of 1,8-naphthalimide derivatives **49** and **50** are given in Table 2.1.

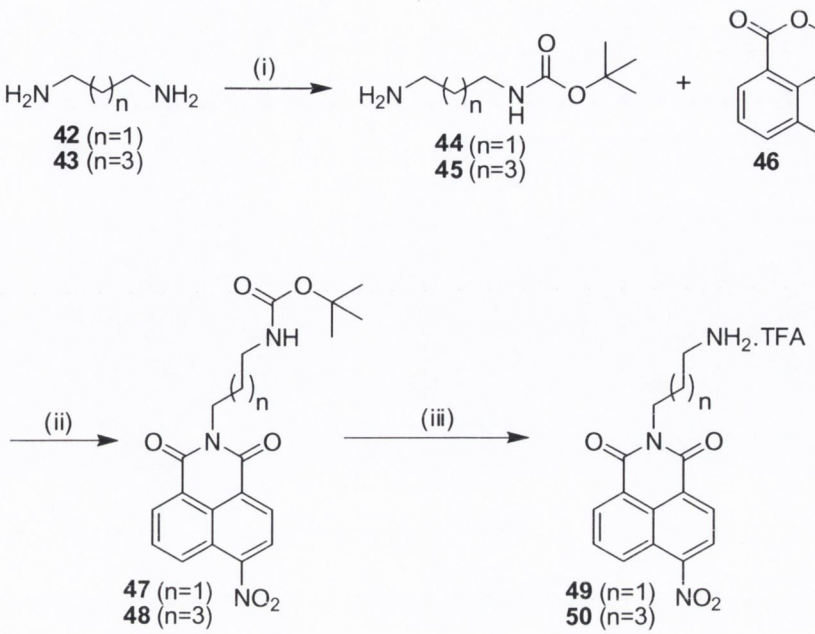

Scheme 2.1 *Synthesis of 1,8-naphthalimide derivatives* ***49*** *and* ***50****. Reagents and conditions: (i)* Boc_2O*,* $CHCl_3$*, O °C to RT, (ii) Toluene,* Et_3N*, (iii) TFA,* CH_2Cl_2 *50%.*

Table 2.1 *Synthesis of 1,8-naphthalimides* ***49*** *and* ***50****.*

Reactant	Linker	Product	Yield
42	C_3	**44**	80%
43	C_5	**45**	82%
44	C_3	**47**	93%
45	C_5	**48**	91%
47	C_3	**49**	100%
48	C_5	**50**	100%

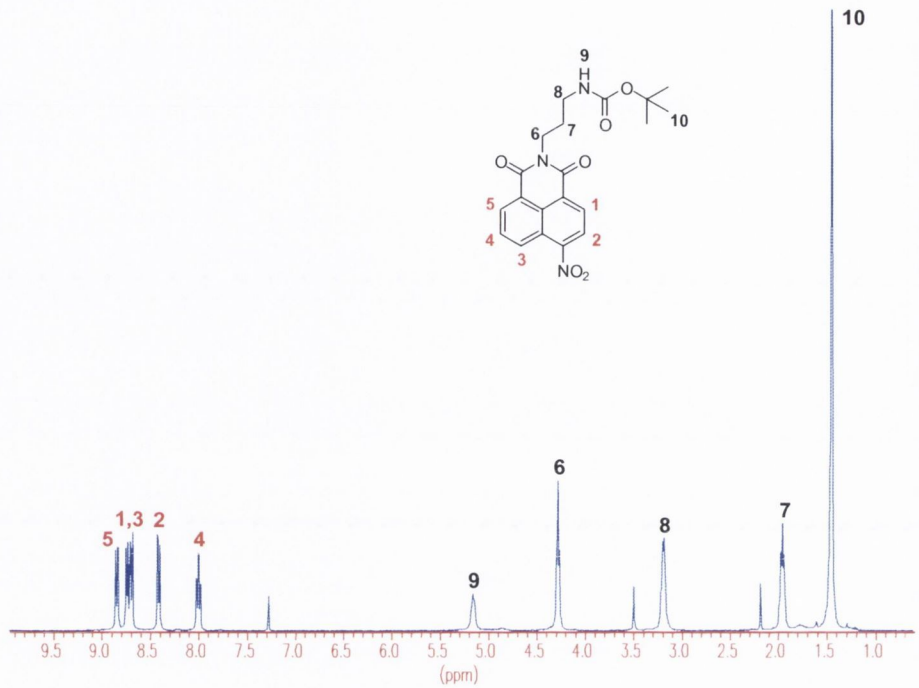

Figure 2.3 *^{1}H NMR spectrum of* ***47*** *($CDCl_3$, 400 MHz).*

2.2.2 Synthesis of mono-4-nitro-1,8-naphthalimide-bipyridine Ligands 53 and 54

A similar approach was applied to the synthesis of the bipyridine ligands functionalised with either one or two 1,8-naphthalimide units. This involved the coupling of the amino functionalised 1,8-naphthalimides **49** or **50** to the mono- or di-acid chloride of bipyridine. The synthesis of one example of each ligand possessing a three carbon linker will be discussed below, as the same procedures were employed for the corresponding five carbon linked compounds. The synthetic route to the mono-1,8-naphthalimide-bipyridine ligands **53** and **54** is outlined in Scheme 2.2.

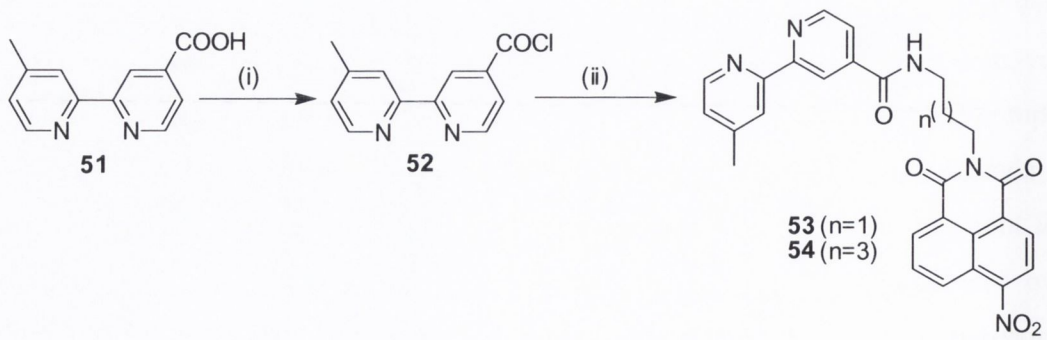

Scheme 2.2 *Synthesis of ligands* ***53*** *and* ***54****. Reagents and conditions: (i) $SOCl_2$, (ii)* ***49/50****, CH_2Cl_2, Et_3N, 0 °C.*

The mono-acid starting material **51** was prepared from 4,4'-dimethyl-2,2'-bipyridine according to a literature procedure.[135] This was converted to the corresponding acid chloride **52**, by stirring in thionyl chloride at reflux for 1 hour after which excess thionyl chloride was removed by bubbling with argon. The acid chloride was thoroughly dried under high vacuum for at least 4 hours, after which it was dissolved in anhydrous CH_2Cl_2 and added drop-wise to a solution of **49** in anhydrous CH_2Cl_2 at 0 °C in the presence of Et_3N. After stirring overnight at room temperature the reaction mixture was diluted by the addition of CH_2Cl_2 and washed several times with 0.1 M HCl and water. After concentration under reduced pressure, the resulting residue was further purified by silica flash column chromatography using 9:1 CH_2Cl_2/MeOH as eluant. The ^1H NMR spectrum of **53** is shown in Figure 2.4, and clearly shows the presence of both 1,8-naphthalimide and bipyridine resonances. Formation of **53** was also confirmed by the presence of a CH_2 resonance at 3.57 ppm, which had shifted downfield in comparison to the starting material by conjugation to the more deshielding amide. The product was further characterised by ^{13}C NMR, IR and elemental analysis.

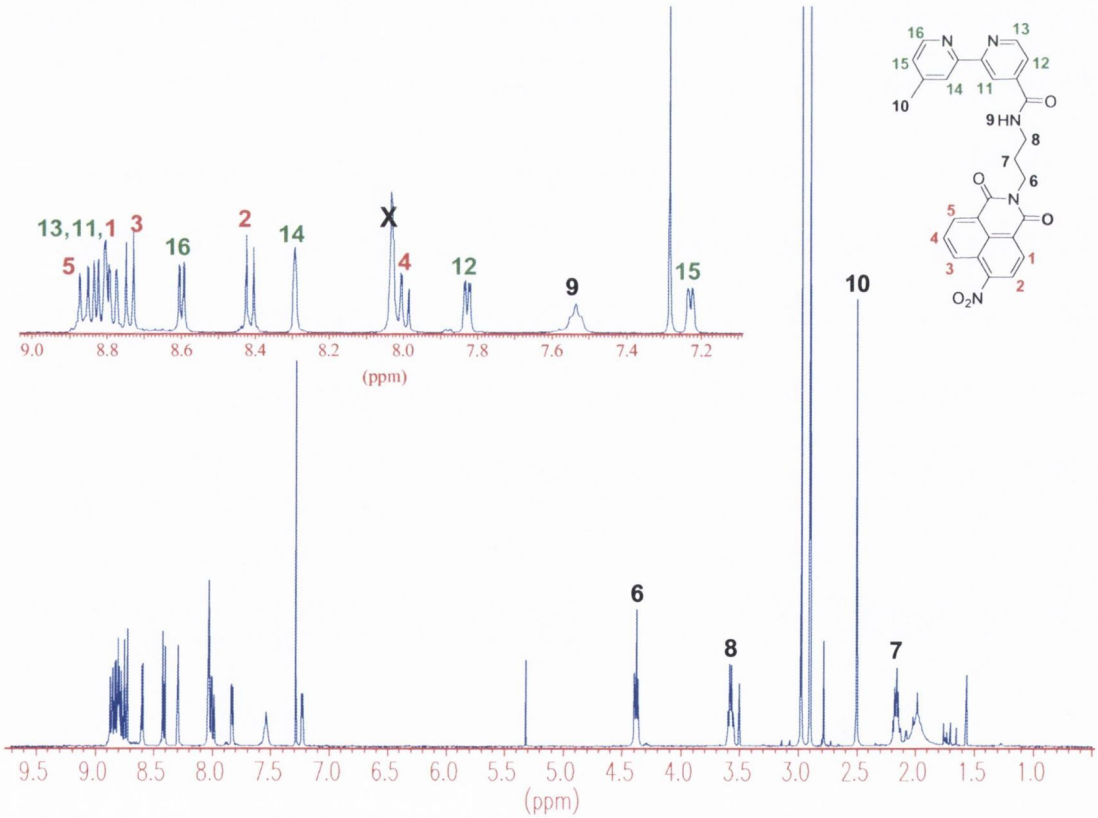

Figure 2.4 *^1H NMR spectrum of **53** ($CDCl_3$, 400 MHz).*

Table 2.2 *Synthesis of mono-4-nitro-1,8-naphthalimide-bipyridine ligands* ***53*** *and* ***54****.*

Reactant	Linker	Product	Yield
49	C_3	**53**	74%
50	C_5	**54**	53%

2.2.3 Synthesis of bis-4-nitro-1,8-naphthalimide-bipyridine Ligands 57 and 58

The two step synthesis of bis-1,8-naphthalimide bipyridine ligand **58** is shown in Scheme 2.3.

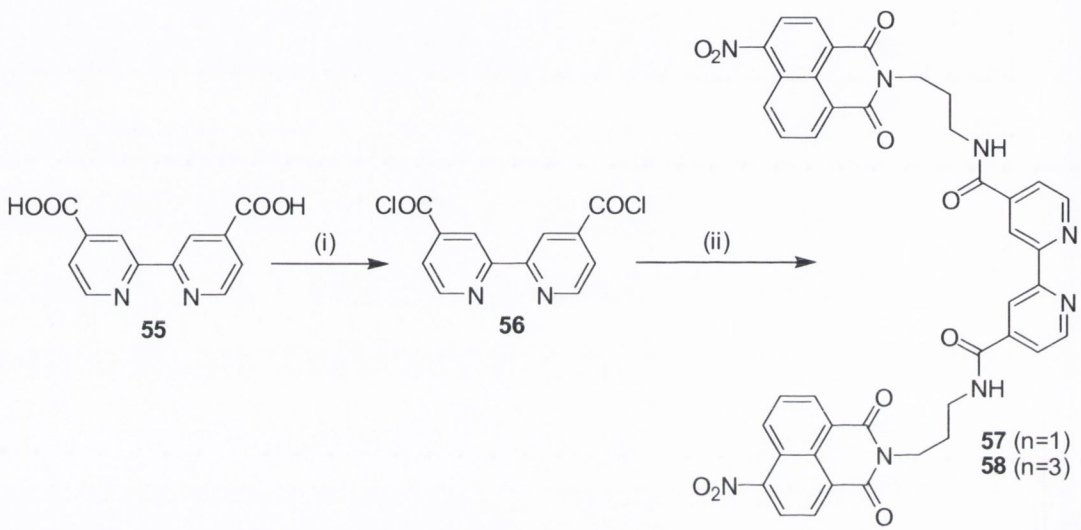

Scheme 2.3 *Synthesis of ligands* ***57*** *and* ***58****. Reagents and conditions: (i)* $SOCl_2$*, (ii)* CH_2Cl_2*,* Et_3N*, 0 °C,* ***49/50****.*

The first step involved the synthesis of the di-acid starting material **55** according to a literature procedure.[136] Unlike the mono-acid bipyridine derivative **51**, this compound is highly insoluble and consequently the reaction mixture was refluxed for approximately 20 hours in order to fully convert to the corresponding acid chloride. The reaction mixture was observed to turn clear once it had gone to completion. The product was isolated and dried in the same manner as before, after which it was dissolved in dry CH_2Cl_2 and added drop-wise to a solution of **49** and Et_3N in anhydrous CH_2Cl_2 at 0 °C. After stirring the resulting solution overnight at room temperature, a highly insoluble precipitate was isolated by suction filtration. This insolubility proved advantageous for purification as trituration of the solid with MeOH gave **57** as a brown solid in high purity in 55% yield. The ^{1}H NMR of **58** is shown in Figure 2.5 and is simpler than that observed for **53** (Figure 2.4) due to the symmetrical nature of the molecule. Once again resonances characteristic of both the 1,8-naphthalimide and the bipyridine moieties are apparent. Two of the linker

CH_2 resonances were found to be located under solvent peaks as indicated in Figure 2.5, their presence was evident from CH and HH COSY analysis of **57**. The CH_2 adjacent to the 1,8-naphthalimide ring system was under the resonance at 4.14 ppm and that adjacent to the amide bond under the resonance at 3.33 ppm. The latter was observed to shift downfield relative to the starting material due to it becoming attached to a more deshielding amide upon product formation. The product was further characterised by ^{13}C NMR, IR and elemental analysis. It was not possible to obtain mass spectrometry of these ligands, which is expected to be due to their insolubility.

Table 2.3 *Synthesis of bis-4-nitro-1,8-naphthalimide-bipyridine ligands **57** and **58**.*

Reactant	Linker	Product	Yield
49	C_3	**57**	55%
50	C_5	**58**	49%

At this stage four new ligands were successfully obtained; the mono-1,8-naphthalimide derivatives **53** and **54**, and the bis-1,8-naphthalimide derivatives **57** and **58**. The next step in the synthesis was to complex each of these ligands.

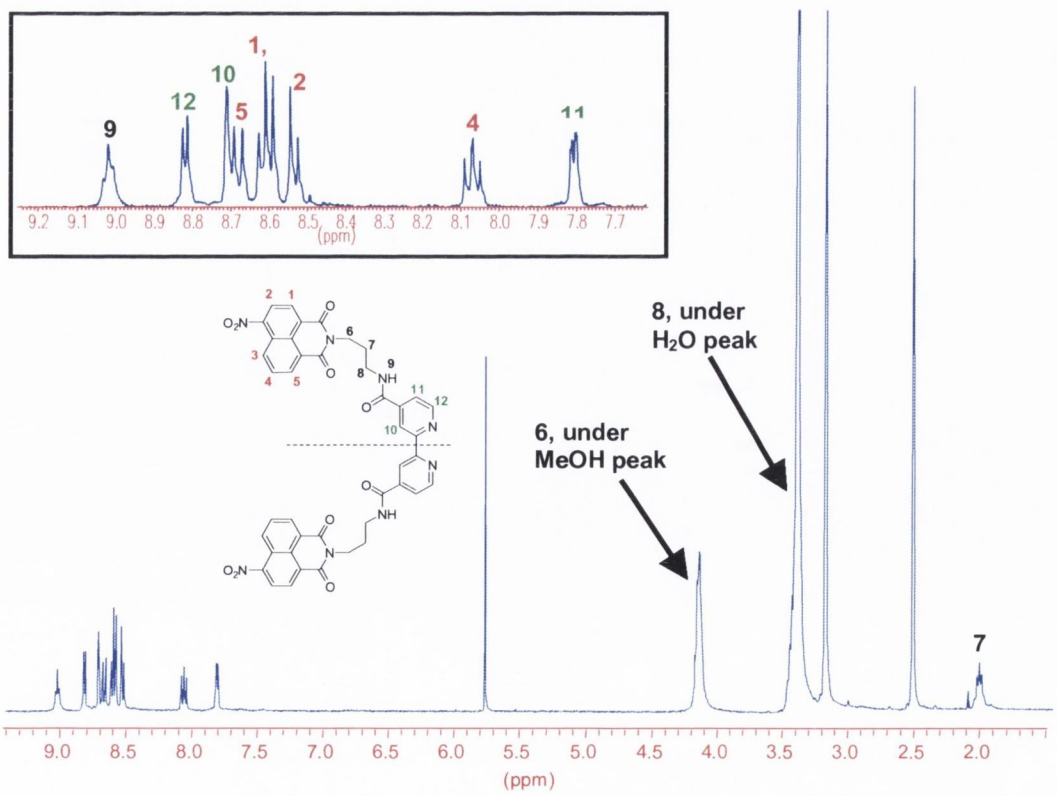

Figure 2.5 *^1H NMR spectrum of **58** ([D6]DMSO, 400 MHz).*

2.2.4 Complexation with $Ru(bpy)_2Cl_2$

Ligands **53** and **57** and their five carbon linker equivalents **54** and **58** were complexed with $Ru(bpy)_2Cl_2$ using the same general procedure. Each of the ligands were dissolved in a mixture of DMF/H_2O 50:50, to which $Ru(bpy)_2Cl_2$ was added and the mixture purged with argon for five minutes. This mixture was then heated at 100 °C overnight, after which the solvent was removed under reduced pressure and the resulting residue re-dissolved in water. This solution was then filtered to remove any un-reacted bis-complex. After this ligand exchange was carried out by the dropwise addition of a concentrated aqueous solution of NH_4PF_6. This lead to precipitation of the PF_6^- salt of each complex. Each of the complexes **37** – **41** were purified as the PF_6^- salts by silica flash column chromatography eluting with $CH_3CN/H_2O/NaNO_{3(sat)}$ 40:4:1. The main impurities present in the reaction mixture were $Ru(bpy)_2Cl_2$, $Ru(bpy)_3^{2+}$, and a highly coloured green/blue compound which was possibly a Ru(III) species formed by oxidation of the products of the reaction. The water soluble chloride salt of the complex was re-formed by dissolution in methanol followed by stirring with Amberlite ion exchange resin (Cl^- form) for 1 hour.

Several methods were initially investigated for purification of these Ru(II)-1,8-naphthalimide conjugates, as detailed in Table 2.4. Complex **39** was the first of these to be synthesised and as such the variety of purification methods detailed below in Table 2.1 only applied to this system. Once a successful means of purification was identified it was then applied to the other systems synthesised. Precipitation of the complex from CH_3CN with Et_2O was not successful in purifying the product. Methods **2** – **4** initially seemed quite promising by TLC, but failed when carried out using preparative plate or column chromatogram as detailed in Table 2.4. Methods **6** and **7** were successful in purifying the complexes, however, due to the large volume of DMF required for method **6**, method **7** was regarded as the most suitable choice for purification of .

After purification, **39** was obtained as a red solid in 52% yield. ESMS analysis showed a peak at 1220.2505 corresponding to the M^{2+} ion. After purification the mono-1,8-naphthalimide analogue **37** was obtained in 60% yield. ESMS analysis of this system showed the presence of a peak at 909.1982 corresponding to the M^{2+} ion. Partial ^1H NMR spectra for **37** and **39** are shown in Figure 2.6 and 2.7 respectively. As for the ligands a simpler spectrum was obtained for the bis-complex due to the C_2 symmetry of the system.

Table 2.4 *Methods attempted for purification of the Ru (II) – naphthalimide conjugate* ***39****.*

No.	Method of purification	Result
1	Precipitation of CH_3CN solution of complex from diethyl ether	Unsuccessful
2	Alumina preparative plate chromatograph – CH_3CN	Unsuccessful
3	Silica preparative plate chromatograph – MeOH	Unsuccessful
4	Alumina column chromatograph – CH_3CN	Unsuccessful
5	Sephadex LH-20 column chromatograph – MeOH eluant	Product slightly cleaner
6	Silica column chromatograph - H_2O / DMF / 2M $NH_4Cl_{(aq)}$ 1:1:2 → H_2O / CH_3CN / 2M $NaNO_{3(aq)}$ 2:2:1	Successful
7	Silica column chromatograph – CH_3CN / H_2O / Sat. $NaNO_{3(aq)}$ 40:4:1	Successful

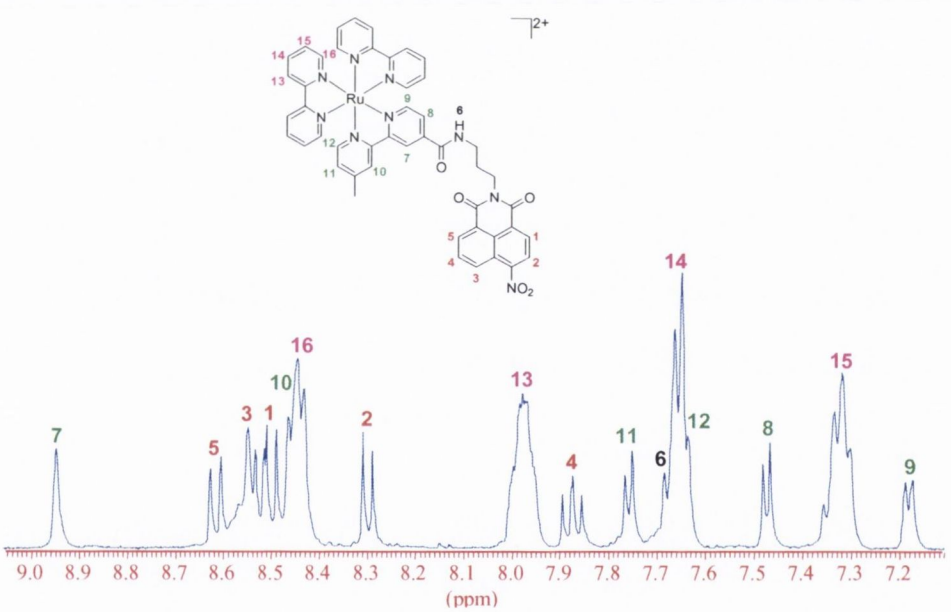

Figure 2.6 *^1H NMR spectrum of* ***45*** *(CD_3CN, 600 MHz), showing the aromatic region.*

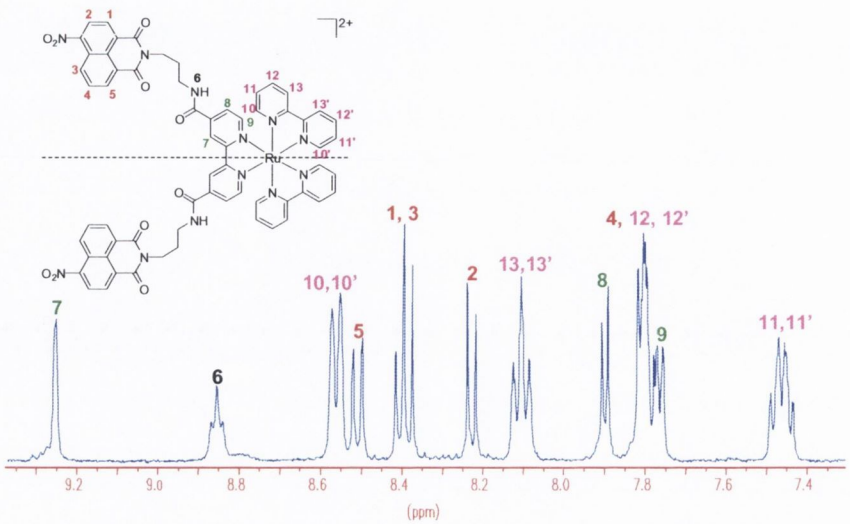

Figure 2.7 *^{1}H NMR spectrum of* ***47*** *(CD_3CN, 400 MHz), showing the aromatic region.*

Table 2.5 *Synthesis of complexes* ***37*** *–* ***40***.

Reactant	Linker	Product	Yield
53	C_3	**37**	60%
54	C_5	**38**	65%
57	C_3	**39**	52%
58	C_5	**40**	49%

2.3 Photophysical Properties of 37 - 41

As compounds **37** – **40** were designed as potential spectroscopic probes for DNA, characterisation of their photophysical properties was firstly carried out. The absorption, excitation and emission spectra of the mono-1,8-naphthalimide derivative **38** and the bis-1,8-naphthalimide derivative **40**, recorded in 10 mM phosphate buffer, pH 7 are shown in Figure 2.8a and 2.8b, respectively.

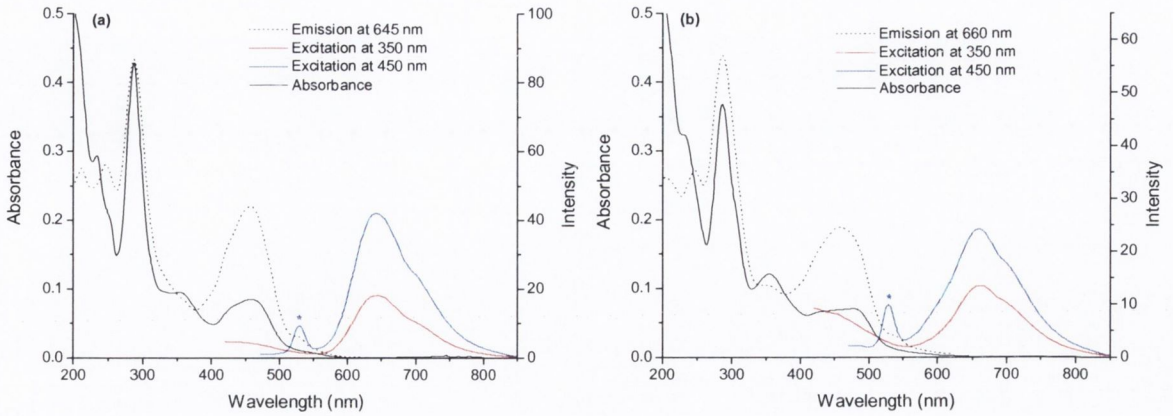

Figure 2.8 *UV/Visible, excitation and emission spectra of (a)* ***38*** *(6.5 μM) and (b)* ***40*** *(6.5 μM), both in 10 mM phosphate buffer, at pH 7. The water Raman band is denoted by *.*

The UV/Visible spectra of the complexes in aqueous solution exhibit bands characteristic of both the 1,8-naphthalimide and Ru(II) polypyridyl chromophores. The intense band centred around 285 nm was attributed mainly to the π-π^* intra-ligand (IL) transitions, and the band at 350 nm to the π-π^* 4-nitro-1,8-naphthalimide transitions. The bands at 456 or 477 nm were assigned to the metal to ligand charge transfer (MLCT) transitions of the Ru(II) complex. Thus bands characteristic of the 1,8-naphthalimide and the Ru (II) MLCT may be resolved, which will be of considerable importance when examining the interaction of these components upon binding of the complexes with DNA.

The MLCT bands are broad and red shifted compared to that of $[Ru(bpy)_3]^{2+}$, particularly for the bis-complexes **39** and **40**. This is due to the presence of the amide substituents on one of the bipyridine ligands, which differ from the non-substituted bipyridine ligands in that they possess a more positive reduction potential. Charge transfer transitions will occur from the metal centre to both the substituted and non-substituted bipyridine ligands. The transition to the non-substituted ligand will contribute mainly in the 450 – 460 nm region, and the lower energy transition to the amide substituted ligand in the 490 – 500 nm region.[137] Hence the maximum absorption appears at 477 nm in the case of **40**, the effect being intermediate in **38** which possesses a single amide substituents, and a corresponding MLCT absorption maximum at 456 nm. Variation of the linker length to a shorter three carbon spacer yields systems with almost identical spectra. The spectrum for the control complex **41** is similar to that observed for the bis-napthalimide complexes **39** and **40**, as the MLCT band is broad and red shifted to the same degree. A summary of the absorption properties of these systems as well as their respective molar absortivities is given in Table 2.6.

Table 2.6 *Absorption properties of* ***37 – 41*** *in 10 mM phosphate buffer, pH 7 at 298 K.*

Complex	λ_{max} (nm) [ϵ(M^{-1} cm^{-1})]		
	π-π* IL	π-π* Naph	MLCT
37	286 [65600]	351 [14500]	458 [13300]
38	286 [73900]	351 [14900]	456 [13700]
39	286 [60900]	355 [21300]	477 [12700]
40	286 [55800]	356 [20100]	477 [11100]
41	286 [55200]	-------	475 [10900]

To examine the degree of stacking of the 1,8-naphthalimides in the bis-systems **39** and **40** and the presence of any ground state electronic interactions additive spectra were constructed. In these spectra the absorbance of the reference complex **41**, the water soluble 1,8-naphthalimide derivative **59**, the summed spectra of these two, and complexes **39** and **40** were compared, all of which had been recorded individually. The spectra resulting for complex **40** are depicted in Figure 2.9. From this examination, we can see that the absorption spectrum of **40** in the MLCT region is effectively the same as it is for the summed components. This indicates that metal complex absorption is unaffected by the conjugation to the 4-nitro-1,8-naphthalimide moieties. However, looking at the 1,8-naphthalimide region, it is apparent that the absorbance is significantly less than calculated, if there was no interaction between the individual components. The absorption at this band is *ca.* 30% reduced relative to that calculated by summing the individual components. This observation suggests the occurrence of significant stacking interactions of the 1,8-naphthalimides, which leads to a hypochromicity in the absorption spectrum. Such interaction could be expected due to the flexible nature of the linker and the propensity of 1,8-naphthalimides to stack in polar solution, due to their planar and hydrophobic nature.[138] Similar observations were made for the bis-propyl linked derivative **39**, the hypochromicity of 1,8-naphthalimide absorption due to stacking being slightly less in this case.

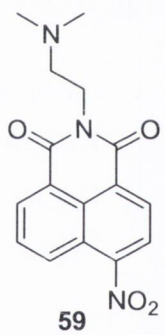

59

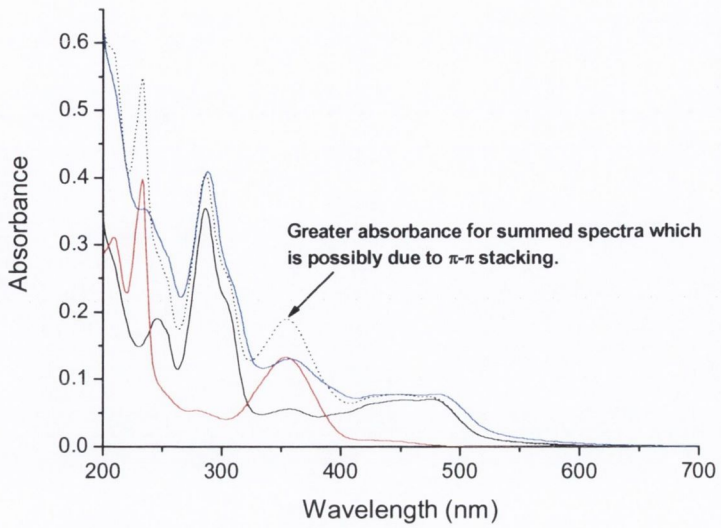

Figure 2.9. *Summed absorption spectra of* ***40****.* ***41*** *(——)(6.5 μM),* ***59*** *(——)(13 μM),* ***41*** *+* ***59*** *(------) and* ***40*** *(——)(6.5 μM). All solutions in 10 mM phosphate buffer, at pH 7.*

In mixed ligand complexes such as **37** – **41**, we observe that separate transitions occur to each of the ligands. It has previously been shown using transient resonance Raman spectroscopy, that in systems of this type incorporating different ligands around the metal centre, subsequent to absorption rapid intramolecular electron transfer occurs, which leads to a triplet MLCT state in which the excited state is localized on the ligand having the most positive reduction potential.[139] Thus, for **37** – **41** we expect the MLCT emission to arise solely from an excited state where the excited electron is localised on the amide substituted bipyridine ligands. The emission maximum would also be expected to be shifted to a lower energy than that of $Ru(bpy)_3^{2+}$. For each of the systems **37** – **41** this was observed to be the case.

Excitation of an aqueous solution of the control complex **41** resulted in an emission band centred at 670 nm. Excitation of the mono-1,8-naphthalimide complexes **37** and **38** at 450 nm, resulted in a single emission band arising from the MLCT state, which was centred at 645 nm. Finally, excitation at 450 nm of the bis-1,8-naphthalimide complexes **39** and **40** resulted in MLCT based emission at 665 nm. The higher energy emission observed for **37** and **38** is due to the presence of a single amide substituent on the ligands, the excited state resulting from charge transfer being slightly higher in energy than when two amides are present.

Excitation at 350 nm, the maximum of absorption for the 1,8-naphthalimide resulted in weak emission from the metal centre, in addition to weak emission from the

1,8-naphthalimide. Some emission from the metal centre was to be expected as there is some contribution to absorption in this region by the metal complex itself, as is apparent in Figure 2.8b. In addition the emission from nitro substituted 1,8-naphthalimides is considerably weaker than that from amino substituted systems which often display intense internal charge transfer (ICT) emission.[140]

Table 2.7 *Emission properties of* ***37 – 41*** *in aerated 10 mM phosphate buffer, pH 7 at 298 K.*

Complex	λ_{em} (nm)	Φ_f (± 10%)
37	645	0.001
38	645	0.001
39	665	< 0.001
40	665	< 0.001
41	670	0.014

Interestingly, strong MLCT emission was observed from reference complex **41**, while all of the 1,8-naphthalimide conjugated complexes were weakly emissive in aqueous solution. This is reflected in the quantum yields obtained as detailed in Table 2.7. Quantum yields were determined for all systems using $Ru(bpy)_3^{2+}$ as a standard. Solutions of each complex were prepared at a number of concentrations all with absorbance less than 0.1. Emission spectra were recorded for each sample and the integrated intensity obtained. Plots of integrated intensity *vs.* absorbance were constructed and the slope of the line through the points determined. This gradient was substituted into Eq. **1** from which the quantum yield was determined.

$$\Phi_x = \Phi_{ST}\left(\frac{Grad_x}{Grad_{ST}}\right)\left(\frac{\eta_x^2}{\eta_{ST}^2}\right) \qquad \textbf{(1)}$$

where the subscripts ST and X denote standard and sample respectively, Φ is the fluorescence quantum yield, Grad the gradient from the plot of integrated fluorescence intensity vs absorbance and η the refractive index of the solvent.

The quantum yield for **41** was found to be 0.014 (± 10%), which is half the value of that reported for $[Ru(bpy)_3]^{2+}$, while the quantum yields for the 1,8-naphthalimide conjugated complexes **37** – **40** were found to be considerably less. Both the

mono-1,8-naphthalimide complexes **37** and **38** possessed quantum yields of 0.001 (± 10%), while the bis-1,8-naphthalimide complexes **39** and **40** possessed quantum yields of less than 0.001 (± 10%). This reduction in the quantum yield, and the resulting weak emission displayed by these complexes, is attributed to an interaction between the 1,8-naphthalimide and the MLCT excited state as depicted in Figure 2.10. As discussed in *Chapter 1*, similar phenomena have been observed for Ru(II)-Viologen[101] and Ru(II)-aminoquinoline[98] conjugates and were attributed to electron transfer processes between the Ru(II) centre (chromophore) and the organic moiety (quencher). We anticipate that a similar process could be occurring here, where the excited state of the metal complex is efficiently quenched by electron transfer to the 1,8-naphthalimide moiety. Thus, **37** – **41** display the first criterion for a chromophore-quencher probe in being essentially non-emissive in solution.[95]

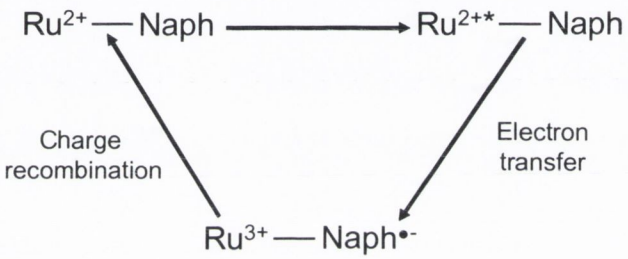

Figure 2.10 *Electron transfer and charge recombination between the two chromophores, leading to weak emission from the Ru (II) MLCT.*

The reduced quantum yield observed for **41** compared to that of $[Ru(bpy)_3]^{2+}$ is a consequence of the energy gap law for radiationless transitions, as has previously been observed for charge transfer excited states.[141] This law, predicts that for a series of related excited states, based on the same chromophore, radiationless decay rates are determined by vibrational overlap between the ground and excited states.[141] This overlap is largely determined by the energy gap between the zero point vibrational levels of the states. In general the smaller the energy gap the more efficient the radiationless decay processes.[141] As previously indicated the emission for complex **41** occurs at a significantly lower energy than that seen for $[Ru(bpy)_3]^{2+}$. From this result we expect a smaller energy gap between the ground and excited states and a concomitant enhancement of non-radiative decay pathways. Although we attribute the reduced quantum yields for the conjugated complexes to interaction between the metal centre and the 1,8-naphthalimides, contribution from increased radiationless transitions to deactivation of the excited state could also be considered.

In summary the bichromophore complexes **37** – **40** display interesting and potentially useful photophysical properties in aqueous solution. They possess multiple absorption bands, which can be attributed to individual chromophores, as expected due to them containing both Ru(II) polypyridyl and 1,8-naphthalimide functionality. The absorption of both components is expected to be sensitive to the surrounding environment and thus is expected to change upon interaction with DNA. Tight binding of the Ru(II) centre will manifest as changes in the MLCT band at ~ 450 nm and binding of the 1,8-naphthalimide as changes in the π-π^* band at ~ 350 nm respectively. Furthermore, the complexes are very weakly emissive in aqueous solution and as such display chromophore – quencher behaviour which fulfils the aim of the initial design. It is thus anticipated, that the interruption of the quenching process upon binding to nucleic acids will form the basis of operation of a novel set of luminescent probes for targeting DNA.

2.4 DNA binding interactions of 37 - 41

In the work presented herein, each of the Ru(II)-1,8-naphthalimide conjugates **37** – **40** were expected to interact with DNA through a combination of electrostatic and π-stacking interactions, with the Ru(II) unit binding externally to the phosphate groups and the 1,8-naphthalimides possibly anchoring the molecule through intercalative binding. Such interactions typically result in changes in the electronic spectra of DNA binding molecules,[142] and thus spectroscopic titrations were carried out to investigate the nature of the binding and affinity towards DNA for these complexes. The results from these studies will be discussed in the following sections.

2.4.1 Changes in the UV/Visible absorption of 37 – 41 with DNA

The interaction of **37** – **41** with salmon testes (st) DNA was firstly investigated using electronic absorption spectroscopy, in which changes in the Ru(II) complex MLCT band at 450 nm and in the 1,8-naphthalimide band at 350 nm were monitored, respectively. St-DNA is commonly used as a source of random sequence DNA and is reported to comprise approximately 2000 base pairs with a GC content of 41.2%.[143,144] The titrations were carried out by the addition of small aliquots of DNA (μl volumes) to a solution of complex, until a plateau in absorbance was reached. At this point all of the complex was regarded as being fully bound to DNA. All titrations were repeated a number of times to ensure reproducibility.

Upon addition of st-DNA to the Ru(II) control complex **41**, no changes were observed in the 1,8-naphthalimide region, while a 9% hypochromic shift was observed at the MLCT band. These results are similar to those obtained previously for the addition of DNA to $[Ru(bpy)_3]^{2+}$, the observed changes having been attributed to electrostatic interactions between the complex and the phosphate backbone of DNA.[29] In the case of the bis-pentyl-linked complex **40**, the addition of DNA resulted in a 27% hypochromism for the 1,8-naphthalimide band, with a smaller change in the absorbance for the MLCT band, which displayed ca. 10% hypochromism, as depicted in Figure 2.11.

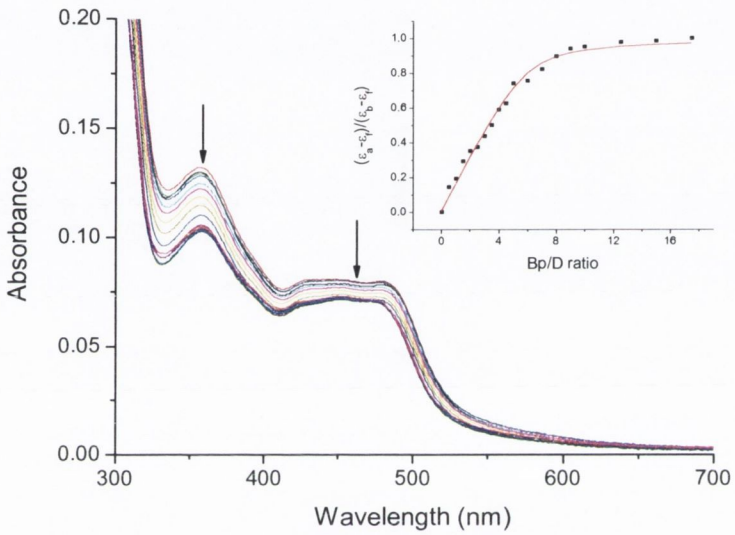

Figure 2.11 *Changes in the UV/Visible spectrum of* ***40*** *(6.5 μM) upon addition of st-DNA (0 – 117 μM base pair) in 10 mM phosphate buffer, pH 7. Inset: Plot of* $(\epsilon_a-\epsilon_f)/(\epsilon_b-\epsilon_f)$ *at 355 nm vs. [DNA] and the corresponding non-linear fit.*

The observed changes in the MLCT absorbance are very similar to those observed previously for **41**, and thus it may be regarded that the metal centre in **40** is externally bound to the phosphate backbone. The changes observed for the 1,8-naphthalimide are typical of intercalation or groove binding, which usually cause a substantial decrease in the oscillator strength of an absorption band. However, the results are somewhat different to those previously obtained for the binding of mono-1,8-naphthalimide compounds to DNA. A number of 1,8-naphthalimide derivatives have previously been shown to intercalate DNA with hypochromicities of 60%.[120,145] In addition, clear isosbestic points were observed in these studies at all DNA/1,8-naphthalimide ratios indicating the presence of only one spectrally distinct 1,8-naphthalimide-DNA complex in solution. The differences for **40**, and indeed all of the conjugate systems studied as part of this research lead to two proposals. Firstly, that full intercalation of the 1,8-naphthalimide components in the

complexes is somewhat inhibited by the presence of the metal complex, leading to reduced hypochromicity, and secondly the multi-component nature of the complexes leads to the presence of a number of distinct bound species in solution. However, it must be noted that the absence of an isosbestic point may also be due to the presence of overlapping absorption bands.

The data from the UV/Visible absorption titration of **40** was analysed in order to obtain a binding affinity for DNA. The model used for this purpose, in addition to others investigated is discussed in the appendix. As expected a range of binding constants and binding site sizes were determined for the different systems as detailed in Table 2.8.

Table 2.8 *DNA binding parameters from fits to absorbance data.*

No.	λ(Naph) Hypochromism	λ(MLCT) Hypochromism	Binding constant K (M^{-1})	Binding site size n (base pairs)	R^2
37	20 %	9 %	3.2×10^6 (± 1.0)	1.63 (± 0.08)	0.99
38	35 %	10 %	4.6×10^6 (± 1.0)	1.67 (± 0.06)	0.99
39	24 %	10 %	9.2×10^6 (± 4.0)	3.46 (± 0.14)	0.99
40	27 %	10 %	2.8×10^6 (± 0.8)	5.99 (± 0.29)	0.99
41	------	9 %	------	------	------

As detailed in Table 2.8 the binding constant obtained for the bis-pentyl-linked complex **40** was 2.8×10^6 M^{-1}, with a binding site size of 6 base pairs, these parameters representing the average that results from different binding geometries. Examination of the results for the corresponding propyl linked complex, **39** illustrated the sensitivity of binding to the linker length. The presence of a propyl linker yielded similar hypochromic effects, 24% at the 1,8-naphthalimide band and 10% at the MLCT band, but with an increased binding constant of 9.2×10^6 M^{-1}. This complex also exhibited a bathochromic shift in absorption maximum of 4 nm upon binding to DNA, an effect commonly associated with a classical intercalative binding mode.[18] Furthermore the binding site size was reduced to ~ 3.5 base pairs suggesting the "bite" size of this complex to be smaller.

The changes in the UV/Visible absorption of **38** are presented in Figure 2.12. In terms of binding constants and binding site sizes the results obtained for the two mono-1,8-naphthalimide complexes **37** and **38** were effectively the same. This is not altogether surprising as the binding affinity of these is most likely to be governed by the insertion of the planar 1,8-naphthalimide into the helix. Therefore, as there is not a second

1,8-naphthalimide present to influence this effect, both exhibit similar binding affinity. The one striking difference between the two systems is the much greater 1,8-naphthalimide hypochromism observed for complex **38** than **37**. A possible explanation for this is that the slightly longer linker used in **38** allows the 1,8-naphthalimide unit to bind in a manner similar to that previously observed for other 1,8-naphthalimide derivatives. The Ru(II) component in **37** restricts insertion of the 1,8-naphthalimide to the same degree as the two constituents are more closely spaced and with the Ru(II) bound externally the 1,8-naphthalimide is unable to insert as far into the helix.

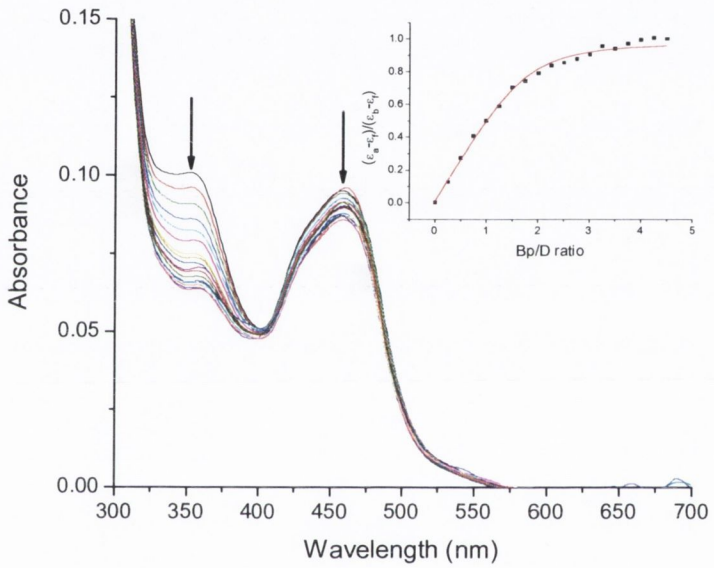

Figure 2.12 *Changes in the UV/Visible spectrum of (a)* ***38*** *(6.5 μM) upon addition of st-DNA (0 – 29.25 μM base pair) in 10 mM phosphate buffer, at pH 7. Inset: Plot of* $(\epsilon_a-\epsilon_f)/(\epsilon_b-\epsilon_f)$ *at 351 nm vs. [DNA] and the corresponding non-linear fit.*

Interestingly, the mono-1,8-naphthalimide derivatives **37** and **38** actually possessed equal, if not slightly greater affinity for DNA than the bis-1,8-naphthalimide complex **40**. This led to the proposal that perhaps only one of the 1,8-naphthalimides in **40** was interacting with DNA and the other remains external to the DNA helix. However, the large binding site size of 6 base pairs would, nevertheless, suggest that all the components of the complex were interacting with DNA. Consequently, it is likely that the longer linker in **40** may allow for significant intramolecular ground state interaction, or potential stacking of the 1,8-naphthalimides; a process which must be perturbed before DNA binding occurs. This would reduce the overall affinity of these systems for DNA. Generally, if a stacking interaction was perturbed an increase in the absorbance would be

expected. However, here the DNA interaction induces a hypochromic shift in the absorption maximum, which may compete with any increases that would otherwise result.

Less flexibility in **39**, due to the shorter linker length, may preclude as efficient stacking and thus the 1,8-naphthalimides may bind independently. Indeed this is supported by the fact that the binding affinity for **39** is twice that for the mono-1,8-naphthalimide complexes **37** and **38**, indicating that the second 1,8-naphthalimide chromophore does not lead to any cooperative binding effects.

In conclusion, all of the bichromophore systems **39** – **40** possessed binding constants of the order of $10^6 - 10^7$ M^{-1}, which are considerably larger than those previously determined for mono- or bis-1,8-naphthalimides, which had K values of the order of 10^4 or 10^5 M^{-1} respectively.[120,145] Despite the fact that the Ru(II) centre seems to inhibit complete interaction of the 1,8-naphthalimides, the overall affinity for DNA is significantly higher than the constituent parts when bound independently. This is most likely due to the bifunctional nature of the complexes; the Ru(II) centre providing initial electrostatic attraction to the DNA helix which places the 1,8-naphthalimides in an ideal environment for high affinity interaction through intercalation or groove binding, as we had anticipated in our initial design.

2.4.2 Changes in the Emission Spectra of 37 – 41 upon Binding to DNA

As detailed in Section 2.3, all of the bichromophore complexes prepared were weakly emissive in solution, possessing quantum yields of 0.001 or less for the metal based emission. This was attributed to an interaction between the 1,8-naphthalimide and the triplet MLCT excited state, a process that most likely involved electron transfer to the 1,8-naphthalimide units. The addition of DNA to all of the bichromophore complexes caused a profound effect on the photophysical properties, where the ^{3}MLCT emission was significantly enhanced.

Three key factors were considered when examining the results from these titrations:

1. The magnitude of the luminescence enhancement. This will provide information on the efficiency with which DNA interrupts the quenching process.
2. The rate at which the enhancement occurred, a measure of which may be obtained by determining the point at which 50% of the emission intensity change is reached. This should reflect the relative affinities of the different systems for DNA.

3. The shape of the binding profile. This may indicate if a single bound species is present in solution or if multiple modes of interaction occur.

2.4.2.1 Studies in Low Ionic Strength Medium (10 mM Phosphate Buffer)

Reference complex **41**, which bears no appended 1,8-naphthalimides displayed no enhancement of Ru(II) based emission upon addition of DNA. This complex is structurally very similar to $Ru(bpy)_3^{2+}$ and was expected to display weak affinity as has previously been observed.[29]

Complex **40** exhibited the greatest emission enhancement upon binding to DNA, giving rise to an eleven fold enhancement in emission intensity, as is evident from Figure 2.13a. Furthermore, the half point in emission intensity change occurred at a base pair/dye (Bp/D) ratio of 5.5.

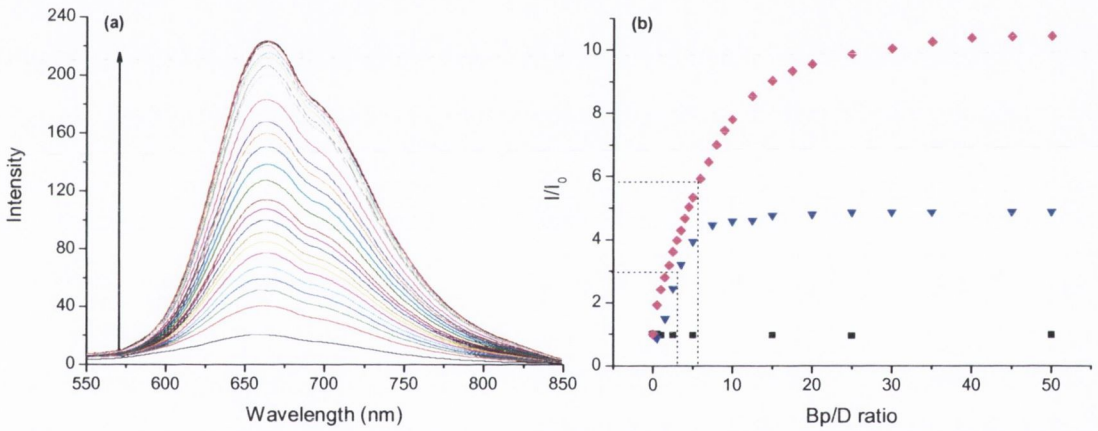

Figure 2.13 *(a) Changes in the MLCT emission of* ***40*** *(6.5 μM) (excitation at 450 nm) upon addition of st-DNA (0 – 325 μM base pairs) in 10 mM phosphate buffer, at pH 7. (b) The relative change in integrated emission intensity of* ***39*** *(▼),* ***40*** *(♦) and* ***41*** *(■) upon addition of st-DNA in 10 mM phosphate buffer, at pH 7.*

From examination of the binding profile, Figure 2.13b, it was apparent that quite high base pair equivalents must be added to reach a plateau. The binding profile shown in Figure 2.13b can be divided into two parts. The first part, up to approximately ten base pair equivalents, is steep and is the region in which most of the emission change occurs. The second part, from ten equivalents up to the plateau, is more gradual, with 25% of the total emission change occurring in this region. The biphasic nature of the emission profile suggests the presence of more than one type of DNA bound species, as was expected of these multi-component conformationally flexible complexes. This is in agreement with the

UV/Visible studies where the absence of isosbestic points suggested a distribution of complex bound to DNA by different modes.

Complex **39**, which was suggested to bind DNA with the highest affinity from UV/Vis absorption studies, however, gave only a five fold emission enhancement. However, the rate at which the emission enhancement occurred was the greatest for this complex, the half-point in intensity change occurring at a Bp/D ratio of 3.2 (this observation was in agreement with the calculated association constant). Additionally, at low base pair equivalents or high loading of complex on DNA, a slight decrease in the emission intensity of *ca.* 10% was observed. Such emission quenching at low ratios of DNA has previously been observed for dinuclear Ru(II) complexes and was attributed to a DNA induced stacking conformation of the Ru(II) complexes which facilitates a partial quenching process.[87] A plateau in the emission was reached at much lower Bp/D ratios for this complex than for its pentyl linked analogue **40**, the emission changes also occurring in a more monophasic manner. This again is in agreement with the overall greater affinity of **39** for DNA. It is also possible that in addition to contributing to lesser stacking interaction of the 1,8-naphthalimides, the shorter linker also restricts the number of possible conformations of the 1,8-naphthalimides with respect to the metal centre, and as a result the number of possible binding modes. This leads to the more simple binding profile in which different regions of change cannot be identified. The longer linker in **40** allows for a greater number of possible conformations and as a result a more "diffuse" binding mode overall. It is clear from these results that the nature of the linker has significant effects on the binding of these complexes to DNA and the resulting emission responses. The reasons for the different emission changes resulting for **39** and **40** will be discussed at a later point when proposing a mechanism for the observed enhancements.

The above results are similar to those obtained for the corresponding mono-1,8-naphthalimide complexes **37** and **38**. Significant differences were observed between **37** and **38**, whereby these complexes displayed two fold and six fold enhancements, respectively. The spectrum for **38** is depicted in Figure 2.14 along with the emission profiles for both of the mono-1,8-naphthalimide Ru(II) complexes. The rate at which the enhancement occurs is similar for both systems, the half point being at 7.8 base pair equivalents for **37** and 6.7 for **38**. This is in agreement with the UV/Visible absorption studies from which it was concluded that both systems bind to DNA in a similar manner, and with similar affinity, in a process that is largely governed by the 1,8-naphthalimide

moiety. Thus the differences in enhancement are most likely due to the differing linker lengths and not to their affinity for DNA.

The shape of the profile for **38** is similar to that of its bis analogue **40**, in that a steep initial increase in emission is observed up to a Bp/D ratio of ca. 7.5, followed by a more gradual change up to the plateau. Also similar to its bis analogue, **37** displays an initial rapid decrease in the emission intensity of *ca.* 10%, followed by a gradual increase up to the plateau. The initial decrease at high loading of complex on DNA may be due to a DNA induced stacking phenomenon. Since this only occurs for the propyl linked complexes **37** and **39** it is most likely due to stacking interactions, enforced by the short linker in which the 1,8-naphthalimides and the metal complex components are forced into close proximity to each other. Consequently, this gives rise to quenching of the MLCT emission. Stacking of the 1,8-naphthalimides may also be induced in complexes **38** and **40.** However, due to the longer (five carbon) linker, the metal centres have a greater degree of freedom and consequently would not be forced into such close proximity.

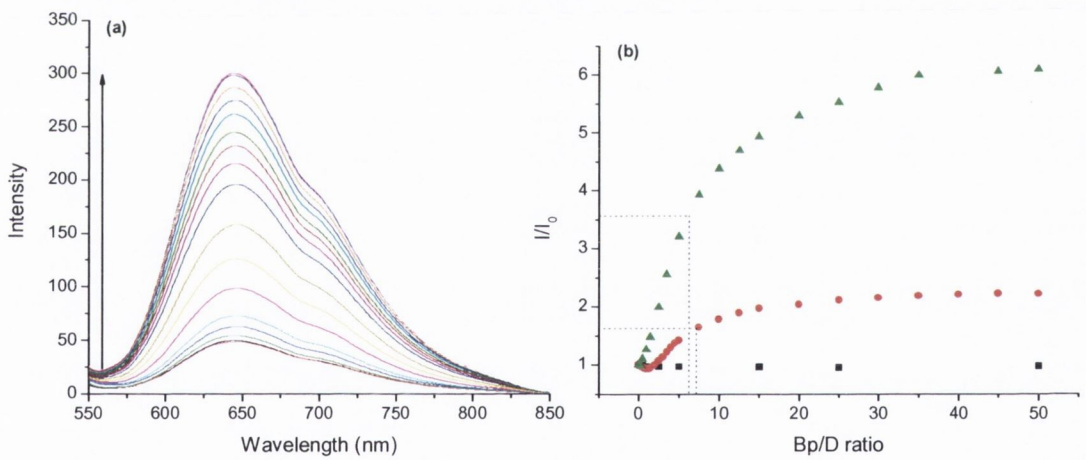

Figure 2.14 *(a) Changes in the MLCT emission of* ***38*** *(6.5 μM) (excitation at 450 nm) upon addition of st-DNA (0 – 325 μM base pairs) in 10 mM phosphate buffer, at pH 7. (b) The relative change in integrated emission intensity of* ***37*** *(●),* ***38*** *(▲) and* ***41*** *(■) upon addition of st-DNA in 10 mM phosphate buffer, at pH 7.*

For comparison, the emission profiles for each of the aforementioned systems is shown in Figure 2.15. From examination of these overlayed changes, it is quite clear that the observed emission enhancements for both of the mono-1,8-naphthalimide complexes are approximately half of those of the corresponding bis-1,8-naphthalimide complexes. This observation will be discussed in the following section when a mechanism for the

observed emission enhancements is proposed. It is also apparent from Figure 2.15 that both of the pentyl linked complexes display a similar overall shape in their emission profiles. Furthermore, quite high equivalents of DNA are necessary to reach a plateau in the emission spectra, a result that perhaps reflects the reduced affinity of these systems for DNA. A similarity in shape is also seen in the profiles for both of the propyl based complexes, which reach an emission plateau at a much earlier point than the corresponding propyl linked systems. Attempts to fit the data from emission studies in all cases proved unsuccessful.

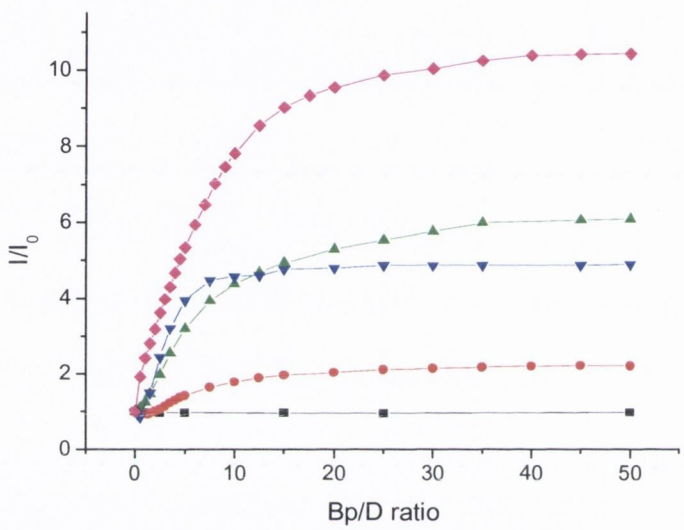

Figure 2.15 *Relative change in the integrated emission intensity of* ***37*** *(●),* ***38*** *(▲),* ***39*** *(▼),* ***40*** *(♦) and* ***41*** *(■) upon addition of st-DNA in 10 mM phosphate buffer, at pH 7.*

2.4.2.2 Studies in High Ionic Strength Medium (10 mM Phosphate Buffer + NaCl)

A drawback associated with many Ru(II) polypyridyl complexes, containing tris bipyridine or tris phenanthroline cores, is their poor affinity for DNA at high ionic strengths, as binding of many of these systems is driven primarily by electrostatic interactions.[29] The complexes studied above contain a Ru(II) centre that is expected to bind to DNA *via* electrostatic interactions, but also contain planar 1,8-naphthalimides that most likely bind by intercalative stacking interactions. Thus **37** - **40** were titrated at varying concentration of NaCl (50 mM and 100 mM), to investigate the effect of increasing ionic strength on the DNA binding process, and the relative contribution of electrostatic *vs.* non-electrostatic modes of interaction. With increasing salt concentration the interaction of Na^+ ions with the negatively charged phosphate backbone of DNA would be expected to become competitive with the interaction of the cationic complex, in effect shielding the negative charge, and as such alter the binding equilibrium of the complex.

This was observed to be the case for each of the complexes **37** – **40**, as the emission enhancement was smaller in the presence of NaCl. Furthermore, the rate at which the enhancement occurred lessened, or the number of DNA equivalents at which the half-point in intensity change was reached increased, as is clear from the values in Table 2.9. This suggests that electrostatic binding of the metal centre to the DNA backbone does play a role in determining the overall affinity of **37** – **40** for DNA. This information is summarised in Table 2.5. An example of the effect that added salt has on the emission response is given in Figure 2.16, where the profiles for **40** under different ionic strength conditions are presented.

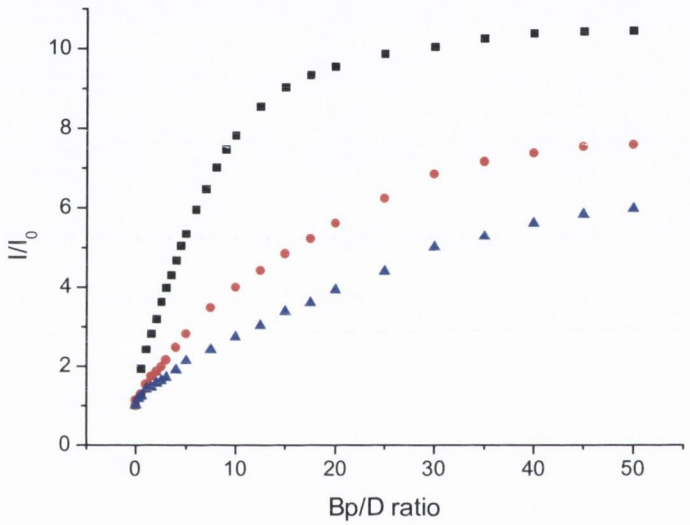

Figure 2.16 *Relative changes in the integrated emission intensity of* ***40*** *(6.5 μM) (excitation at 450 nm) with increasing concentration of st-DNA (0 – 325 μM), in 10 mM phosphate buffer (■) alone, and with 50 mM NaCl (●) and 100 mM NaCl (▲).*

Table 2.9 *Emission titration data of the Ru(II) conjugates with st-DNA.*

No.	10 mM phosphate buffer		10 mM phosphate buffer + 50 mM NaCl		10 mM phosphate buffer + 100 mM NaCl	
	Enhancement factor	Bp/D ratio where $F_{(obs)} = 0.5F_{(final)}$	Enhancement factor	Bp/D ratio where $F_{(obs)} = 0.5F_{(final)}$	Enhancement factor	Bp/D ratio where $F_{(obs)} = 0.5F_{(final)}$
37	2.1	7.8	1.9	10.5	1.8	13.9
38	6.1	6.7	5.5	9.4	4.0	16.1
39	4.9	3.2	4.3	4.3	3.8	8.6
40	10.7	5.5	7.6	11.5	6.3	17.0
41	------	------	------	------	------	------

At 50 mM NaCl concentration the greatest enhancement was still observed for **40**, reaching the half way point in emission enhancement at a Bp/D ratio of 11.5. However, the enhancement under these conditions is not as strong. The order of enhancements is again the same for the mono-1,8-naphthalimide complexes at 1.9 fold and 5.5 fold for **37** and **38**, respectively. As was the case in 10 mM phosphate buffer the half point in emission enhancement was effectively the same for both **37** and **38,** occurring at a Bp/D ratio of 10.5 and 9.4, respectively. This again would indicate a similarity in binding modes for these two systems. Complex **39** displayed a small decrease in overall emission enhancement at 4.3 fold, and reached the half point in emission enhancement at a Bp/D ratio of 4.3. This is considerably less than was required for **37**, **38** and **40**, which again points to the greater affinity for DNA possessed by this complex.

At 100 mM NaCl the same trends were observed, whereby **40** showed the greatest enhancement at 6.3 fold, and reached the half point in emission intensity change at a Bp/D ratio of 17. The order of enhancement was the same for the mono-1,8-naphthalimide complexes **37** and **38**, at 1.8 fold and 4 fold respectively. The half point in emission enhancement was approximately the same for **37** and **38**, occurring at a Bp/D ratio of 13.9 and 16.1, respectively. Complex **39** again appeared to be the most strongly bound to DNA, displaying an enhancement of 3.8 fold, and the half point in enhancement occurring at a Bp/D ratio of 8.6

In summary, the most important information obtained from the above salt dependence studies is that each of **37** – **40** were observed to remain bound to DNA at high concentration of NaCl. Furthermore, a shift in equilibrium from bound complex was evident from both the smaller emission enhancement, and the higher base pair equivalents necessary to reach the half point in enhancement. From these studies it may be concluded that electrostatic binding of the metal centre to DNA does play a role in determining the overall affinity. However, given the fact that **37** – **40** remain bound at high ionic strength, non-electrostatic interactions are therefore the predominant means from which the DNA affinity of these systems derives.

2.4.2.3 Mechanism of Emission Enhancement for 37 – 40

Each of the bichromophore complexes **37** – **40** displayed large emission enhancements with added DNA. In a 'simple' Ru(II) complex such as $Ru(phen)_3^{2+}$, emission enhancement upon DNA binding is attributed to shielding of the Ru(II) complex core from quenching by oxygen and solvent molecules, and reduced vibrational

deactivation of the excited state due to rigidification of the structure.[33] This mechanism may play a small role in the emission enhancement for **37** – **40**, in which the 1,8-naphthalimide moiety tightly binds DNA, and in doing so locks the Ru(II) centre in place in the protected environment of the DNA grooves, thereby shielding it from quenching. As previously mentioned in Section 2.3, **37** – **40** possess very low quantum yields. This may be attributed to interaction between the two chromophores, in which the ruthenium ^{3}MLCT is quenched by electron transfer to the 1,8-naphthalimide. The emission enhancement upon DNA binding could therefore be proposed to be the result of the interruption of this quenching pathway.

In proposing exactly how DNA binding leads to emission enhancement a number of points should be considered:

1) The 1,8-naphthalimide binds with high affinity to DNA through intercalation or groove binding.
2) The Ru(II) centre binds weakly through external association.
3) Binding decreases the efficiency of quenching pathways.
4) Greater emission enhancements are observed for systems with longer linker lengths.

As discussed above, the linker moiety of **37** – **40** may be expected to adopt conformations that give small chromophore – quencher separation distances. As electron transfer is highly sensitive to the distance between the donor and acceptor, as described in **Eq. 2.1**,[146] efficient transfer will result, and consequently give rise to weak emission from the metal centre.[97]

$$\mathbf{k_{ET} = k_{ET}^{0} exp(-\beta R)} \qquad \mathbf{(2.1)}$$

where, k_{ET}^{0} is the rate constant of adiabatic intramolecular electron transfer, R is the donor-acceptor centre–to–centre distance and β is dependent on the nature of the environment which affects the electronic coupling between the donor and acceptor. For DNA this β value has been determined to be approximately 0.7 Å.[147,148]

It is expected that the separation distance between the donor and acceptor is larger for the DNA bound complex than for the complex free in solution. In terms of equation **2.1**, such DNA binding leads to larger values of R, as the chromophores separate, giving a corresponding decrease in the rate of electron transfer. This reduction in k_{ET} is the origin of the increase in emission from ^{3}MLCT. These processes are represented schematically in

Figure 2.17. It should be pointed out that the drawing in Figure 2.17 does not suggest anything about the degree or stacking of the 1,8-naphthalimides with either the Ru(II) core or with themselves. It merely serves to emphasise the change in distance between the components upon binding to DNA.

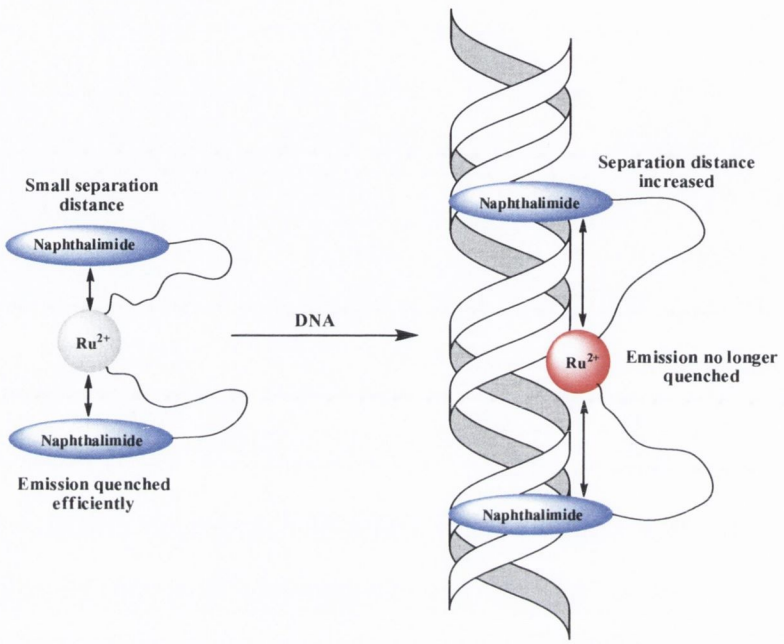

Figure 2.17 *Representation of the quenching of the Ru(II) complex in solution and the "switching on" effect resulting from DNA binding.*

The differences in emission enhancements observed for systems with varying linker length may be related to such distance dependence of quenching. From examination of the results for the bis-1,8-naphthalimide complexes **39** and **40**, it is apparent that a longer linker length lead to greater emission enhancement. It has already been proposed that DNA binding causes a separation of the components of **37** - **41**. Therefore, for complex **40**, with a five carbon unit linker, the separation caused by binding is greater than that for complex **39**, with a three carbon unit linker. This increased separation causes a greater decrease in the rate of electron transfer and a correspondingly larger increase in emission. This effect is mirrored in the mono-1,8-naphthalimide complexes **37** and **38**, whereby a greater enhancement is also observed for the five carbon unit linked derivative in comparison to that containing a three carbon unit linker.

The differences observed between corresponding mono- and bis-1,8-naphthalimide systems, in which the enhancement observed for the bis system is approximately twice that observed for the mono system, could be attributed to the number of 1,8-naphthalimide moieties attached to the Ru(II) centre. Greater emission enhancements were observed for

the bis systems **39** and **40** as quenching caused by two 1,8-naphthalimide moieties is being interrupted upon DNA binding, as opposed to one 1,8-naphthalimide in the mono substituted complexes **37** and **38**.

One further observation made is that although large increases in emission are observed in certain cases, the intensities do not reach values that would be expected if the quenching pathway was completely switched off. DNA does not eliminate quenching completely but rather retards it. This can be seen in Table 2.10 where the quantum yield for each system fully bound to DNA is given. None of the values reach that of the unquenched complex, which was determined to be 0.014.

Table 2.10 *Emission quantum yields of* ***37 – 40*** *bound to DNA (Ref. to* $Ru(bpy)_3^{2+}$*).*

Complex	Φ_f (± 10%)
45	0.003
46	0.005
47	0.003
48	0.009

In summary the results from the UV/Visible absorption and emission studies of **37 – 40** in the presence of DNA, showed that functionalisation of a Ru(II) polypyridyl complex with 1,8-naphthalimide moieties is a successful strategy for increasing their affinity for DNA. Binding affinities in the range $10^6 - 10^7$ M^{-1} were determined for **37 – 40**, which are substantially greater than that observed for $Ru(bpy)_3^{2+}$.[31] The resulting systems also displayed useful emission responses upon binding DNA, along with varying degrees of enhancement depending on the molecular arrangement. In particular, **40** displayed a large emission increase of 10.7 fold, and although it cannot be described as a "*light switch*" it is approaching the criteria for classification as such. From the UV/Visible absorption and the emission studies, **37 – 40** were proposed to bind in a manner involving intercalation or groove binding of the 1,8-naphthalimide chromophores and external association of the metal complex with the backbone of DNA. From these promising results further spectroscopic measurements were carried out in order to gain more complete understanding of the nature of these interactions. The results from these studies will be discussed in the following sections.

2.4.3 DNA Thermal Denaturation Studies of 37 – 41

If the temperature of a solution containing double stranded DNA is raised by a sufficient amount, strand separation or melting occurs, as depicted in Figure 2.18.[149] The temperature that marks the midpoint of the transition is called the helix-coil transition temperature or T_m.[149] At the T_m, half of the nucleic acid exists in the helical state and the other half in the single-stranded state, with the two forms in equilibrium with each other. Melting transitions can be detected by UV/Visible absorbance, circular dichroism, NMR, viscosity, electrophoresis or calorimetry, with UV/Visible absorbance being the most commonly used.[149] Nucleic acids absorb light in the UV region with a maximum absorbance at approximately 260 nm. This absorbance increases as native (double helical) DNA melts into the denatured form, and thus by monitoring this hyperchromicity a melting profile can be obtained, where the inflection point is the T_m. The increase in absorbance is due to a reduction of electronic interactions in the stacked form. The absorbance of the single strand form approaches that of the nucleic acid taken as monomers where no interaction between the bases occur.

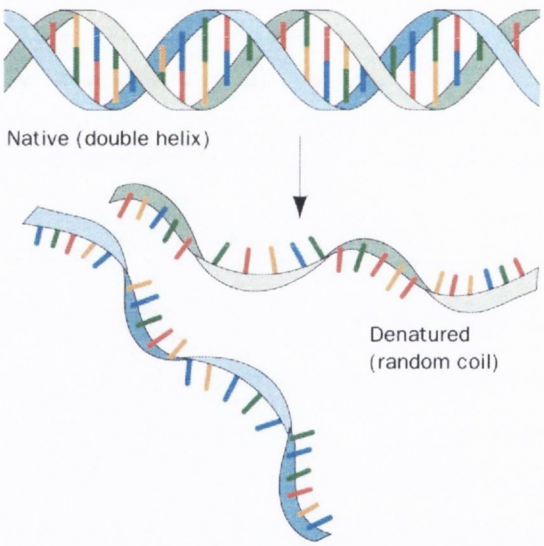

Figure 2.18 *Schematic representation of the melting of a DNA double helix.*[9]

Molecules that bind nucleic acids generally bind to the helical state with higher affinity as it has more uniform structural features that favour complex formation.[149] This stabilises the DNA structure, shifting the equilibrium between the double and single stranded forms in favour of the former. The result of this is that more energy is necessary to separate the strands. The base stack of the DNA double helix provides an environment for intercalation of a drug. In contrast, stacking with single stranded DNA is much weaker, and consequently intercalators stabilise the double helix and cause an increase in T_m.

Binding by groove binding species has also been shown to preferentially stabilise helical structures and cause increases in T_m.[150]

In the absence of metal complex the T_m value for ct-DNA was determined to be 69 °C. This temperature was found to change significantly in the presence of **37** – **39**, as shown in Figure 2.19.

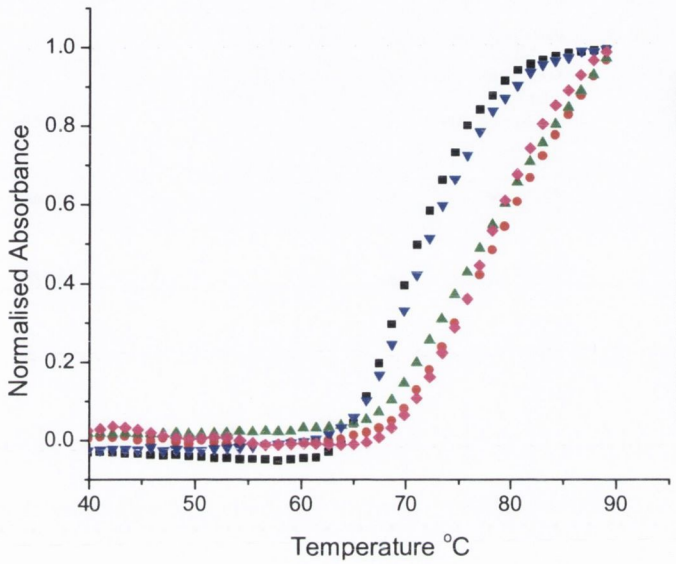

No.	T_m
DNA	69 °C (± 10%)
37	75.8 °C (± 10%)
38	75.0 °C (± 10%)
39	76.0 °C (± 10%)
40	70.2 °C (± 10%)

Figure 2.19 *Thermal denaturation curves of st-DNA (150 μM) in 10 mM phosphate buffer, at pH 7, in the absence (■) and presence of* ***37*** *(▲),* ***38*** *(●),* ***39*** *(♦), and* ***40*** *(▼), all at a Bp/D ratio of 5.*

As the melting transition had not gone to completion at 90 °C for these systems it was necessary to extrapolate the curve by fitting to a sigmoidal function with Sigmaplot 10.0. Thus, the values reported should be regarded as approximations and are likely underestimated. A T_m of 76.0 °C was determined for the bis-1,8-naphthalimide complex **39**, the complex which displayed the greatest binding affinity for DNA. Interestingly, complex **40**, which has a pentyl linker, gave only a small increase in T_m, suggesting that the complex was more loosely associated with DNA, or bound in a manner which does not stabilise the helix. This is in agreement with the more diffuse binding mode proposed in Section 2.4.1. The T_m values for **39** and the corresponding mono-1,8-naphthalimide analogue, **37**, were effectively the same, suggesting that for **39** only one of the 1,8-naphthalimide moieties was possibly interacting with DNA. However, it must be emphasised that the thermal denaturation studies do not provide unequivocal evidence for a particular binding mode, as changes may arise from both groove binding[150] and

intercalative interactions.[151] Given that both 1,8-naphthalimide units in **39** may bind to DNA, the above results indicate that the binding mode leads to similar stabilisation of the helix, as would the binding of a single 1,8-naphthalimide moiety. Complex **37** may bind by classical intercalation whereas **39** may bind by partial insertion of both 1,8-naphthalimides. The T_m for **38** at 75.0 °C was similar to that observed for **40**, once again pointing to the similarity in binding of these two complexes to DNA.

2.4.4. Circular Dichroism Studies of 37 – 41

Circular dichroism is defined as the difference in absorption of incident left and right circularly polarised light.[152] The phenomenon only occurs with asymmetric molecules and the differences in absorption are generally small but measurable. The technique is particularly useful in the study of biological macromolecules, for probing both conformational changes of the macromolecule itself and its interaction with small molecules. The heterocyclic bases of DNA are achiral, but become chiral when placed within the framework of the chiral sugar-phosphate backbone.[152] Different sequences and conformations of nucleic acids possess characteristic CD spectra, that of B-DNA consisting of a positive band at 275 nm and a negative band at 248 nm. Many DNA binding ligands are achiral and as such do not display CD.[153] However, they may upon interaction with DNA acquire an induced CD (ICD) signal through the coupling of electric transition moments of the ligand and the DNA bases.[152] The presence of an ICD signal is therefore an immediate indication of ligand-DNA interaction. Equally the interaction of chiral molecules with DNA may cause changes in the CD signal intrinsic to the molecule.

Assignment of a binding mode from changes in the CD spectrum of a DNA binding molecule is not definitive, although in general small changes of $< 10\ M^{-1}\ cm^{-1}$ imply intercalation, whereas larger signals are indicative of groove binding.[152] In addition, only those bands outside the region of absorption of the DNA may be considered in proposing a binding mode as changes in the DNA region may be due to ICD of the ligand as well as structural changes in the DNA itself, which would be induced by binding of the ligand.

Circular dichroism measurements were carried out using **37** – **41**, in which the concentration of ct-DNA was kept constant, and that of the metal complexes was varied to give a range of Bp/D ratios. The CD spectra resulting from the addition of reference **41** to ct-DNA are shown in Figure 2.20. From examination of these spectra it is clear that no induced CD signal occurs outside the region of absorption of the DNA. In addition, only a

small change in CD signal occurs in the region of the spectrum below 300 nm. These results further confirm the weak nature of the interaction of **41** with DNA.

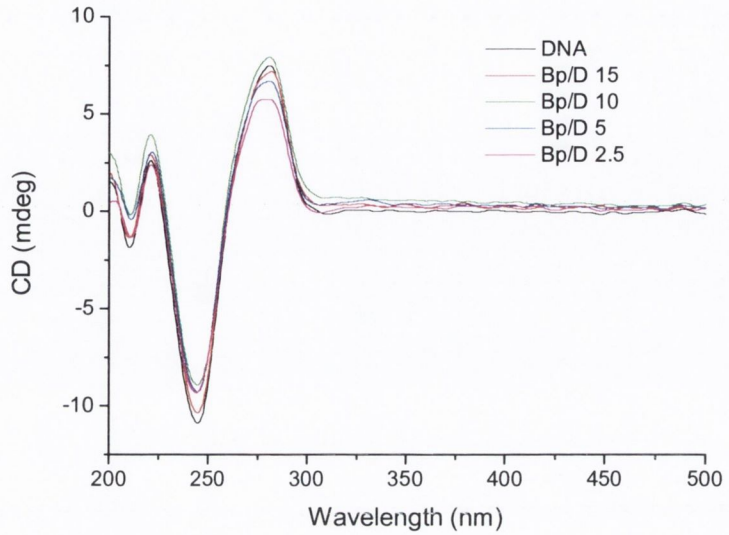

Figure 2.20 *Circular dichroism spectra of ct-DNA (150 μM) in 10 mM phosphate buffer, at pH 7, in the absence and presence of* ***41*** *at varying ratios.*

All of the Ru(II)-1,8-naphthalimide conjugates **37** – **40** exhibited similar CD behaviour. The spectra obtained from the addition of **38** to ct-DNA are shown in Figure 2.21. A substantial ICD is observed at long wavelength with the maximum appearing at about 470 nm. This corresponds to the MLCT absorption of the metal complex and implies that the Ru(II) component of **38** is associated with the DNA helix. The changes are relatively small, but due to the minimal extended planar nature of the ligands in the metal complex are unlikely to result from any form of intercalative binding. Consequently, it is suggested that the Ru(II) centre binds externally in a manner that places it in loose association with the grooves of DNA, resulting in a small ICD signal. CD changes were also observed in the region of absorption of the 1,8-naphthalimide moiety at around 350 nm. The Ru(II) polypyridyl complexes display broad absorption which tails into this region and thus the changes cannot be assigned to either chromophore. This is also true of the large ICD at *ca.* 310 nm. Significant changes in CD were also observed in the region of absorption of DNA. However, as previously indicated, these changes could result from either a conformational change in the DNA, caused by bound complex, or from ICD of the bound complexes themselves. As such conclusions cannot be made from the CD changes observed in this region.

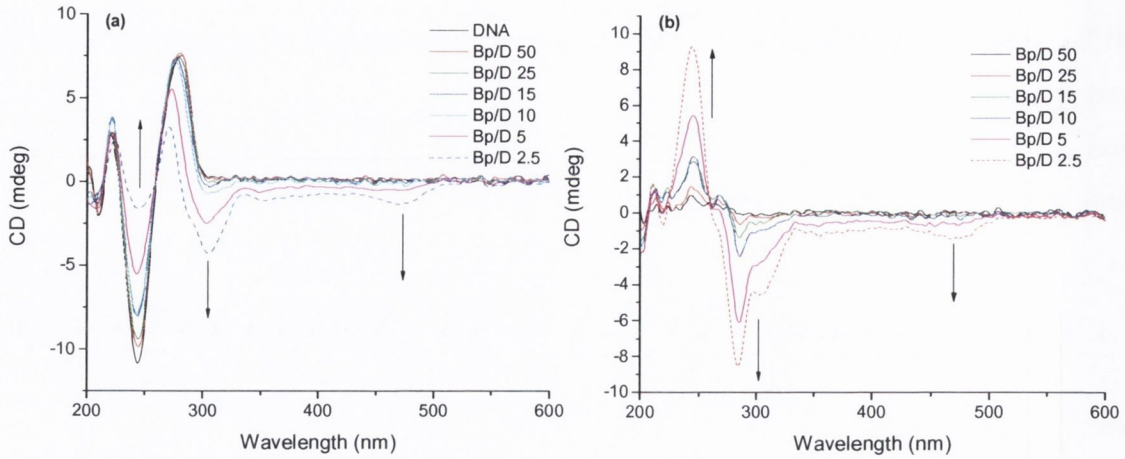

Figure 2.21 *Circular dichroism spectra of (a) ct-DNA (150 μM) in 10 mM phosphate buffer, pH 7, in the absence and presence of* ***38*** *at varying ratios, and (b) the difference spectra obtained.*

The most important conclusion that may be taken from the CD studies on **37** – **40** is that the Ru(II) component of the bichromophore systems does bind DNA and in doing so experiences the helicity of the DNA. Even though the changes are quite small they do indicate that the metal centre when bound is in the chiral environment of the sugar. This is in contrast to the results obtained for the reference complex **41**, which displayed no ICD in the region of absorption of the metal complex.

2.4.5 Ethidium Bromide Displacement Assay of 37 – 40

Ethidium bromide (EtBr) can be used as a fluorescent probe to investigate the binding interaction of small molecules with DNA.[154] Addition of a DNA binding compound to DNA bound EtBr results in a decrease in fluorescence due to dislodgement of the bound intercalator. EtBr is weakly emissive in solution but fluoresces strongly when bound to DNA.[154] The relative decrease in fluorescence can be directly related to the extent of binding of the particular species under investigation. The addition of complexes **37** – **40** to a mixture of EtBr and DNA were found to displace the EtBr molar ratios of one or less than one, *i.e.* they displayed equal or greater affinity for DNA than EtBr. This again confirms the high affinity of these complexes for DNA, which is in agreement with the results obtained from UV/Visible titration discussed in Section 2.4.1.

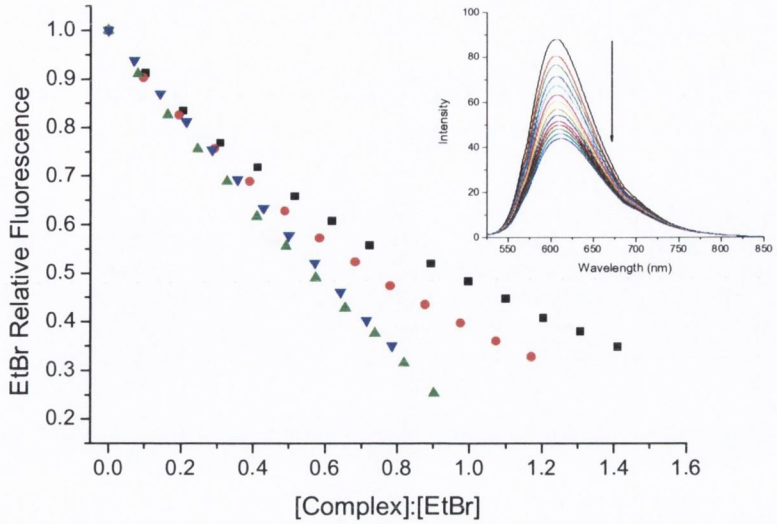

Figure 2.22 *Decrease in fluorescence of DNA bound EtBr upon addition of* ***37*** *(■),* ***38*** *(●),* ***39*** *(▲) and* ***40*** *(▼) in 10 mM phosphate buffer, pH 7. Insert: The emission changes for DNA bound EtBr (excitation at 545 nm) with increasing conc. of* ***37****.*

Some general trends may be identified in the binding affinities determined from EtBr displacement. Its is apparent from the displacement profiles shown in Figure 2.22 that the bis-1,8-naphthalimide complexes **39** and **40** displace EtBr more effectively than their mono-1,8-naphthalimide analogues, **37** and **38** respectively. This important result confirms that both of the 1,8-naphthalimides moieties are binding DNA, and a situation where one of them is redundant in terms of DNA binding does not occur.

2.4.6 Summary of Results (37 – 40)

In conclusion, the family of bifunctional complexes **37** – **40**, containing Ru(II) polypyridyl and 4-nitro-1,8-naphthalimide subunits, have been shown to possess well defined photophysical properties that could be perturbed in the presence of DNA. All complexes were found to bind DNA with affinity constants in the range $10^6 - 10^7$ M^{-1}. The most striking results from this study were the emission enhancements accompanying DNA binding. All conjugates displayed large enhancements upon binding, with the bis-pentyl complex **40** giving the greatest change at eleven fold. This complex cannot strictly be described as a "light switch" for DNA, as has been applied to Ru(II) dppz complexes, but it does essentially exhibit off↔on emission behaviour. Such an effect can be attributed to interruption of intramolecular electron transfer quenching of the Ru(II) moiety by the

appended 1,8-naphthalimides. This process was shown to be quite dependent on distance, with greater enhancements observed for pentyl linked complexes **38** and **40** than the corresponding propyl linked derivatives **37** and **39**. Consideration of these results and those from thermal denaturation, circular dichroism and ethidium bromide displacement suggests a binding mode which most likely involves tight association of the 1,8-naphthalimide moieties, with weaker association of the metal centre on the exterior of the helix or partially placed in the grooves. Due to the multi-component nature of **37** – **40** numerous different binding modes may be present, with various different orientations and distances between the subunits.

An important feature of these complexes is that the Ru(II) centre, which is essentially external to the helix, reports effectively through its MLCT emission on the change in local environment of the 1,8-naphthalimides. Consequently, these systems may be regarded as potentially useful luminescent probes for DNA. One drawback with the molecular arrangement discussed thus far was the large number of DNA equivalents necessary to reach an emission plateau with **40**, the system that displayed the greatest enhancement. However, the nitro substituents on the 1,8-naphthalimide is also a significant determinant for binding. Therefore, it was decided to make a simple modification to structure **40** by incorporation of different 1,8-naphthalimide functionality, and investigate the effect that this had on DNA binding.

2.5 Structural Modification of 40

It has been suggested in the literature that 3-nitro-1,8-naphthalimides are more effective intercalators than their 4-nitro counterparts, as in the latter, the nitro group may be twisted slightly out of plane due to steric repulsion by the neighbouring H-atom in the 5-position of the ring system,[155] as depicted in Figure 2.23. This diminished planarity makes intercalation or insertion into the DNA helix less favourable. The higher intercalating ability of 3-nitro-1,8-naphthalimides would therefore make them desirable for use as DNA binding agents, and in particular for incorporation into bifunctional complexes of the type discussed in the preceding sections of this chapter.

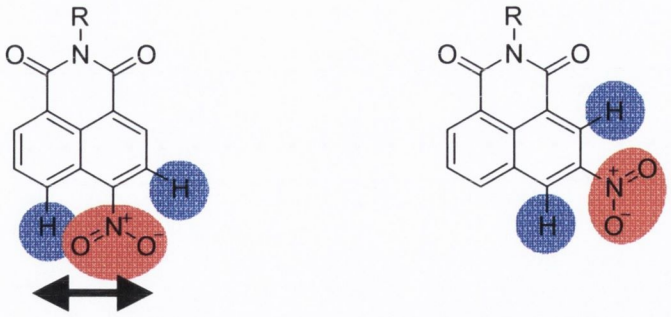

Steric repulsion between nitro and H5

No steric repulsion of nitro by neighbouring H atoms

Figure 2.23 *Steric repulsion experienced by the nitro group when in the 4-position.*

With this in mind, compound **60** was designed to investigate this phenomenon. This complex comprises two 3-nitro-1,8-naphthalimide subunits linked to a Ru(II) polypyridyl core by a five carbon unit aliphatic chain, and hence is a structural analogue of **40**. This system was synthesised according to the same general procedure as discussed for its 4-nitro analogue **40**. This firstly involved synthesis of the appropriate 3-nitro-1,8-naphthalimide **61** in the same manner as for the compounds discussed in Section 2.2.1, followed by deprotection to give the corresponding *N*-alkylamino terminated derivative **62**. This was subsequently coupled to 4,4'-dicarboxy-2,2'-bipyridine *via* the acid chloride intermediate as before, to give **63**. Ligand **63** was coupled in the same manner described in Section 2.2.3, affording the desired complex.

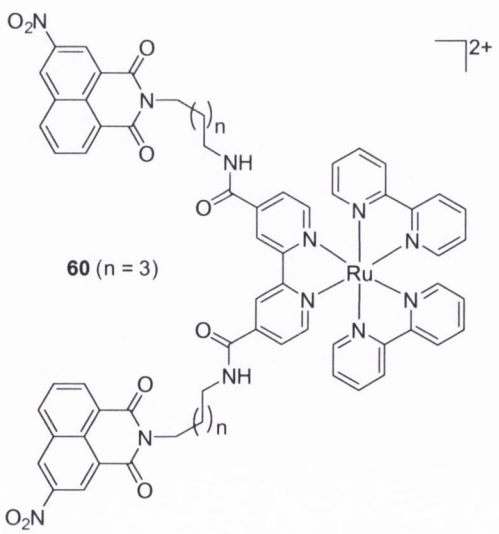

2.5.1 Photophysical Properties of 60

The photophysical properties of **60** were somewhat different to those of its 4-nitro analogue **40**. The absorption, excitation and emission spectra of **60** are shown in Figure 2.24.

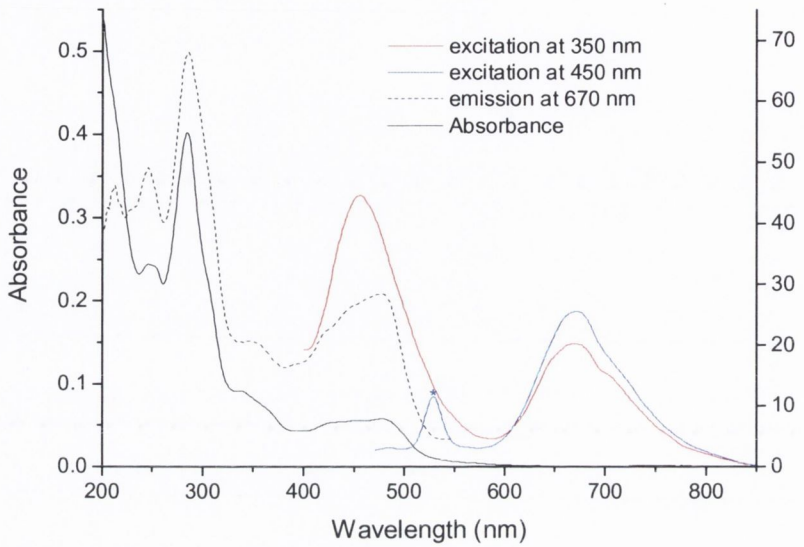

Figure 2.24 *UV/Visible, excitation and emission spectra of* ***60*** *(6.5 μM) in 10 mM phosphate buffer, at pH 7. The water Raman band is denoted by *.*

In comparison to **40** the maximum of the 1,8-naphthalimide absorption band of **60** was shifted to a slightly shorter wavelength of 338 nm, with ϵ = 13400 M^{-1} cm^{-1}, which is just over half that observed for **40**. It is very likely that intramolecular stacking of the 3-nitro-1,8-naphthalimides in solution occurs to a greater degree in this system, than in **40**, and therefore a greater hypochromicity in absorption is observed. The absorption maximum of the metal complex component of **60** occurs at 480 nm, the same wavelength as for **39** and **40**, respectively, but again the molar absortivity was somewhat reduced at 8400 M^{-1}.

Significant differences were also observed in the emission properties of **60** in that a reasonably intense emission band was observed at 456 nm, corresponding to an emission originating from the 1,8-naphthalimide moiety. This is in contrast to that observed for **37** – **40**, which displayed much weaker such emission, as discussed in Section 2.3. This emphasises the significant effect that this small structural modification of the 1,8-naphthalimide ring system has on the photophysical properties of the resulting complex. It is possible that changing the nitro substituent to the 3-position results in less efficient energy transfer to the metal centre, and therefore some emission is observed from the 1,8-naphthalimide itself. The quantum yield of the MLCT emission from **60** was

determined to be < 0.001, an observation which can be attributed to quenching of the metal centre by electron transfer to the 1,8-naphthalimide moieties. The system therefore possesses photophysical properties in solution that render it ideal for use as a chromophore – quencher probe for DNA, *i.e.* weakly emissive comprising two flexibly linked components. The following sections will deal with the interaction of **60** with DNA and its potential for use as a photophysical probe.

2.5.2 DNA Binding Interactions of 60

2.5.2.1 Changes in the UV/Visible Absorption of 60 with DNA

The changes in the absorption spectrum of **60** in 10 mM phosphate buffer upon addition of st-DNA was significantly different to those observed for **37** – **40**. An initial increase in the absorbance of *ca.* 10% was seen in the 1,8-naphthalimide region (338nm) up to the addition of approximately 0.6 base pair equivalents of DNA, as shown in Figure 2.25.

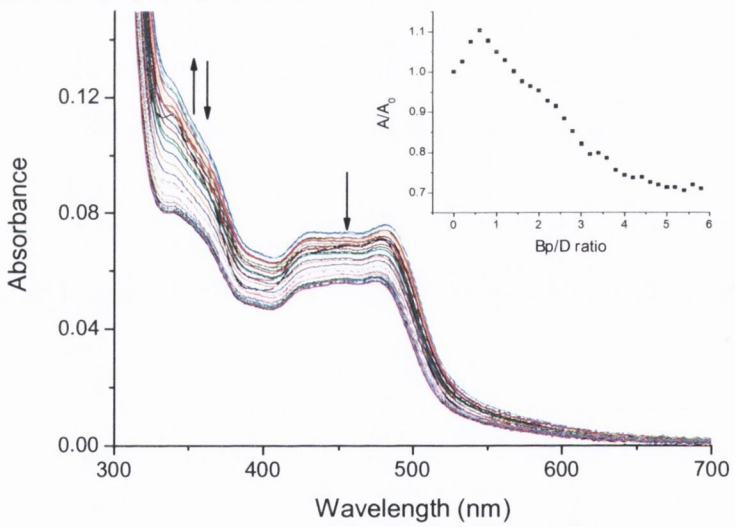

Figure 2.25 *Changes in the UV/Visible spectrum of* ***60*** *(6.5 μM) in 10 mM phosphate buffer, at pH 7 upon addition of st-DNA (0 – 37.7 μM). Inset: Relative change in the absorbance at 350 nm vs. equivalents of DNA.*

As previously discussed, the relatively low molar absorptivity in this region was indicative of extensive stacking of the 1,8-naphthalimide moieties. Hence, the increase in absorbance could to be due to a perturbation of this stacking process by low equivalents of DNA. A subsequent decrease in absorbance of *ca.* 30% (relative to the starting point) followed the increase, which may be due to insertion of the 1,8-naphthalimides into the

DNA helix. Due to the increased complexity of this possible binding process the data from the UV/Visible absorption titrations was not fitted to the Bard model, and therefore a binding constant for the DNA interaction was not determined for **60**. In contrast to these results, the change in absorbance of the MLCT band of 18% was significantly greater for this system than that observed for **40**. This suggests that the metal centre is perhaps more strongly bound to the DNA helix as it is anchored more tightly in place by the improved binding of the 1,8-naphthalimide groups.

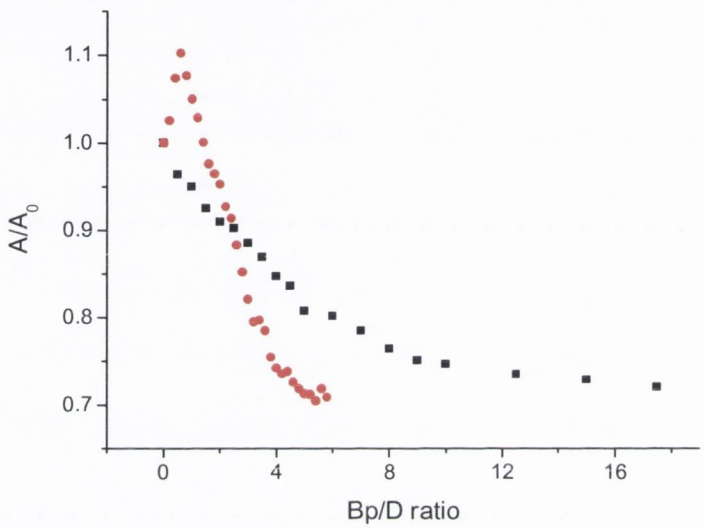

Figure 2.26 *Changes in the 1,8-naphthalimide absorption of* ***40*** *(6.5 μM) (■) and* ***60*** *(μM) (●) at 350 nm in 10 mM phosphate buffer,at pH 7 upon addition of st-DNA.*

Although a binding constant was not determined, a comparison of the absorption profile for titration of **60** with DNA compared to that of **40** may give an indication of the relative binding affinity. To achieve this, an overlay of the two absorption profiles is shown in Figure 2.26, which shows that the changes for **60** reach a plateau at a much lower Bp/D ratio. Therefore, it seems that **60** may possess higher affinity for DNA than its 4-nitro analogue **40**. Consequently, it would seem from these initial studies that modification of the ring system does lead to an improved DNA binding ability.

2.5.2.2 Changes in the Emission Spectrum of 60 upon Binding to DNA

2.5.2.2.1 Studies in Low Ionic Strength Medium (10 mM Phosphate Buffer)

As for complexes **37** – **40**, the addition of DNA to a solution of **60** in 10 mM phosphate buffer resulted in a profound increase in the emission from the metal centre. A twelve fold luminescent enhancement was observed, with the half point of the intensity

change occurring at a Bp/D ratio of 1.3. From examination of the titration profile shown in Figure 2.27, two distinct regions can be identified. The first occurs up to a Bp/D ratio of 0.6, and is steeper than the remainder of the titration profile. This is the same region in which the aforementioned increase in absorbance was observed, and thus assigned to the first stage in DNA binding, in which the stacking of the 1,8-naphthalimides was disrupted. Upon increasing concentration of DNA the profile gradually reaches a plateau at a Bp/D ratio of approximately 5. In terms of emission changes, this complex can be regarded as being bound to DNA with much greater affinity than its analogue **40**. The emission enhancement and the rate of enhancement are greatest for **60**, and the point at which it plateaus are all greatest for complex **60**. This can be clearly seen in Figure 2.28, where the intensity changes for **40** and **60** are compared. The change in the MLCT emission for **60** has reached a plateau at a Bp/D ratio of *ca.* 5, in agreement with the behaviour seen in the UV/Visible absorption spectrum. At the same Bp/D ratio only approximately 50% of the overall emission enhancement had been reached for compound **40**.

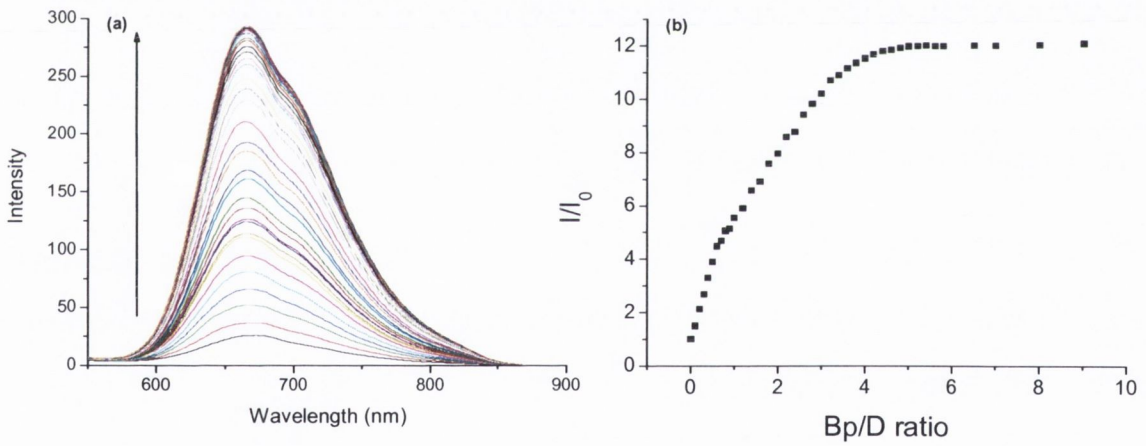

Figure 2.27 *(a) Changes in the MLCT emission spectrum of* ***60*** *(6.5 μM) (excitation at 450 nm) upon addition of st-DNA (0 – 58.5 μM base pairs) in 10 mM phosphate buffer, at pH 7. (b) The relative change in integrated emission intensity.*

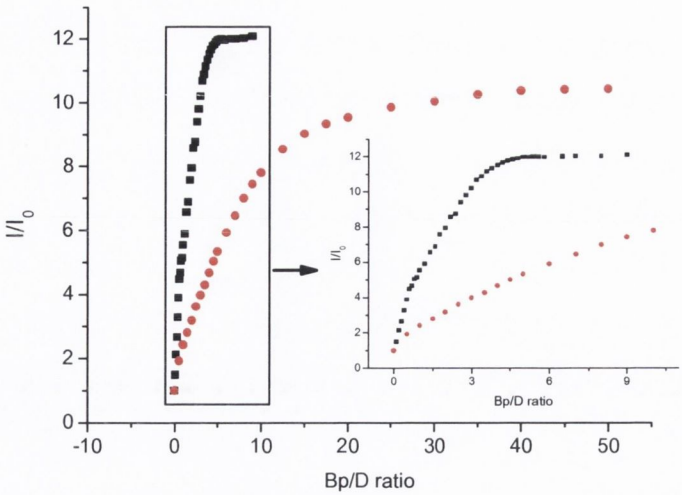

Figure 2.28 *Comparison of the emission intensity changes for* ***40*** *(●) and* ***60*** *(■) upon addition of st-DNA.*

The modification of complex **40** yielding complex **60** has resulted in a system with substantially improved luminescence response to added DNA. Compound **60** displayed both a greater change in MLCT emission in the presence of DNA at twelve fold, and stronger binding to the DNA, ascribed from the smaller number of equivalents of DNA necessary to reach a plateau. The next step with **60** was to evaluate its sensitivity to increasing ionic strength of the titration medium.

2.5.2.2.2 Studies in High Ionic Strength Medium (10 mM Phosphate Buffer + NaCl)

The effect of increasing ionic strength on the DNA binding ability of **60** was also investigated in the same manner described above. The emission changes in the presence of different concentrations of NaCl are shown in Figure 2.29. As observed above, the profiles at each salt concentration displayed two distinct regions of change.

With 50 mM NaCl, the first part of the profile remains essentially the same as in 10 mM phosphate buffer, in that a steep change occurred up to a Bp/D ratio of approximately 0.6 base. The change then became more gradual up to the plateau, which in this case corresponds to a ten fold emission enhancement. The second part of the profile is more gradual than that observed in 10 mM phosphate buffer solution, the half point in the overall emission change in this case being reached at a Bp/D ratio of 1.3. The initial part of the profiles in 10 mM phosphate buffer and 10 mM phosphate buffer with 50 mM NaCl are very similar. As much of the overall enhancement occurs in this region in both cases, the simple measurement of the rate of change places them both approximately then same. In the case of 100 mM NaCl background concentration, a two step profile was also observed,

with much of the overall change occurring before the addition of one base pair equivalent. The half way point in intensity change occured at a Bp/D ratio of approximately 1.4, very close to the values in 10 mM phosphate buffer and 10 mM phosphate buffer + 50 mM NaCl.

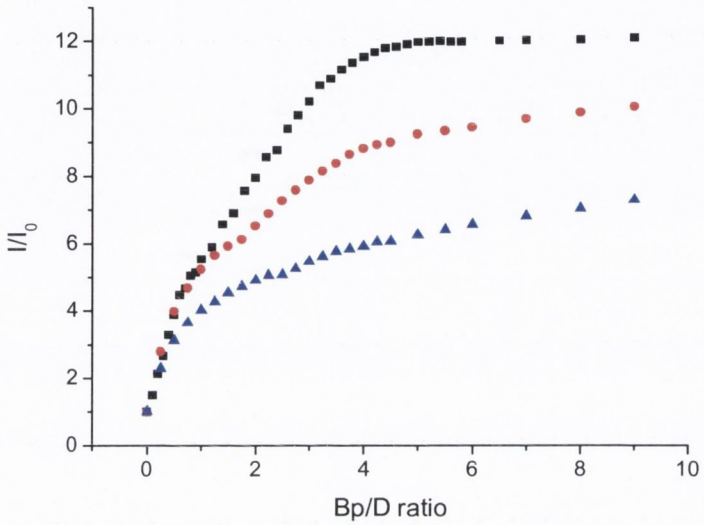

Figure 2.29 *Relative changes in the emission of* ***60*** *(6.5 μM) (excitation at 450 nm) with increasing concentration of st-DNA (0 – 58.5 μM), in 10 mM phosphate buffer (■), 10 mM phosphate buffer + 50 mM NaCl (●) and 10 mM phosphate buffer + 100 mM NaCl (▲).*

A back titration was also carried out on **60**, in which nine base pair equivalents of DNA were added to **60**, followed by titration using NaCl, in an attempt to displace the bound complex from the DNA. A relative intensity of one in Figure 2.30 represents complex fully bound to DNA, and of zero represents the complex free in solution. As expected, increasing NaCl concentration gives rise to a gradual decrease in the intensity of the MLCT emission. From the profile in Figure 2.30b it is clear that the complex remains bound to DNA at high salt concentration, the intensity not returning to that of free complex even in the presence of 300 mM NaCl.

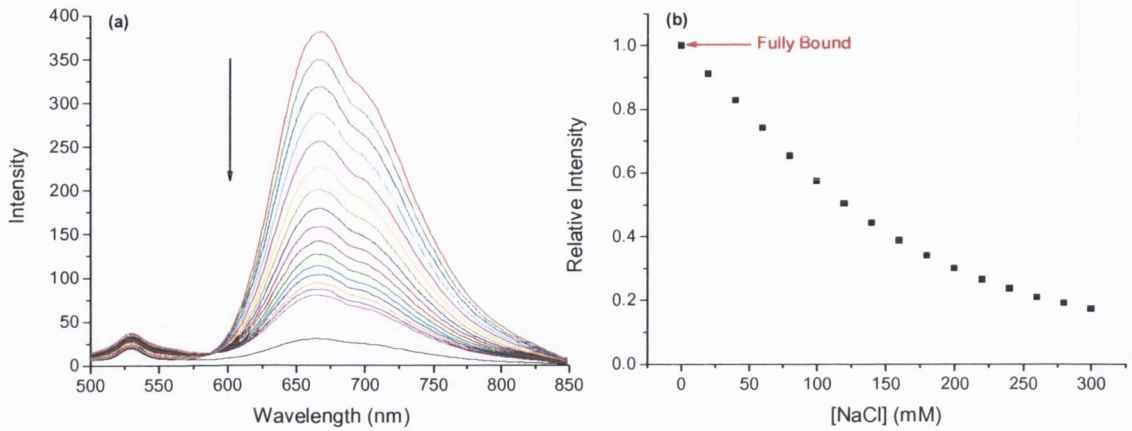

Figure 2.30 *(a) Changes in the MLCT emission spectrum of DNA bound* ***60*** *(6.5 μM) (excitation at 450 nm) in 10 mM phosphate buffer, at pH 7, with increasing concentration of NaCl. (b) the binding profile from monitoring the integrated emission intensity.*

It is apparent from these luminescence studies that varying salt concentrations do not give rise to the same degree of changes in the emission as seen preciously for **37** – **40**, Section 2.4.2. This would suggest that **60** binds DNA with greater affinity, and in a manner than is more reliant on modes of binding that are insensitive to added salt such as intercalation. This is in agreement with that proposed above, where it was postulated that the 3-nitro substituents would lead to greater affinity for DNA due to enhanced intercalating ability. This would suggest a binding mode whereby the 3-nitro-1,8-naphthalimides were more deeply inserted into the helix, and hence more effectively prevented from interaction with the metal complex. Additionally, the quantum yield of **60** was determined to be 0.012 when bound to DNA, which is quite close to that of the reference complex **41**. Thus, binding of **60** to DNA almost completely switches off the ET quenching pathway, a result that is again in agreement with a binding mode whereby the 3-nitro-1,8-naphthalimides are more effectively sequestered by the DNA bases thorough stacking interaction, and prevented from interacting with the metal complex excited state.

2.5.2.2.3 Studies in the Presence of Different DNA Sequences

In general, the emission intensities of Ru(II) polypyridyl complexes do not vary much with DNA sequence. Some exceptions are however, the $[Ru(TAP)_2POQ\text{-}NMet]^{2+}$ system discussed in *Chapter 1*, which displayed greater emission enhancement in the presence of AT rich sequences, as a competitive ET mechanism from guanine residues in

GC rich sequences to metal complex becomes significant, and the parent $Ru(TAP)_3^{2+}$ complex.[100] This complex is an example of the possibility of achieving enhanced sequence recognition using a chromophore – quencher assembly. Therefore it was decided to investigate the emission properties of **60** in the presence of $[poly(dAdT)]_2$ and $[poly(dGdC)]_2$ in the hope of revealing similar sequence specific effects.

The emission profile of **60** in the presence of $[poly(dG\text{-}dC)]_2$, shown in Figure 2.31, was quite similar to that observed in the presence of st-DNA.

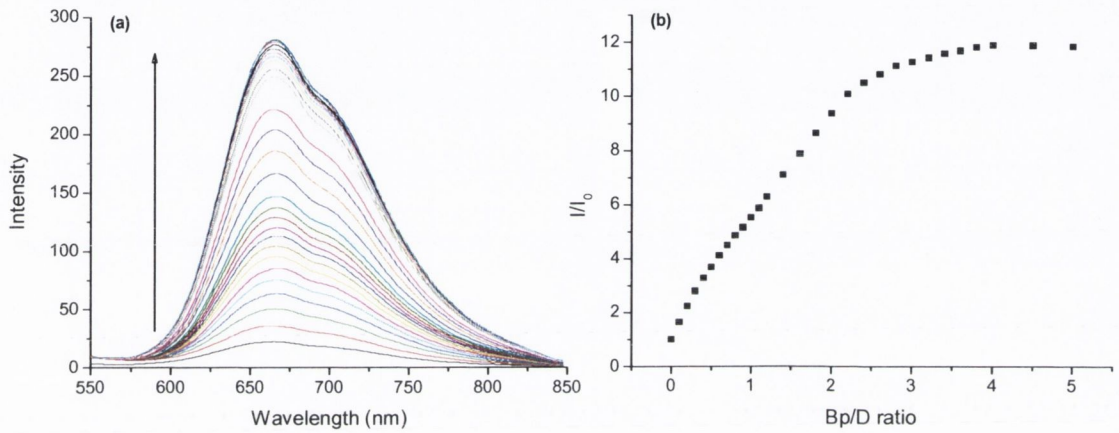

Figure 2.31 *(a) Changes in the MLCT emission of* ***60*** *(6.5 μM) (excitation at 450 nm) upon addition of* $[poly(dG\text{-}dC)]_2$ *(0 – 32.5 μM base pairs) in 10 mM phosphate buffer, at pH 7. (b) The relative change in integrated emission intensity.*

An initial rapid change in emission intensity was observed up to a BP/D ratio of approximately 0.6, followed by a more gradual increase up to the plateau. The second part of the profile is slightly steeper than that seen in the presence of st-DNA, and as such a plateau is reached at slightly lower base pair equivalents. The half point of the intensity change occurs at approximately 1.1 base pair equivalents. However, the overall intensity change is the same for both st-DNA and $[poly(dG\text{-}dC)]_2$.

The profile in the presence of $[poly(dA\text{-}dT)]_2$ followed the same basic shape but the magnitude of the overall change was less at 7.3 fold, as shown in Figure 2.32. An initial change was observed up to a Bp/D ratio of approximately 0.6, followed by a more gradual increase to the plateau. The half-point in emission intensity change occured at approximately 1.2 base pair equivalents.

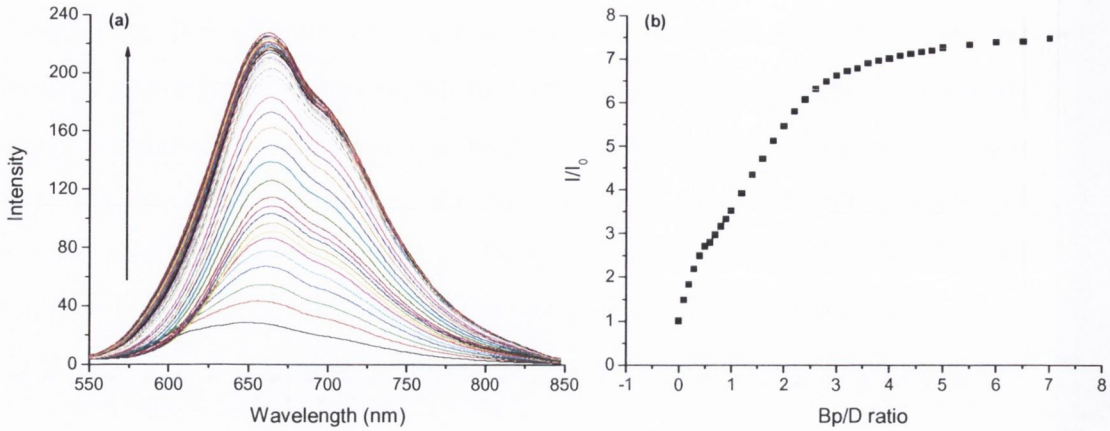

Figure 2.32 *(a) Changes in the MLCT emission of* ***60*** *(6.5 μM) (excitation at 450 nm) upon addition of [poly(dA-dT)]$_2$ (0 – 45.5 μM base pairs) in 10 mM phosphate buffer, at pH 7. (b) The relative change in integrated emission intensity.*

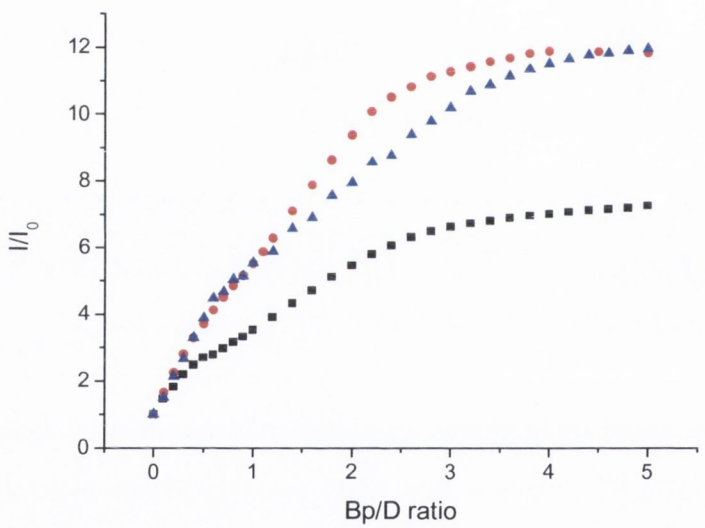

Figure 2.33 *Relative changes in the MLCT emission of* ***60*** *(6.5 μM) (excitation at 450 nm) with increasing concentration of [poly(dG-dC)]$_2$ (●), [poly(dA-dT)]$_2$ (■) and st-DNA (▲), all in 10 mM phosphate buffer, pH 7. Recorded as the integrated intensity of the MLCT emission band.*

Shown in Figure 2.33 are the overlayed emission profiles for **60** with added st-DNA, [poly(dG-dC)]$_2$ and [poly(dA-dT)]$_2$ respectively. From examination of this it is apparent that the emission from the MLCT excited state in **60** was enhanced to a greater degree in the presence of GC rich sequences than AT rich sequences. This selectivity is the opposite to that observed for the Ru(II)-quinoline system referred to above. Overall, the changes in the presence of st-DNA, [poly(dG-dC)]$_2$ and [poly(dA-dT)]$_2$ follow the

same shape profile, the difference being the degree of observed emission enhancement. Consequently, **60** may be regarded as possessing similar affinity for the different DNA sequences, a conclusion that was supported by ethidium bromide displacement assays as will be discussed in a later section.

Two issues resulting from these selectivity studies need to be addressed. Firstly, despite showing equal binding affinity for both GC and AT rich sequences, some feature of binding to the former leads to greater emission enhancement, and secondly, binding to st-DNA leads to a very similar enhancement as observed for the binding of **60** to $[poly(dG\text{-}dC)]_2$, even though the former possesses a heterogeneous base content. Some of the main differences between AT and GC regions are structural in nature, where for instance the minor groove in AT rich regions is narrower,[156] and AT base pairs have a greater propensity to adopt twisted propeller conformations, as depicted in Figure 2.34.[157]

Figure 2.34 *Representation of the propeller twist perturbation at a nucleic acid base pair.*

It is likely that the narrower minor groove in $[poly(dA\text{-}dT)]_2$ enforces a different binding mode to that which results with the other two DNA polymers. Hence, the Ru(II) centre may not fit into the groove in the same manner, and this can result in a different degree of emission enhancement. The explanation fits with the results obtained for the titration of **60** with $[poly(dG\text{-}dC)]_2$ and st-DNA, which although quite different to each other in terms of sequence, are very similar in terms of overall three dimensional structure.

Besides structural differences the two types of base pair also display differing charge distribution.[157] While AT base pairs have relatively small and well spread out positive and negative charges, GC base pairs have a large positive partial atomic charge on the cytosine, and a large negative partial atomic charge on the guanine moiety. These distributions are represented schematically in Figure 2.35. It is possible that complex **60** binds at GC and AT sites in a similar manner, *i.e.* insertion of the 1,8-naphthalimides between the base stack with external association of the metal complex component. However, the distinct charge distribution at each site may have differing effects on the quenching process in the metal complex. The process is interrupted more efficiently by

GC base pairs than by AT base pairs. To the best of our knowledge no literature precedent currently exists for sequence specific luminescence enhancement by such a mechanism. This proposal, however, does not address the similarities in enhancement for st-DNA and $[poly(dG\text{-}dC)]_2$. More extensive photophysical studies, with these and other DNA polymers are necessary, to gain a more complete understanding of the mechanism responsible for the differential luminescence enhancement. At this point the explanation based on structural differences between the nucleic acids is regarded as being more likely.

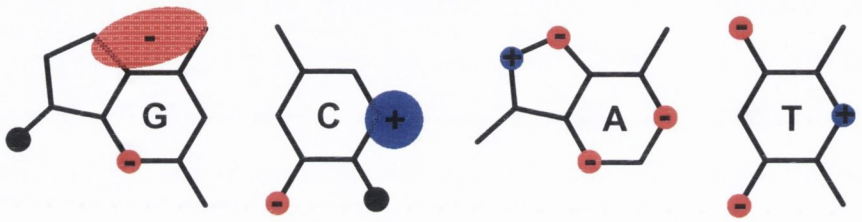

Figure 2.35 *Representation of the charge distribution in GC and AT base pairs.*

2.5.2.3 DNA Thermal Denaturation Studies of 60

Thermal denaturation studies were also carried out on **60** to further investigate the nature of the binding interaction with DNA. These measurements were carried out in the same manner as for **37** – **40**, as described in Section 2.4.3, and are shown in Figure 2.36. From examination of Figure 2.36, it is apparent that **60** stabilises duplex DNA to a greater extent than observed for the 4-nitro-1,8-naphthalimide analogue **40**, giving an increase in T_m of 2 °C at a Bp/D ratio of 10 and 5.7 °C at a Bp/D ratio of 5. These results again emphasise the higher affinity of **60** for DNA, and suggests that the mode of interaction likely involves classical intercalation of the 1,8-naphthalimides. The mode of interaction of this system is not "diffuse" in nature like that of **40** despite them having the same degree of flexibility and access to a large number of conformations. Interestingly, at both P/D ratios the melting transition went to completion in the temperature range employed, whereas **37** – **39** displayed large increases in T_m, but with profiles that had not reached a plateau at 90 °C.

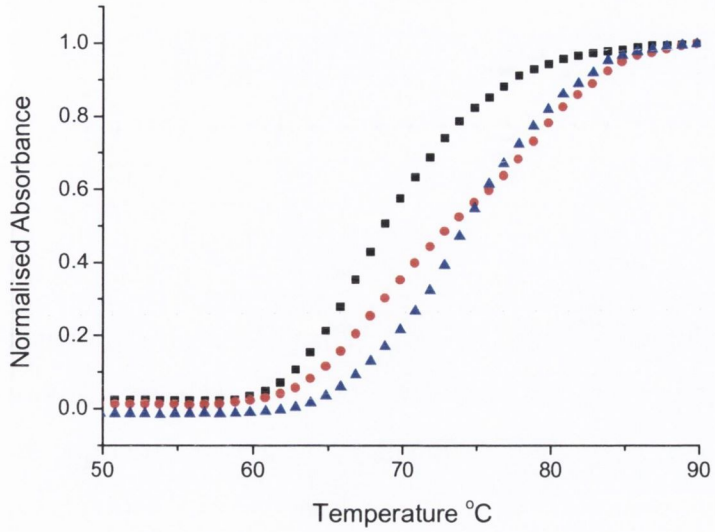

Sample	T_m
DNA	68 °C (± 10%)
60 (Bp/D 10)	70 °C (± 10%)
60 (Bp/D 5)	73.7 °C (± 10%)

Figure 2.36 *Thermal denaturation curves of st-DNA (150 μM) in 10 mM phosphate buffer, pH 7, in the absence (■) and presence of* ***60*** *at P/D ratio of 20 (●) and 10 (▲).*

2.5.2.4 Circular Dichroism Studies of 60

The CD changes observed for **60** were very similar to those observed for **37** – **40**, in that an ICD of moderate strength occurred in the MLCT region with much larger changes in the region of absorption of the DNA. Thus a detailed discussion will not be given here. The important conclusion from CD changes of DNA in the presence of **60** is that the metal centre is held in place in the chiral environment of DNA. The CD spectrum of **60** in the presence of DNA is included in the Appendix.

2.5.2.5 Ethidium Bromide Displacement Assay of 60

It was not possible to calculate binding constants from UV/Visible titration data as discussed in Section 2.4.2.1, and as such displacement assays were useful in this case in providing a measure of the overall affinity of **60** for DNA. The affinities determined using the EtBr displacement assay are detailed in Table 2.11. The complex displayed extremely high affinity for DNA, the overall affinity being approximately twice that of ethidium bromide.[154] No selectivity in binding was, however, observed to the DNA alternating co-polymers $[poly(dG\text{-}dC)]_2$ and $[poly(dA\text{-}dT)]_2$, in contrast to the selectivity in emission response of the system to these sequences.

Table 2.11 *Binding affinities of* ***60*** *from EtBr displacement assays.*

DNA type	Binding constant
Salmon testes	1.7×10^7
$[poly(dA\text{-}dT)]_2$	2.1×10^7
$[poly(dG\text{-}dC)]_2$	2.1×10^7

Modification to the initial design by incorporation of a 3-nitro-1,8-naphthalimide in place of a 4-nitro-1,8-naphthalimide has proved successful in generating a more efficient binder and probe of DNA. UV/Visible and emission studies showed **60** to be fully bound to DNA at lower base pair equivalents than its 4-nitro analogue. In addition, larger shifts in melting temperature were observed, and DNA bound ethidium bromide was displaced at lower concentrations. A very interesting, but as yet not fully understood, selectivity in emission response was also observed depending on the DNA sequence. Similar to **40**, complex **60** also approaches the criteria for classification as a "light switch" as it essentially exhibits off / on emission behaviour.

2.6 Conclusions

The results presented in this chapter have shown the strategy of combining Ru(II) polypyridyl with 1,8-naphthalimide functionality in a single complex, to be successful in generating novel photophysical probes for DNA. This study is the first step in building an understanding of the important structural features of such assemblies that control their DNA binding behaviour and resulting spectral responses.

All of the systems presented in this chapter comprised flexible linkers, the lengths of which were shown to have significant effects on the DNA binding properties. It was shown that the pentyl linkers gave rise to greater emission enhancement than the corresponding propyl analogues. This was most likely due to greater separation of chromophore and quencher upon DNA binding. The presence of two 1,8-naphthalimides *vs.* one in these structures was also shown to give rise to greater emission responses for the former.

Slight structural modification of the 1,8-naphthalimide moiety, involving a change in the substitution pattern, had a significant effect on the binding properties of the resulting complexes. Complex **60** displayed improved DNA binding ability and emission response in comparison to its analogue **40**, verifying that the modification to the design was correct. Thus, in addition to the linker, the structural properties of the quencher were also shown to

be important in determining the DNA binding properties of a particular system. This aspect emphasised the ease with which the properties of the assembly may be varied and the possibility that numerous different systems may be prepared using the same basic synthetic methodology. As such the components of the system – the Ru(II) polypyridyl complex (chromophore), the linker and the 1,8-naphthalimide (quencher) may be regarded as modules to be varied depending on the properties required. In subsequent chapters these modules will be systematically varied and their influence on DNA binding investigated.

Chapter 3

Flexible Ru(II)-1,8-naphthalimide Conjugates

3.1 Introduction

In *Chapter 2*, the attachment of a 3- or 4-nitro-1,8-naphthalimide to a Ru(II) polypyridyl complex was found to result in quenching of the metal based MLCT emission, by electron transfer from the Ru(II) centre to the attached chromophore. The addition of DNA was shown to interrupt the quenching process and result in large emission enhancements, in a similar manner to that previously observed for Ru(II)-quinoline conjugates.[97] However, in addition to quenching, the attachment of organic chromophores to Ru(II) polypyridyl complexes may also result in an enhancement of the lifetime.

For instance, Ford and Rogers have shown that it was possible to prolong the luminescence lifetime of Ru(II) polypyridyl complexes, by conjugation to an organic chromophore. An example of such a system is the flexibly linked Ru(II)-pyrene conjugate **65**, which possessed an excited state lifetime of 11.2 μs in degassed acetonitrile.[158]

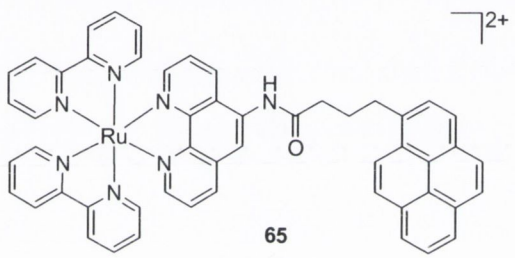

65

This is considerably longer than the lifetime of *ca.* 0.9 μs determined for $Ru(bpy)_3^{2+}$ under identical conditions.[25] Pyrene has a low lying triplet state, that is close in energy to the metal based triplet, and thus the extended lifetime was attributed to a reversible energy transfer, or equilibration, between the triplet states. The observed emission was shown to arise almost exclusively from the ^{3}MLCT, and as such the pyrene was regarded as acting as an energy reservoir. It was shown in separate studies that singlet – singlet energy transfer between the pyrene and the Ru(II) MLCT was also efficient.[159,160] It was subsequently demonstrated that the incorporation of three pyrene moieties around the Ru(II) centre allowed for both efficient sensitization of the MLCT excited state due to singlet – singlet energy transfer, in which the pyrene essentially acts as an antenna, and extended lifetimes due again to the sensitized ^{3}MLCT states being in equilibrium with the triplet states of the pyrene.[161] This work was further extended to arrays incorporating six pyrene moieties which possessed considerably extended excited state lifetimes of 18.1 μs in degassed acetonitrile solution.[162]

Pyrene – Ru(II) conjugates have been extensively studied in organic media, where the goal of many of these studies has been to explore their potential applications in materials science.[163] However, luminescent metal complexes with long excited state

lifetimes are also desirable, for use as biological probes as discussed above, as their emission will persist after the natural background luminescence has diminished. Despite this potential, the interaction of such systems with biological macromolecules such as DNA has been relatively unexplored. The exception to this is conjugate **66**, whose interaction with and photophysical response to DNA was previously investigated within the Gunnlaugsson and Kelly groups, and is detailed in the PhD thesis of Dr. Aoife O' Brien.[164] The photophysical properties of this system proved quite complicated to investigate, but it was shown to bind DNA by intercalation of the pyrene moiety. The binding of **66** to DNA resulted in a moderate emission enhancement, the magnitude of which was reasonably sensitive to the ionic strength of the medium. The DNA binding did not disrupt the equilibrium between the Ru(II) and pyrene moieties, but it did seem to protect the metal centre from quenching by molecular oxygen. This system emphasised the utility of bifunctional molecules as DNA binders and probes, the pyrene acting as an anchor in this case, holding the Ru(II) centre tightly in place with respect to the helix. However, solubility problems and an unusual photoinduced ether bond cleavage limited the potential utility of this system as a DNA probe.

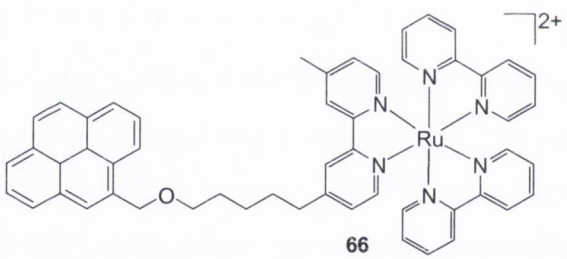

66

Of particular relevance to the work described in this thesis is the system developed by Castellano and co-workers, **67**, which comprised a Ru(II) polypyridyl core with appended 4-piperidinyl-1,8-naphthalimide (PNI) chromophores.[165] This system is somewhat different to **65** and **66** in that the components are linked in a more rigid manner. The PNI chromophore was chosen as an energy donor, as it displays intense singlet fluorescence which overlapped with the Ru(II) MLCT absorption band in the visible region, and as such was expected to favour efficient Förster-type resonance energy transfer. Additionally, the PNI chromophore possesses low lying triplet states, that are nearly isoenergetic with the ^{3}MLCT states, allowing for the possibility of an excited state equilibrium similar to that observed for the pyrene derivatives discussed above. Both of these processes were shown to occur, and the excited state lifetime of **67**, when recorded in degassed acetonitrile, was shown to be extremely long lived at 60.8 μs. Therefore, this study showed that a selection of organic chromophores, with appropriate singlet and triplet

energies conjugated to a Ru(II) centre, can yield visible light harvesting complexes with extended excited state lifetimes.

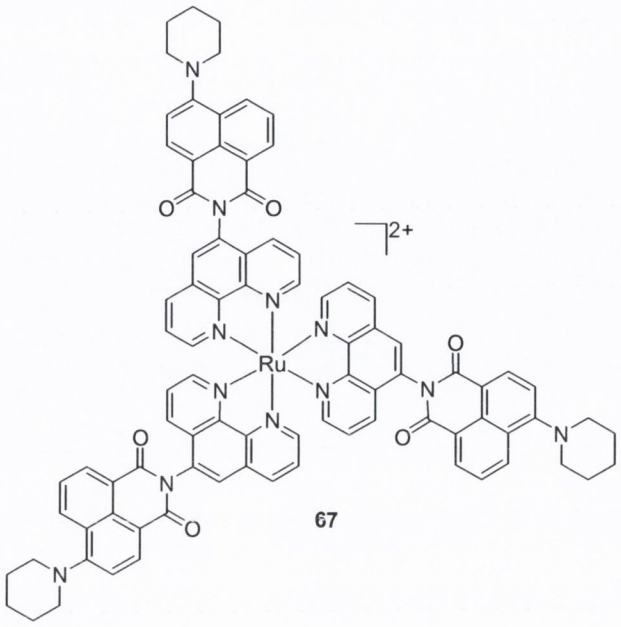

67

In this Chapter complexes comprising a Ru(II) polypyridyl core, appended with a C_5 linker to an unsubstituted 1,8-naphthalimide are considered. Both the mono, **68** and bis, **69** complexes were prepared.

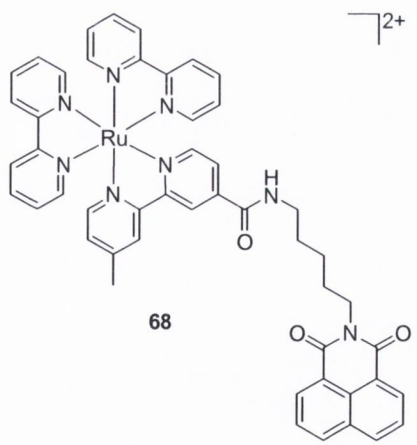

68

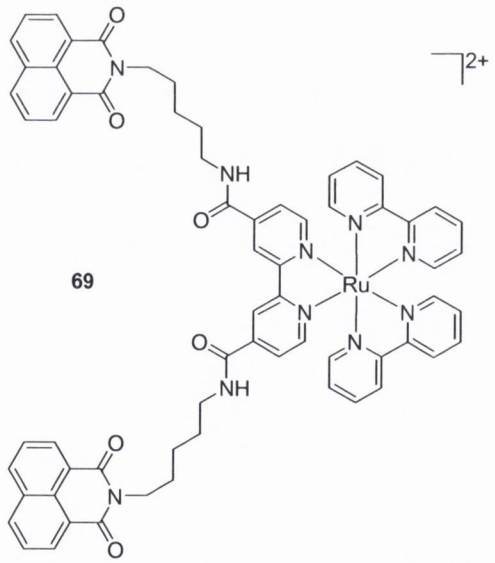

69

The unsubstituted 1,8-naphthalimide chromophore was chosen as an energy donor as it displays singlet fluorescence which should overlap the Ru(II) MLCT absorption, and possesses low lying triplet excited states which are very close in energy to those calculated for the Ru(II) complex core.[119] Therefore like pyrene, and 4-piperidinyl-1,8-naphthalimide, the donor is a promising candidate for both singlet energy transfer and

triplet state equilibrium. The proposed photophysical scheme for **68** and **69** is shown in Figure 3.1.

Another important property of the un-substituted 1,8-naphthalimide, distinguishing it from the nitro derivatives employed in *Chapter 2*, is that it is not sufficiently oxidizing to accept an electron from the excited states of the Ru(II) complex. Therefore, it should not be expected to quench the MLCT emission, in the manner observed in *Chapter 2*. This was deduced from theoretical calculation, using the simplified Rehm-Weller equation (**.1**), from which a driving force for electron transfer of approximately 0.12 eV for **68** and 0.26 eV for **69** was determined, respectively.[166] From the positive free energy changes calculated for both systems, it is apparent that electron transfer from the excited Ru(II) complex to the 1,8-naphthalimide would be thermodynamically unfavourable in both cases.

$$\Delta G = -[(E_{1/2}\ \mathbf{Naph/Naph^{\bullet -}} - E_{1/2}\ \mathbf{Ru^{3+/2+}})] - E^* \qquad (3.1)$$

where E* is the excitation energy of the vibrationally relaxed MLCT excited state, estimated from the luminescence maximum as just described.

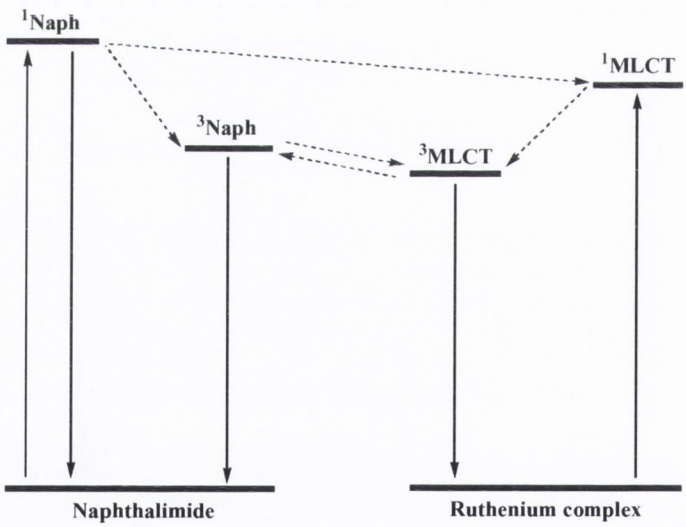

Figure 3.1 *Qualitative energy level diagram for* ***68*** *and* ***69*** *showing possible energy transfer from ^{1}Naph to ^{1}MLCT, and excited state equilibrium between ^{3}Naph and ^{3}MLCT. Radiative transitions are represented by solid lines and non-radiative transitions by dashed lines.*

As demonstrated in *Chapter 2*, DNA binding can have significant effects on the efficiency of electron transfer processes in donor – acceptor systems.[100] In the systems

described in this Chapter it was expected that energy transfer from the 1,8-naphthalimides to the Ru(II) centre would occur, due to the closely lying energy levels of their excited states. There are two possible mechanisms by which energy transfer can occur; the Förster or the Dexter mechanism. The former, also known as fluorescence resonance energy transfer (FRET), relies on the distance dependent transfer of energy from a donor fluorophore to an acceptor, and is widely used in biology for measuring extremely small distances (Å scale) with high accuracy.[167] The rate of Förster or resonance energy transfer decreases as R^{-6}.[146] Energy transfer by the Dexter or exchange mechanism is also highly distance dependent, with the rate of energy transfer decreasing exponentially with increasing separation of the donor and acceptor.[146]

The presence of energy transfer processes in **68** and **69** will firstly be investigated using a variety of spectroscopic techniques. In addition, the nature of their interaction with and affinity for DNA will be determined, as will the effect if any that DNA binding has on the communication between the 1,8-naphthalimide and Ru(II) chromophores. The presence of intramolecular stacking interactions of the 1,8-naphthalimides in **69** will also be investigated, and whether this could act as an additional signalling process for DNA interaction.

3.2 Synthesis

The mono-1,8-naphthalimide complex **68** and bis-1,8-naphthalimide complex **69** were synthesised, purified and characterised in the same manner as their 4-nitro-1,8-naphthalimide containing counterparts discussed in *Chapter 2*. The synthesis of each of these conjugates is briefly discussed in the following sections.

3.2.1 Synthesis of Ru(II)-mono-1,8-naphthalimide Conjugate 68

Complex **68** was synthesised according to the procedure in Scheme 3.1. The first step involved condensation of the protected amine **45** with 1,8-naphthalic anhydride, **70**, by suspension of the two reactants in toluene, in the presence of Et_3N, and heating of the mixture at reflux for 24 hours under an argon atmosphere. The reaction mixture was worked up in the same manner as described in *Chapter 2*. This afforded **71** as an orange oily solid in 82% yield. Removal of the protecting group was effected by stirring **71** in 1:1 TFA/CH_2Cl_2 for 1 hour. After drying under high vacuum the product **72** was obtained as a pale brown solid in quantitative yield. Coupling to bipyridine was achieved in the same manner as described in *Chapter 2*, in which the acid chloride, **52** was dissolved in

anhydrous CH_2Cl_2 and added dropwise to a solution of **72** in anhydrous CH_2Cl_2 at 0 °C, in the presence of Et_3N. Workup and purification was carried out as for the ligands in *Chapter 2*, giving the product **73** as a pale brown solid in 83% yield. Ligand **73** was complexed in the same manner as described in *Chapter 2*, affording the product **68** as a red solid in 86% yield. Full characterisation data for each of the intermediates in the synthesis of **68** is given in *Chapter 7*.

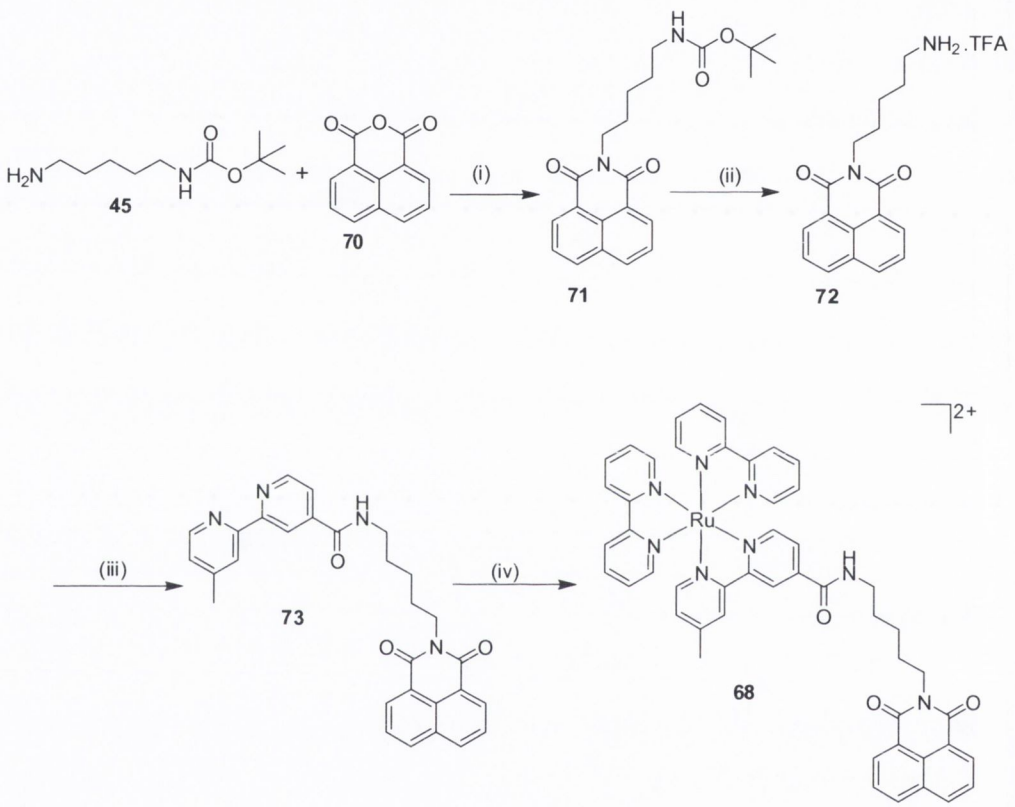

Scheme 3.1 *Synthesis of complex* ***68****. Reagents and conditions: (i) Toluene, Et_3N, (ii) TFA/CH_2Cl_2 1:1, (iii)* ***52****, CH_2Cl_2, Et_3N, 0 °C, (iv) $Ru(bpy)_2Cl_2$, DMF/H_2O.*

The ^1H NMR spectrum (400 MHz, CD_3CN) of **68** is shown in Figure 3.2. Additionally, ESMS analysis of this complex showed the presence of a peak at 892.2420 corresponding to the M^{2+} ion.

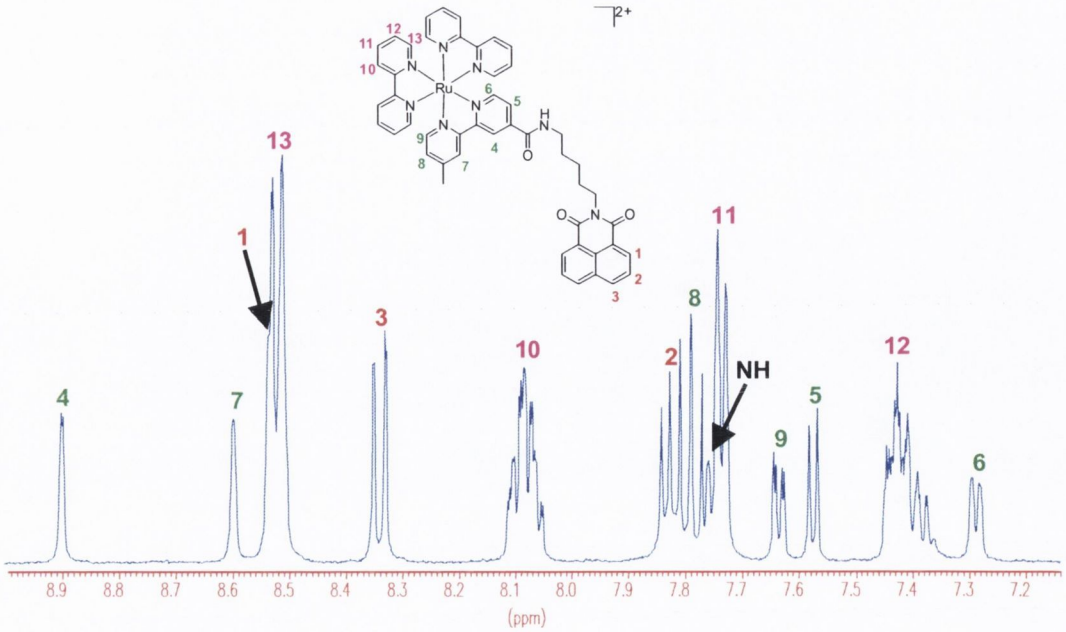

Figure 3.2 *^{1}H NMR spectrum of* ***68*** *(400 MHz, CD_3CN) showing the aromatic region.*

3.2.2 Synthesis of Ru(II)-bis-1,8-naphthalimide Conjugate 69

Complex **69** was synthesised according to the procedure in Scheme 3.2.

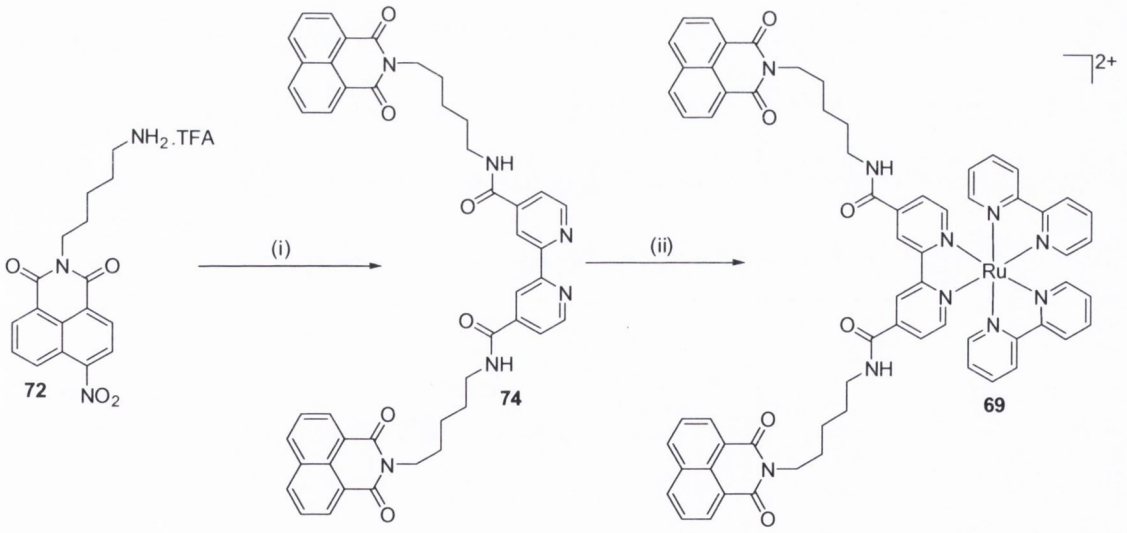

Scheme 3.2 *Synthesis of complex* ***69****. Reagents and conditions: (i)* ***52****, CH_2Cl_2, Et_3N, 0 °C, (ii) $Ru(bpy)_2Cl_2$, DMF/H_2O.*

The acid chloride **56** was dissolved in anhydrous CH_2Cl_2 and added dropwise to a solution of **72** in anhydrous CH_2Cl_2 at 0 °C, in the presence of Et_3N. Workup of the resulting residue was carried out as in *Chapter 2*, which afforded the product **74** as a purple

solid in 95% yield. Complexation and purification were carried out as before giving the product **69** as a red solid in 76% yield.

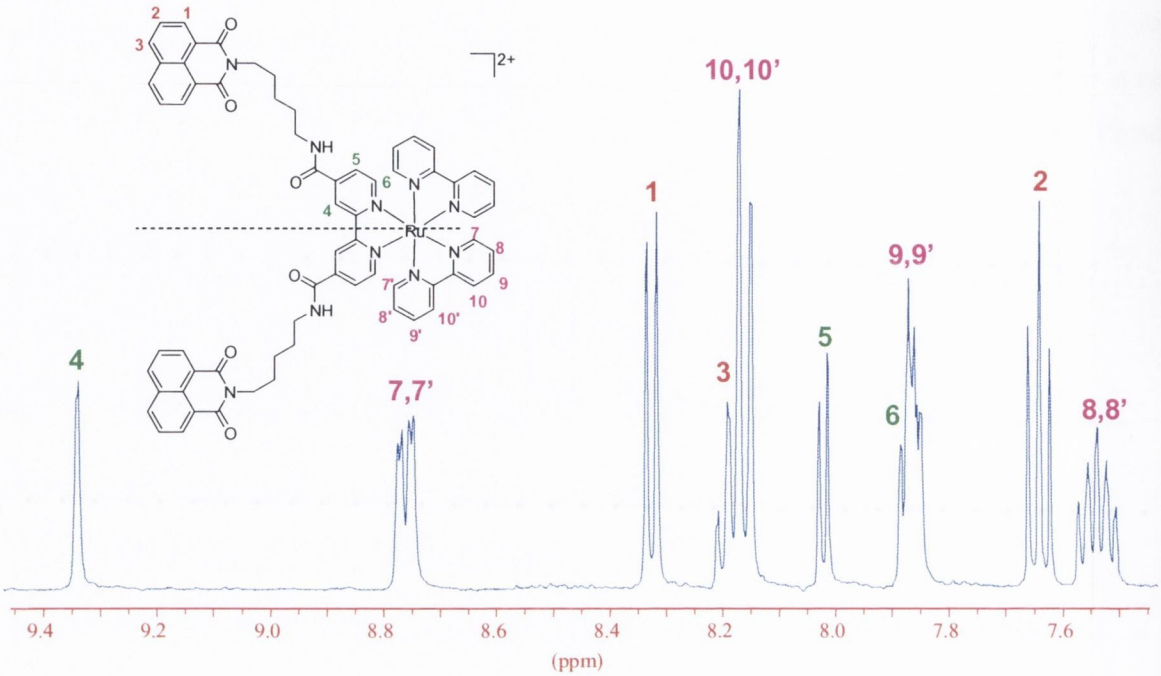

Figure 3.3 *^{1}H NMR spectrum of **69** (400 MHz, CD_3CN) showing the aromatic region.*

The ^{1}H NMR spectrum of **69** (400 MHz, CD_3CN) is shown in Figure 3.3, which is simpler than that of **68** due to the C_2 symmetry in the former. Additionally, ESMS analysis of this complex showed the presence of a peak at 1186.3412 corresponding to the M^{2+} ion. This complex was further characterised by ^{13}C NMR, IR and elemental analysis.

3.3 Photophysical Properties of 68 and 69

3.3.1 UV/Visible Absorption of 68 and 69 in Aqueous Solution

The absorption, excitation and emission spectra of **68** and **69** are depicted in Figures 3.4a and 3.4b, respectively. As for their 4-nitro-1,8-naphthalimide analogues, the UV/Visible absorption spectra of **68** and **69** in buffered aqueous solution exhibit bands characteristic of both chromophores. Complex **68** displayed an intense band centred around 286 nm, which was attributed mainly to π-π^* intraligand transitions, a band at 338 nm assigned to the π-π^* 1,8-naphthalimide transitions, and a longer wavelength absorption band at 459 nm due to the metal to ligand charge transfer (MLCT) transitions of the Ru(II) centre. In the case of **69**, these bands appear at 286 nm, 345 nm and 480 nm, respectively.

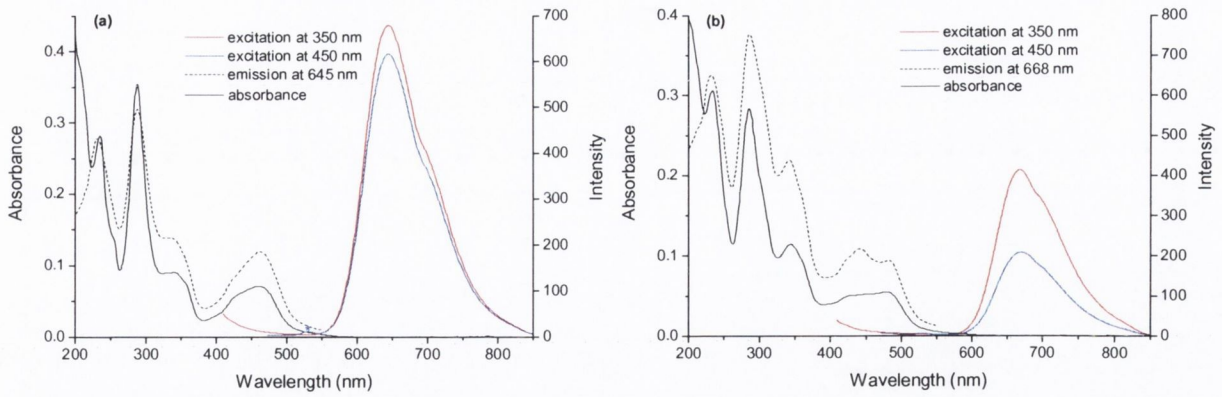

Figure 3.4 *UV/Visible, excitation and emission spectra of (a)* ***68*** *(6.5 μM) and (b)* ***69,*** *both in 10 mM phosphate buffer, at pH 7. The water Raman band is denoted by *.*

The MLCT bands of both **68** and **69** were somewhat broad and red shifted compared to that of $Ru(bpy)_3^{2+}$, due to the presence of the amide substituted bipyridine ligands, *c.t. Chapter 2.*[137] The main difference is in the position of the 1,8-naphthalimide transitions, which were blue shifted. A summary of the absorption properties of **68** and **69** is given in Table 3.1, along with the properties of reference complex **41** for comparison.

Table 3.1 *Absorption properties of* ***68, 69*** *and* ***49*** *in 10 mM phosphate buffer, at pH 7 at 298 K.*

Complex	λ_{max} (nm) [ϵ (M^{-1} cm^{-1})]		
	π-π* IL	π-π* Naph	MLCT
68	287 [55000]	338 [14300]	459 [10900]
69	286 [43700]	345 [16500]	480 [8000]
41	286 [55200]	------	475 [10900]

It is important to note, that similar to the complexes discussed in *Chapter 2*, bands corresponding to the 1,8-naphthalimide and Ru(II) chromophores of **68** and **69** may be resolved, which will be of considerable importance when examining the interaction of the components of each complex with DNA.

To examine the degree of stacking of the 1,8-naphthalimides, and the presence of any ground state electronic interactions in the bis-1,8-naphthalimide complex **69**, an additive spectrum was constructed, using the reference Ru(II) complex **41** and the water soluble 1,8-naphthalimide derivative **75**. This spectrum is shown in Figure 3.5. The first apparent feature is the greater absorbance in the MLCT region for the summed spectra in comparison to complex **69**. This observation suggests that there is some

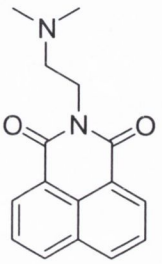

75

degree of electronic interaction between the Ru(II) centre and the 1,8-naphthalimide in the ground state. In the 1,8-naphthalimide region, centred at 345 nm, the absorbance is significantly less for **69** than that in the calculated spectrum, where no interaction exists between the individual components. Absorbance at this band is *ca.* 47% reduced, in comparison to that observed for the combined components. This observation is indicative of extensive stacking interactions of the 1,8-naphthalimides, that leads to hypochromicity in absorbance.[138] This could be expected due to the flexible linkers and the propensity of 1,8-naphthalimides to stack in polar solution, due to their planar and hydrophobic nature.[138]

The degree of stacking of the 1,8-naphthalimides in **69** (47%) is greater than that of the 4-nitro-1,8-naphthalimides in **40** (30%) (discussed in the previous Chapter) and may be attributed to the presence of the nitro substituents, which reduce the overall stacking ability of the chromophore, due to the substituent being slightly twisted out of plane. The observation that the 1,8-naphthalimide components of **69** are self associated is significant in relation to DNA binding, which could perturb any such stacking process. Electronic interactions between the 1,8-naphthalimides and the Ru(II) centre, may also contribute to the overall hypochromicity in the absorption region of the 1,8-naphthalimide in **69**. However, it was not possible to evaluate individual contributions to the overall diminished absorbance in this region.

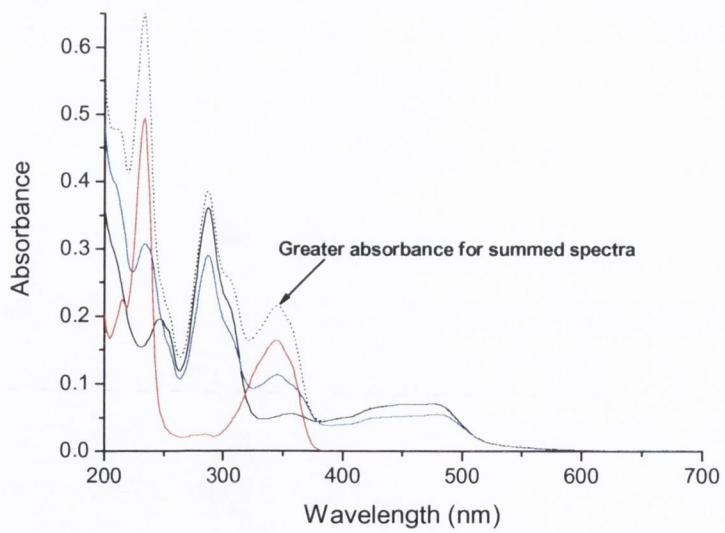

Figure 3.5 *UV/Visible absorption spectra of* ***41*** *(6.5 μM) (——),* ***75*** *(13 μM) (——),* ***41*** *+* ***75*** *(------) and* ***69*** *(6.5 μM) (——). All solutions in 10 mM phosphate buffer, at pH 7.*

3.3.2 Emission Properties of 68 and 69 in Aqueous Solution

Excitation of an aqueous solution of **68** at 450 nm resulted in a single observable emission band at 645 nm, as shown in Figure 3.4a. Excitation of **69** at the same wavelength resulted in an emission band centred at 670 nm, as shown in Figure 3.4b. The decreasing energy of these emission bands compared to $Ru(bpy)_3^{2+}$, is attributed to the presence of the amide substituted bipyridine ligands, as discussed in *Chapter 2*.[168] As was expected in the initial design, emission from the Ru(II) centre was not quenched in these systems by the presence of the 1,8-naphthalimide chromophores. This may clearly be seen from the quantum yields in Table 3.2, for excitation at 450 nm, where the quantum yield of 0.014 determined for **69** is the same as that calculated for **41**. The quantum yield of **68** was determined as 0.018, which also suggests the absence of any quenching of the metal centre. The excited states of **68** and **69** were, however, shown to be quenched by dissolved oxygen, the quantum yields being somewhat increased upon degassing for both systems, Table 3.2.

Table 3.2 *Emission properties of **68** and **69** in 10 mM phosphate buffer,at pH 7 at 298 K. Both at 6.5 μM concentration. Excitation at 450 nm.*

Complex	λ_{em} (nm)	Φ_f (± 10%) aerated	Φ_f (± 10%) de-gassed*
68	645	0.018	0.025
69	670	0.014	0.020

*Degassing was performed by bubbling argon through a solution of complex for at least 10 minutes.

Excitation of an aqueous solution of **68** at its 1,8-naphthalimide absorption maximum at 338 nm resulted in an intense Ru(II) emission at 645 nm, whereas excitation of **69** at 345 nm resulted in emission centred at 670 nm. This is in striking contrast to the conjugates discussed in *Chapter 2*, where excitation at this wavelength resulted in extremely weak emission from the metal centre, contributing significantly less to Ru(II) based emission than direct excitation at the MLCT. For both **68** and **69** significant contribution to MLCT based emission was observed in the region of absorption of the 1,8-naphthalimide, suggesting the presence of efficient singlet – singlet energy transfer, from ^{1}naphthalimide to the ^{1}MLCT excited state.

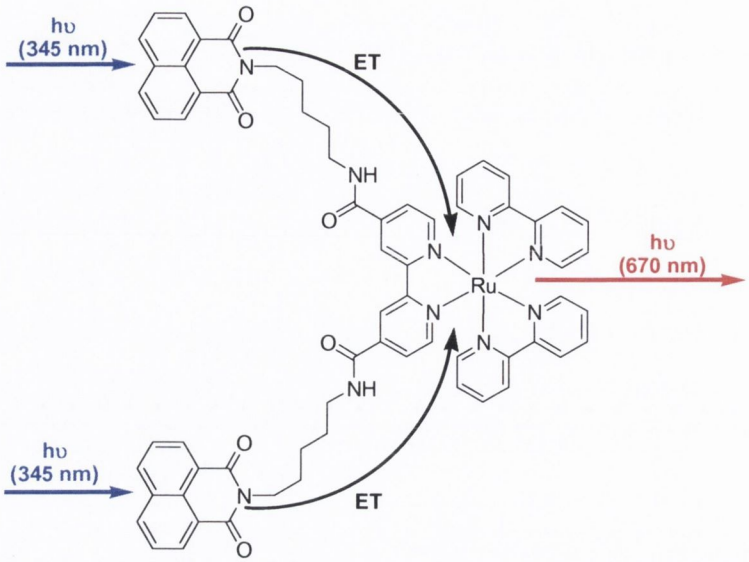

Figure 3.6 *Representation of the antenna effect in which the excited state energy of the 1,8-naphthalimides is transferred to the Ru (II) MLCT excited state.*

This is most clearly seen in the excitation spectra for these derivatives, where the contribution from excitation at the 1,8-naphthalimide absorption band relative to direct excitation at the MLCT can be seen. In fact the absorption and excitation spectra are close to being super-imposable. Furthermore, very weak emission from the 1,8-naphthalimide was observed in both cases, suggesting that most of the excitation energy is passed on to the Ru(II) centre through an energy transfer mechanism. The contribution to Ru(II) emission from the 1,8-naphthalimides in **69**, was much greater than for **68**, which indicates that the 1,8-naphthalimide acts as an antenna, by harvesting the light energy and passing it on to the Ru(II) excited state. This process is represented schematically in Figure 3.6.

The significant contribution from the 1,8-naphthalimide to the Ru(II) emission can also be seen clearly in Figure 3.7, where the excitation spectra for emission from the MLCT state of **41** and **69** are compared. Here, the contribution from direct excitation at the MLCT is approximately the same for both systems, however, the contribution around 350 nm is much smaller for **41**, which suggests that there is less contribution to the metal based emission than direct excitation of the MLCT absorption band. In contrast to these results, for **69** a much greater contribution is observed at 350 nm, resulting in almost twice the relative intensity in comparison to direct excitation at the MLCT. These observations suggest an efficient energy transfer pathway from the un-substituted naphthalimide to the Ru(II) centre.

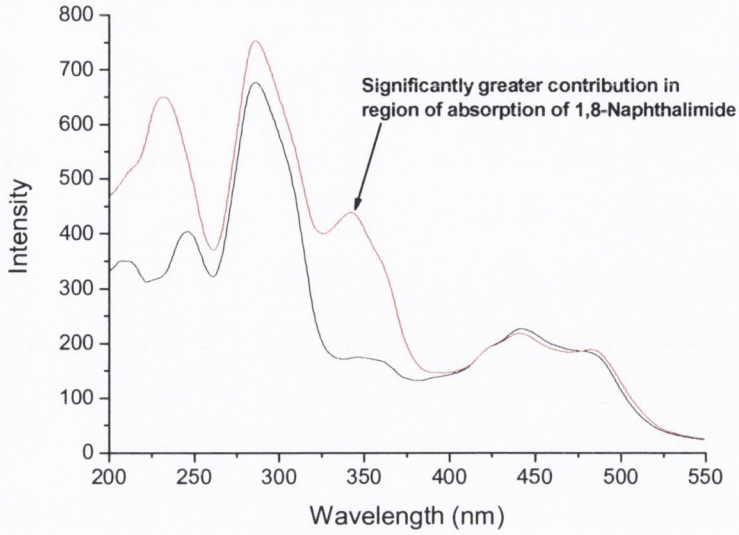

Figure 3.7 *Excitation spectra (emission at 670 nm) of* ***41*** *(——) and* ***69*** *(——), both at 6.5 μM concentration in 10 mM phosphate buffer, at pH 7.*

Complexes **68** and **69** have fulfilled a number of the design criteria set out at the beginning of this Chapter, in that they are strongly emissive in aqueous solution and display a light harvesting antenna effect by the constituent 1,8-naphthalimides. Due to the greater light harvesting effect in complex **69**, this derivative was chosen for further photophysical studies as detailed in the following section.

3.3.3 Further Photophysical Study of 69

The emission properties of **69** and **41** were recorded in gassed and degassed acetonitrile (CH_3CN) solutions. Reference compound **41** displayed an emission maximum (λ_{max}) at 650 nm in CH_3CN solution, as shown in Figure 3.8a. Quantum yields of 0.021 and 0.061 were determined for this complex in gassed and degassed CH_3CN solution, respectively, Table 3.3. The three fold emission enhancement observed upon degassing is typical for Ru(II) polypyridyl complexes, as their luminescence is known to be quenched by oxygen.[169]

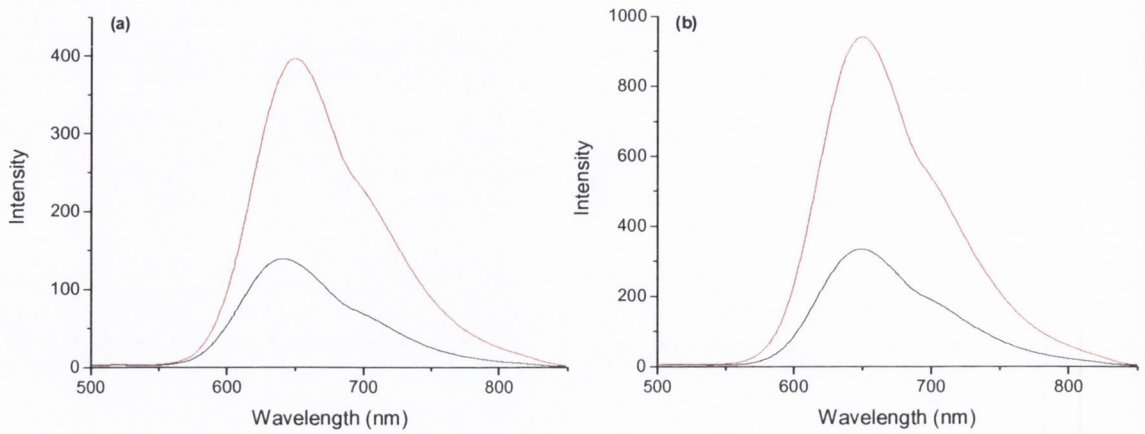

Figure 3.8 *Emission spectra of (a)* ***69*** *and (b)* ***41*** *in gassed (——) and degassed (——) CH_3CN, both at 6.5 μM (excitation at 450 nm).*

Complex **69** displayed quite similar behaviour, exhibiting a λ_{max} at 650 nm, as shown in Figure 3.8b, and Φ_F of 0.021 and 0.064 in gassed and degassed CH_3CN, respectively, Table 3.3. Greater enhancements in emission quantum yield were observed upon degassing an CH_3CN solution of **69**, over an aqueous solution, due to the higher oxygen content in the former ($[O_2] = 1.9 \times 10^{-3}$ mol/L for CH_3CN under 0.21 Atm O_2).[170] From initial analysis, **69** therefore seems to display very similar emission behaviour in CH_3CN solution to its reference **41**.

Table 3.3 *Emission properties of* ***41*** *and* ***69*** *in CH_3CN at 298 K.*

Complex	λ_{em} (nm)	Φ_f (± 10 %) gassed	Φ_f (± 10 %) de-gassed*
41	650	0.021	0.061
69	650	0.021	0.064

*Degassing was achieved by purging of a solution of the complex in CH_3CN with argon for 10 minutes.

To further characterise the excited state properties of **69** and **41**, excited state lifetimes were recorded in CH_3CN and aqueous buffer solution, under both gassed and degassed conditions, using time correlated single photon counting (excitation at 337 nm, with absorbance at 337 nm of 0.2). These experiments were necessary to determine if triplet equilibrium was occurring between the excited states of the 1,8-naphthalimide and Ru(II) components of **69**. A summary of the results are given in Table 3.4.

***Table 3.4** Lifetimes of **41** and **69** determined at 298 K *.*

No.	τ_{em} (ns) buffer	τ_{em} (ns) deoxygenated buffer	τ_{em} (ns) acetonitrile	τ_{em} (ns) deoxygenated acetonitrile
41	320.4	341.0	352.5	1082.0
69	351.1	388.5	389.4	1385.8

*Each lifetime represents an average of six measurements. In all cases the data was fit to a single exponential function, with R^2 values in the range 0.98 – 0.99.

Both complexes **41** and **69** possessed similar lifetimes under all of the conditions investigated, as detailed in Table 3.4. Hence, it appears that an equilibrium does not exist, between the triplet excited state of the 1,8-naphthalimide and that of the Ru(II) complex. If such an equilibrium existed, the lifetime of **69** would be expected to be very much increased over that of the reference compound **41**. The minor increases in lifetime displayed by **69** over the reference may be attributed to the singlet – singlet energy transfer from the 1,8-naphthalimide.

In summary, from the analysis of the photophysical properties of **68** and **69** in solution it may be concluded that the 1,8-naphthalimide moieties act as antennae, passing their excited state energy to the metal centre as expected. This was particularly evident in the excitation spectra for both derivatives, where significant contribution to Ru(II) emission was observed in the region of absorption of the 1,8-naphthalimide. However, given that the excited state lifetime of **69** was not extended, compared to the reference **41** with no appended 1,8-napthalimides, it seems that equilibrium between the triplet states of the chromophores does not occur. Despite this, **68** and **69** possessed many of the features that were regarded as desirable for use as nucleic acid probes. It was expected that these complexes would display interesting and potentially useful photophysical changes upon binding to DNA, the investigation of which is discussed in the following section.

3.4 DNA Binding Interactions of 68 and 69

Similar to the complexes discussed in *Chapter 2*, **68** and **69** were expected to interact with DNA through external electrostatic binding of the Ru(II) centre to the phosphate backbone and intercalation of the 1,8-naphthalimide moieties. The nature of their binding interaction was investigated using a number of spectroscopic techniques.

Significant changes in the spectroscopic properties of both systems were observed, a discussion of which is provided in the following sections.

3.4.1 Changes in the UV/Visible Absorption of 68 with DNA

The interaction of both complexes with st-DNA and with the alternating co-polymers $[poly(dG\text{-}dC)]_2$ and $[poly(dA\text{-}dT)]_2$ was investigated using UV/Visible absorption spectroscopy, in which the changes in the MLCT band at 450 nm, and the 1,8-naphthalimide band at 338 nm were monitored, upon titration with the nucleic acids. The titrations were carried out and analysed in the same manner as described in *Chapter 2*.

As previously noted, the addition of DNA to the control complex **41** resulted in a 10% hypochromism in the MLCT band, which was attributed to electrostatic interaction between the complex and the phosphate backbone of DNA. In the case of complex **68**, the addition of st-DNA resulted in a 37% hypochromism at the 1,8-naphthalimide band, with a smaller change of 16% in the absorbance of the MLCT band, as shown in Figure 3.9.

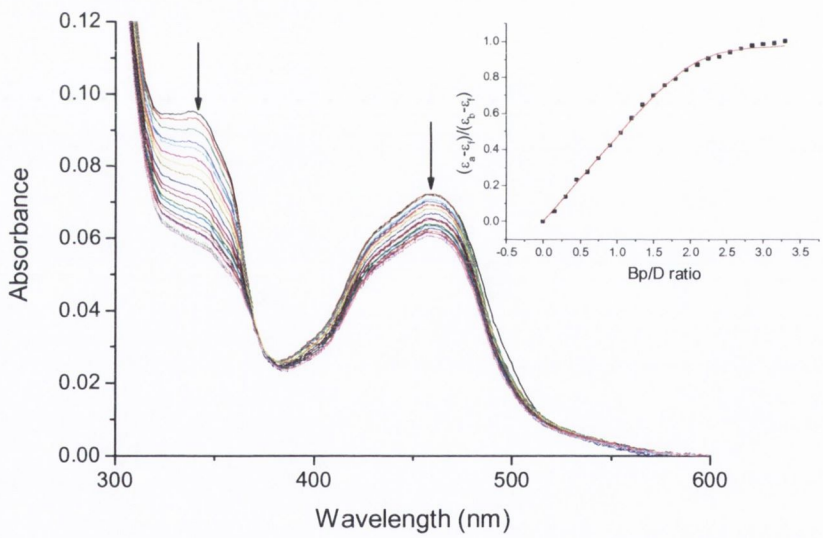

Figure 3.9 *Changes in the UV/Visible spectrum of* ***68*** *(6.5 μM) upon addition of st-DNA (0 – 21.45 μM base pairs) in 10 mM phosphate buffer, at pH 7. Inset: Plot of* $(\epsilon_a-\epsilon_f)/(\epsilon_b-\epsilon_f)$ *at 350 nm vs. equivalents of DNA and the corresponding non-linear fit.*

The changes in absorbance at the MLCT band were greater than those observed for **41**, which suggests that the metal centre in **68** is more tightly bound to DNA. The decrease in the absorbance of 37% for the 1,8-naphthalimide moiety is very similar to that observed for **38**, discussed in *Chapter 2*. However, the 10% hypochromism seen for the MLCT band of **38** was less than that observed for **68**. It seems therefore, that in **68**, the overall

binding mode is similar to that of its 4-nitro-1,8-naphthalimide analogue **38**, the difference being the tighter apparent binding of the metal centre to DNA in **68**. A binding constant of 9.0×10^6 M^{-1} and binding site size of 2.18 base pairs was determined for **68**.

Analysis of the results indicate that the non-substituted 1,8-naphthalimide moiety leads to a system with greater overall affinity for DNA, while the nitro substituent leads to a decreased intercalation ability.

Table 3.5 *DNA binding parameters for* ***68*** *from fits to absorbance data.*

No.	λ(Naph) Hypochromism	λ(MLCT) Hypochromism	Binding constant K (M^{-1})	Binding site size n (base pairs)	R^2
st-DNA	37%	16%	9.0×10^6 (± 1.0)	2.18 (± 0.02)	0.99
[poly(dG-dC)]$_2$	33%	11%	1.3×10^7 (± 0.4)	1.65 (± 0.02)	0.99
[poly(dA-dT)]$_2$	34%	10%	1.0×10^7 (± 0.3)	1.51 (± 0.02)	0.99

Titrations with [poly(dG-dC)]$_2$ yielded moderately different changes in the absorbance at both the 1,8-naphthalimide and the MLCT bands. Addition of the alternating co-polymer resulted in a 33% hypochromic shift for the former band and a *ca.* 11% shift for the latter band, as detailed in Table 3.5. The binding site size was somewhat smaller, being 1.65 base pairs, and the binding constant was determined as 1.3×10^7 M^{-1}. An attempt was also made to fit the data placing a limit on the binding site size to 2 base pairs. This would allow for a more direct comparison of the binding constants obtained with the different types of DNA. However, any such attempts proved unsuccessful and yielded fits with very large associated errors. Overall the affinity may be regarded as being slightly greater than that for st-DNA. The binding, however, seems to occur in a manner that does not hold the metal centre as tightly bound to the helix, or the 1,8-naphthalimides as deeply intercalated, thus giving smaller hypochromic effects.

The hypochromicities in the presence of [poly(dA-dT)]$_2$ were the same as observed for [poly(dG-dC)]$_2$. The binding constant and binding site size were marginally less at 1.0×10^7 M^{-1} and 1.51 respectively. However, taking into account the error associated with this measurement they may be regarded as being approximately the same. Hence, **63** does not show sequence selectivity in binding to these alternating co-polymers.

3.4.2 Changes in the UV/Visible Absorption of 69 with DNA

The titration of **69** with st-DNA resulted in a large hypochromicity of 56% at the 1,8-naphthalimide band, and also a large hypochromicity of 41% at the MLCT band, as shown in Figure 3.10 and Table 3.6.

The most significant result from this particular experiment was the very large hypochromic shift in absorbance of the MLCT band upon DNA binding, being more than twice that observed for any of the bichromophore systems discussed thus far. This could suggest that the Ru(II) centre is being anchored in the DNA grooves, aided by the 1,8-naphthalimide moieties. Partial intercalation of the Ru(II) complex may also be possible, although not very likely due to the minimal extended planar nature of the bipyridine ligands.[31] The binding constant for these interactions was determined as 1.5 x 10^7 M^{-1}, with a slightly larger binding site size of 2.48 base pairs. The increased binding constant falls short of increases that would be expected for cooperative binding effects, which is most likely due to stacking interactions of the 1,8-naphthalimides; an energetically favourable process that must be overcome before they can insert into the helix.

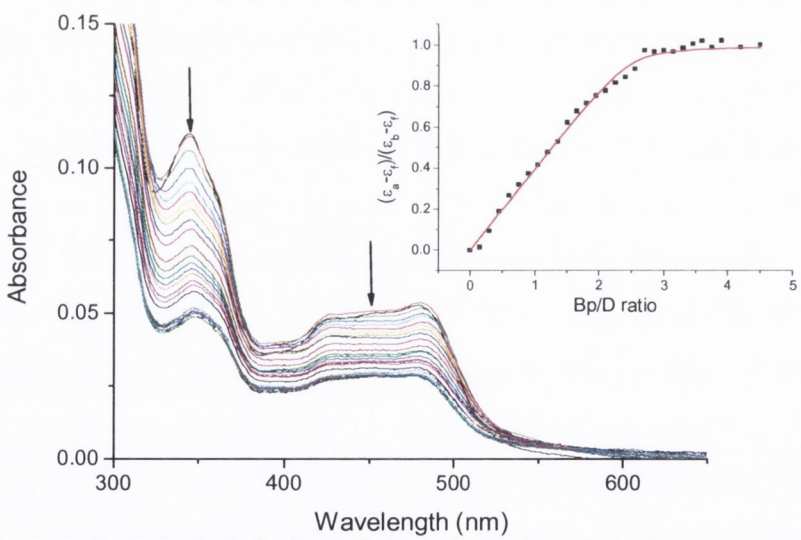

Figure 3.10 *Changes in the UV/Visible spectrum of* ***69*** *(6.5 μM) upon addition of st-DNA (0 – 29.25 μM base pairs) in 10 mM phosphate buffer, at pH 7. Inset: Plot of* $(\epsilon_a-\epsilon_f)/(\epsilon_b-\epsilon_f)$ *at 355 nm vs. equivalents of DNA and the corresponding non-linear fit.*

Table 3.6 *DNA binding parameters for* ***69*** *from fits to absorbance data.*

No.	λ(Naph) Hypochromism	λ(MLCT) Hypochromism	Binding constant K (M^{-1})	Binding site size n (base pairs)	R^2
st-DNA	56%	41%	1.5×10^7 (± 0.5)	2.48 (± 0.02)	0.99
[poly(dG-dC)]$_2$	55%	40%	1.0×10^7 (± 0.4)	2.20 (± 0.03)	0.99
[poly(dA-dT)]$_2$*	42%	19%	--------	--------	---

* Addition of [poly(dA-dT)]$_2$ to a solution of **69** resulted in an initial increase in absorbance that was subsequently followed by a decrease. For this reason attempts to fit the data to the Bard model were unsuccessful.

Addition of [poly(dG-dC)]$_2$ to a solution of **69** gave very similar changes in both 1,8-naphthalimide and MLCT absorption bands, as detailed in Table 3.6, with a binding constant of 1.0×10^7 M^{-1} and binding site size of 2.20.

The absorbance changes for **69** upon titration of [poly(dA-dT)]$_2$ was quite different, with an initial increase in absorbance of 6%, up to *ca.* 0.3 base pair equivalents followed by a decrease of 42% (from the starting point). This behaviour is similar to that seen for the 3-nitro-1,8-naphthalimide complex **60**, and may once again be attributed to some initial disruption in 1,8-naphthalimide stacking by low DNA concentration. However, this presents the question of why this phenomenon was not observed with the other DNA polymers? Upon examining the profile in Figure 3.10 closely, it is, however, apparent that the first addition of DNA results in a very small change in absorbance, with more rapid change occurring from this point on. This is, however, not observed with [poly(dG-dC)]$_2$. Competing with this process is binding of the 1,8-naphthalimides to DNA, and the associated hypochromism. A slightly higher affinity for GC sequences means that the effect is not observed at all, with the situation being intermediate with st-DNA. It must be emphasised that the differences are very subtle, a slight preference for a particular sequence being responsible for this effect. The addition of [poly(dA-dT)]$_2$ to **69** also gave a much smaller decrease in MLCT absorption at 19%. This along with the smaller 1,8-naphthalimide hypochromism suggests that in this case the 1,8-naphthalimides are not as deeply inserted into the helix, and as a result the Ru(II) centre remains externally bound to a greater degree. In addition to this, the narrower minor groove in AT regions may prevent as efficient binding of the Ru(II) centre, or of the system as a whole to the nucleic

acid. Additionally, binding of this complex from the major groove may account for the observed changes.

Both **68** and **69** displayed extremely high affinity for DNA, with binding constants of the order of 10^7 M^{-1} determined for both systems, these being orders of magnitude greater than those observed for the separate components. Of particular significance were the very large hypochromic shifts at the MLCT absorption band of **69** upon interaction with DNA, which are not normally associated with Ru(II) complexes containing simple tris-bipyridine cores.[31] This result emphasised the utility of a second 1,8-naphthalimide moiety, whose presence pulls the Ru(II) centre very tightly in place with respect to the helix. Neither **68** or **69** displayed an apparent preference in binding affinity for AT or GC sequences, although the absorbance decreases for **69** in the presence of $[poly(dA\text{-}dT)]_2$ were less than those in the presence of the other two DNA polymers employed. This was most likely due to a poorer fit of the system as a whole into the DNA helix, in which the Ru(II) centre was restricted by the narrower minor groove, and as a result the 1,8-naphthalimide was not able to insert as efficiently into the helix. The binding behaviour was further investigated using emission spectroscopy as detailed in the following sections.

3.4.3 Changes in the Emission Spectra of 68 and 69 with DNA

As detailed in Section 3.3 both **68** and **69** were substantially emissive in aqueous solution, in contrast to their nitro-1,8-naphthalimide containing analogues **37** – **41** discussed in *Chapter 2*. Furthermore, it was shown that emission from the Ru(II) centre was sensitized by energy transfer from the 1,8-naphthalimides. Hence, it was anticipated that any possible DNA binding might perturb the energy transfer processes, and consequently, emission titrations were carried out to establish if this was the case. Absorption studies demonstrated that 1,8-naphthalimide and MLCT absorption bands were well resolved. Hence, it was possible to excite the two chromophores independently, and monitor the photophysical behaviour in the presence of DNA. Significant differences were observed in the emission responses of **68** *vs.* that of **69** upon binding to st-DNA, $[poly(dG\text{-}dC)]_2$ and $[poly(dA\text{-}dT)]_2$, respectively. Therefore the results for each complex in the presence of the different DNA sequences, and the mechanisms underlying the observed changes will be discussed separately.

3.4.3.1 Emission Titration of 68 with st-DNA

Complex **68** was firstly studied in the presence of st-DNA. Upon direct excitation of the metal centre at 450 nm, a slight increase in MLCT emission intensity was observed, as shown in Figure 3.11. The emission profile was characterised by a rapid initial intensity increase, up to *ca.* one base pair equivalent, followed by a very gradual increase up to the plateau at *ca.* 10 base pair equivalents, with an overall luminescence enhancement of 1.2 fold. The enhancement may be attributed to protection of the metal centre from quenching by oxygen and solvent molecules upon DNA binding. As such binding places the metal centre in the protected environment of the grooves whereby access of external molecules to the complex is restricted.

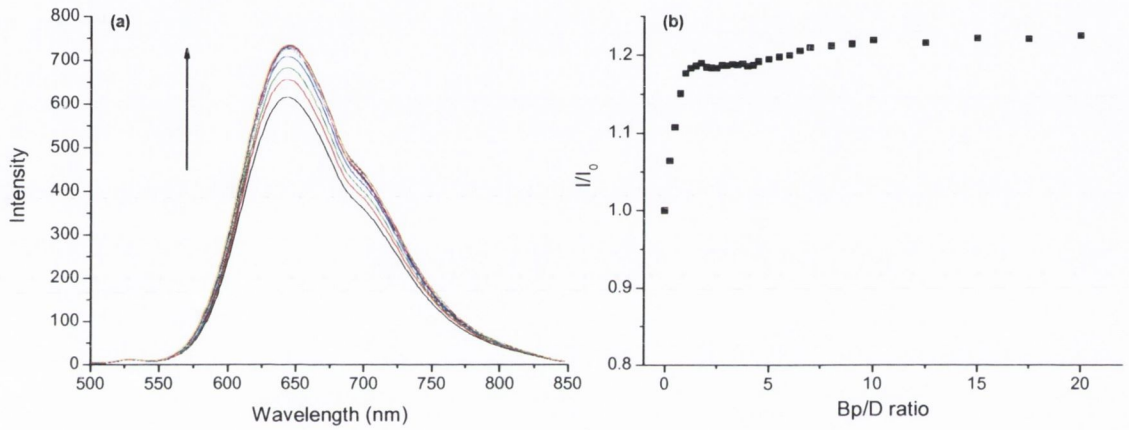

Figure 3.11 *(a) Changes in the MLCT emission spectrum of* ***68*** *(6.5 μM) (excitation at 450 nm) upon addition of st-DNA (0 – 130 μM base pairs) in 10 mM phosphate buffer, at pH 7. (b) The change in integrated MLCT emission intensity as a function of Bp/D.*

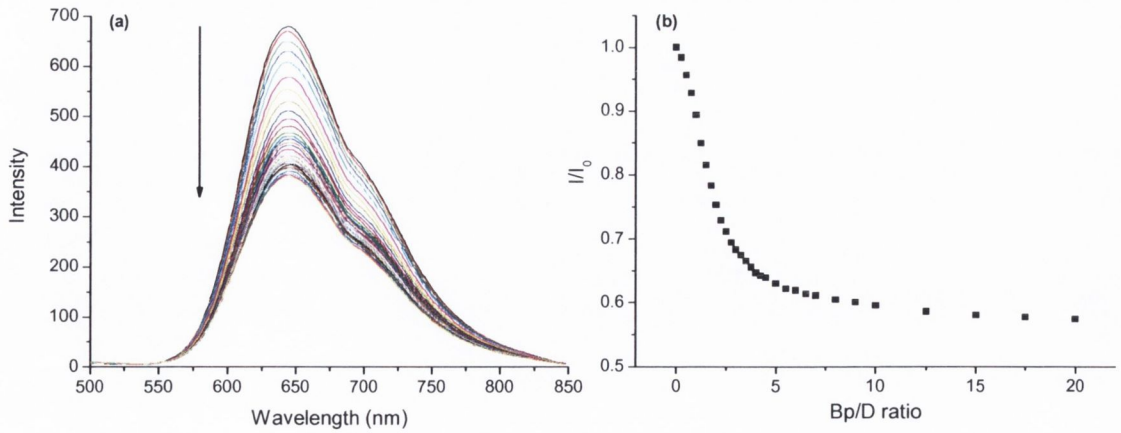

Figure 3.12 *(a) Changes in the MLCT emission spectrum of* ***68*** *(6.5 μM) (excitation at 338 nm) upon addition of st-DNA (0 – 130 μM base pairs) in 10 mM phosphate buffer, at pH 7. (b) The change in integrated MLCT emission intensity as a function of Bp/D.*

Upon excitation of the 1,8-naphthalimide at 338 nm, quite different behaviour was observed, as is evident in Figure 3.12. Here, the intensity of MLCT emission was observed to decrease in this case by *ca.* 43%. However, the emission profile was again characterised by two different regions of change, the first being a rapid decrease in intensity up to *ca.* 3 base pair equivalents, followed by a more gradual decrease up to *ca.* 15 base pairs. No concomitant changes were seen in the 1,8-naphthalimide emission.

The decreased contribution to emission from the Ru(II) centre from the 1,8-naphthalimide, can be clearly seen in the excitation spectrum for **68** in the absence and presence of DNA, Figure 3.13. At the titration end-point, the 1,8-naphthalimide contribution to Ru(II) emission had essentially disappeared, and the spectrum resembled that of **41**, which contains no appended 1,8-naphthalimides. This decrease in intensity may be a result of two factors; firstly diminished absorption by the 1,8-naphthalimide, upon DNA interaction, and secondly, interference with energy transfer from the 1,8-naphthalimide to the Ru(II). Contribution from the former is likely to be considerable, as a 37% hypochromism had previously been observed for **68** upon DNA interaction. The DNA binding may also decrease the efficiency of energy transfer due to spatial separation, or altered orientations of the chromophores as previously predicted by equation **2**. These factors will be discussed in more detail in Section 3.4.3.3.

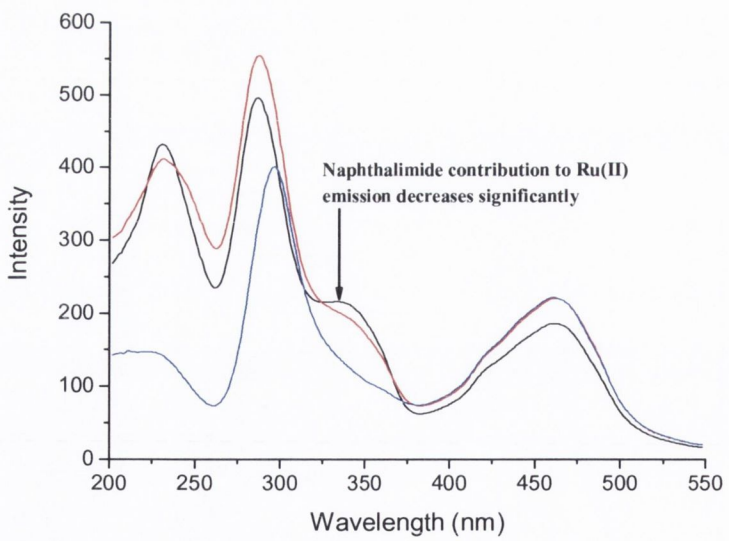

Figure 3.13 *Excitation spectrum of* ***68*** *(6.5 μM) (emission at 645 nm) in 10 mM phosphate buffer, at pH 7 in the absence (——) and presence of st-DNA at a Bp/D ratio of 1 (——) and 20 (——).*

3.4.3.2 Emission Titration of 68 with [poly(dG-dC)]$_2$

The addition of [poly(dG-dC)]$_2$ to a solution of **68** resulted in a somewhat different emission response to that seen above. Excitation of **68** at 450 nm, upon titration with [poly(dG-dC)]$_2$ resulted in no net luminescence change from the metal centre, in contrast to the changes seen above for binding to st-DNA. The absence of emission enhancement upon addition of [poly(dG-dC)]$_2$ points to a binding mode, in which the Ru(II) centre is not held in place in the protected environment of the grooves. The spectra for titration of **68** with [poly(dG-dC)]$_2$ are contained in the appendix.

The MLCT emission intensity (excitation at 338 nm) upon titration with [poly(dG-dC)]$_2$ was observed to decrease by 48%, which is slightly greater than that in the presence of st-DNA. The titration profile was, however, mono-phasic, where the emission decrease occurred gradually. The overall changes resulting from titration with [poly(dG-dC)]$_2$ were easily identified in the excitation spectrum. Here, the absence of change in the MLCT emission upon direct excitation at the MLCT absorption band was apparent, as was the very much decreased 1,8-naphthalimide contribution, the excitation spectrum in this region resembling **41**, with no appended 1,8-naphthalimides.

3.4.3.3 Emission Titration of 68 with [poly(dA-dT)]$_2$

The titration of [poly(dA-dT)]$_2$ with **68** resulted in the same changes in absorbance as that for [poly(dG-dC)]$_2$. However, the emission response was markedly different, with excitation at 450 nm resulting in a *ca.* 1.25 fold enhancement in MLCT emission intensity. The profile for the enhancement was mono-phasic reaching a plateau at *ca.* 1.5 base pair equivalents. This emission enhancement is in striking contrast to that seen upon titration with [poly(dG-dC)]$_2$, and suggests that the binding to AT regions more effectively protects the Ru(II) centre from quenching. This will be elaborated upon when proposing a mechanism for the observed emission changes. The spectra for the titration of **68** with [poly(dA-dT]$_2$ are contained in the appendix.

The response of this system when excited at 338 nm was also different. In this case, a very slight increase in the intensity was observed, up to *ca.* one base pair equivalent, followed by a decrease of *ca.* 13% from the initial intensity, which reached a plateau at *ca.* 3 base pair equivalents. The slight initial increase in intensity is most likely due to contribution from direct excitation of the metal centre in this region. The decrease in the intensity that follows is presumably due to interaction of the 1,8-naphthalimide moiety, as will be discussed in Section 3.4.3.4. It is also worth mentioning that in this case

the overall change, upon excitation at 338 nm is quite small, and indeed smaller than the corresponding hypochromism observed in the absorption spectrum.

The changes in the excitation spectrum of **63** demonstrate the overall changes. Here, the significantly enhanced contribution from direct excitation of the MLCT was apparent along with the very small decrease in contribution in the region of absorption of the 1,8-naphthalimide.

In summary, significant differences in emission response were observed for the binding of **68** to the two DNA alternating co-polymers, particularly upon excitation at the 1,8-naphthalimide absorption band at 338 nm. This may be clearly seen in Figure 3.14 and 3.15, respectively, where the spectra of free complex in buffer solution, complex fully bound to $[poly(dG\text{-}dC)]_2$ and complex fully bound to $[poly(dA\text{-}dT)]_2$ are compared. Greater decreases in MLCT emission intensity were observed in the presence of the GC rich alternating co-polymer, whereas greater enhancement resulted in the presence of the AT rich species. A summary of the emission responses of **68** to st-DNA, $[poly(dG\text{-}dC)]_2$ and $[poly(dA\text{-}dT)]_2$ is provided in Table 3.7.

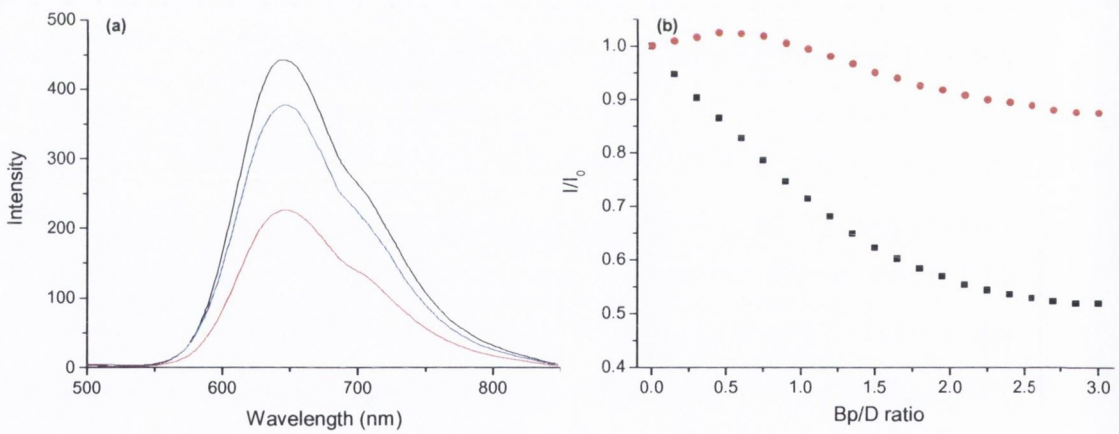

Figure 3.14 *(a) Emission spectrum of* ***68*** *(6.5 μM) (excitation at 338 nm) in the absence (——) and presence of* $[poly(dG\text{-}dC)]_2$ *(——) and* $[poly(dA\text{-}dT)]_2$ *(——). (b) The emission response for titration with* $[poly(dG\text{-}dC)]_2$ *(■) and* $[poly(dA\text{-}dT)]_2$ *(●). All in 10 mM phosphate buffer, at pH 7.*

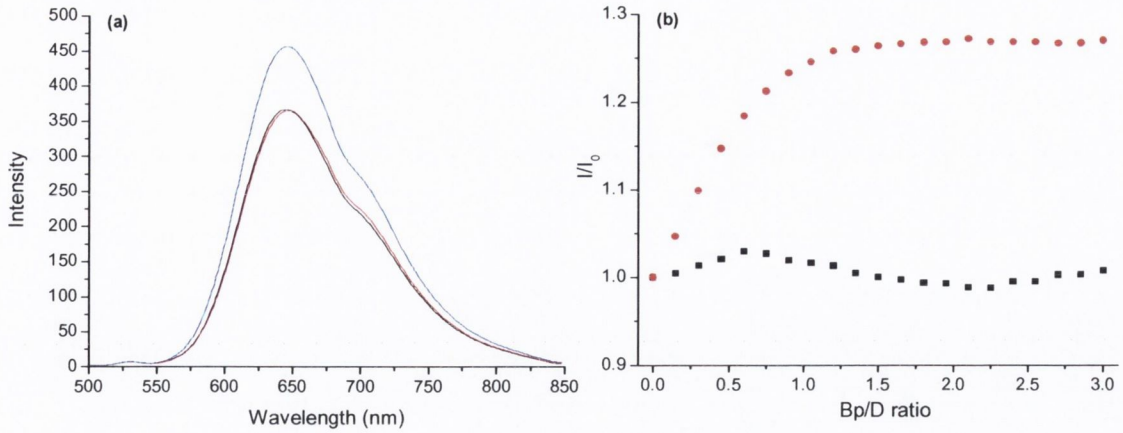

Figure 3.15 *(a) Emission spectrum of* ***68*** *(6.5 μM) (excitation at 450 nm) in the absence (——) and presence of [poly(dG-dC)]$_2$ (——) and [poly(dA-dT)]$_2$ (——). (b) The emission response for titration with [poly(dG-dC)]$_2$ (■) and [poly(dA-dT)]$_2$ (●). All in 10 mM phosphate buffer, at pH 7.*

Table 3.7 *Emission responses of* ***68*** *to added DNAs.*

DNA type	Excitation at 450 nm	Excitation at 338 nm
st-DNA	↑ 20%	↓ 43%
[poly(dG-dC)]$_2$	------	↓ 48%
[poly(dA-dT)]$_2$	↑ 25%	↓ 13%

3.4.3.4 Model for the Emission Changes of 68 upon Titration with DNA

In order to provide a model that is consistent with the different responses, to the different types of DNA, a number of results must be addressed:

1. Enhancement in the MLCT emission upon excitation at 450 nm was observed with st-DNA and [poly(dA-dT)]$_2$, but not with [poly(dG-dC)]$_2$; the changes with st-DNA being intermediate to those observed for the other DNAs.
2. Greater decreases in the MLCT emission intensity was observed upon excitation at 338 nm with [poly(dG-dC)]$_2$ over [poly(dA-dT)]$_2$, with the changes for st-DNA, again, being intermediate between the two.

Concerning the first point above, it seems that emission enhancement is most favourable when the complex binds to AT sites. Luminescent enhancement is still observed with mixed sequence st-DNA as it contains 58.8% AT residues. This could be the reason for the change being intermediate between that observed with [poly(dA-dT)]$_2$

and [poly(dG-dC)]$_2$. The Φ_F of MLCT emission for **68** bound to DNA was 0.024, which is a significant increase to that of free **68** of 0.018. It is unlikely that complexes such as **68** containing a $Ru(bpy)_3^{2+}$ like core would photoreact with DNA. Therefore the preferential enhancement observed with [poly(dA-dT)]$_2$ is most likely due to local structural difference in AT regions, such as the narrower minor groove, that would protect the complex from quenching more effectively. This effect is very subtle as no emission enhancement was observed with [poly(dG-dC)]$_2$. An intermediate effect was observed with st-DNA, due to its heterogeneous base content, which further supports this hypothesis.

The luminescence quenching that occurred upon excitation at 338 nm was more complex, and occured with all of the DNA sequences employed. Changes in the absorbance of the 1,8-naphthalimide moiety upon DNA interaction will contribute in some part to the observed changes, as suggested earlier. However, **68** displays equal hypochromicity at 338 nm upon binding to both [poly(dG-dC)]$_2$ and [poly(dA-dT)]$_2$, while giving rise to significant differences in the emission spectra. Furthermore, the intensity decrease in the presence of [poly(dG-dC)]$_2$ of 48% was significantly greater than the observed decrease in the absorbance, which showed a 33% reduction at 338 nm. This suggests that other mechanisms, such as differential interruption of the energy transfer pathway between the 1,8-naphthalimide and Ru(II) complex, may also play a role.

One of the main differences between GC and AT rich sequences is greater redox reactivity in GC sequences, which is imparted by the guanine moieties. It has previously been shown, that electron transfer from all of the nucleotide bases to the singlet excited state of 1,8-naphthalimides is exergonic by at least 1 eV.[120] Therefore it is possible that such a process may also occur upon binding of **68** to DNA. Here, electron transfer would be expected to quench the 1,8-naphthalimide excited state, with concomitant reduction in its sensitization ability. Therefore, addition of [poly(dG-dC)]$_2$ (rich in guanine residues) would be expected to quench the 1,8-naphthalimide excited state to the greatest extent, and as a result the population of the ^{3}MLCT. This possible mechanism is represented schematically in Figure 3.16. A factor which must also be considered is whether or not the Ru(II) centre is better protected from quenching upon binding to AT sites. This would possibly compensate to a greater extent for the decreases resulting from diminished absorption, and electron transfer quenching by the DNA nucleotides. In order to establish the exact nature of these processes more comprehensive photophysical studies in the presence of DNA, such as the use of fluorescence lifetime and transient absorption

experiments, are necessary. This will be the subject of future research within the Gunnlaugsson group.

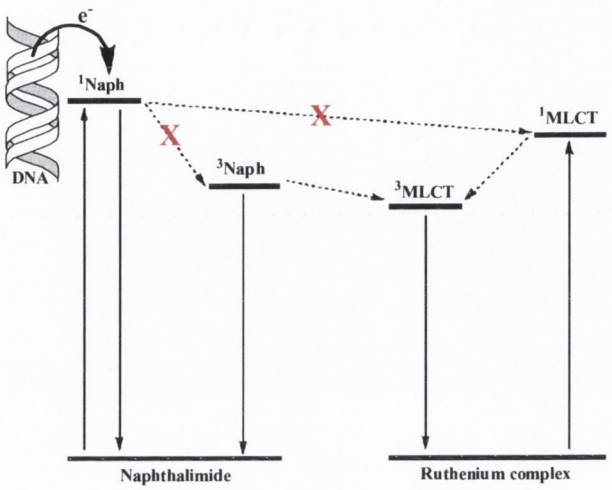

Figure 3.16 *Representation of electron transfer from DNA to the 1,8-naphthalimide and subsequent disruption of energy transfer.*

The presence of a sequence selective emission response is highly significant, as as such behaviour is not commonly exhibited by Ru(II) polypyridyl complexes. As previously mentioned exceptions to this are the $[Ru(TAP)_2POQ\text{-}NMet]^{2+}$ and $Ru(TAP)_3^{2+}$ systems discussed in *Chapters 1* and *2*, which displayed greater emission enhancement in the presence of AT rich sequences.[100] The sequence selective emission response of **63**, when excited at 338 nm is quite novel, as the Ru(II) centre independently reports on the more efficient quenching of the 1,8-naphthalimide excited state by GC rich sequences.

3.4.3.5 Emission Titration of 69 with st-DNA

The emission behaviour of **68** in the presence of the different types of DNA discussed above proved quite complex, exhibiting some very interesting sequence selective responses. The emission behaviour of **69** was thus next considered. It was expected that the results from this investigation would be even more complex, due to the added element of stacking of the 1,8-naphthalimide moieties in **69**. As previously stated, the interaction of **69** with st-DNA was characterised by a 56% and 41% hypochromism at the 1,8-naphthalimide and MLCT bands, respectively.

Upon titration of **69** with st-DNA, and excitation at 450 nm, an initial increase in the MLCT emission intensity of approximately 1.25 fold was observed (0 – 0.45 base pair equivalents), followed by a decrease in the emission intensity to a plateau at approximately

3.5 base pairs equivalents, as shown in Figure 3.17. The final intensity represented a decrease of 46%. The decreased intensity observed for **69** in comparison to **68** is representative of the larger hypochromicity in MLCT absorption that occurs with addition of DNA to the former.

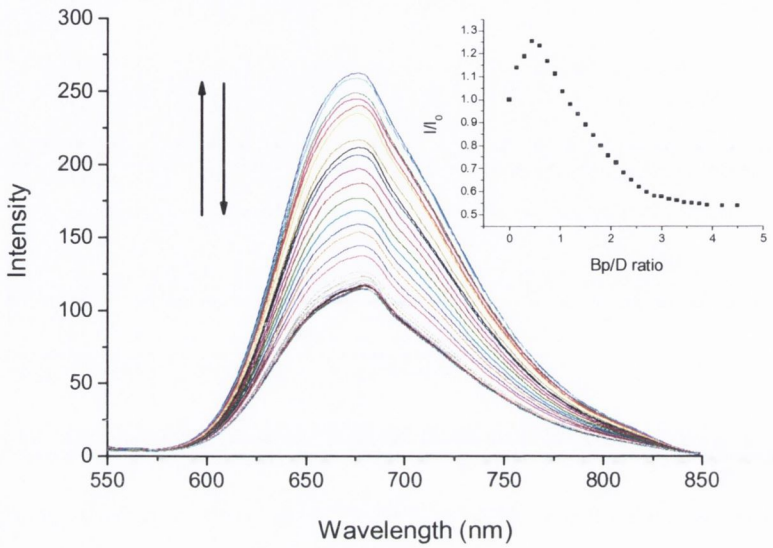

Figure 3.17 *Changes in the MLCT emission spectrum of* ***69*** *(6.5 μM) (excitation at 450 nm) upon addition of st-DNA (0 – 29.25 μM base pairs) in 10 mM phosphate buffer, at pH 7. Inset: The change in integrated MLCT emission intensity as a function of Bp/D.*

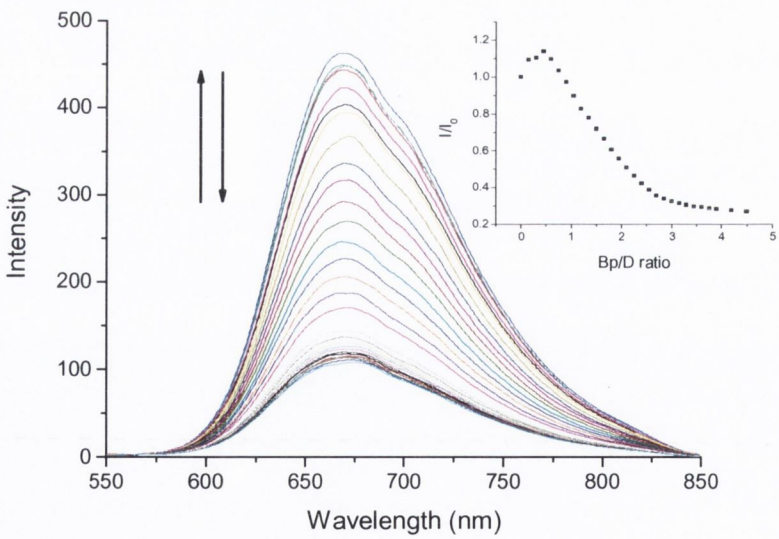

Figure 3.18 *Changes in the emission spectrum of* ***69*** *(6.5 μM) (excitation at 345 nm) upon addition of st-DNA (0 – 29.25 μM base pairs) in 10 mM phosphate buffer, at pH 7. Inset: The change in integrated MLCT emission intensity as a function of Bp/D.*

As for **68** more pronounced changes in emission intensity were observed upon excitation at the 1,8-naphthalimide band, which for **69** is centred at 345 nm. An initial increase of *ca.* 1.14 fold was observed up to 0.45 base pair equivalents, followed by a decrease of 73% from the initial intensity, Figure 3.18. These changes are highly significant, and may not be attributed solely to the decreased oscillator strength of the absorption in this region. This will be discussed in Section 3.4.3.7.

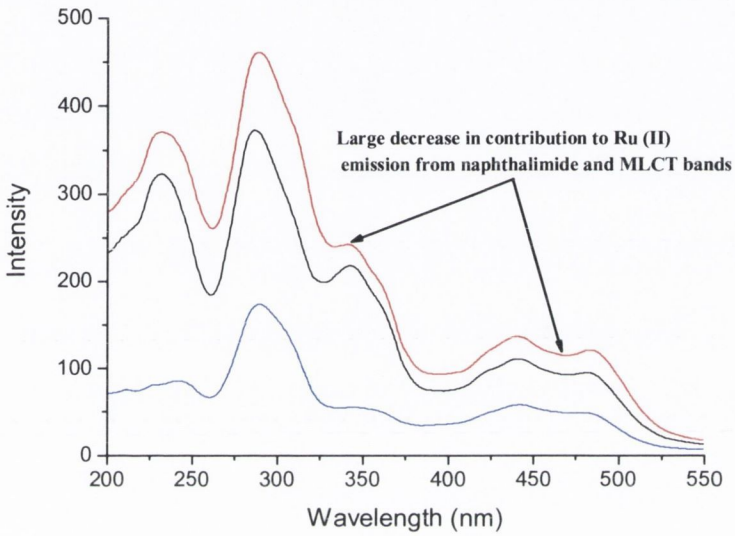

Figure 3.19 *Excitation spectrum of* ***69*** *(6.5 μM) (emission at 670 nm) in 10 mM phosphate buffer, at pH 7 in the absence (——) and presence of st- DNA at a Bp/D ratio of 0.6 (——) and 4.5 (——).*

The decreased contribution to the MLCT emission from both bands at the end point of the DNA titration was also seen in the excitation spectrum, Figure 3.19. Here, the contribution of both bands to the Ru(II) emission has essentially disappeared when fully bound to DNA. Furthermore, the excitation spectrum in the 350 nm region closely resembled that of **41**, which has no appended 1,8-naphthalimides.

3.4.3.6 Emission Titration of 69 with [poly(dG-dC)]$_2$

The effect of [poly(dG-dC)]$_2$ on the emission of **69** was also studied, having resulted in a 55% and 40% hypochromism at the 1,8-naphthalimide and MLCT absorption bands respectively, which is similar to that observed upon titration with st-DNA. Upon excitation at 450 nm, the titration of [poly(dG-dC)]$_2$ gave rise to an initial increase of *ca.* 1.17 fold (0 – 0.45 base pair equivalents), followed by quenching of the MLCT emission

up to *ca.* 3 base pair equivalents. The final intensity represented an overall decrease of 42%. The spectra for the titration of **69** with $[poly(dG\text{-}dC)]_2$ are contained in the appendix.

These changes are different to those observed for **68**, which effectively displayed no change in the MLCT emission, upon excitation at 450 nm, with titration of $[poly(dG\text{-}dC)]_2$. This is possibly reflective of the more intimate association of the Ru(II) centre of **69** with the DNA helix, which could be imparted by the presence of the second 1,8-naphthalimide moiety.

Significant changes in emission intensity were also observed upon excitation at 345 nm for titration with $[poly(dG\text{-}dC)]_2$, displaying an initial increase in the MLCT emission by *ca.* 1.1 fold (0 – 0.3 base pair equivalents), followed by a large decrease of 73% overall, reaching a plateau at *ca.* 3 base pair equivalents. The overall decrease in intensity from the starting point is the same as with the addition of st-DNA, but the initial increase in intensity is slightly less with addition of $[poly(dG\text{-}dC)]_2$. The decreased contribution to MLCT emission at both absorption bands may clearly be seen in the excitation spectrum, shown in the appendix. In the DNA bound form the 1,8-naphthalimide contribution to the Ru(II) emission of **69** has essentially disappeared.

3.4.3.7 Emission Titration of 69 with $[poly(dA\text{-}dT)]_2$

The addition of $[poly(dA\text{-}dT)]_2$ to a solution of **69** resulted in a 42% and 19% hypochromicity in the 1,8-naphthalimide and MLCT absorption bands respectively, quite different to the results from the titration with the other DNA polymers. These results were also mirrored in the emission titration. Upon excitation at 450 nm, the titration of $[poly(dA\text{-}dT)]_2$ resulted in an initial increase in the emission intensity of approximately 1.5 fold (0 – 0.6 base pair equivalents), followed by a decrease in the emission intensity (plateau at *ca.* 3 base pair equivalents), giving an overall emission intensity change of 14%. This was significantly less that observed for the st-DNA or $[poly(dG\text{-}dC)]_2$ titrations.

Excitation of a solution of **69** at 345 nm gave similar results, displaying an initial increase in emission intensity of *ca.* 1.34 fold (0 – 0.45 base pair equivalents), followed by a *ca.* 70% quenching (plateau 3 base pair equivalents). The final intensity represents a decrease of *ca.* 47% overall. The decreased contribution to MLCT emission at both absorption bands may clearly be seen in the excitation spectrum, shown in the appendix. Overall, the emission responses of **69** to added DNA are quite sensitive to the particular base content.

3.4.3.8 Model for the Emission Changes of 69 upon Titration with DNA

A summary of the emission response of **69** to st-DNA, $[poly(dG\text{-}dC)]_2$ and $[poly(dA\text{-}dT)]_2$ is given in Table 3.8.

Table 3.8 *Emission responses of* ***69*** *to added DNAs.*

DNA type	Excitation at 450 nm	Excitation at 345 nm
st-DNA	↑ 25% ↓ 46%	↑ 14% ↓ 73%
$[poly(dG\text{-}dC)]_2$	↑ 17% ↓ 42%	↑ 10% ↓ 73%
$[poly(dA\text{-}dT)]_2$	↑ 50% ↓ 14%	↑ 34% ↓ 47%

In proposing a photophysical mechanism to account for the above changes for **69** upon titration with DNA a number of points must be considered:

1. Upon excitation at both 450 nm and 345 nm the titration of st-DNA, $[poly(dG\text{-}dC)]_2$ and $[poly(dA\text{-}dT)]_2$ all resulted in an initial increase in emission intensity followed by a decrease.
2. Upon excitation at 450 nm the greatest increase and smallest overall decrease in emission intensity was observed for addition of $[poly(dA\text{-}dT)]_2$.
3. Upon excitation at 345 nm the smallest initial increase and greatest overall decrease in emission intensity was observed for addition of $[poly(dG\text{-}dC)]_2$.
4. The metal centre in **69** is not sufficiently reactive in the excited state to undergo electron transfer from DNA.
5. The metal centre in **69** is held more tightly in contact with DNA than that in **68**.
6. Solution studies suggested that an equilibrium does not exist between the triplet excited states of the 1,8-naphthalimide and Ru(II) polypyridyl complex.

The initial increase observed when exciting the Ru(II) complex at 450 nm is most likely due to binding of the metal centre to DNA, which results in it being protected from quenching, as was also observed for the mono-1,8-naphthalimide complex **68**. The greatest increase is observed with added $[poly(dA\text{-}dT)]_2$ due to the narrower minor groove of this DNA polymer, in which bound metal complex is protected from quenching more effectively. The increase is subsequently followed by a decrease, which is suggested to be due to the diminished absorption capability of the complex. In fact the quantum yield of emission from the metal centre upon excitation at 450 nm increased slightly from 0.014 for free complex, to 0.017 for complex bound to st-DNA, supporting this hypothesis.

Emission enhancement also occurs at low Bp/D equivalents upon excitation at the 1,8-naphthalimide band of **69**. This does not occur for mono-1,8-naphthalimide complex **68**, implicating the second 1,8-naphthalimide in the initial enhancement. It is proposed that the initial increase in intensity is due to disruption of stacking of the 1,8-naphthalimides, by the presence of a small quantity of DNA, which results in more efficient energy transfer to the metal centre. This disruption of stacking and subsequent DNA interaction of **69** is represented schematically in Figure 3.20.

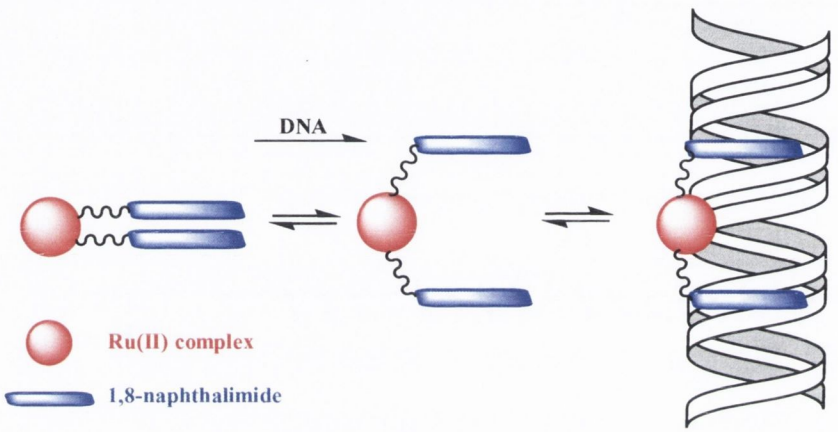

Figure 3.20 *Schematic representation of stacked and unstacked 1,8-naphthalimides and the influence of DNA on this process.*

The decrease in emission intensity from the metal centre that results upon excitation at 345 nm, may be attributed to two factors. Firstly quenching of the 1,8-naphthalimide singlet excited state by electron transfer from the nucleotides, as previously discussed. The second factor to be considered is diminished population of the excited state resulting from a decreased oscillator strength of absorption, which will have a similar effect to the quenching by electron transfer.

Complexes **68** and **69** display quite interesting and useful emission responses to added DNA. In both cases communication between the constituent chromophores was shown to be significantly altered upon interaction with DNA. Upon excitation of **68** at 450 nm a preferential enhancement of emission is observed with $[poly(dA\text{-}dT)]_2$. However, upon excitation at 338 nm a decrease in Ru(II) emission resulted with all of the DNA polymers employed, which was attributed to diminished light harvesting ability of the 1,8-naphthalimide. Decreased energy transfer from the 1,8-naphthalimide to the Ru(II) centre resulting from an increased separation distance caused by DNA binding may also

play a role. However, the contribution cannot be evaluated without studies on further derivatives incorporating different length linker moieties.

Complex **69** displayed quite different emission behaviour to its analogue **69**, which were representative of the increased complexity imparted by the second 1,8-naphthalimide chromophore. Upon excitation at 450 nm an initial increase in intensity was observed, followed by a decrease, with the greatest increase and smallest overall decrease observed with the titration with $[poly(dA\text{-}dT)]_2$. Upon excitation at 345 nm this system displayed an initial increase in intensity followed by a decrease. The initial increase was proposed to be due to perturbation of stacking of the 1,8-naphthalimides by DNA, the result being more efficient energy transfer to the Ru(II) centre. The greatest decrease was observed with addition of $[poly(dG\text{-}dC)]_2$.

In both cases the observed spectroscopic changes were consistent with intercalative binding of the 1,8-naphthalimide, and groove association of the Ru(II) centre, similar in nature to the binding of the complexes discussed in *Chapter 2*. The changes at the MLCT absorption band of **69** were of particular significance, and to the best of our knowledge greater than any changes previously observed for the binding of a tris-bipyridine Ru(II) complex to DNA. Further information on the binding mode was obtained from thermal denaturation, circular dichroism, and ethidium bromide displacement studies, as detailed in the following sections.

3.4.4 DNA Thermal Denaturation Study of 68 and 69

Thermal denaturation studies were carried out to further elucidate the nature of the interaction of **68** and **69** with DNA. The addition of both **68** and **69** to a solution of DNA, resulted in significant shifts in the T_m value, as is evident in Figure 3.21, with **68** giving a shift in T_m of 6.8 °C. Surprisingly a much smaller stabilisation was observed with **69**, giving a shift in T_m of 2 °C. It seems from these results that **68** binds by a classical intercalative mode, whereas **69** binds in a non-classical mode, such as partial intercalation or groove binding of the two 1,8-naphthalimides, which does not stabilise the helix to the same extent, similar to the systems discussed in *Chapter 2*.

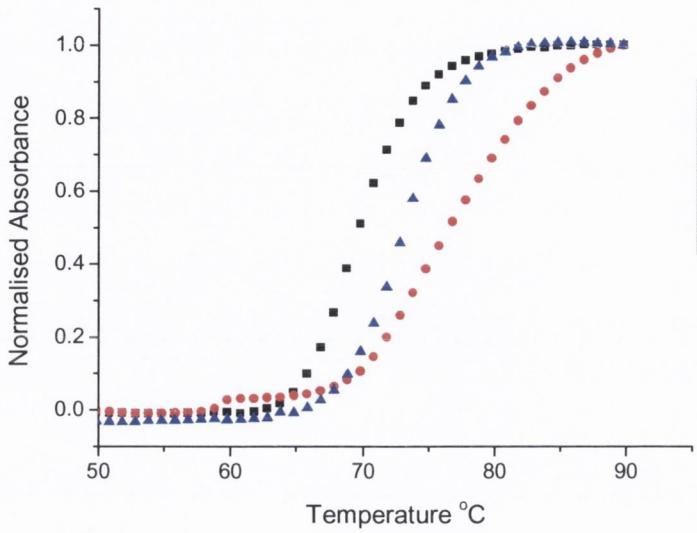

No.	T_m
68	77.0 (± 10%)
69	73.2 (± 10%)

Figure 3.21 *Thermal denaturation curves of ct-DNA (150 μM) in 10 mM phosphate buffer, at pH 7, in the absence (■) and the presence of* ***68*** *(●) and* ***69*** *(▲) at a Bp/D ratio of 5.*

3.4.5 Circular Dichroism Study of 68 and 69

Circular dichroism titrations were carried out on **68** and **69**, in which the concentration of DNA was kept constant and that of the metal complex was varied to give a range of Bp/D ratios. Both conjugates displayed similar CD behaviour, the spectra for **68** being shown in Figure 3.22

Here, a small ICD was observed at long wavelength with the maximum appearing at approximately 470 nm for the MLCT absorption band, which confirms that the Ru(II) component of **68** is associated with the DNA. The relatively small change observed might be due to a binding mode in which the Ru(II) centre binds externally, being partially inserted into the grooves of the DNA. As was observed for the systems in *Chapter 2*, a small ICD was also observed in the region of absorption of the 1,8-naphthalimide at ca. 350 nm. Large changes in CD signal were seen in the region of absorption of DNA, which is possibly due to a combination of conformational changes of the DNA induced by the bound complex, or alternatively due to ICD of the bound complexes themselves.

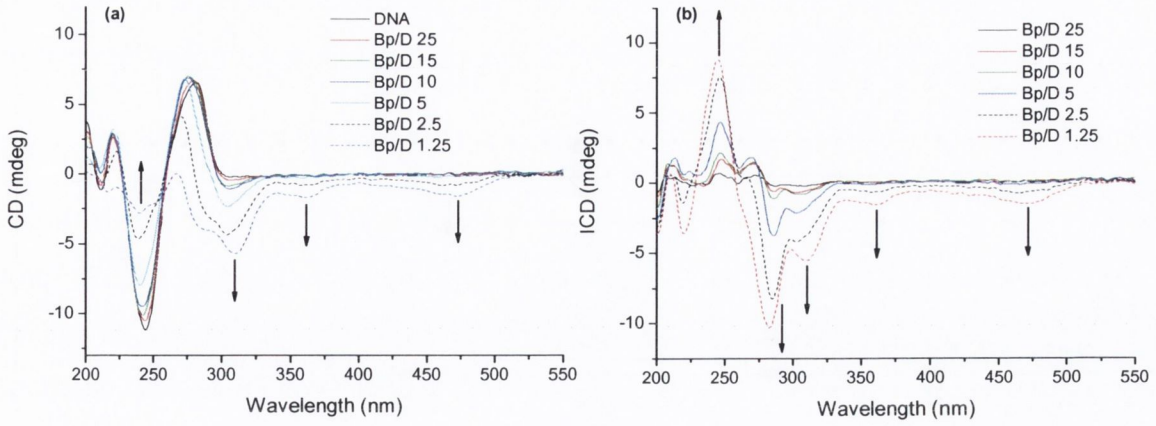

Figure 3.22 *Circular dichroism curves of (a) ct-DNA (150 μM) in 10 mM phosphate buffer, at pH 7 in the absence and presence of* ***68*** *at varying ratios, and (b) the difference spectra obtained.*

3.4.6 Ethidium Bromide Displacement Assay of 68 and 69

The interaction of **68** and **69** with DNA was further characterised using the EtBr displacement assay, as discussed in *Chapter 2*. The displacement profiles for **68** and **69** are shown in the appendix. The binding affinities determined from this assay were in good agreement with those calculated from fits to the UV/Visible absorption data. Complex **68** was shown to possess a slightly lower affinity for DNA compared to that of EtBr, with a calculated binding constant K of 8 x 10^6 M^{-1}. Complex **69** displayed equal affinity for DNA as EtBr with a binding constant of 1 x 10^7 M^{-1}. The important information obtained from these studies is that both the 1,8-naphthalimides in **69** contribute to the DNA binding affinity, as it binds with slightly greater affinity than **68**. However, the absence of cooperativity in the binding action is again indicative of considerable ground state interaction of the 1,8-naphthalimides, which lowers the overall affinity of the system for DNA.

3.5 Conclusions

In this chapter it has been shown that the interruption of energy transfer from a 1,8-naphthalimide donor to a Ru(II) polypyridyl complex acceptor, may also be used as a basis for probing DNA. As was anticipated, both **68** and **69** display an antenna effect in which light was harvested by the 1,8-naphthalimide moieties, resulting in energy transfer to the Ru(II) and subsequent emission. In addition, they possessed reasonably high Φ_F, and did not undergo quenching processes like the systems discussed in *Chapter 2*.

Complex **69** did not possess lifetimes significantly longer than the reference complex **41**. Consequently, it was concluded that triplet equilibrium does not occur between the Ru(II) centre and the appended organic functionalities.

Both systems were shown to strongly bind DNA and undergo large changes in spectroscopic properties upon doing so. Again the bifunctional nature of the molecules proved useful, as two sets of photophysical properties were available for probing the interaction. The Ru(II) centre through its MLCT emission may be regarded as a reporter of the interaction with DNA, and the associated excited state processes undergone by the 1,8-naphthalimide moiety. Both decreased absorbance and electron transfer quenching of the 1,8-naphthalimide moiety, were reported by significant changes in the Ru(II) MLCT based emission. The MLCT emission was modulated to varying degrees with different DNA sequences, in particular due to changes in the sensitization ability of the 1,8-naphthalimide. More pronounced quenching was observed in the presence of GC rich sequences, which was attributed to enhanced electron transfer quenching of the 1,8-naphthalimide excited state by guanine nucleotides. Consequently, **68** and **69** display quite useful sequence selective emission responses, properties not commonly possessed by Ru(II) polypyridyl complexes.

From consideration of all of the DNA binding studies conducted on these systems, an overall binding mode was proposed, involving insertion of the 1,8-naphthalimide chromophores in to the DNA helix, and groove association of the Ru(II) complex. The binding behaviour of both systems proved complex to analyse, in particular that of the bis-complex **69**. While the addition of a second 1,8-naphthalimide moiety does improve the binding and spectroscopic responses upon binding to DNA, it results in more complex behaviour in comparison to **68**. This is possibly due to both stacking interactions of the 1,8-naphthalimides in solution, as well as a greater number of possible binding modes resulting from the presence of the second chromophore.

Flexible linkers were employed in the systems described in this chapter and in *Chapter 2*. Although these did result in conjugates which displayed excellent spectroscopic responses to DNA, they also allowed for quite independent movement of the constituent components of each complex, and therefore a large number of possible modes of interaction with DNA. The next logical step in the research was therefore to employ more rigid linkers, which did not allow for the same degree of freedom of the 1,8-naphthalimide and Ru(II) units when linked to each other. Complexes comprising such an arrangement will be discussed in the following chapter.

Chapter 4

Rigid Ru(II)-1,8-naphthalimide Conjugates

4.1 Introduction

In the two preceding chapters the properties of systems comprising flexible linkers were presented. It was shown that the nature of the linker influences the inherent photophysical properties of the system, and in defining the geometric arrangement of the subunits with respect to each other, profoundly influences the nature of the available binding modes to DNA. It was subsequently demonstrated, that the addition of DNA resulted in substantial changes in spectroscopic properties of each of these families of complexes.

In this chapter the effect of a more rigid arrangement of the components, on the DNA binding properties of Ru(II)-1,8-naphthalimide conjugates is described. Furthermore, the effect that such an arrangement has on the photophysical properties of the complexes, and the degree of interaction between the constituent chromophores will also be studied, in light of the potential application as probes.

A number of modifications to the design presented in the previous chapters have been made. Firstly, the flexible linker was replaced by a more rigid aromatic group, which allows only for limited rotational flexibility of the system; secondly, only mono-1,8-naphthalimides were addressed to limit intramolecular interactions; thirdly, the importance of shape selective recognition of DNA was considered, through the use of two types of connectivity around the central aromatic ring. The first in which the Ru(II) polypyridyl and 1,8-naphthalimide units have a para arrangement with respect to each other, and the second in which they have a meta arrangement to each other. These arrangements are designated as linear and wedged, respectively, for simplicity. While such a linker does not allow for changes in the overall distance between the two chromophores, it does allow for changes in their orientation with respect to each other. The resulting complexes are shown in Figure 4.1.

It was anticipated that their different arrangements would result in substantial differences in the DNA binding modes of these systems, where in the linear systems (**76** and **78**) the 1,8-naphthalimide and Ru(II) units point away from each other, whereas in the wedged systems (**77** and **79**) they have a more complementary orientation with respect to each other. More importantly, it was expected that in restricting the number of potential DNA interactions, a more systematic understanding of the factors influencing the strength of DNA binding could be elucidated.

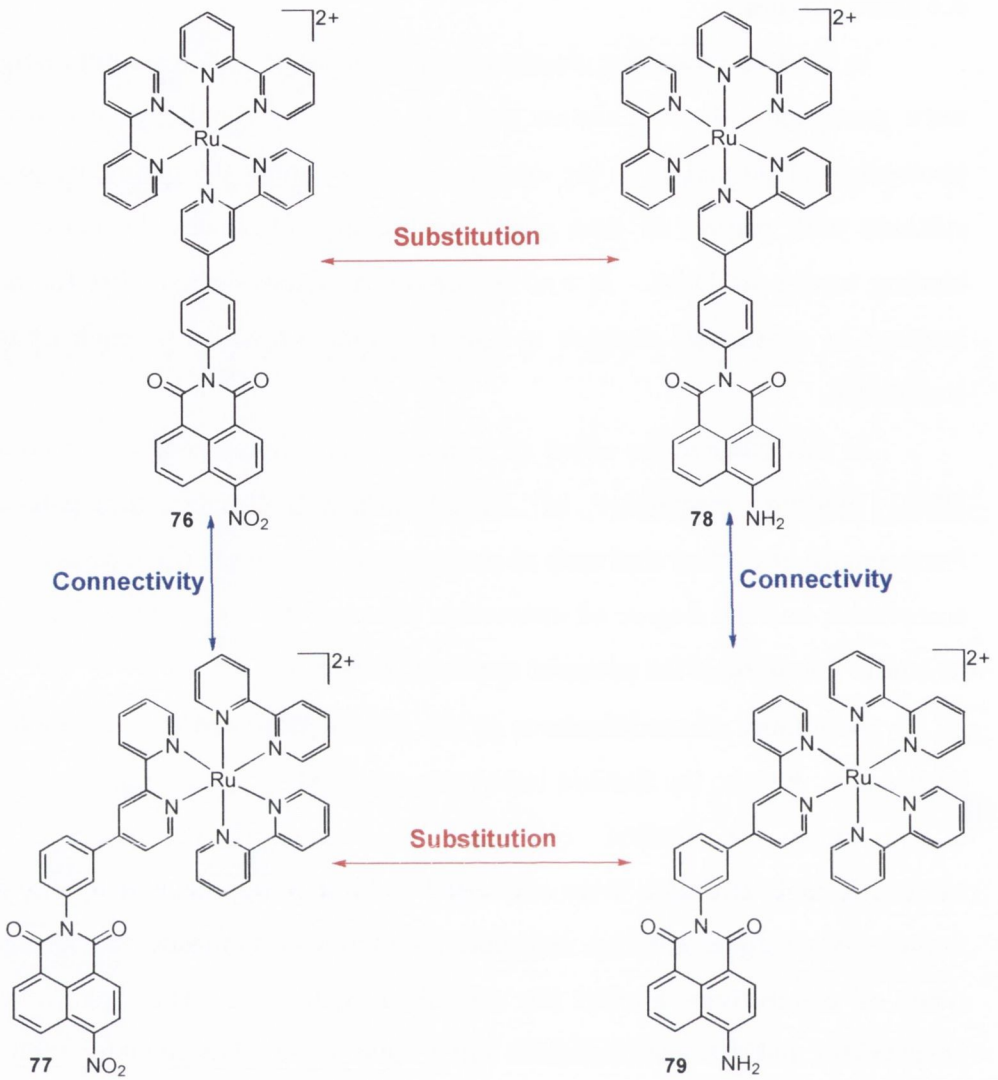

Figure 4.1 *Target complexes* ***76*** *–* ***79*** *and their relationship to one another.*

As was discussed in the preceding chapters, the substituents on the 1,8-naphthalimide ring profoundly affect the photophysical properties of the resulting conjugates. It was therefore decided to also incorporate a substitution study into the research presented in this chapter. Complexes **78** and **79** were identified as targets, as they should easily be prepared by reduction of their nitro analogues **76** and **77**. This was regarded as being the most efficient way of investigating the effect of varying substitution. The nitro complexes **76** and **77** should be weakly emissive, due to the electron transfer processes discussed in *Chapter 2*, whereas their amino analogues **78** and **79** should be strongly emissive due to the diminished reducing ability of the 4-amino-1,8-naphthalimide.

In the context of DNA binding the 1,8-naphthalimide is anticipated to contribute to high affinity binding through intercalation, while the Ru(II) centre should contribute to the

overall interaction through electrostatic association with the helix or insertion into the grooves.

4.2 Synthesis

The synthesis of rigid complexes **76** – **79** was different to that of the flexible derivatives discussed in the previous chapters, hence a detailed discussion will be provided here. The route to complexes **76** and **78**, in which the bipyridine and 1,8-naphthalimide moieties are para to each other will be discussed as an example. A very similar procedure was applied in the synthesis of **77** and **79**.

4.2.1 Synthesis of Aniline Substituted Bipyridines 86 and 87

The preparation of aniline functionalised bipyridine **86** was achieved according to a literature procedure, as outlined in Scheme 4.1.[171] Its analogue **87** comprising a meta arrangement was synthesised using the same general procedure. Full characterisation is given in *Chapter 7*.

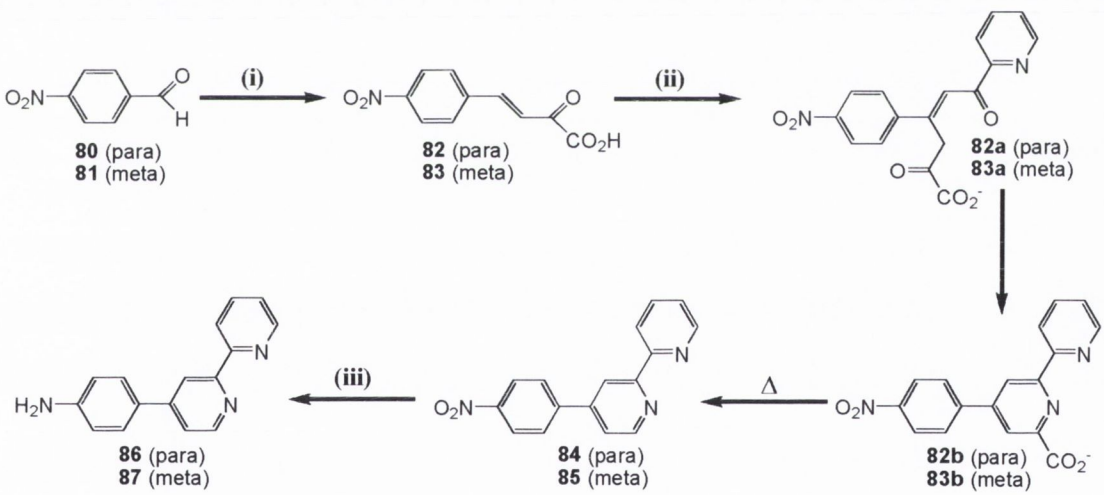

Scheme 4.1 *Synthesis of amino substituted bipyridines* ***86*** *and* ***87****. Reagents and conditions: (i)* $CH_3COCO_2^-$*, EtOH, 2M NaOH, 2M HCl, (ii) 2-pyridacyl pyridinium iodide,* NH_4OAc*,* H_2O*, (iii)* H_2NNH_2*, Pd/C, EtOH.*

The first step involved condensation of the benzaldehyde **80** with sodium pyruvate, under basic conditions at 0 °C, followed by acidification to afford the chalcone **82**, as a yellow solid in 54% yield. The first pyridine moiety was incorporated by reflux of **82** with 2-pyridacyl pyridinium iodide in water, to give the intermediate **82a**. Also present in the reaction mixture was NH_4OAc, which reacted at the two carbonyl groups in **82a**, resulting

in ring closure and formation of the intermediate carboxyl salt **82b**. This was vigorously heated under vacuum to yield the decarboxylated product **84**, which was purified by reflux with activated charcoal. This afforded the product as a pale yellow solid in 87% yield. The final step involved reduction of the nitro group using hydrazine in the presence of a 10% Pd/C catalyst, to yield the aniline functionalised bipyridine **86**, as an off white solid in 86% yield. The route to the amine **87**, for use in the synthesis of complexes **77** and **79** is very similar to that for **86**, using 3-nitro-benzaldehyde as starting material in place of the 4-nitro derivative used above. The yields obtained in synthesis of this derivative are presented in Table 4.1.

Table 4.1 *Synthesis of aniline substituted bipyridines.*

Reactant	Linkage	Product	Yield (%)
80	para	**82**	54
81	meta	**83**	63
82	para	**84**	87
83	meta	**85**	37
84	para	**86**	86
85	meta	**87**	97

4.2.2 Synthesis of 1,8-naphthalimide-bipyridine Ligands 88 and 89

The amine **86** was successfully condensed with 4-nitro-1,8-naphthalic anhydride by refluxing the two compounds in anhydrous ethanol, under an argon atmosphere for 24 hours. Following ether precipitation, the desired ligand **88**, was obtained as a pale-yellow solid in 84% yield. This novel ligand was characterised using ^{1}H NMR, ^{13}C NMR, elemental analysis, mass spectrometry and IR. The ^{1}H NMR spectrum (400 MHz, $CDCl_3$) of **88** is shown in Figure 4.1. Resonances corresponding to the 1,8-naphthalimide and bipyridine moieties are evident, in addition to those for the bridging aromatic ring (see assignment in Figure 4.2).

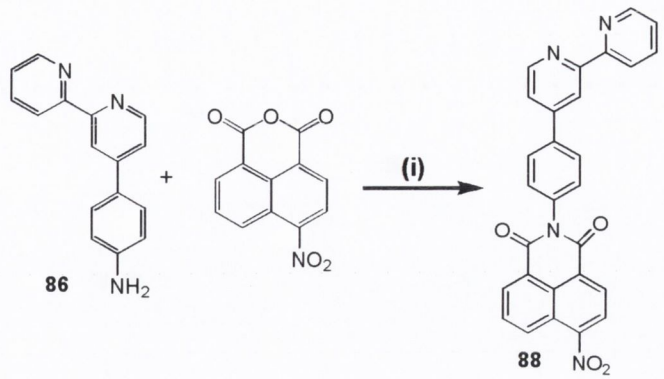

Scheme 4.2 *Synthesis of 1,8-naphthalimide-bipyridine ligand* ***88****. Reagents and conditions: (i) EtOH, Argon atmosphere, 24 hours.*

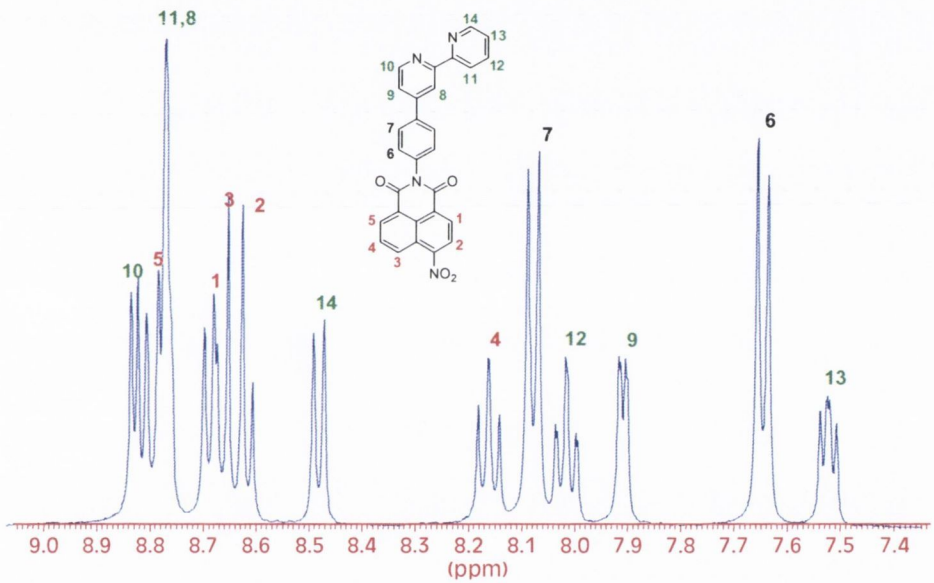

Figure 4.2 *^{1}H NMR spectrum of* ***88*** *($CDCl_3$, 400 MHz).*

Derivative **89**, comprising a meta arrangement of the 1,8-naphthalimide and bipyridine around the connecting ring was synthesised using the same procedure, as detailed in Table 4.2.

Table 4.2 *Synthesis of 1,8-naphthalimide-bipyridine ligands* ***88*** *and* ***89****.*

Reactant	Linkage	Product	Yield (%)
86	Para	**88**	84
87	meta	**80**	84

The procedure employed allows for easy preparation of the ligands **88** and **89** in both small and large quantities. However, numerous different procedures were attempted, before successful condensation of the aromatic amine **86** with 4-nitro-1,8-naphthalic anhydride was achieved, details of which are given in Table 4.3. The failure of **86** to react under many of these conditions is quite surprising, as this amine had previously been condensed with the unreactive 1,4,5,8-naphthalic dianhydride.[171]

Table 4.3 *Conditions investigated for condensation of* ***86*** *with 4-nitro-1,8-naphthalic anhydride. In all cases anhydrous solvents were used.*

Reaction conditions	Result
Toluene, DMAP (catalytic), acetic anhydride, 24 h reflux	Unsuccessful
Toluene, DMAP (equivalent), acetic anhydride, 24 h reflux	Unsuccessful
Toluene, $N(CH_3)_4OH$, 24 h reflux	Unsuccessful
Toluene, KO^tBu, 24 h reflux	Unsuccessful
Toluene, KO^tBu, molecular sieves, 24 h reflux	Unsuccessful
DMA, molecular sieves, 24 h reflux	Unsuccessful
DMA, molecular sieves, 17 h reflux, pyridine, acetic anhydride, 20 h reflux	Unsuccessful
Pyridine, molecular sieves, 24 h reflux	Unsuccessful
Pyridine, ZnOAc, 24 h reflux	Unsuccessful
Glacial acetic acid, 24 h reflux	Unsuccessful
Ethanol, 24 h reflux	**Successful**

Fortunately, the desired product was successfully formed by reflux of the amine and the anhydride in dry ethanol under an inert atmosphere. This reaction has the added advantage of being extremely easy to work up, with pure product being obtained by direct precipitation of the reaction mixture into ether. It does seem quite surprising that these mild reaction conditions afford the desired product in high yield and in high purity after reflux for 24 hours. Analysis of the reaction mixtures from the unsuccessful attempts showed either the presence of pure starting material, or insoluble oligomeric material. Thus it seems that in these cases the reaction either did not go at all, or the conditions were too harsh, and decomposition of both the starting materials and any product formed occurred. We propose that the mechanism for product formation under the successful conditions involves firstly reaction of the amine at the anhydride ring. The acid present in

the opened ring then undergoes esterification with the ethanol solvent, and the resulting ester reacts in the ring closing reaction to give the product. This process is presented in Scheme 4.3.

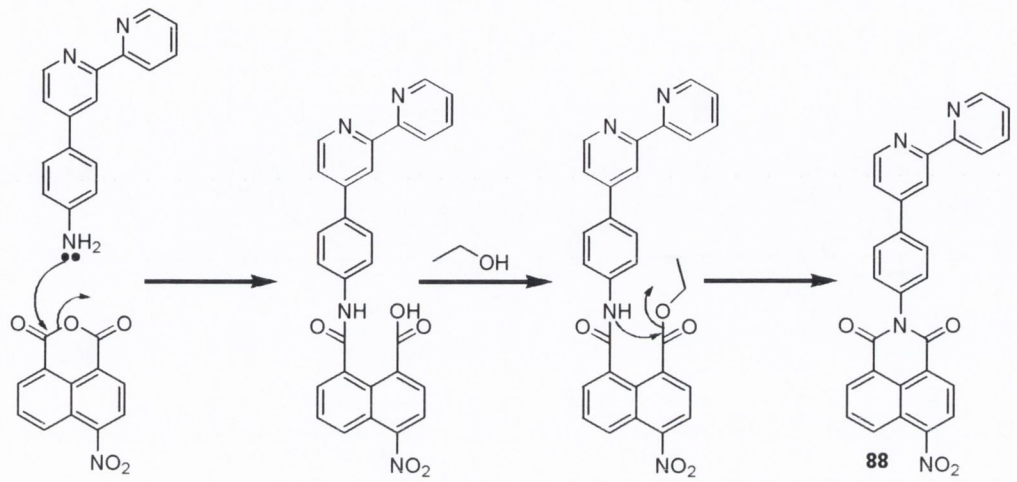

Scheme 4.3 *Proposed mechanism for the formation of ligand* ***88****.*

4.2.3 Complexation of 88 and 89 with $Ru(bpy)_2Cl_2$

Ligands **88** and **89** were complexed in the same manner as for the systems described in *Chapter 2*, Section 2.2.4, as shown in Scheme 4.4. This involved dissolution of the ligand and $Ru(bpy)_2Cl_2$ in DMF/H_2O, degassing of the mixture by bubbling with argon for five minutes, and then stirring of the mixture at 100 °C overnight. The complexes were purified as described before. The 4-nitro-1,8-naphthalimide based **76** and **77** were then reduced to their corresponding 4-amino-1,8-naphthalimide analogues **78** and **79**, in MeOH using 10% Pd/C, at 1 atm of H_2, for 24 hours. Filtration of the reaction mixture through celite afforded the desired products **78** and **79** in high purity. Novel compounds were characterised using the full range of techniques described in *Chapter 2*, see *Chapter 7* for further details. There was a very large degree of overlap in the ^1H NMR spectra (recorded in CD_3CN) of both complexes and as such assignment of all the resonances was not possible. ^{13}C NMR spectra (recorded in CD_3CN) were also obtained, in which all the expected resonances were visible. The successful formation of the complexes was also clearly evident from accurate mass spectrometry, where **76** displayed a peak at 886.1572, corresponding to the M^{2+} ion, and **78** displayed a peak at 856.1822, corresponding to the M^{2+} ion.

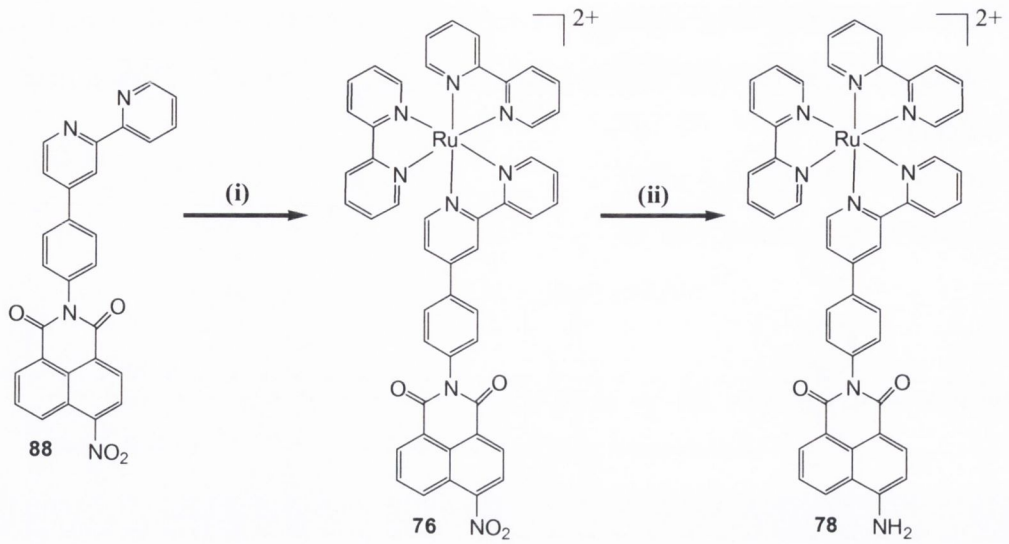

Scheme 4.4 *Complexation of ligand* ***88*** *with* $Ru(bpy)_2Cl_2$ *and reduction of the resulting complex. Reagents and conditions: (i)* $Ru(bpy)_2Cl_2$*, DMF /* H_2O*, argon, (ii) MeOH, Pd/C, 1 atm* H_2*.*

4.3 X-ray Crystallographic Study

Numerous attempts, using a variety of solvent systems, were made to grow crystals suitable for X-ray crystallographic structure analysis of the complexes discussed in *Chapter 2* and *3*. However, none of these attempts proved successful, with the formation of oils or powders occurring in all cases. The failure of these complexes to crystallise was likely due to their flexible nature, and the large number of potential conformations. The rigid complexes described in this chapter lack such flexibility, and it has therefore been possible to grow crystals of some of these systems, the details of which will be discussed in the following sections.

4.3.1 X-ray Crystallographic Study of Complex 77

X-ray quality crystals of **77** were successfully obtained by slow diffusion of diisopropyl ether into an acetonitrile solution of the complex as the PF_6 salt. The structure along with labelling of certain atoms is presented in Figure 4.3. A list of bond lengths, bond angles and dihedral angles corresponding to this structure is given in Table 4.4.

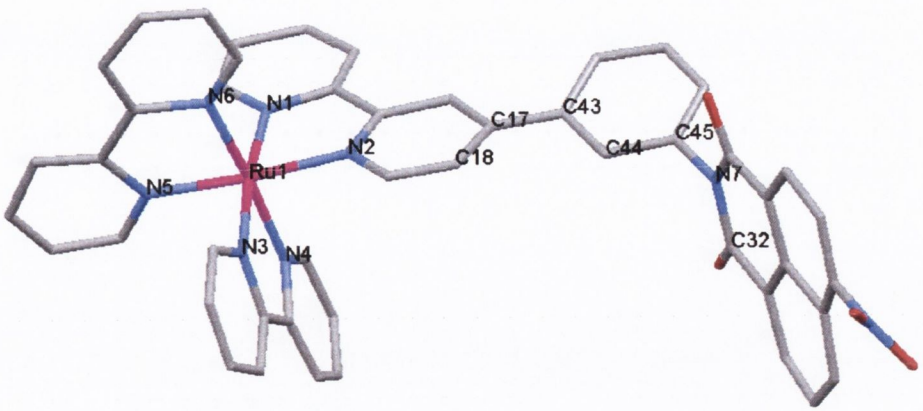

Figure 4.3 *X-ray crystal structure of 77, grey represents carbon atoms, red oxygen atoms, blue nitrogen atoms and magenta ruthenium atoms. Hydrogen atoms and counter-ions have been omitted for clarity.*

The ruthenium – nitrogen bond lengths are within the range 2.028 – 2.074 Å, the bond length in $Ru(bpy)_3^{2+}$ being in the middle of this range at 2.056 Å.[172] Thus the bond lengths are typical of those expected with a tris-polypyridyl ruthenium complex, and substitution of the bipyridine does not seem to have a significant effect. The geometry around the metal is somewhat removed from an ideal octahedral environment, as is evident in the calculated bond angles, this deviation also being in agreement with the properties of $Ru(bpy)_3^{2+}$ in the solid state.

One of the more important features of the structure are the dihedral angles between the two components of the conjugate, the 1,8-naphthalimide moiety being significantly twisted out of plane with respect to the aromatic ring connecting it to the metal centre. The dihedral angle between the two was measured as 78.15°, approaching that of an orthogonal conformation. The fact that the 1,8-naphthalimide is twisted out of plane to such an extent may have interesting consequences on the DNA binding behaviour of this complex, assuming that **77** adopts a similar conformation in solution, which is likely due to the restricted rotation around the connecting ring. The 1,8-naphthalimide would be expected to insert into the helix, but because of the orientation the ligand part of the system will remain externally bound. This will be discussed in more detail when the results of DNA binding studies have been presented. It is also worth commenting on the orientation of the nitro group at the 4-position of the 1,8-naphthalimide, which is twisted out of plane as suggested in *Chapter 2*.

Table 4.4 *Selected bond lengths, bond angles and dihedral angles for 77.*

Bond	Length (Å)	Bond	Angle (deg)
N1 Ru1	2.035	N1 Ru1 N2	78.67
N2 Ru1	2.055	N1 Ru1 N3	172.02
N3 Ru1	2.031	N1 Ru1 N4	94.60
N4 Ru1	2.057	N1 Ru1 N5	96.90
N5 Ru1	2.074	N1 Ru1 N6	90.09
N6 Ru1	2.028	N2 Ru1 N3	96.67
		N2 Ru1 N4	86.28
		N2 Ru1 N5	174.91
Bond	**Angle (deg)**	N2 Ru1 N6	96.91
C44 C45 N7 C32	78.15	N3 Ru1 N4	78.53
C18 C17 C43 C44	17.97	N3 Ru1 N5	88.01
		N3 Ru1 N6	96.95
		N4 Ru1 N5	96.63
		N4 Ru1 N6	174.78
		N5 Ru1 N6	80.50

The packing diagram of **77** is shown in Figure 4.4, viewed along the c* axis. From examination of the packing diagram it is apparent that there are eight metal complexes per unit cell. Of these the 1,8-naphthalimide moieties of four complexes stack over each other in the centre of the cell, and the other four point outwards. Presumably those 1,8-naphthalimides pointing outwards interact with others in adjacent cells.

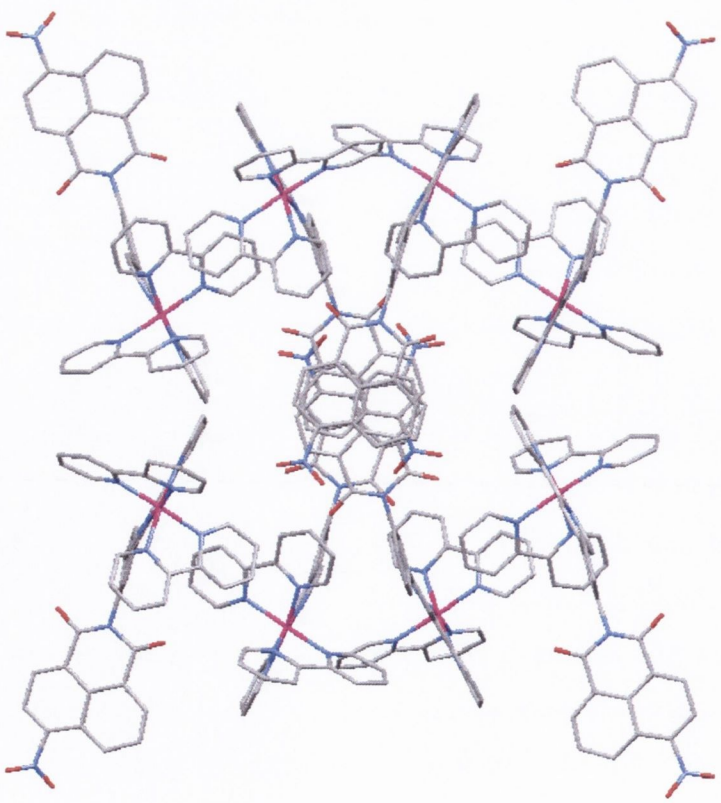

Figure 4.4 *Crystal packing diagram of 77, viewed along the c* axis. Hydrogen atoms and counter-ions have been omitted for clarity.*

4.3.2 X-ray Crystallographic Study of Complex 76

Attempted crystallisation of **76** by diffusion of diisopropyl ether into an acetonitrile solution of the complex, resulted in the formation of spherical crystals, a photograph of which is given in Figure 4.5. Several repeated attempts gave the same result, with one of the attempts resulting in the formation of small rectangular crystals. The spherical objects in Figure 4.5 are solid and of crystalline nature, as is evident from the circled particle which was scratched with a needle. Despite this they failed to diffract after repeated attempts. One of the rectangular crystals did however, diffract, although the data was not of sufficient quality to enable a crystal structure to be fully solved to within acceptable limits of error for publication. The structure resulting from this is, nevertheless, shown in Figure 4.6, as it does illustrate the overall molecular arrangement. Hence, it is useful for comparison to the structure obtained for **77**.

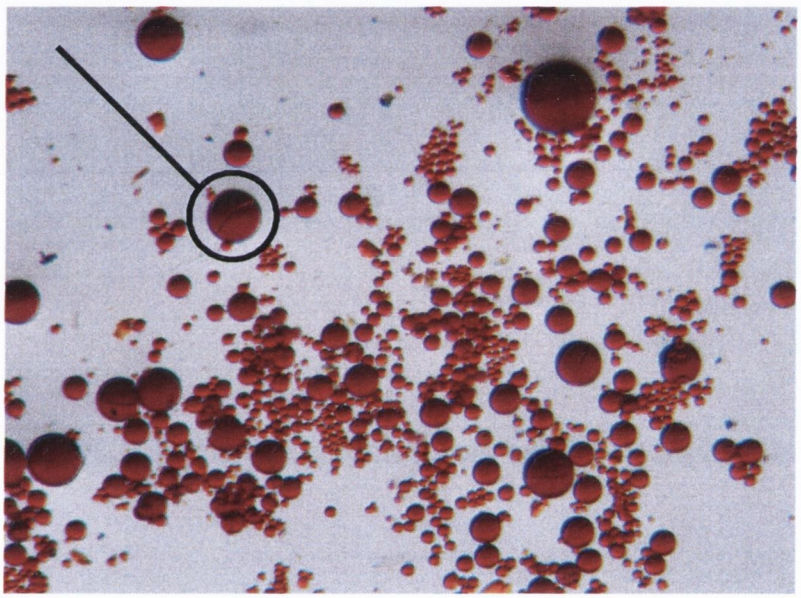

Figure 4.5 *Photograph of crystals obtained of linear complex* ***76****.*

From the structure it is clear that the 1,8-naphthalimide is substantially twisted out of plane with respect to the connecting aromatic ring, similar to that observed for **77**. However, in the structure for **76**, the 1,8-naphthalimide is as expected pointing away from the metal complex component of the system. Hence, it is likely that these different structural arrangements will have significant effects on the DNA binding ability of such complexes, as was anticipated in the initial design.

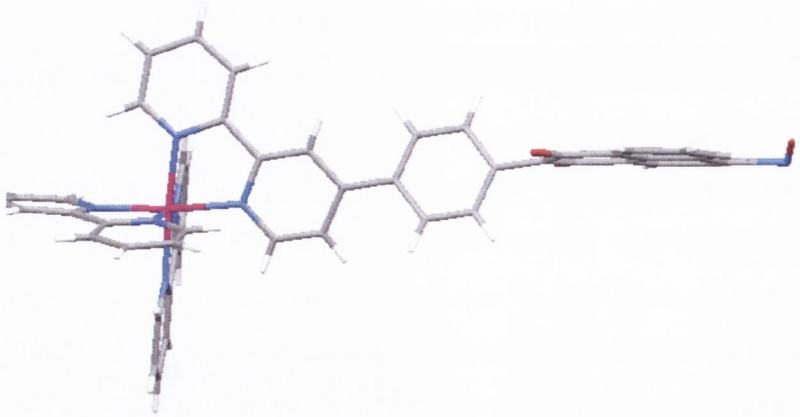

Figure 4.6 *X-ray crystal structure of* ***76****, grey represents carbon atoms, white hydrogen atoms, red oxygen atoms, blue nitrogen atoms and magenta ruthenium atoms.*

In light of these structural observations, for future discussion, complexes **76** and **78** will be referred to as linear and complexes **77** and **79** as wedged.

4.4 Photophysical Properties of 76 – 79

4.4.1 UV/Visible Absorption Properties of 76 – 79

The photophysical properties of **76** – **79** were next investigated. The notation shown in Figure 4.7 will be used throughout the remainder of this chapter, as a structural representation of each conjugate. It was anticipated that both the substituent on the 1,8-naphthalimide ring and the connectivity between the two chromophores, would have an effect on the photophysical properties of the resulting conjugates. The linear derivatives are considered in detail and are described below.

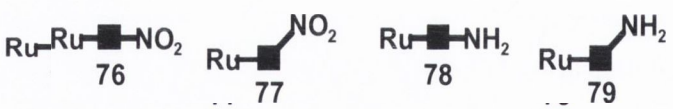

Figure 4.7 *Molecular arrangement of complexes* ***76*** *–* ***79****.*

The absorption, excitation and emission spectra of **76** and its amino analogue **78** are depicted in Figure 4.8a and 4.8b, respectively. Examination of the UV/Visible absorption spectrum of **76** reveals bands characteristic of both the Ru(II) polypyridyl and 4-nitro-1,8-naphthalimide chromophores, where the intense band centred around 287 nm was attributed mainly to π-π^* intraligand transitions, the band at 350 nm to the 1,8-naphthalimide π-π^* transitions, and the band centred at 457 nm to the MLCT

transitions of the Ru(II) centre, which was very slightly red shifted compared to that of $Ru(bpy)_3^{2+}$. The absorption properties of **78** were somewhat different. The band at 287 nm was still present, although its molar absortivity was slightly reduced compared to **76**. A single band was observed at 451 nm corresponding to both the 4-amino-1,8-naphthalimide and the Ru(II) MLCT transitions. A summary of these absorption properties is given in Table 4.5.

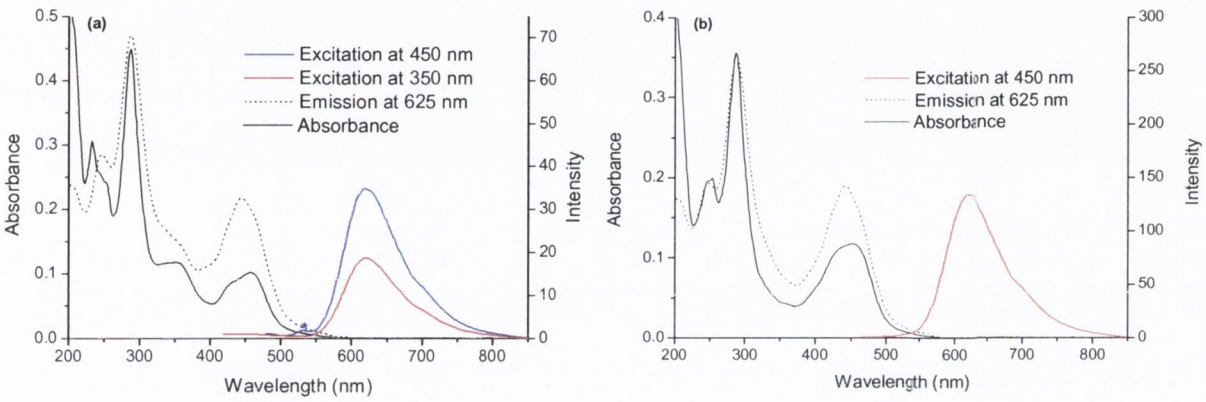

Figure 4.8 *UV/Visible, excitation and emission spectra of (a)* ***76*** *(6.5 μM) and (b)* ***78*** *(6.5 μM), both in 10 mM phosphate buffer, at pH 7. The water Raman band is denoted by *.*

Table 4.5 *Absorption properties of* ***76*** *–* ***79*** *in 10 mM phosphate buffer, pH 7 at 298 K.*

Complex	λ_{max} (nm) [ϵ (M^{-1} cm^{-1})]		
76	287 [68000]	350 [18000]	457 [15000]
77	287 [78200]	351 [19000]	457 [14800]
78	287 [54200]	------	451 [18000]
79	287 [53000]	------	451 [18000]

The systems discussed in this chapter all contain a single 1,8-naphthalimide moiety, and as such intra-molecular interactions involving 1,8-naphthalimide stacking is not expected. However, due to the potentially greater conjugation afforded by the aromatic linkers in these complexes, ground state electronic interactions between the components may be significant. For this reason additive spectra were recorded, in which the absorbance of $Ru(bpy)_3^{2+}$, the appropriate water soluble nitro or amino 1,8-naphthalimide derivative (**59** or **90**), the

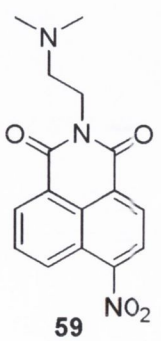

59

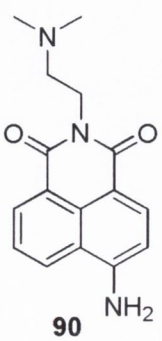

90

summed spectra of these two, and complexes **76** or **78** were compared. The resulting spectra for **76** and **78** are contained in the appendix.

From examination of these Figures it is apparent that for **76**, there is a close agreement between the actual spectrum and that calculated from summation of the constituent components of the complex. The main difference is the slight red shift in absorption maximum of the MLCT band, due to the lower energy excited state as outlined earlier. Overall the close agreement suggests negligible ground state electronic interaction between the 1,8-naphthalimide and Ru(II) units in **76**, and also precludes intermolecular stacking interactions of the 1,8-napthalimide moieties at the concentration employed in this study.

The behaviour of **78** was, however, quite different. The absorption of this complex was significantly less than that predicted from summation of its components. This would immediately suggest that there was a significant electronic interaction between the two components, leading to a reduced overall oscillator strength for either or both of the overlapping absorption bands. Hence, the ground state properties of these rigid complexes are very sensitive to the nature of the substituents at the 4-position of the 1,8-naphthalimide ring system.

Very similar UV/Visible absorption behaviour was observed for the meta arranged complexes **77** and **79**, as shown in the appendix. The absorption properties for **77** and **79** are also detailed in Table 4.5. From examination of the data it is clear that very similar absorption properties are possessed by corresponding linear and wedged complexes, and that the different arrangements do not significantly alter the ground state properties.

4.4.2 Emission Properties of 76 – 79

Excitation of an aqueous solution of the 4-nitro-1,8-naphthalimide containing complexes **76** and **77** resulted in essentially no emission from the 1,8-naphthalimide moiety, and MLCT based emission at around 625 nm. The absence of a 1,8-naphthalimide associated emission band suggests that sensitization of the MLCT excited state through some energy transfer process occurs, in a similar manner to the complexes discussed in *Chapter 3*. Excitation of an aqueous solution of **78** and **79** at 450 nm resulted in similar behaviour, in that no emission was observed from the 1,8-naphthalimide, but a band at 625 nm corresponding to MLCT emission occurred. The λ_{max} and Φ_F for **76** – **79** are detailed in Table 4.6.

Table 4.6 *Emission properties of* ***76*** *–* ***79*** *in 10 mM phosphate buffer, pH 7 at 298 K.*

Complex	λ_{em} (nm)	Φ_f (± 10 %)
76	625	0.004
77	625	0.001
78	625	0.019
79	625	0.018

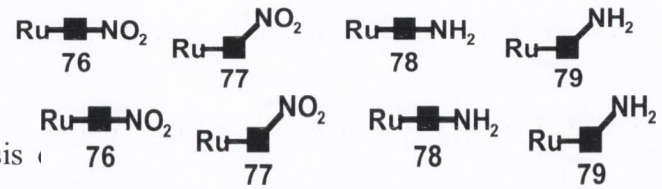

Ru NO2 76 Ru NO2 77 Ru NH2 78 Ru NH2 79

From analysis of **76** and **77**, it is clear that significant quenching of the MLCT excited state by the 1,8-naphthalimide moieties occurs. This most likely involves an electron transfer, similar to that observed in *Chapter 2*. Both systems displayed essentially no 1,8-naphthalimide emission suggesting that energy transfer from the 1,8-naphthalimide singlet state to the MLCT singlet state may occur. The ^{1}MLCT state produced as a result of this process then crosses to the triplet state, which is quenched by the electron transfer mechanism just described.

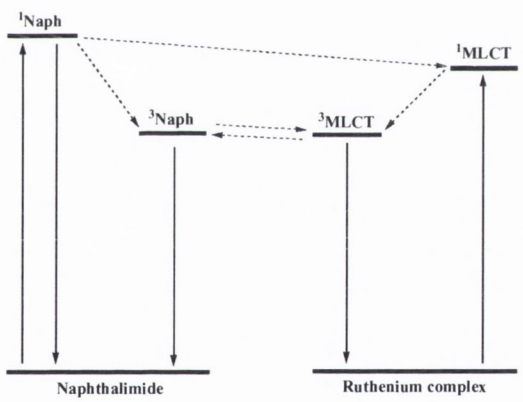

Figure 4.9 *Qualitative energy level diagrams describing the possible energy transfer from ^{1}Naph to ^{1}MLCT and excited state equilibrium between ^{3}Naph and ^{3}MLCT, in amino substituted complexes* ***78*** *and* ***79****. Radiative transitions are represented by solid lines and non-radiative transitions by dashed lines.*

The emission displayed by the amino complexes **78** and **79** was quite different to that from the nitro complexes **76** and **77**. No emission was observed from the 1,8-naphthalimide moiety in either **78** or **79**, suggesting the presence of efficient energy transfer to the metal centre. A similar observation has previously been made by Castellano and co-workers for 4-piperidinyl-1,8-naphthalimide-Ru(II) conjugates, and was attributed

to efficient singlet-singlet energy transfer between the two components.[165] These systems possessed very long lifetimes, due to the presence of an equilibrium between the triplet states of the 1,8-naphthalimide and the Ru(II) polypyridyl complex, and it was anticipated that similar processes could be occurring in **78** and **79**, in that efficient energy transfer from ^{1}Naph to ^{1}MLCT occurs, as shown in Figure 4.9. The quantum yields of these systems, being somewhat less than that of $Ru(bpy)_3^{2+}$,suggests that interaction of the triplet states may also occur,. This may be due to an equilibrium or energy transfer process to ^{3}Naph, which results in an overall decrease in population of the ^{3}MLCT. However, it is also worth bearing in mind that upon excitation at 450 nm, not all of the light is absorbed by the metal centre, due to the overlap of the 1,8-naphthalimide and MLCT absorption bands.

From consideration of the above photophysical properties it is clear that the strategy employed in the design of **76** – **79** was successful in yielding systems with varying photophysical properties, by simply changing the nature of the substituents at the 4-position of the appended 1,8-naphthalimide moiety. In addition, from examination of the crystal structures it is apparent that the use of the more rigid aromatic linkers in these systems, allows for more precise control of the orientation of 1,8-naphthalimide and Ru(II) polypyridyl components with respect to each other. This could have effects on the communication of the two chromophores, as discussed above, and is also expected to have interesting consequences on the nature of their interaction with DNA. This will be discussed in the following sections.

4.5 DNA Binding Interactions of 76 – 79

Due to the bifunctional nature of **76** – **79**, these complexes were expected to interact with DNA through a combination of electrostatic and π-stacking interactions, where the metal complex unit binds externally to the phosphate groups, while the 1,8-naphthalimides bind through intercalative or groove binding interaction. To determine the nature of their binding to and affinity for DNA a number of spectroscopic titrations were carried out. Significant changes in the photophysical properties of each system were observed upon interaction with DNA.

4.5.1 Changes in the UV/Visible Absorption of 76 – 79 with DNA

The interaction of each complex with st-DNA was firstly investigated using electronic absorption spectroscopy, in which changes in MLCT and/or the

1,8-naphthalimide bands were monitored, where appropriate. The titrations were carried out in the same manner as described in *Chapter 2*.

The titration of DNA with the linear nitro complex **76** resulted in a 34% hypochromism at the 1,8-naphthalimide band, with a smaller change of *ca.* 15% in absorbance of the MLCT band, as depicted in Figure 4.10. The changes observed for the 1,8-naphthalimide band are similar to those observed for the more strongly bound species in the previous chapters, and are typical of intercalation.[18] The changes in the MLCT band are greater than those observed for reference complex **41**, which only displayed a 9% hypochromism. This confirms that the metal centre in **76** is possibly more tightly bound to DNA, probably being anchored by the 1,8-naphthalimide moiety. The greater affinity is also apparent in the binding constant determined from fitting to UV/Visible titration data.

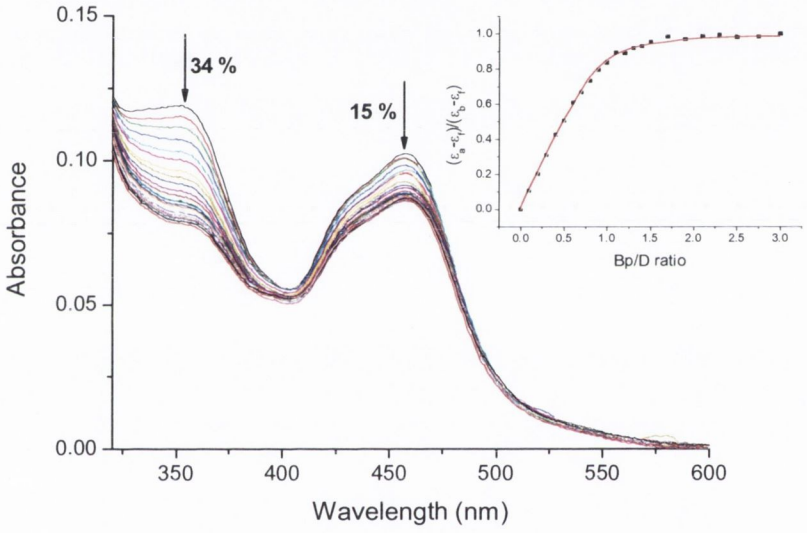

Figure 4.10 *Changes in the UV/Visible spectrum of* ***76*** *(6.7 μM) upon addition of st-DNA (0 – 20.1 μM base pairs), in 10 mM phosphate buffer, at pH 7. Inset: Plot of* $(\epsilon_a-\epsilon_f)/(\epsilon_b-\epsilon_f)$ *at 355 nm vs. equivalents of DNA and the corresponding non-linear fit.*

A binding constant of 4.5 x 10^6 M^{-1} and binding site size of *ca.* 1 base pair was determined for this system. The former is of the same order as that determined for **45** and **46**, respectively, discussed in *Chapter 2* of this thesis. The affinity is, however, two orders of magnitude greater than the constituent components, emphasising the effectiveness of the bifunctional nature of these complexes as DNA binders. It is also interesting to note that despite displaying similar affinity for DNA to the flexibly linked complexes discussed in *Chapter 2*, a greater MLCT hypochromism results for the interaction of **76** with the nucleic acid. Here, binding of the 1,8-naphthalimide seems to pull the Ru(II) centre into close

proximity to the helix, as the rigid linker does not allow for independent interaction of the two components.

The addition of DNA to the wedged nitro complex **77** resulted in significantly greater changes in the absorbance than its linear analogue, as shown in the appendix, and listed in Table 4.7. In addition, the affinity for DNA was significantly greater, with a calculated binding constant of 1.9 x 10^7 M^{-1} and binding site size of 1.36 base pairs. The reason for the greater spectroscopic changes and the overall higher affinity displayed by this complex may be related to the structure, and particularly the orientation of the 1,8-naphthalimide and Ru(II) components with respect to each other. From examination of the crystal structure of **77** it is apparent that a cleft exists between the two components, that should allow for tight binding of both the 1,8-napththalimide and Ru(II) centre, the binding occurring in a manner in which each component complements the other. However, in the linear system **76** such a cleft does not exist, and the components of the complex point away from each other. Therefore, in binding to DNA the components of the complex cannot complement each other in the same manner as for **77**, resulting in smaller overall changes in photophysical properties and reduced DNA binding affinity.

Table 4.7 *DNA binding parameters from fits to absorbance data.*

No.	λ(Naph) Hypochromism	λ(MLCT) Hypochromism	Binding constant K (M^{-1})	Binding site size n (base pairs)	R^2
76	34 %	15 %	4.5 x 10^6 (± 0.7)	0.98 (± 0.02)	0.99
77	45 %	21 %	1.9 x 10^7 (± 0.6)	1.36 (± 0.02)	0.99
78	30 %		3.0 x 10^6 (± 1.0)	0.88 (± 0.06)	0.98
79	29 %		1.1 x 10^7 (± 0.5)	1.50 (± 0.06)	0.98

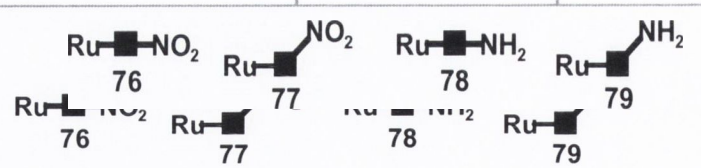

Unlike the nitro derivatives, the amino substituted complexes **78** and **79** do not possess spectroscopically distinct bands for the two components. Therefore, the absorbance changes displayed by these complexes were somewhat different. The changes for the linear amino derivative **78** are shown in Figure 4.11, and in Table 4.7. A binding constant of 3.0 x 10^6 M^{-1} and binding site size of 0.88 were determined from fitting to the data, being quite similar to those of the linear nitro complex above.

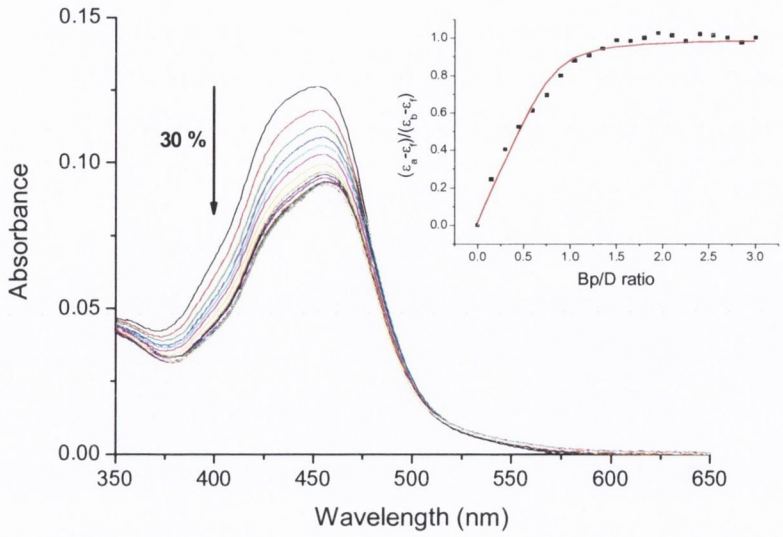

Figure 4.11 *Changes in the UV/Visible spectrum of* ***78*** *(7.0 μM) upon addition of st-DNA (0 – 21 μM base pairs), in 10 mM phosphate buffer, at pH 7. Inset: Plot of* $(\epsilon_a-\epsilon_f)/(\epsilon_b-\epsilon_f)$ *at 451 nm vs. equivalents of DNA and the corresponding non-linear fit.*

It is likely that these two linear complexes bind in a similar fashion, with the orientation of the two components being the most important factor in determining the nature of the interaction with DNA. The significant difference is a 5 nm shift in absorption maximum of the 451 nm band of **78**, shifts such as this usually being associated with classical intercalation.[18] This may be a consequence of the twisting of nitro groups in the 4-position of 1,8-naphthalimides out of plane, due to steric interactions, as discussed in detail in *Chapter 2*. An amino group does not experience this type of twisting to the same degree, and as such its presence in a 1,8-naphthalimide derivative may allow for more complete insertion into the helix and spectral responses more like those of classical intercalators.

The wedged amino complex **79** displayed a hypochromicity of the long wavelength band of 29%, and a bathochromic shift of 7 nm, as shown in the appendix, which is almost exactly the same as that resulting from the addition of DNA to complex **78**. However, a binding constant of 1.1 x 10^7 M^{-1} and binding site size of 1.50 base pairs were determined for this system, Table 4.7.

The binding constant is significantly larger than that of the corresponding linear complex, which again emphasises the tighter binding interaction associated with a wedged arrangement of the chromophores. From UV/Visible absorption studies it is clear that **76** – **79** bind DNA with high affinity, having binding constants of the order of 10^6 – 10^7 M^{-1}.

Furthermore, the nature of the interaction with and the binding affinity for DNA is quite sensitive to the arrangement of the Ru(II) and 1,8-naphthalimide components around the connecting ring, more intimate association with the DNA helix being observed for a meta arrangement. The nature of this interaction was further investigated using emission spectroscopy as detailed in the following section.

4.5.2 Emission Titration of 76 – 79 with DNA

As discussed in Section 4.3 the emission properties of **76** – **79** were very much dependent on the substituent at the 4-position of the 1,8-naphthalimide ring system. Nitro substituted derivatives **76** and **77** were weakly emissive in solution, whereas emission from their amino analogues **78** and **79** was considerably stronger. Significant differences in spectral response to added DNA were also observed between the corresponding nitro and amino substituted complexes, and as such they will be discussed separately.

4.5.2.1 Emission Titration of Nitro Complexes 76 and 77 with DNA

The emission spectrum of linear nitro complex **76**, obtained by excitation at 450 nm, was found to change dramatically in the presence of increasing concentrations of DNA. Two distinct phases of change were observed in the emission profile. Firstly, an initial rapid decrease in emission intensity of 28% was observed up to 1.2 base pair equivalents, followed by a more gradual increase to a plateau, as shown in Figure 4.12.

The initial decrease in emission intensity is most likely due to DNA induced stacking of the complexes.[87] In this stage of titration the ratio of complex:DNA is high, and the fact that the complex has a high binding affinity is expected to result in complex – complex interactions. As discussed in *Chapter 2*, such stacking interactions place the metal centres in close proximity to each other, and quenching of emission results. The intensity increase at higher DNA ratios is quite modest at 1.1 fold overall, but not unexpected due to the more rigid nature of **76**.

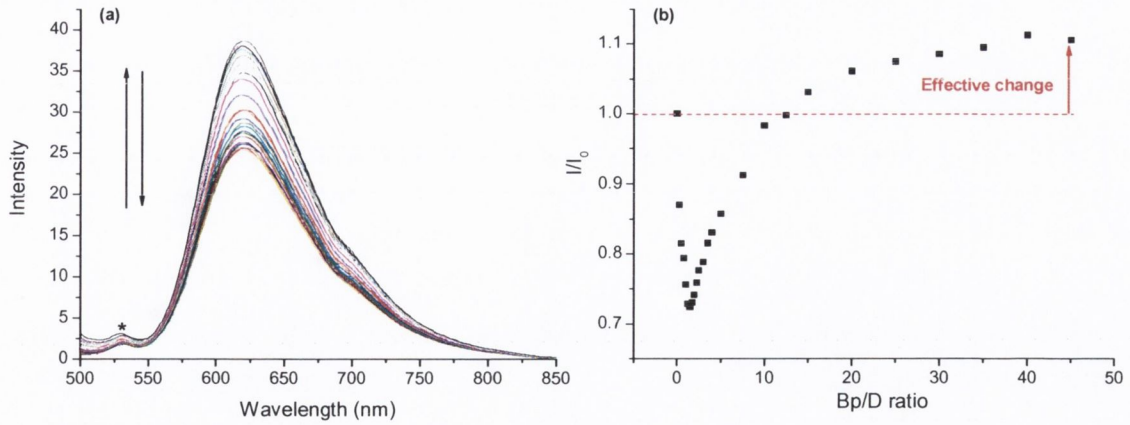

Figure 4.12 *(a) Changes in the MLCT emission spectrum of* ***76*** *(6.6 μM) (excitation at 450 nm) upon addition of st-DNA (0 – 297 μM base pairs) in 10 mM phosphate buffer, at pH 7. (b) The change in integrated MLCT emission as a function of Bp/D. The water Raman band is denoted by *.*

Quenching of the MLCT emission of **76** in solution occurs by electron transfer to the 1,8-naphthalimide moiety, in a similar manner as for the flexible complexes discussed in *Chapter 2*. However, due to the flexible nature of the complexes discussed in *Chapter 2*, the distance between the metal centre and the 1,8-naphthalimide, and their communication, was modulated upon binding DNA. Such behaviour cannot occur for **76**, due to its inherent rigidity. The observed emission increases for **76** must therefore be due to protection of the metal centre by DNA from quenching by other species such as solvent and dissolved oxygen. The emission enhancement observed is therefore most likely due to a combination of reduced quenching, and also a redistribution of complex bound to DNA from a self-stacking mode to a non-stacked mode. The latter may also help explain the large equivalents of DNA necessary to reach a plateau in the emission intensity, as shown in Figure 4.12. Control experiments verified that the binding process was not time-dependent.

A similar emission profile was observed for wedged nitro complex **77** upon the addition of DNA, as shown in Figure 4.13. Here, the initial intensity decrease is again likely due to a DNA induced stacking conformation, which forces the metal centres into close proximity. However, here the changes were greater than seen for **76**, which may be a consequence of the molecular arrangement, with stacking of the 1,8-naphthalimides forcing the metal centres into closer proximity than in **76**. The subsequent emission enhancement is also larger for **77** than for **76**. This could be a consequence of the

molecular arrangement, where insertion of the 1,8-naphthalimide into DNA places the metal centre in closer proximity to the DNA, and hence into a more protected environment.

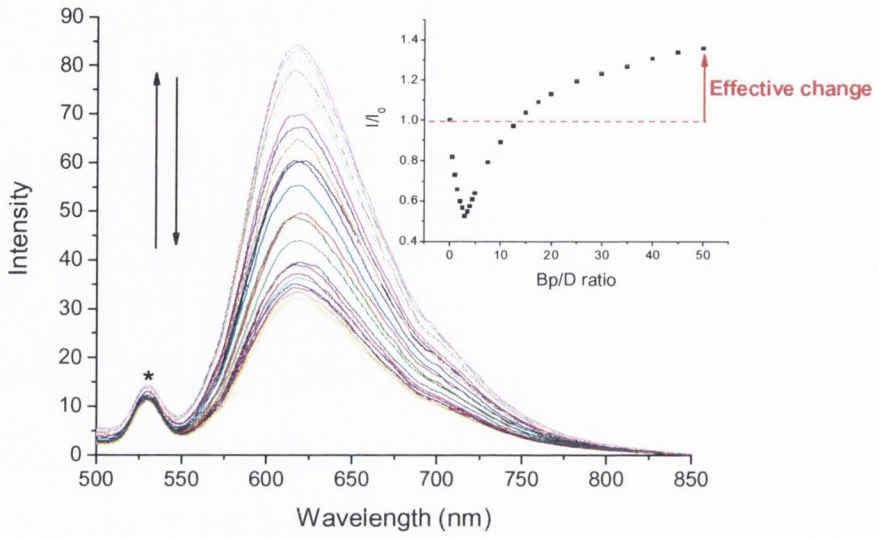

Figure 4.13 *Changes in the emission spectrum of 77 (6.9 μM) (excitation at 450 nm) upon addition of st-DNA (0 – 345 μM base pairs) in 10 mM phosphate buffer, at pH 7. Inset: The change in integrated emission intensity as a function of Bp/D. The water Raman band is denoted by *.*

Quite large equivalents of DNA were necessary to reach the plateau for both **76** and **77**. This would initially suggest that the metal centre itself is quite loosely associated with the DNA. However, UV/Visible studies demonstrated the tight binding of both components of these complexes to DNA. Hence, it is possible that a large number of equivalents of DNA are necessary to effect a redistribution of the complex from the stacked form.

The two rigid 4-nitro-1,8-naphthalimide containing complexes **76** and **77**, emphasise the significant importance that the linker in a chromophore – quencher assembly may have on the resulting spectral responses to added DNA. Both complexes were weakly emissive, and as such were expected to display different luminescence behaviour to the other complexes discussed in this thesis. However, very slight emission enhancements were observed for both of these systems, as the distance between the metal centre and the 1,8-naphthalimide, and consequently the rate of electron transfer could not alter upon interaction with DNA. This is in striking contrast to the systems discussed in *Chapter 2*. Complexes **76** and **77** serve to emphasise how the interaction with DNA and resulting spectral responses may be significantly altered, not only by changing the nature of the

substituents on the 1,8-naphthalimide moiety, but also the nature of the linker, in particular its conformational properties. Both of these conjugates are locked into a non-emissive state, which cannot be significantly altered upon binding DNA.

4.5.2.2 Emission Titration of Amino Complexes 78 and 79 with DNA

The emission from **78**, due to excitation at 450 nm, upon titration with DNA is shown in Figure 4.14. Again, as was observed above, two distinct phases of change can be identified. The first region up to ca. five base pair equivalents, is steep and represents most of the intensity change. The change then becomes more gradual reaching a plateau of 1.8 fold overall enhancement in emission intensity at approximately 30 base pair equivalents. This enhancement may be regarded as being purely due to tight binding of the 1,8-naphthalimide, which holds the metal centre in close proximity to the DNA, with subsequent loss of quenching.

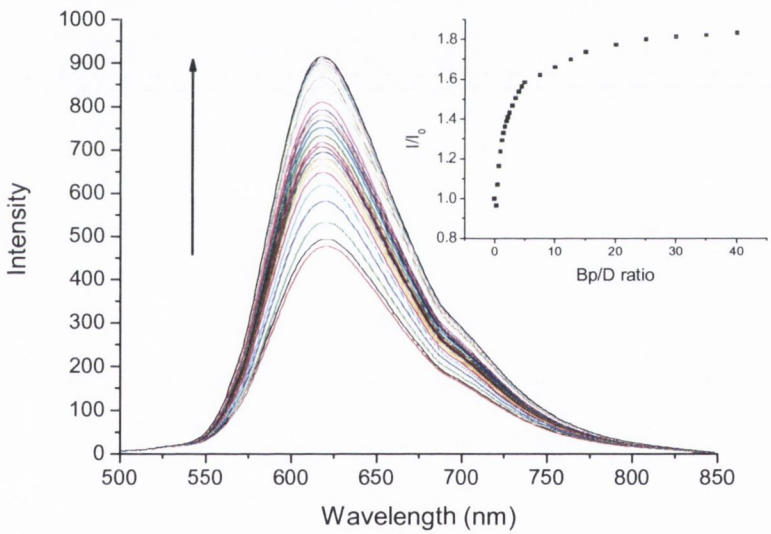

Figure 4.14 *Changes in the emission spectrum of* ***78*** *(6.9 μM) (excitation at 450 nm) upon addition of st-DNA (0 – 345 μM base pairs) in 10 mM phosphate buffer, at pH 7. Inset: The change in integrated emission intensity as a function of Bp/D.*

DNA titrations were also carried out at varying salt concentrations. The results of these studies are shown in Figure 4.15, which demonstrate, as expected, that the overall emission enhancement upon addition of DNA decreases as a function of added NaCl. However, even at 100 mM NaCl substantial luminescent enhancements are observed, which suggest that non-electrostatic interactions are the most prominant in the binding of this complex to DNA. This was anticipated in the initial design of these complexes, the

1,8-naphthalimide providing high affinity binding through intercalation into DNA, with the metal centre remaining externally bound through electrostatic attraction to the phosphate backbone.

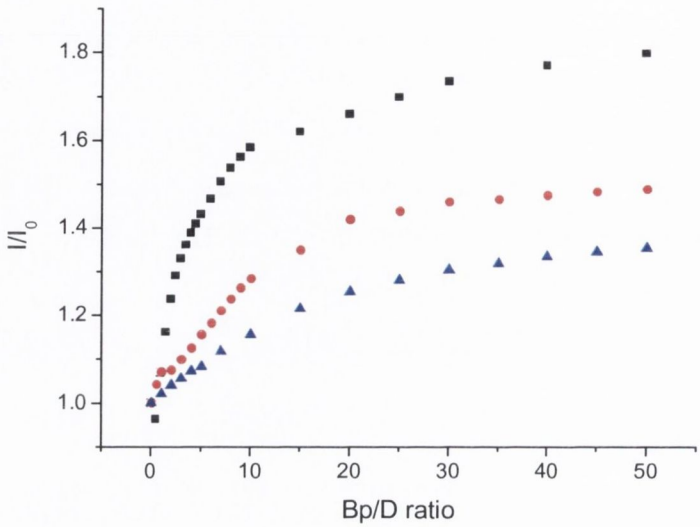

Figure 4.15 *Relative changes in the emission of* ***78*** *(6.5 μM) (excitation at 450 nm) with increasing concentration of st-DNA (0 – 58.5 μM), in 10 mM phosphate buffer (■), 10 mM phosphate buffer + 50 mM NaCl (●) and 10 mM phosphate buffer + 100 mM NaCl (▲).*

The emission changes displayed by the wedged complex **79** upon addition of DNA are shown in the appendix. These were significantly greater than those for its linear analogue **78**, being characterised by a rapid initial increase (0 – 2 base pairs), followed by a very gradual increase up to a plateau at approximately 15 base pair equivalents, with an overall emission enhancement of 2.6 fold. The significantly greater enhancement that occurs for this system in comparison to its linear analogue **78** is clear in Figure 4.16, where the emission profiles of both complexes are compared to that of $Ru(bpy)_3^{2+}$. This greater enhancement may be related to the arrangement of the constituents of the complex around the connecting ring. A meta arrangement creates a cleft as discussed in Section 4.4.1, the result of this being that the shape of the complex is more complementary to that of the DNA. Upon insertion of the 1,8-naphthalimide into the helix, the Ru(II) centre in **79** is held more tightly bound to the DNA than that in **78,** and as a result is more effectively protected from quenching. Overall complex **79** displays a better fit in binding DNA.

Further examination of the spectra for titration of **79** reveals an interesting feature. The first two additions of DNA seem to induce not only luminescence enhancement, but also a slight red shift in the emission maximum. It is not fully understood why this

phenomenon occurs but may be due to a different mode of interaction at low DNA ratios, in which the substituted bipyridine ligand is intercalated or partially intercalated. Addition of further DNA effects a redistribution to a mode of interaction that does not induce such a red shift.

As for the linear system **78,** studies on **79** were also carried out at varying salt concentration. As before, an emission enhancement occurred in the presence of 50 mM and 100 mM NaCl, although the magnitude of the change was decreased relative to that in 10 mM phosphate buffer alone, see appendix. Nevertheless, this shows that **79** does remain bound to DNA, even at high ionic strength, and hence, non-electrostatic modes of interaction are also important in its binding to DNA.

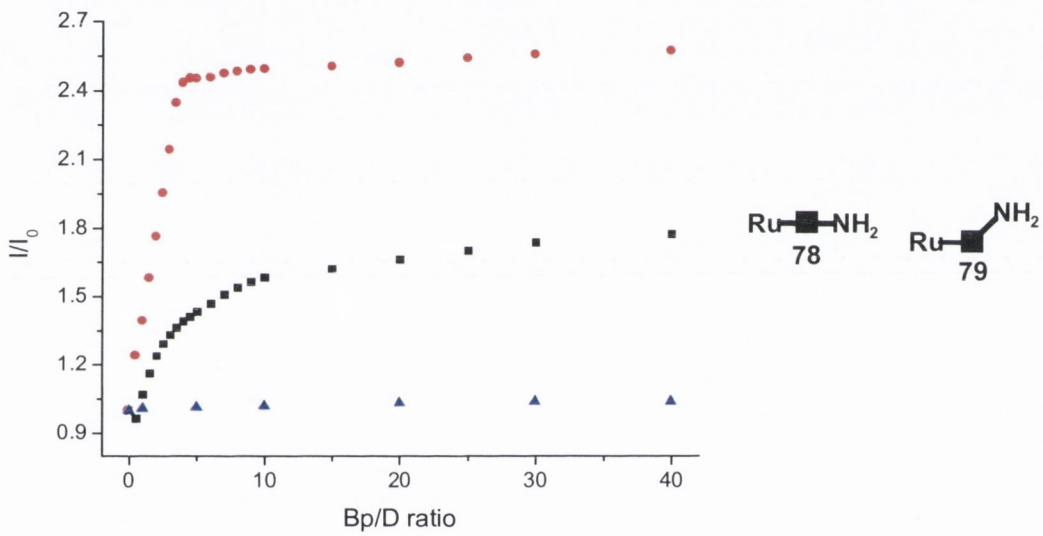

Figure 4.16 *Comparison of the emission intensity changes for* $Ru(bpy)_3^{2+}$ *(▲), **78** (■) and **79** (●) upon addition of DNA.*

In addition to possessing contrasting photophysical properties to their nitro analogues, the amino complexes **78** and **79** also display different emission responses upon titration with DNA, where the emission intensity was enhanced by *ca.* 1.8 fold for **78** and 2.6 fold for **79**, respectively. These results are again, consistent with stronger binding of wedged complexes to DNA due to greater complementary in shape.

It has been shown from the above studies, that a more precise control of the orientation of the components in bichromophore complexes, of the type presented in this thesis, can have significant consequences on the nature of their interaction with DNA. Each of the complexes **76** – **79** were shown to binds DNA with very high affinity, possessing binding constants of the order of 10^6 – 10^7 M^{-1}. A wedged arrangement of the chromophores was shown to result in greater affinity for DNA, due to a greater

complementarity in shape of the complex to that of the helix. The emission profiles displayed by each system were characterised by two phases of change. However, the nature of the changes was substantially different for the amino complexes *vs.* that of the nitro complexes, where both **78** and **79** displayed emission enhancements upon titration with DNA. The emission changes were shown to be moderately sensitive to added salt, suggesting non-electrostatic modes of interaction to be important in the overall binding process.

The nitro substituted complexes **76** and **77** displayed quite pronounced quenching of emission at low equivalents of DNA, followed by a gradual increase upon increasing concentration of DNA. These observations were attributed to DNA induced self stacking at low concentrations of the nucleic acid, followed by a redistribution to an un-stacked form at higher concentrations. In order to verify the more efficient binding that results with a wedged arrangement, and gain further understanding of the interaction, further spectroscopic measurements were carried out, as detailed in the following sections.

4.5.3 DNA Thermal Denaturation Studies of 76 – 79

Thermal denaturation studies were carried on **76** – **79** in the presence of DNA, as in the previous chapters. In the absence of metal complex the T_m value for DNA was determined to be 67 °C.

As previously seen, the melting transition for both **76** and **77** did not reach a plateau at 90 °C, Figure 4.17. Hence, it was not possible to fit the data to a sigmoidal function and extrapolate to the end point accurately, and as such exact melting values cannot be reported, but may be regarded as being greater than 75 °C. However, the different extent of the stabilisation between the linear and wedged systems is apparent from these changes, where **77** resulted in a significantly greater shift to higher temperature in the melting profile. This result is complementary to those from the UV/Visible absorption and emission studies, and emphasises the higher affinity of this system in comparison to the linear analogue

The shifts in melting temperature associated with binding of the amino derivatives **78** and **79** to DNA were less than those for their nitro analogues **76** and **77**, as shown in Figure 4.17, with a shift of approximately 4 °C for both **78** and **79**. As before, the wedged system seems to result in a slightly greater stabilisation than its linear analogue. It is possible that the nitro derivatives, being more electron deficient undergo greater stacking

interactions with the DNA bases than their amino analogues and lead to slightly greater stabilisation of the helix.

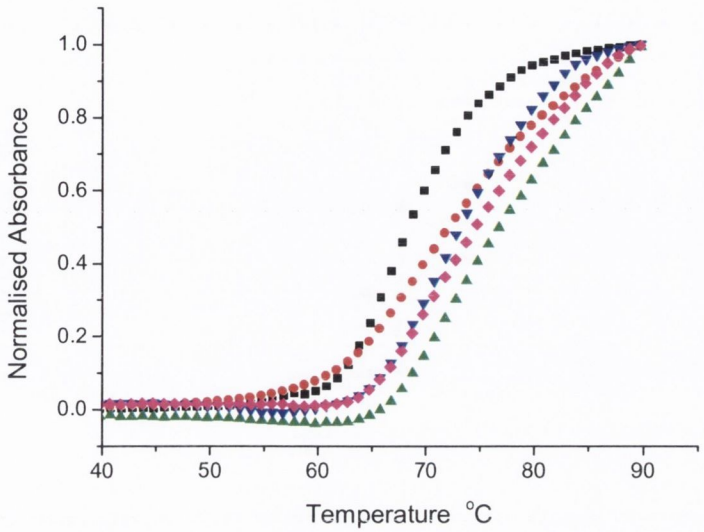

Sample	T_m
DNA	77 °C (± 10%)
76 (Bp/D 5)	> 75 °C (± 10%)
77 (Bp/D 5)	> 75 °C (± 10%)
78 (Bp/D 5)	73 °C (± 10%)
79 (Bp/D 5)	73 °C (± 10%)

Figure 4.17 *Thermal denaturation curves of ct-DNA (150 μM) in 10 mM phosphate buffer, at pH 7, in the absence (■) and presence of* ***76*** *(●),* ***77*** *(▲),* ***78*** *(▼) and* ***79*** *(♦) at a Bp/D ratio of 5.*

In summary the result from the thermal denaturation studies of **76** – **79** in the presence of DNA, complement the results from UV/Visible absorption and emission titrations. The significant stabilisation of the helix associated with binding of these systems highlights the high affinity that they all possess for DNA. The results also support the binding model which places the wedged systems in more tight association with the helix.

4.5.4 Circular Dichroism Studies of 76 – 79

Circular dichroism titrations were carried out on **76** – **79**, in which the concentration of DNA was kept constant and that of the metal complex was varied to give a range of Bp/D ratios. The spectra obtained for wedged nitro complex **77** are depicted in Figure 4.18. From examination of these results, it is apparent that this system displays similar CD behaviour to that observed for the Ru(II)-1,8-naphthalimide conjugates discussed in the previous chapters; a small ICD is observed at long wavelength corresponding to the MLCT absorption, in addition to large changes in the DNA region, attributable to both changes in the CD signal of the DNA itself and ICD of the metal complex in this region. These results are indicative of association of the metal centre in

the grooves, which results in an induced CD.[152] As observed for the systems discussed in the previous chapters, practically no changes were seen for the 1,8-naphthalimide moiety.

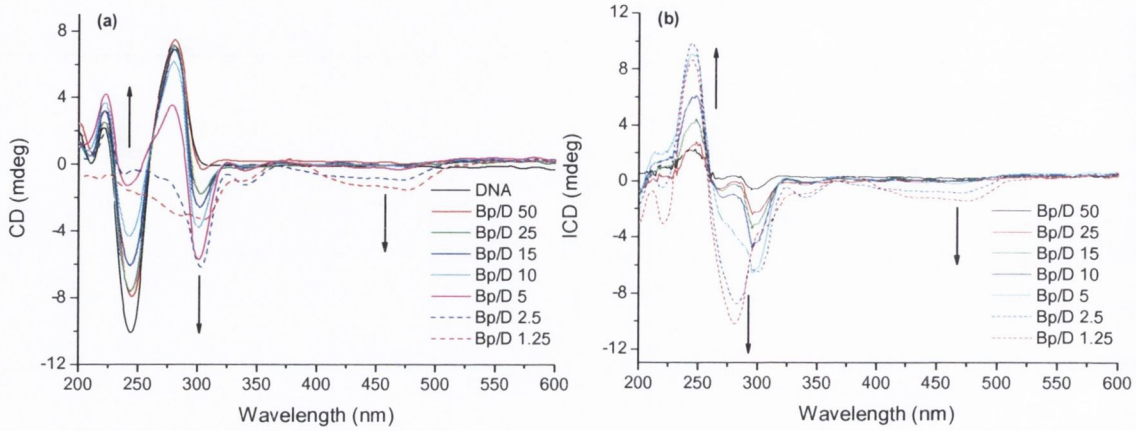

Figure 4.18 *Circular dichroism curves of (a) ct-DNA (150 μM) in 10 mM phosphate buffer, at pH 7, in the absence and presence of* ***77****, at varying ratios, and (b) the difference spectra obtained.*

Significantly different CD behaviour was exhibited by the linear nitro complex **76**. The changes at the MLCT band were the same as for **77**. However, these were concomitant with changes in the region of absorption of the 1,8-naphthalimide.

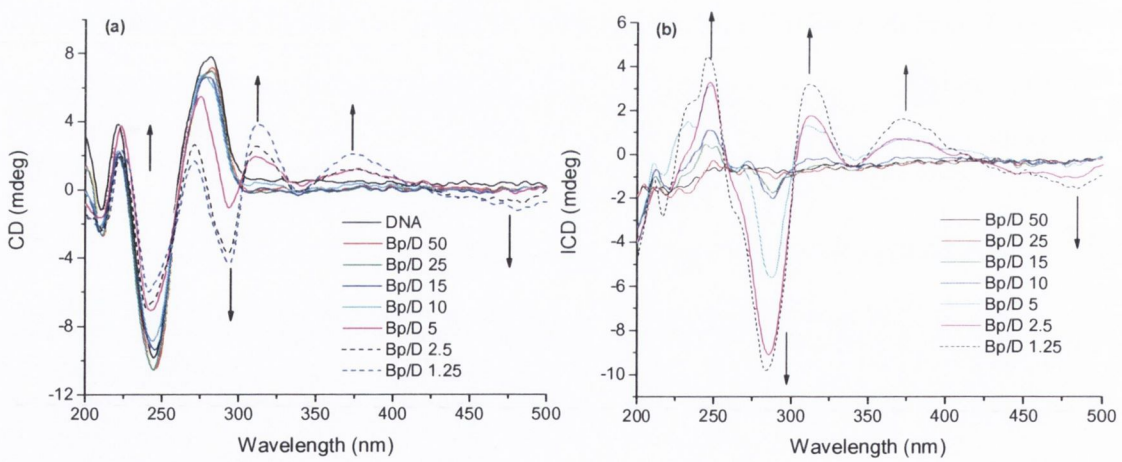

Figure 4.19 *Circular dichroism curves of (a) ct-DNA (150 μM) in 10 mM phosphate buffer, at pH 7, in the absence and presence of* ***76*** *at varying ratios, and (b) the difference spectra obtained.*

From examination of the 300 – 400 nm region in Figure 4.19 two bands are apparent that had not been seen in previous examples. However, it was initially not clear

from the CD spectra in Figure 4.19 as to the origin of these bands. To investigate this phenomenon a CD experiment was run, in which a solution of **68** was used as the baseline, and then DNA was added to give a final solution of Bp/D = 1.25. The results of this experiment are presented in Figure 4.20.

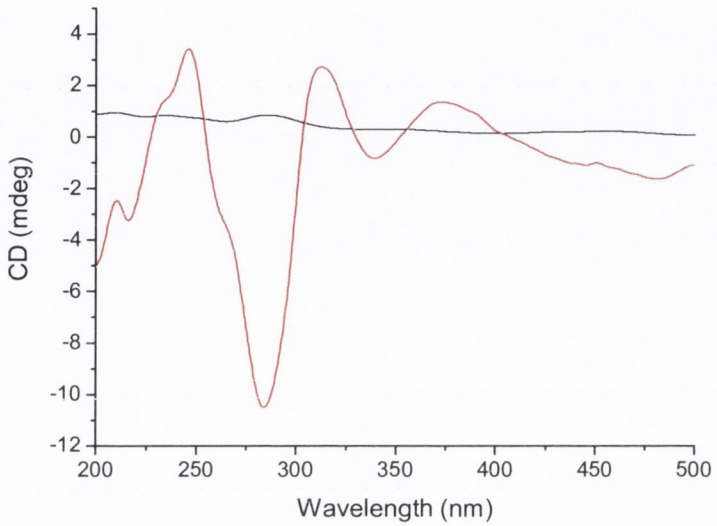

Figure 4.20 *Circular dichroism curves of* ***76*** *(——) and* ***76*** *+ DNA (——) (Bp/D 1.25) (****76*** *as baseline), both in 10 mM phosphate buffer, at pH 7. Recorded after the accumulation of 30 scans for each sample.*

The spectrum contains features very much representative of an exciton CD signal, which has a characteristic bisignate shape, with one positive and one negative band located either side of the absorption maximum of the free ligand, and results from the close proximity of two identical transition moments of equal energy.[152] Here, a positive signal at 378 nm and negative signal at 340 nm are observed, respectively, with a crossover at 355 nm. This type of behaviour is a result of the formation of dimers or higher order complexes by stacking in the grooves or externally to the double helix. Such results have previously been observed for species such as methylene blue.[173] The phenomenon only occurs at high loading of the complex on DNA, and thus the results are in agreement with the propsed DNA induced stacking of this complex under similar conditions. Why this phenomenon occurs here and not for the wedged analogue is unclear. Previous emission results showed that the complexes stacked with added DNA, and that the process was more significant for the wedged complex. It is possible that the absence of an exciton CD signal for **77** is simply due to the different orientation of the 1,8-naphthalimides when stacked within the DNA helix.

The two amino derivatives **78** and **79** displayed similar CD behaviour to each other and indeed to the complexes discussed in previous chapters, as shown in the appendix. The most significant feature observed for these derivatives was the growth of a band in the region of absorption of the metal centre. Large changes were also observed in the region of absorption of DNA, in the same manner discussed previously.

The results from these CD studies yielded similar information as was seen for the flexible complexes discussed in the previous chapters. The overall results point to a binding mode in which the metal centre is tightly associated with the helix, thus experiencing its chirality. Considered with the other spectroscopic studies presented so far, it is likely that the DNA binding involves insertion of the 1,8-naphthalimide into the helix, with tight association of the metal centre, through external binding or partial insertion into the grooves.

4.5.5 Ethidium Bromide Displacement Assay of 76 – 79

The addition of each of the complexes **76** – **79** to DNA bound ethidium bromide, resulted in a decrease in fluorescence from the latter, due to dislodgement from DNA, Figure 4.21. The same trends in binding affinities as those calculated from UV/Visible absorption titrations could be identified. From examination of Figure 4.21 it is clear that **76** displays significantly weaker affinity for DNA than its wedged analogue **77**, with greater equivalents of the former necessary to displace the DNA bound EtBr. A similar trend was observed for **79** and **78**. This is in agreement with the broader trends that have emerged from the above studies of these four systems; i.e. the wedged (meta) arrangement around the connecting rings allows for more favourable interaction with DNA than the linear (para) analogues.

The binding constants determined from EtBr displacement, Figure 4.21, were in general agreement with those calculated from fitting to UV/Visible absorption data, with the exception being **78** (which was determined to have a binding constant of 3.0×10^6 from UV/Visible absorption titration and 1.1×10^7 M^{-1} from EtBr displacement). It was remarked when previously discussing the UV/Visible absorption results, that for this complex and its wedged analogue, the changes observed are representative of both the 1,8-naphthalimide and MLCT absorption bands. Additionally, the fitting of the UV/Visible absorption data takes the binding site size of the compound into consideration, whereas the value from displacement is an average value relative to another known DNA binder. These factors may contribute to the observed discrepancy. The important result to

note, however, is the affinity of each system relative to the other, the wedged arrangement allowing for more efficient DNA binding.

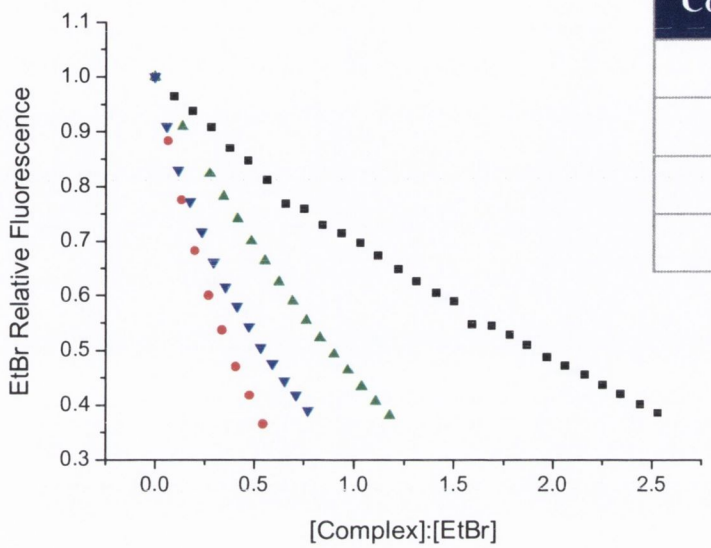

Complex	K
76	5.2×10^6
77	2.6×10^7
78	1.1×10^7
79	1.7×10^7

77 > 79 > 78 > 76

Figure 4.21 *Decrease in fluorescence of DNA bound EtBr upon addition of* ***76*** *(■),* ***77*** *(●),* ***78*** *(▲), and* ***79*** *(▼) in 10 mM phosphate buffer, at pH 7.*

4.6 Conclusions

The results presented in this chapter have further contributed to our overall understanding of the properties of the bifunctional Ru(II)-1,8-naphthalimide conjugates, in particular the effect of variations in substitution and connectivity. It has been demonstrated that the use of a more rigid aromatic group as the linking moiety, allowed for more precise control of the orientation of the components of the complex with respect to each other. Effects were observed in both the solution photophysical properties of the resulting conjugates in solution, and upon DNA binding. A wedged, or meta arrangement, around the connecting ring was shown to result in greater affinity for DNA, and greater changes in the spectroscopic properties, due to greater complementarity in the shape of the complex to that of the DNA.

Complexes **76** and **77** were shown to display substantially different spectroscopic responses upon addition of DNA, to their flexible analogues discussed in *Chapter 2*. Both complexes were shown to undergo a DNA induced stacking process at low equivalents of the nucleic acid, with concomitant emission quenching. This was followed by an emission enhancement with further added DNA, which was possibly a result of redistribution and protection from quenching in the local environment of the DNA.

The effect of substitution on the 1,8-naphthalimide ring system was also investigated. Complexes **78** and **79** were also prepared, which possessed an amino group at the 4-position of the 1,8-naphthalimide moiety. These systems possessed substantially different photophysical properties to their nitro analogues, being strongly emissive in solution. Furthermore, both displayed significant emission enhancement upon binding to DNA, an observation that was attributed solely to the protection of the complex from quenching by external species. Similar differences were observed between the wedged and linear forms discussed above; the former displaying substantially greater binding affinity for DNA. Overall through study of complexes **76** – **79**, it has been shown that binding of Ru(II)-1,8-naphthalimide conjugates may be tuned through the overall shape of the complex.

An overall binding mode for conjugates **76** – **79** was proposed, which involves insertion of the 1,8-naphthalimide into the helix with concomitant external, and groove association of the Ru(II) centre. The tight binding, typical of intercalative interaction was also apparent from thermal denaturation studies, where large shifts were observed in the T_m of DNA. Ethidium bromide displacement assays further confirmed this high affinity binding, with binding constants in the range $10^6 - 10^7$ M^{-1} for **76** – **79**. Finally, ICD in the region of absorption of the Ru(II) centre, confirmed the metal complex component of each conjugate to be tightly bound to DNA, probably associated to some degree in the grooves.

Due to the excellent DNA binding ability of the systems discussed in this chapter it was decided to investigate their ability to act as DNA photocleavers, with the ultimate aim of applying them as such within cells as novel photodynamic therapy (PDT) agents. These studies will be presented in full in *Chapter 6*.

Chapter 5

Rigid 1,8-naphthalimide-diquat Conjugates

5.1 Introduction

In the previous chapters of this thesis, the focus has been on the interaction of 1,8-naphthalimide conjugated Ru(II) complexes with DNA. Excellent affinity for DNA has been observed for many of these systems, signalled by significant changes in their spectroscopic properties, particularly the Ru(II) based MLCT emission.

In this chapter, a series of organic compounds, comprising 1,8-naphthalimide and diquat functionality were developed and their photophysical properties investigated. Diquat, **91** is a derivative of 2,2'-bipyridine, in which the two bipyridine nitrogens have been bridged by an ethylene group. This compound is a commonly used herbicide that produces desiccation and defoliation.[174] Furthermore, diquat possesses well defined electrochemical properties, and undergoes two sequential reduction processes.[175] Its ease of reduction may have interesting consequences when bound to DNA, with diquat derivatives having previously exhibited electron transfer from the DNA bases.[176] More extensively studied as DNA binding, and as redox active agents, are the viologens. Molecules incorporating viologen functionality have previously been shown to bind DNA with high affinity and undergo photoinduced electron transfer processes with the bases.[177,178] The organic dppz based system **92**, has also been previously studied by Thomas and co-workers, and shown to display excellent binding affinity for DNA, being of the same order as dppz based Ru(II) complexes.[179,180]

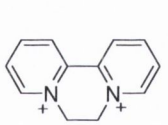

91

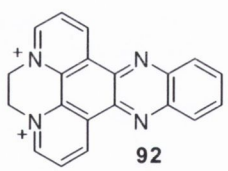

92

In light of the excellent binding affinity observed for rigid complexes **76** – **79** described in the previous Chapter and to understand the influence of the metal centre on binding to DNA it was decided to quaternize ligands **88** and **89**, and to investigate the DNA binding behaviour of the resulting conjugates. Four systems were considered: the 4-nitro-1,8-naphthalimide based structures **93** and **94**, the 4-amino-1,8-naphthalimide based structure **95**, and the reference compound **96**, which was regarded as necessary to evaluate the contribution to DNA binding from the diquat portion of the molecule, and to provide a reference for the photophysical properties of this portion of the molecule.

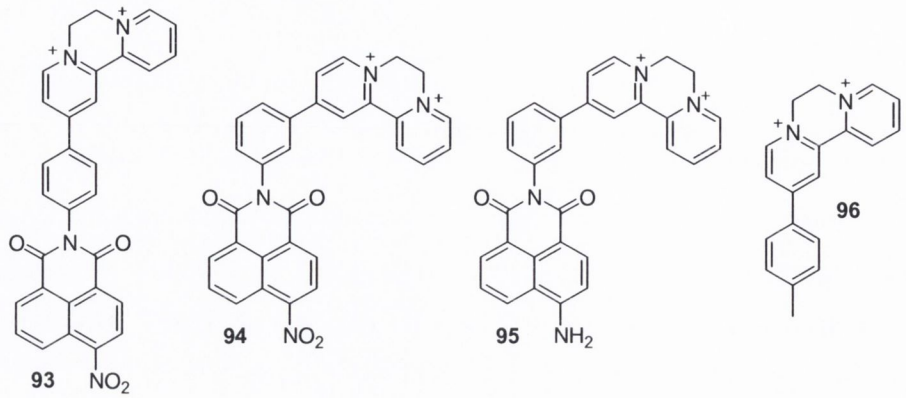

5.2 Synthesis of 93 – 96

The synthesis of **93** – **96** was achieved through quaternisation of an appropriate bipyridine as discussed in the following sections.

5.2.1 Synthesis of 4-nitro-1,8-naphthalimide-diquat Conjugates 93 and 94

The nitro derivative **93** was synthesised as outlined in Scheme 5.1. This involved reflux of ligand **88**, in dibromoethane for 48 hours, and isolation of the resulting precipitate by suction filtration. Washing of the precipitate with acetone and ether, to remove unreacted starting material, gave the product as a brown solid in 80% yield. The starting material was sparingly soluble in dibromoethane at room temperature, but dissolved fully as the reaction mixture reached reflux temperature. A precipitate then formed as the reaction progressed. The bromide counter-ions in the product were exchanged for chloride by dissolution in MeOH, followed by stirring with Amberlite ion exchange resin (Cl^- form) for 1 hour.

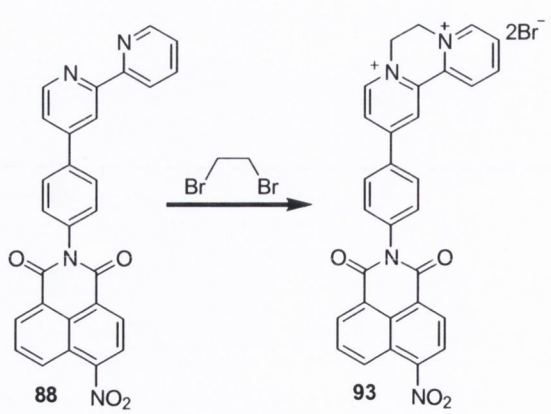

Scheme 5.1 *Synthesis of 1,8-naphthalimide-diquat conjugate* ***93****.*

Analysis of the reaction mixture by ^{1}H NMR (D_2O, 400 MHz) after shorter periods of reflux, showed the presence of a mixture of starting material and product. Product formation was evident from the appearance of a resonance in the ^{1}H NMR spectrum at approximately 5.30 ppm, integrating for 4 protons, corresponding to the two CH_2's of the bridge. Furthermore, electrospray mass spectrometry showed the presence of a peak at 499.1411 corresponding to the M^{2+} ion. This compound was further characterised by ^{13}C NMR, IR and elemental analysis, details of which are provided in the experimental chapter. A similar procedure was applied in the synthesis of the wedged 4-nitro-1,8-naphthalimide-diquat derivative **94**, starting from the corresponding 1,8-naphthalimide-bipyridine ligand, as detailed in Table 5.1

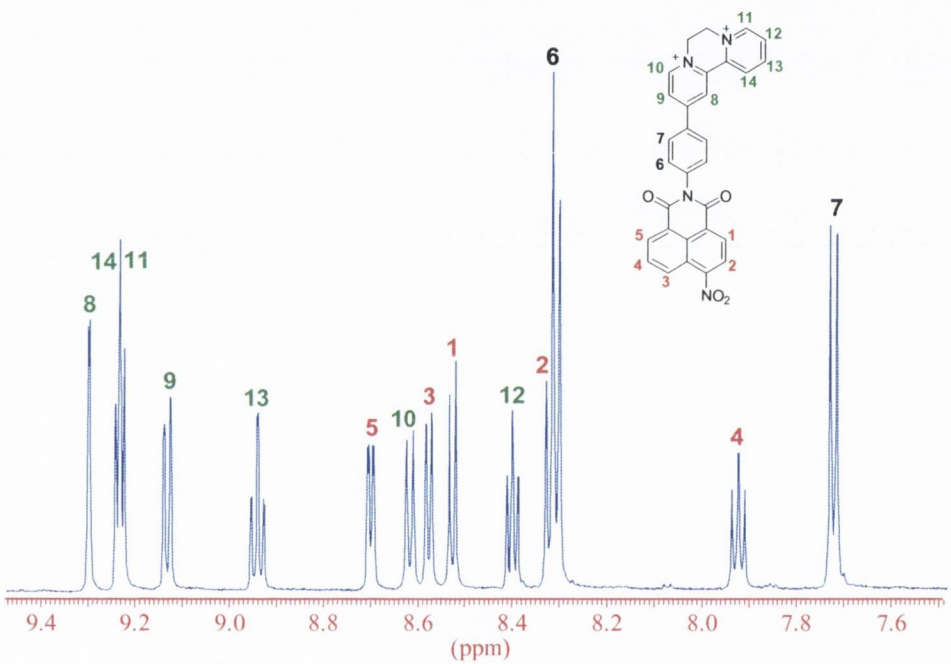

Figure 5.1 *The ^{1}H NMR spectrum of* ***93*** *(D_2O, 600 MHz) showing the aromatic region.*

Table 5.1 *Synthesis of 4-nitro-1,8-naphthalimide-diquat conjugates.*

Reactant	Linker	Product	Yield
88	para	**93**	80 %
89	meta	**94**	82 %

5.2.2 Synthesis of 4-amino-1,8-naphthalimide-diquat Conjugate 95

A number of methods were explored for the synthesis of the amino derivative **95**. These included reduction of the corresponding nitro conjugate **94**, by hydrogenation, and

condensation of amine **87** with 4-amino-1,8-naphthalic anhydride to afford an amino substituted ligand precursor. The reduction of ligand **89**, followed by bridging of the bipyridine nitrogens proved to be a successful route to the desired product, as shown in Scheme 5.2. The first method investigated for reduction of the ligand **89** involved suspension in MeOH, in the presence of 10% Pd/C, followed by heating at reflux for 1 hour. Hydrazine was then added and the mixture heated at reflux for a further 24 hours. Although the starting material was sparingly soluble in MeOH, it was anticipated that the amine present in the product would render it more soluble, and thus more material would go into solution as the reaction progressed. However, this was not observed to be the case and little product was formed. A slightly different procedure was therefore employed, in which the starting material was dissolved in DMF/MeOH and subsequently reacted as before. This successfully yielded the product **99** as an orange solid in 94% yield.

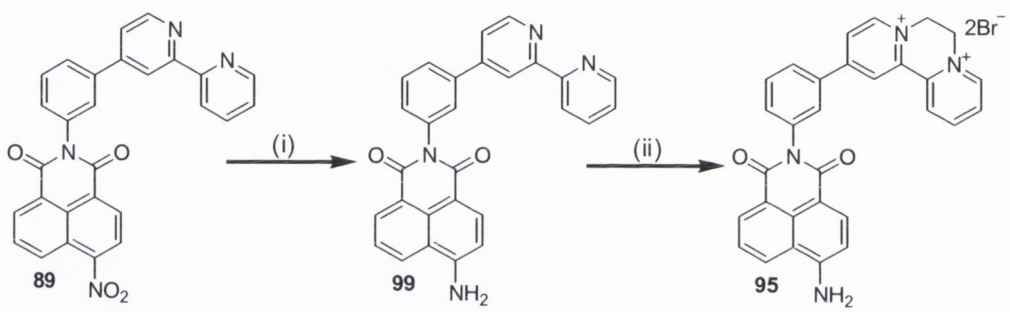

Scheme 5.2 *Synthetic route to* ***95****. Reagent and conditions: (i) DMF/MeOH, Pd/C,* H_2NNH_2*, (ii) dibromoethane.*

An attempt to bridge the reduced ligand **99** was then carried out as for the nitro derivatives, involving reflux for 48 hours in dibromoethane. Upon ^{1}H NMR analysis of the reaction mixture some decomposition or side reaction of the product was evident, after long reaction time, and therefore a shorter reaction time was explored. The starting material was observed to fully dissolve after *ca.* 30 min at reflux. Shortly after this (*ca.* 10 min) a precipitate began to appear after which reflux was continued for 4 hours. The residue was then dissolved in water and filtered to remove unreacted starting material.

^{1}H NMR analysis of this product showed that **95** was successfully formed, although a small amount of impurity was also present, and therefore purification was carried out as detailed in *Chapter 7*. Successful formation of product was evident from the ^{1}H NMR spectrum as shown in Figure 5.2, where a resonance integrating for 4 protons was observed at 5.21 ppm, corresponding to the CH_2's of the bridge. Furthermore, electrospray mass

spectrometry showed the presence of a peak at 471.1806 corresponding to the M^{2+} ion. Due to the lengthy nature of the workup a substantial amount of product was lost, and as such the yield of this reaction was very low at 1.6%.

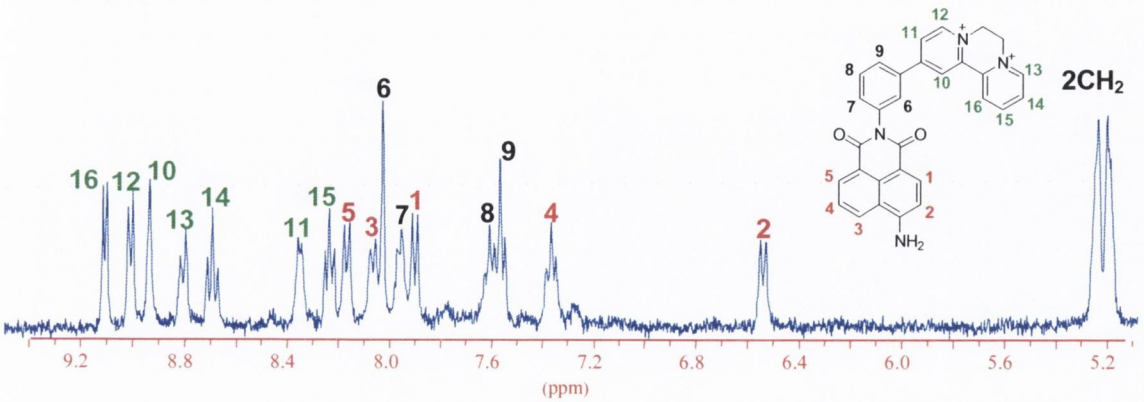

Figure 5.2 *The ^{1}H NMR spectrum of* ***95*** *(D_2O, 400 MHz).*

5.2.3 Synthesis of Reference Diquat Derivative 96

Synthesis of the control compound **96** was achieved through quaternisation of **97**, as shown in Scheme 5.3. This involved suspension of **97** in dibromoethane, followed by heating at reflux for 4 hours. The reaction was worked up as for that in the formation of **93**, giving the product as a yellow solid in 92% yield. Bipyridine **97** was prepared according to the literature procedure.[171] The formation of **96** was apparent from the appearance of resonances in the ^{1}H NMR spectrum at 5.25 and 5.18 ppm, both integrating for two protons, corresponding to the two CH_2's of the bridge. The spectrum and assignment are depicted in Figure 5.3. Furthermore, electrospray mass spectrometry showed the presence of a peak at 275.1555 corresponding to the M^{2+} ion. This compound was further characterised by ^{13}C NMR, IR and elemental analysis, details of which are provided in the experimental chapter.

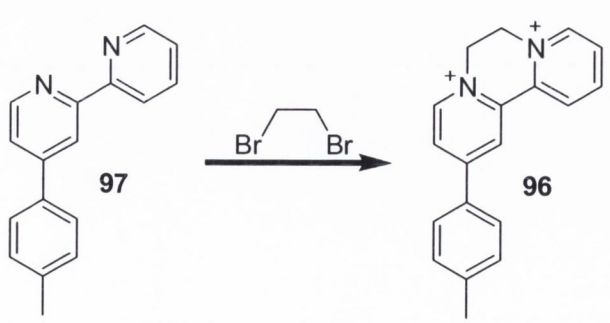

Scheme 5.3 *Synthesis of reference* ***96****.*

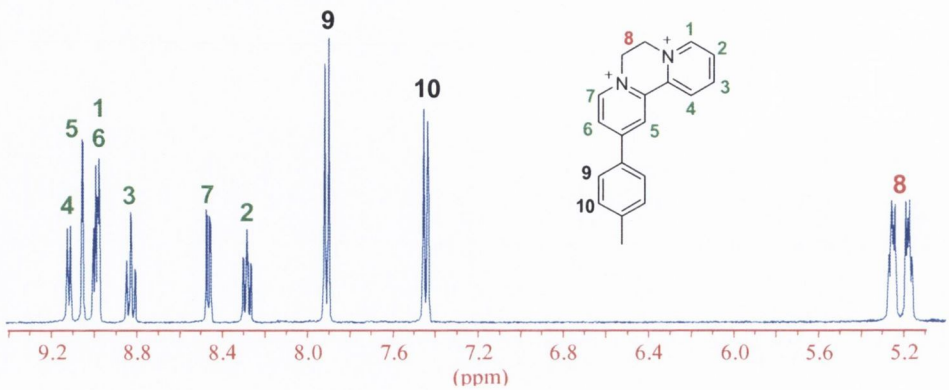

Figure 5.3 *The ^1H NMR spectrum of* ***96*** *(D_2O, 400 MHz) showing the 5.2 to 9.4 ppm region.*

5.3 Photophysical Properties of 93 – 96

5.3.1 UV/Visible Absorption Properties of 93 – 96

Having successfully synthesised **93** – **96** the next step was to characterise their photophysical properties in buffered aqueous solution. The linear derivative **93** displayed three different absorption maxima, Figure 5.4. The first occurring at 232 nm, and the other two overlapping (but distinguishable) bands with λ_{max} at 320 and 336 nm, respectively.

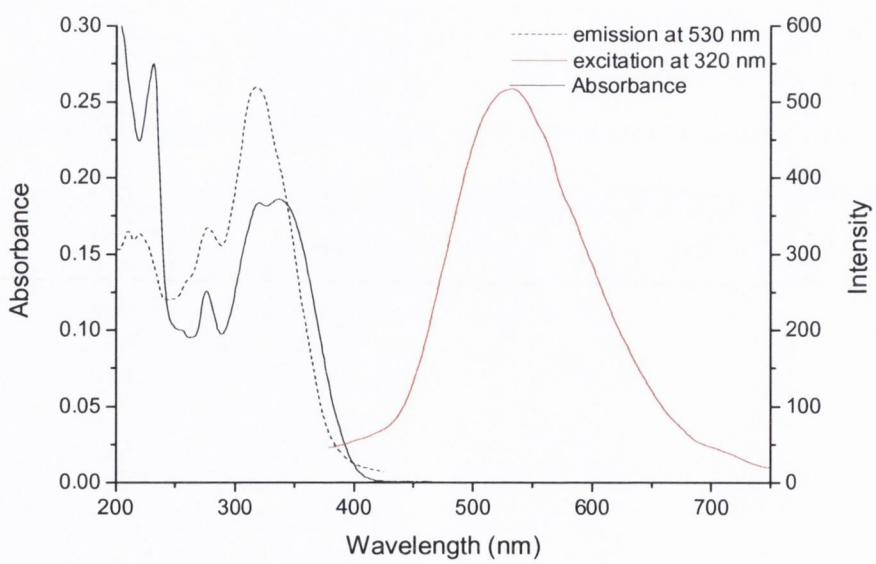

Figure 5.4 *UV/Visible, excitation and emission spectra of* ***93*** *(6.5 μM) in 10 mM phosphate buffer, at pH 7.*

This absorption spectrum of **93** was compared to that of the 1,8-naphthalimide control **59** and for diquat control **96**, see Figure 5.5. Considering these spectra, it is likely that the higher energy part of the 330 nm band consists mainly of contribution from the diquat part of the molecule, while the lower energy part corresponds to both chromophores. Rather than displaying two distinct bands at approximately 300 and 355 nm, a broad band centred at ~ 330 nm was observed, indicating that significant electronic interaction occurs between the two components.

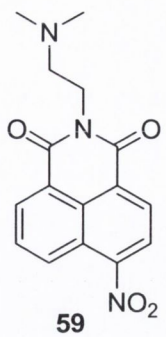

59

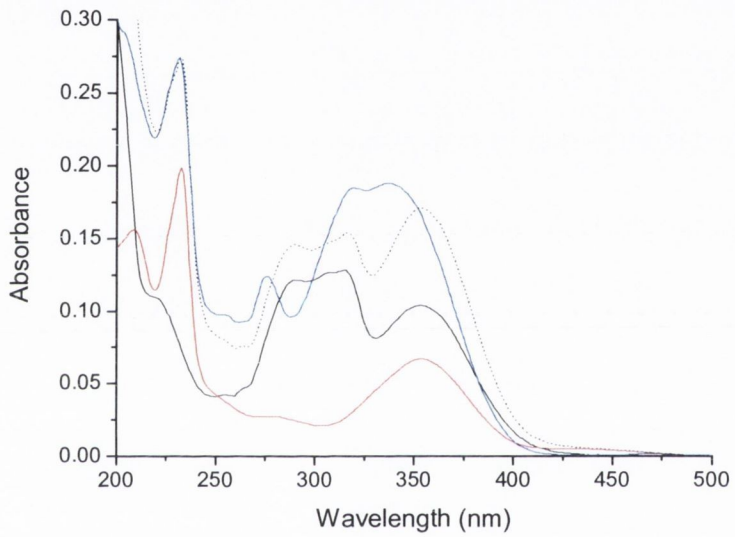

***Figure 5.5** Summed absorption spectra of **93**. **96** (——), **59** (——), **96** + **59** (------) and **93** (——). All solutions at 6.5 μM concentration in 10 mM phosphate buffer, at pH 7.*

(It should be mentioned that the 1,8-naphthalimide reference used was substituted with an alkyl amine at the imide nitrogen and not an aromatic group as in the conjugate **93**. This was necessary for solubility reasons, and is not expected to differ significantly in absorption properties to a system functionalised with an aromatic ring.[120])

The wedged nitro derivative **94** displayed quite similar absorption properties to its linear analogue, however, only one absorption maximum was discernible at long wavelength, occurring at 319 nm. The lower energy region of the absorption band was less prominent in this case. Additive spectra for **94** are also contained in the appendix, from which it is clear that a similar degree of ground state interaction occurs for this compound.

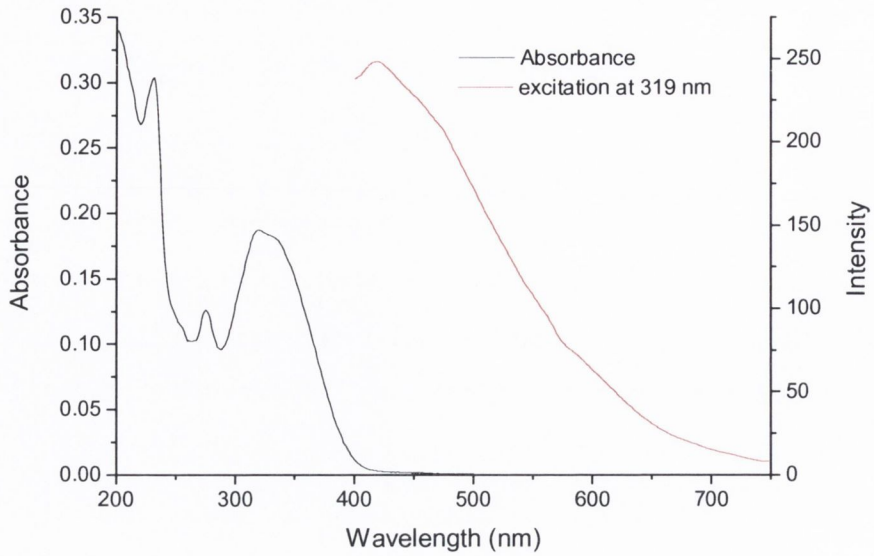

Figure 5.6 *UV/Visible and emission spectra of* ***94*** *(6.5 μM) in 10 mM phosphate buffer, at pH 7.*

The absorption spectrum for amino compound **95** displayed a band at 434 nm, assigned as the internal charge transfer absorption of the 1,8-naphthalimide, and a second band at 311 nm assigned to the diquat moiety, Figure 5.7.

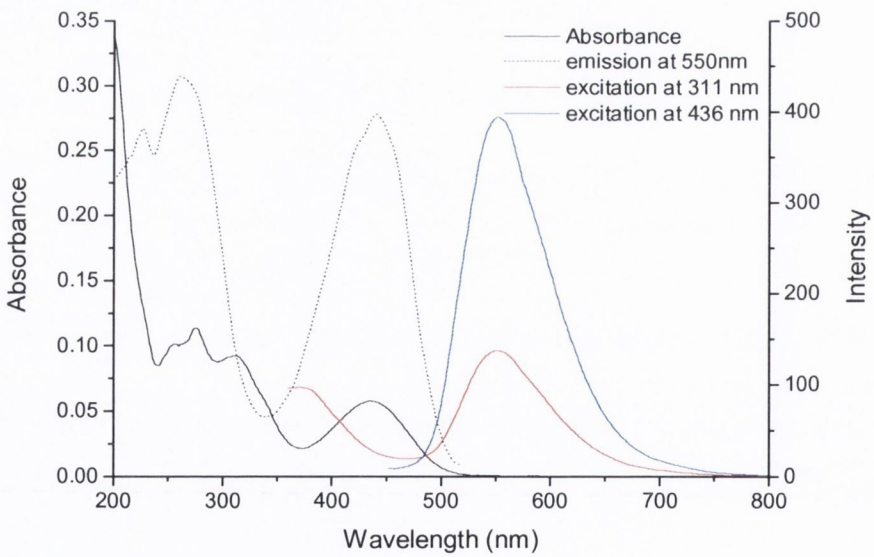

Figure 5.7 *UV/Visible, excitation and emission spectra of* ***95*** *(6.5 μM) in 10 mM phosphate buffer, at pH 7.*

An additive spectrum was also constructed for **95**, Figure 5.8, which showed that the conjugation had little effect on the 1,8-naphthalimide based absorption. However, the

rest of the absorption spectrum was significantly different than that expected, the 350 nm band due to the diquat having essentially disappeared. Diminished absorption was also observed at *ca.* 319 nm, suggesting that the conjugation has a significant effect on the absorption properties of the diquat moiety. A summary of these absorption properties is given in Table 5.2.

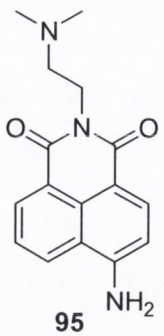

95

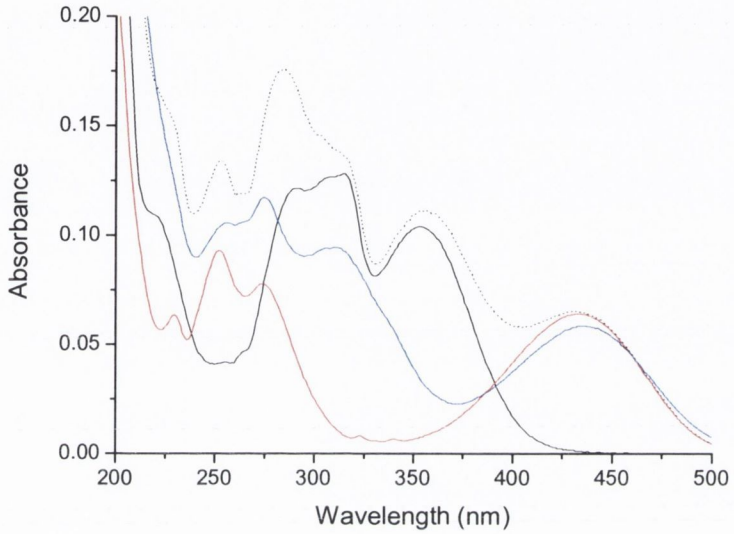

Figure 5.8 *Summed absorption spectra of* ***95****.* ***96*** *(——),* ***90*** *(——),* ***96*** *+* ***90*** *(------) and* ***95*** *(——). All solutions at 6.5 μM concentration in 10 mM phosphate buffer, at pH 7.*

Table 5.2 *Absorption properties of* ***93*** *–* ***96*** *in 10 mM phosphate buffer, pH 7 at 298 K.*

Compound	λ_{max} (nm) [ϵ (M^{-1} cm^{-1})]		
93	232 [42000]	320 [28300]	336 [29000]
94	232 [50000]	319 [29100]	
95	296 [20400]	311 [14200]	434 [8890]
96	292 [19000]	315 [19600]	353 [15900]

5.3.2 Emission Properties of 93 – 96

The emission properties of **93** – **96** were also investigated and shown to be quite sensitive to the particular molecular arrangement of the constituent chromophores. Excitation of **96** resulted in an emission spectrum with two discernable maxima, Figure 5.9, occurring at 415 nm and 530 nm, respectively. From consideration of the emission properties of the conjugated systems discussed below, it is likely that the 530 nm band corresponds to emission from the diquat, while the 451 nm band is due to the attached aromatic ring, or possibly a state involving interaction of the two components.

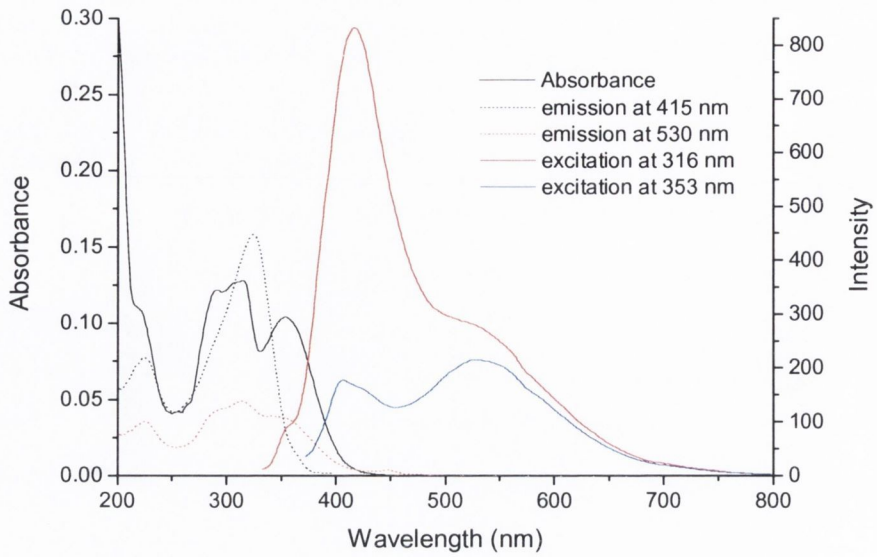

Figure 5.9 *UV/Visible, excitation and emission spectra of* ***96*** *(6.5 μM) in 10 mM phosphate buffer, at pH 7.*

Excitation of **93** gave a single emission band centred at 530 nm, as shown in Figure 5.5. This emission is not typical of a 4-nitro-1,8-naphthalimide,[140] but from comparison to the spectra in Figure 5.9 may be attributed to the diquat portion of the molecule. Furthermore, from examination of the excitation spectrum it is apparent that maximum emission from **93** arises when excited at 319 nm, which corresponds to the absorption of the diquat. The absence of any 1,8-naphthalimide emission may be indicative of a single excited state, arising from mixing of energy levels of the constituent chromophores, or quenching of the 1,8-naphthalimide excited state by the attached diquat moiety. Although an exact comparison cannot be made to other systems reported in the literature to date, a conjugate comprising flexibly linked 1,8-naphthalimide and viologen moieties was previously studied as a DNA photosensitizer, where an intramolecular electron transfer quenching of the 1,8-naphthalimide singlet excited state by the viologen was shown to occur.[181] Such a mechanism may also occur for the more rigidly linked derivatives under discussion here.

Conjugate **94** displayed quite different photophysical behaviour, giving a single broad emission band, as shown in Figure 5.6. This system seems to display both diquat based emission (with an assumed emission maximum at 530 nm), and a 4-nitro-1,8-naphthalimide emission. The degree of interaction between the two chromophores in this system was not as pronounced as in the linear analogue, which only displayed a single emission maximum. This observation would favour an explanation of

the photophysical properties involving a mixing of the energy levels, as discussed above. If electron transfer quenching was responsible for the single emissive state in **93**, it would also be expected to occur for **94**, as the 1,8-naphthalimide and diquat are also held quite closely together in space. Therefore, a mixing of the energy levels, which depends on the orientation of the components, may be responsible for the observed properties, where the linear arrangement allows for effective overlap, while the wedged arrangement does not.

Excitation of a solution of the amino substituted derivative **95** also gave two emission bands, centred at approximately 370 nm and 550 nm, Figure 5.7. The band at 550 nm resulted from both excitation at 311 nm and 436 nm (with the intensity being greater for excitation at the latter wavelength), and was assigned to an excited state corresponding to a mixing of the energy levels of the two components. This is quite different to that observed for the nitro analogue **94**, where little or no interaction was observed in the excited state. A separate emission band was also observed for **95** upon excitation at 311 nm, with λ_{max} at 400 nm, which again is not typical of either the 1,8-naphthalimide or the diquat, and therefore is most likely due to an excited state resulting from interaction of the two components.

From these results it is obvious that conjugates **93** – **96** possessed luminescence properties which may be useful in determining the nature of their interaction with DNA. The emission features of **93** – **95** were shown to be dependent on both the connectivity of the two chromophores and the substituents at the 4-position of the 1,8-naphthalimide ring. The solution properties of the nitro derivatives **93** and **94** were next characterised by cyclic voltammetry, as detailed in the following section.

5.4 Electrochemistry

Bridged bipyridine compounds such as diquat display well defined reduction and oxidation processes.[175] 1,8-naphthalimides also display interesting electrochemistry depending on their particular structure.[121] The electrochemical behaviour of **93** and **94** in aqueous solution is shown in Figure 5.10 and 5.11 respectively. The cyclic voltammograms were recorded by Mr. Gareth Keeley of the Lyons group, at the School of Chemistry, Trinity College Dublin.

System **93** displays three reduction processes in the potential window investigated, occurring at – 0.28 V, – 0.48 V and – 0.78 V respectively. The peaks at – 0.28 V and – 0.78 V correspond to sequential reduction processes at the diquat moiety,[175] while that at – 0.49 V was attributed to the reduction of the 1,8-naphthalimide (no literature values for

nitro substituted 1,8-naphthalimides being available). The oxidation peak at – 0.41 V corresponds to oxidation of reduced diquat, compounds incorporating this moiety usually displaying reversible redox behaviour.

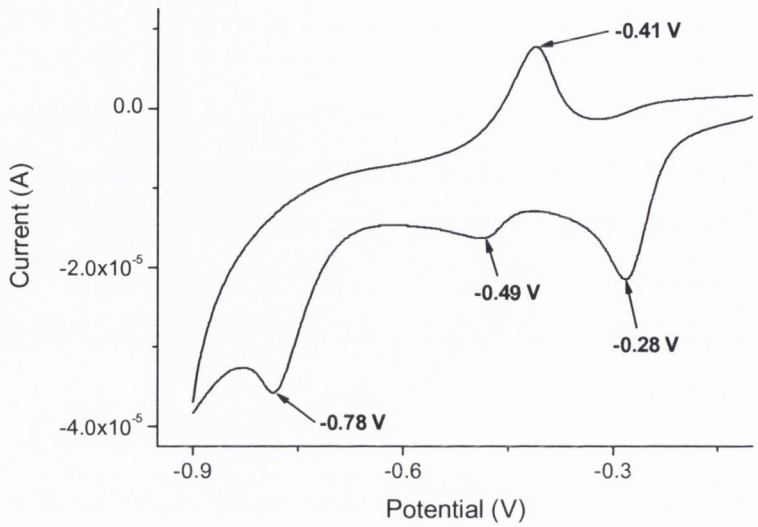

Figure 5.10 *Cyclic voltammogram of* ***94*** *vs. Ag / AgCl in 0.1 M phosphate buffer, at pH 7.*

The redox behaviour of **94** was somewhat different, where two reduction processes were observed in the potential window, at – 0.28 V and – 0.44 V respectively, Figure 5.11.

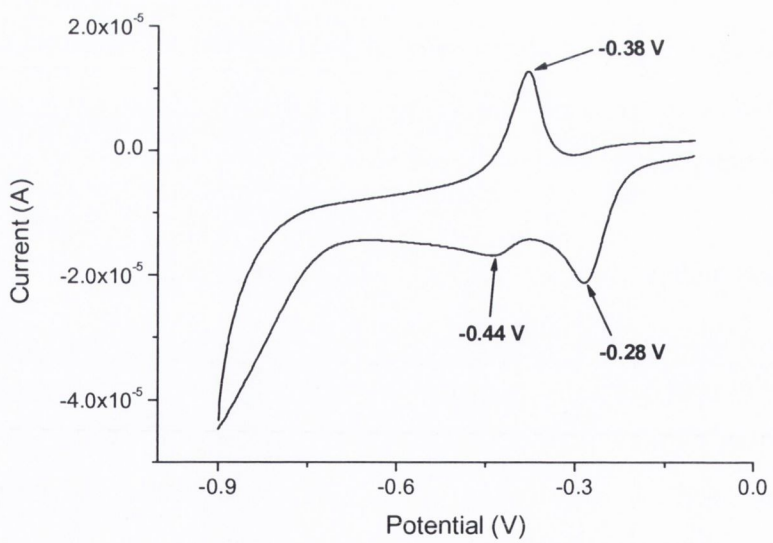

Figure 5.11 *Cyclic voltammogram of* ***94*** *vs. Ag / AgCl in 0.1 M phosphate buffer, at pH 7.*

These correspond to reduction of the 1,8-naphthalimide and the diquat moieties, respectively. In this case, the second reduction of the diquat was not observed. This we propose to be due to the smaller degree of interaction between the 1,8-naphthalimide and

the diquat moiety, resulting from the wedged arrangement of this system, in contrast to the linear arrangement in **93**. The oxidation process for **94** occurs at a similar potential to that of **93,** as can be seen in Figure 5.11.

The redox behaviour of the 4-nitro-1,8-naphthalimide-diquat conjugates **93** and **94**, provided further evidence of the interaction between the constituent chromophores resulting from the para arrangement around the connecting ring. Nevertheless, the first two reduction potentials for these systems also demonstrate the ease with which they can be reduced. This may have interesting consequences on the behaviour of these derivatives in the presence of DNA, and their ability to lead to redox damage of the polymer.

5.5 DNA Binding Interactions of 93 - 96

5.5.1 Changes in the UV/Visible Absorption of 93 – 96 with DNA

The interaction of **93** – **96** with DNA under different ionic strength conditions was firstly investigated using UV/Visible absorption, as detailed in the following sections. As before the arrangements and substitution of the conjugates was expected to result in different DNA binding behaviour.

5.5.1.1 Studies in Low Ionic Strength Medium (10 mM Phosphate Buffer)

The changes in absorption resulting from the addition of st-DNA to the reference compound **96**, when recorded in 10 mM phosphate buffer, are represented in Figure 5.12. A significant hypochromism of 32% was observed at the longer wavelength band upon titration of DNA, as well as an 8 nm bathochromic shift of the absorption maximum. Fitting of the absorbance data to the Bard model, as described in the *Chapter 2*, gave a binding constant of 2.8 x 10^6 M^{-1} and binding site size of 5.84 base pairs. The spectroscopic changes observed, *i.e.* the significant hypochromism and red shift of the absorption maximum, are consistent with intercalation,[18] although the binding site size of almost six base pairs would suggest otherwise, since it would usually indicate an external mode of association of lesser affinity, for which large equivalents of DNA are necessary in order to reach a plateau.

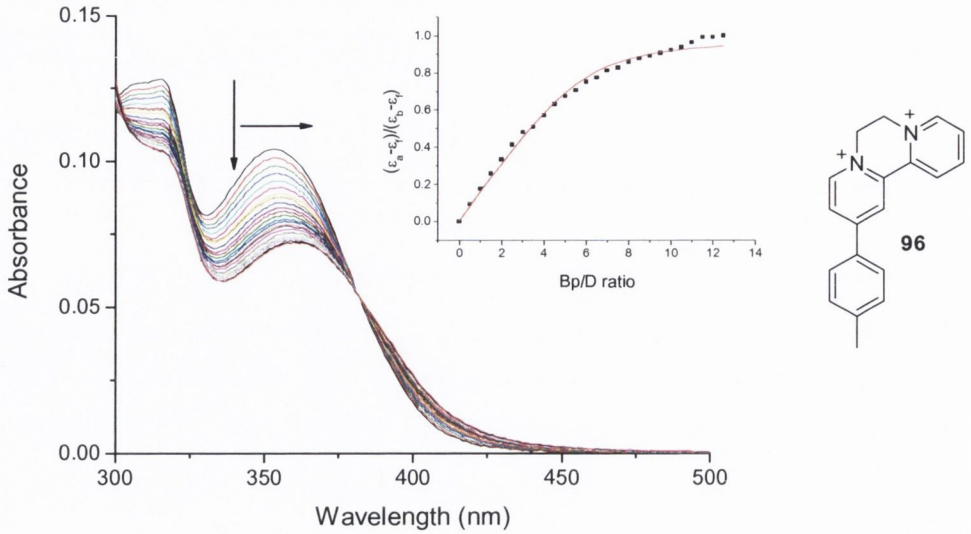

Figure 5.12 *Changes in the UV/Visible spectrum of* ***96*** *(6.5 μM) upon addition of st-DNA (0 – 81.25 μM base pairs) in 10 mM phosphate buffer, at pH 7. Inset: Plot of* $(\epsilon_a-\epsilon_f)/(\epsilon_b-\epsilon_f)$ *at 353 nm vs. equivalents of DNA and the corresponding non-linear fit.*

The changes in the absorption spectrum resulting from the titration of DNA with **93** are represented in Figure 5.13. Addition of st-DNA to this system resulted in a 25% hypochromism in the long wavelength absorption band. The shoulder at 319 nm also displayed a smaller change of 17%. As will be discussed later, it was expected that most of these absorbance changes corresponded to the interaction of the 1,8-naphthalimide moiety with DNA.

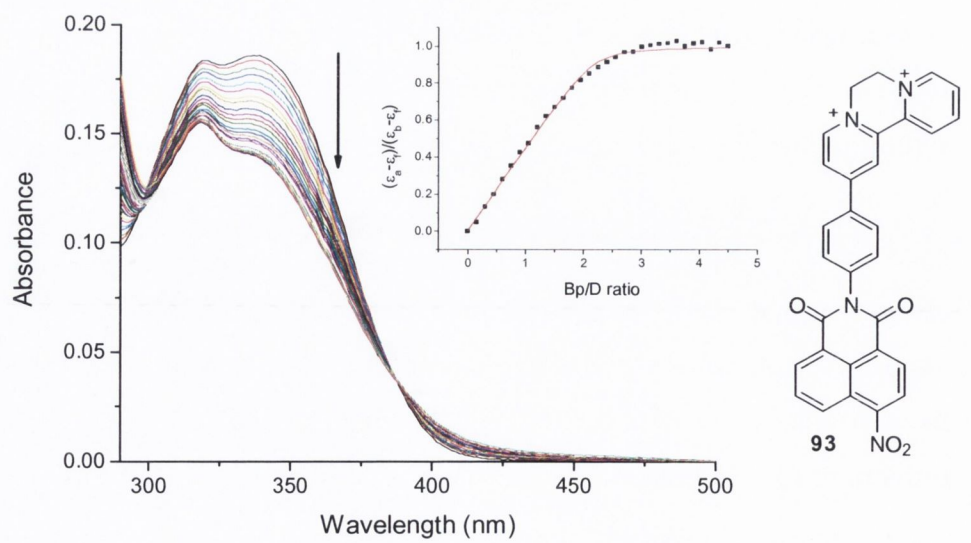

Figure 5.13 *Changes in the UV/Visible spectrum of* ***93*** *(6.5 μM) upon addition of st-DNA (0 – 29.25 μM base pairs) in 10 mM phosphate buffer, at pH 7. Inset: Plot of* $(\epsilon_a-\epsilon_f)/(\epsilon_b-\epsilon_f)$ *at 336 nm vs. equivalents of DNA and the corresponding non-linear fit.*

A binding constant of 1.7 x 10^7 M^{-1} and binding site size of 2.26 base pairs were determined from fitting of the titration data to the Bard model. The binding constant for this system is significantly greater than those of the individual components, which suggests a tight intercalative binding to DNA. In fact, the binding of the 1,8-naphthalimide is approximately three orders of magnitude greater than that previously observed for mono-1,8-naphthalimide compounds.[120,145] In contrast to the systems discussed in previous chapters, an isosbestic point was also observed at 388 nm, suggesting that less DNA bound species are present in solution.

Next the wedged nitro compound **94** was considered, the results for which are shown in Figure 5.13. In this case, a 21% hypochromism was observed for the 319 nm band with no shift in the absorption maximum. Again a greater change was observed at the longer wavelength part of the band, which was attributed to interaction of the 1,8-naphthalimide. An isosbestic point was also observed for this system, occurring at 388 nm.

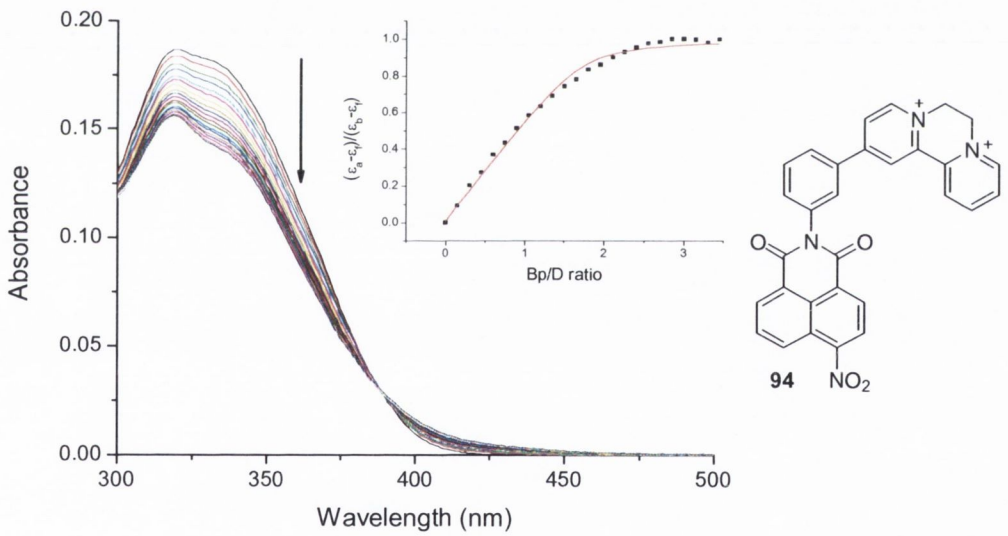

Figure 5.14 *Changes in the UV/Visible spectrum of* ***94*** *(6.5 μM) upon addition of st-DNA (0 – 22.43 μM base pairs) in 10 mM phosphate buffer, at pH 7. Inset: Plot of* $(\epsilon_a-\epsilon_f)/(\epsilon_b-\epsilon_f)$ *at 319 nm vs. equivalents of DNA and the corresponding non-linear fit.*

From fitting of the absorbance data, a binding constant of 6.5 x 10^6 M^{-1} and binding site size of 1.95 base pairs was determined. The binding affinity of **94** for DNA is less than that observed for the linear analogue **93**. This is in marked contrast to that discussed in *Chapter 4*, where the wedged arrangement of the components, resulted in both greater affinity and spectroscopic responses upon titration with DNA. It is worth mentioning that

the charged components of the molecules presented herein are significantly less bulky, and therefore, would be expected to possess different structural requirements for binding to DNA. Furthermore, hydrophobic contact of the ligands of **76** – **79** in the grooves of DNA is likely to contribute considerably to the overall DNA affinity, while such contacts would not be significant for **93** and **94**. The actual fit of **93** and **94** in binding DNA may be very different to that of their Ru(II) complex counterparts. A linear arrangement may allow for more complete insertion of the 1,8-naphthalimide into the helix, and consequently a greater apparent affinity for DNA, in contrast to that observed for the Ru(II) analogues.

In the case of the amino substituted derivative **95** the changes at the diquat and 1,8-naphthalimide absorption bands could be monitored independently. Upon addition of st-DNA to **95**, a 42% hypochromism was observed for the 1,8-naphthalimide band at 434 nm, while a much smaller change of 11% was observed for the 311 nm band, Figure 5.15. In addition to the large hypochromism, an 11 nm shift in absorption maximum was also observed at the 434 nm band, which is usually indicative of intercalation.[18]

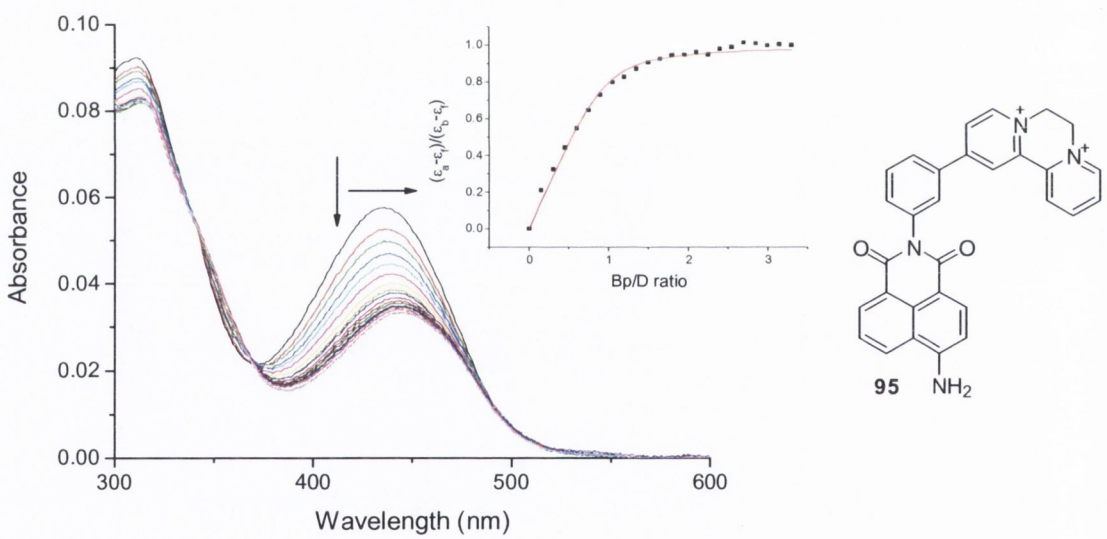

Figure 5.15 *Changes in the UV/Visible spectrum of* ***95*** *(6.5 μM) upon addition of st-DNA (0 – 21.45 μM base pairs) in 10 mM phosphate buffer, at pH 7. Inset: Plot of* $(\epsilon_a-\epsilon_f)/(\epsilon_b-\epsilon_f)$ *at 434 nm vs. equivalents of DNA and the corresponding non-linear fit.*

Here, binding seems to be primarily governed by the 1,8-naphthalimide moiety, and thus it was expected that the overall mode of interaction would involve intercalation of this part of the molecule, and groove binding, or external association, of the cationic diquat moiety. Fitting the titration data gave a binding constant of 2.3 x 10^6 M^{-1} and binding site size of 1.98 for the interaction of **95** with st-DNA, the affinity being slightly reduced

compared to **94**. Several isobestic points were observed upon titration of **95** with DNA, occurring at 339 nm, 370 nm and 487 nm, respectively.

It should be emphasised again at this point, that for nitro systems **93** and **94**, a greater absorbance change was observed at the longer wavelength part of the band monitored. Considering that study of **95** has shown that the majority of absorbance changes with added DNA occurred due to changes in the 1,8-napthalimide transition, it may be proposed that changes at the longer wavelength part of the bands of **93** and **94** was also due to interaction of the 1,8-naphthalimide moiety.

5.5.1.2 Studies in Varying Ionic Strength Medium

For control compound **96**, electrostatic binding to DNA would be expected to play a significant role. As such, a mode of binding which places the molecule external to the helix, or associated in the grooves, would be expected to dominate. To investigate this, and provide further information on the binding mode, a salt back titration was carried out, in which **96** bound to DNA was displaced upon titration with NaCl. The profile resulting from this titration is shown in Figure 5.16. It is clear from these results that the interaction of **96** with DNA is highly dependent on the ionic strength of the medium, as **96** was fully displaced after the addition of approximately 30 mM of NaCl solution. Hence, this confirms that electrostatic interactions govern the overall association of **96** with DNA.

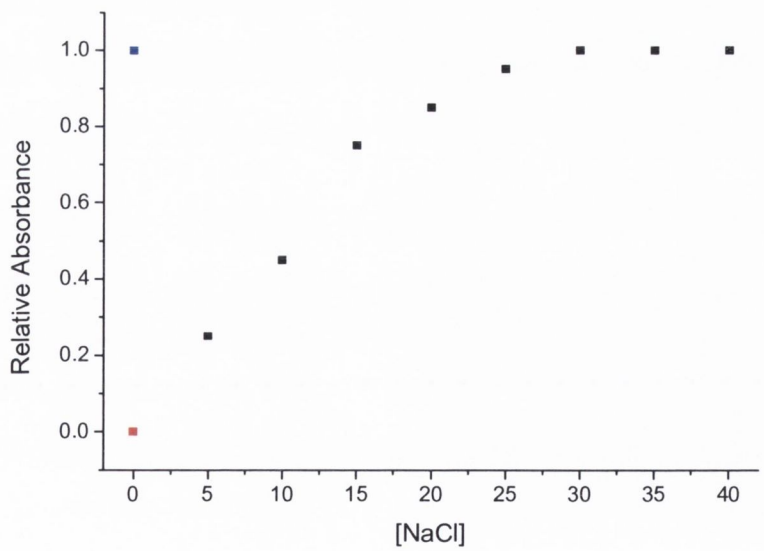

Figure 5.16 *UV/Visible absorption back titration of* ***93*** *(6.5 μM). Absorption of unbound compound (■), fully bound compound (■) and bound compound with increasing concentration of NaCl (■).*

As each of the conjugate systems **72** – **75** displayed excellent affinity for DNA, back titrations were also carried out for each of these compounds. The profiles resulting from these titrations are overlayed in Figure 5.17.

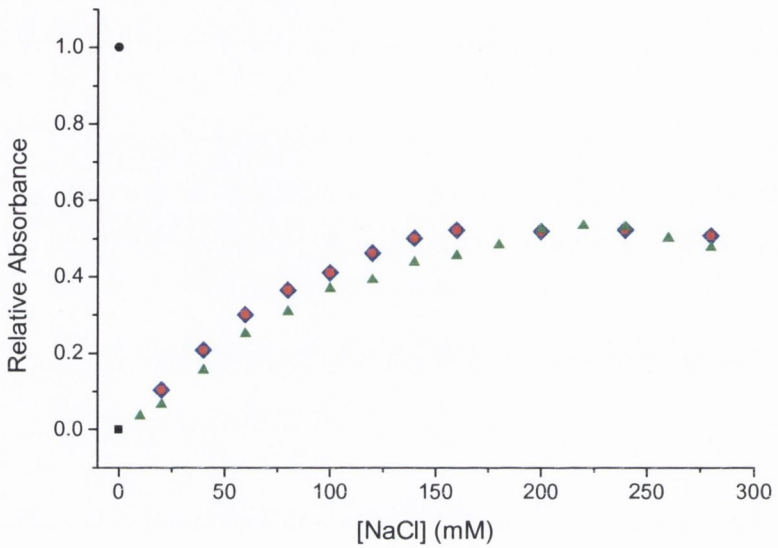

Figure 5.17 *UV/Visible absorption back titration of* ***93*** *–* ***96****. Absorption of unbound compound (■), fully bound compound (●) and bound* ***93*** *(♦),* ***94*** *(●) and* ***95*** *(▲) with increasing concentration of NaCl.*

For each of these systems the absorbance gradually increased towards that of free compound, but reached a plateau at *ca.* 150 mM NaCl, at about the half-way point in absorbance between free and bound compound. No further change occurred with the addition of up to 280 mM NaCl, indicating that a significant amount of compound remains bound to DNA at high ionic strength, and therefore that non-electrostatic modes of interaction are contributing largely to the binding of **93** – **96** to DNA.

5.5.1.3 Studies in the Presence of $[poly(dG\text{-}dC)]_2$ and $[poly(dA\text{-}dT)]_2$

Studies in the presence of different DNA alternating co-polymers were also carried out with **93** – **95**, with the aim of establishing if these compounds displayed any sequence selectivity in their binding. The observed hypochromicities, binding constants and binding site sizes for each system are summarised in Table 5.3. However, none of the systems displayed a marked preference in affinity for either $[poly(dA\text{-}dT)]_2$ or $[poly(dG\text{-}dC)]_2$ as can be seen from the values in the Table. Full details are provided in appendix 5.

In summary **93** – **96** displayed excellent affinity for DNA with binding constants of the order of 10^6 – 10^7 M^{-1}. Similar to the complexes discussed in *Chapter 4*, the nature of

the interaction with, and binding affinity for DNA, was sensitive to the arrangement of the diquat and 1,8-naphthalimide components around the connecting ring. Here a more intimate binding was associated with the para (or linear) arrangement. The requirements for high affinity binding of **93** – **95** to DNA are quite different to that of their Ru(II) complex counterparts, most likely due to the less bulky nature of the charged centre in the former. Salt dependence studies showed that non-electrostatic binding modes govern the overall affinity of the systems for DNA. The exact nature of these interactions was further investigated using emission spectroscopy, as described in the following section.

Table 5.3 *DNA binding parameters from fits to absorbance data.*

No	Hypochromism	Bathochroism	Binding constant K (M^{-1})	Binding site size n (base pairs)	R^2
Salmon testes DNA					
93	25 %	------	1.7×10^7 (± 0.5)	2.26 (± 0.04)	0.99
94	21 %	------	6.5×10^6 (± 1.8)	1.95 (± 0.06)	0.99
95	42 %	11 nm	2.3×10^6 (± 0.5)	1.98 (± 0.05)	0.99
96	32 %	8 nm	2.8×10^6 (± 0.5)	5.84 (± 0.21)	0.99
[poly(dG-dC)]$_2$					
93	22 %	------	9.4×10^6 (± 2.3)	1.50 (± 0.04)	0.99
94	23 %	------	2.8×10^6 (± 0.8)	0.98 (± 0.06)	0.99
95	43 %	11 nm	3.4×10^6 (± 0.6)	1.76 (± 0.06)	0.99
96	------	------	------	------	---
[poly(dA-dT)]$_2$					
93	19 %	------	6.6×10^6 (± 1.7)	1.56 (± 0.04)	0.99
94	20 %	------	1.6×10^6 (± 0.6)	0.98 (± 0.10)	0.99
95	41 %	9 nm	4.7×10^6 (± 1.1)	1.60 (± 0.06)	0.99
96	------	------	------	------	---

5.5.2 Emission Titration of 93 – 96 with DNA

The systems described in this chapter are quite different to those in *Chapters 2 – 4*, as the Ru(II) centre has been replaced by a diquat moiety. As such their emission response to DNA was expected to be quite different.

5.5.2.1 Studies with st-DNA

Excitation of **96** at 353 nm, upon titration with st-DNA, resulted in a significant 61% decrease in the emission intensity of the 530 nm band, as shown in Figure 5.18. Compounds containing diquat or paraquat (viologen) functionality are very well known oxidizing agents, and therefore the observed emission quenching is likely due to ET from the DNA bases.[176] Furthermore, quenching of this magnitude implies intimate association of **96** with the nucleotides, in a manner that allows for ET from the bases to **96**. The evidence suggests at least partial intercalation of **96**, possibly favoured by the presence of the extra aromatic ring. It is interesting to note that no significant emission change was observed at the 415 nm band, which was previously suggested to originate from an excited state localised on the aromatic ring connected to the diquat moiety. It therefore appears that the charged diquat component contributes mostly to the observed affinity.

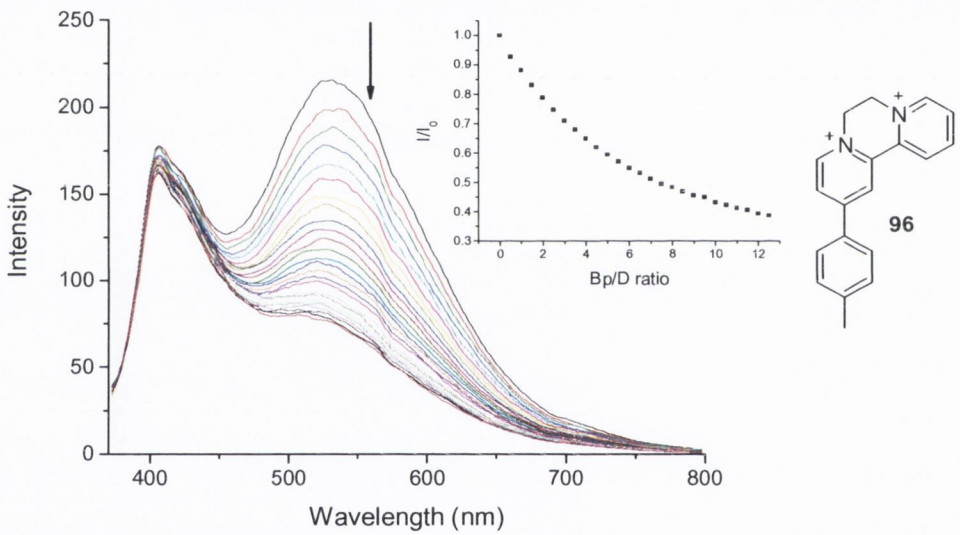

Figure 5.18 *Changes in the emission spectrum of* ***96*** *(6.5 μM) (excitation at 353 nm) upon addition of st-DNA (0 – 81.25 μM) in 10 mM phosphate buffer, at pH 7.*

Excitation of **93** at 336 nm upon titration with st-DNA, resulted in a 90% decrease in emission intensity from the excited state, as shown in Figure 5.19. This decrease was attributed to PET from the DNA bases to **93**. The quenching was more efficient than that of **96**, which is agreement with the superior intercalating ability and the higher affinity of this compound for DNA. Alternatively, intercalation of the 1,8-naphthalimide may place the diquat part of the molecule in close proximity to the DNA helix, and therefore close to the bases, whereby it can undergo electron transfer. Which of these mechanisms predominates cannot be deduced from the experimental results.

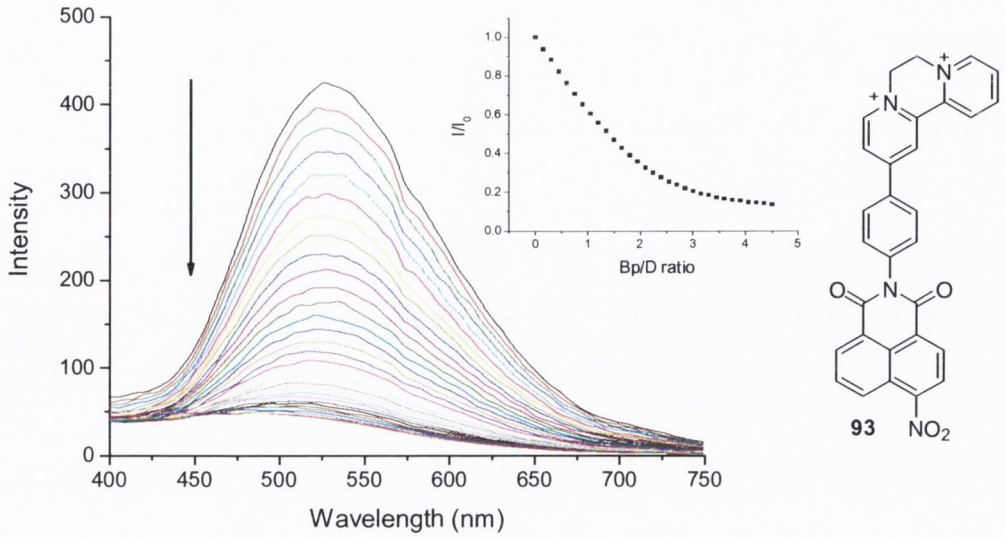

Figure 5.19 *Changes in the emission spectrum of* ***93*** *(6.5 μM) (excitation at 336 nm) upon addition of st-DNA (0 – 29.25 μM) in 10 mM phosphate buffer, at pH 7.*

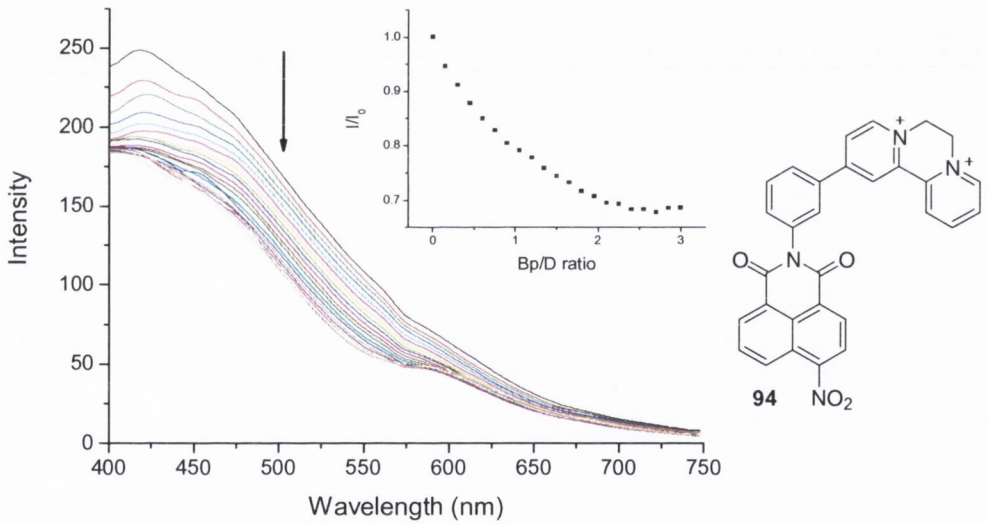

Figure 5.20 *Changes in the emission spectrum of* ***94*** *(6.5 μM) (excitation at 319 nm) upon addition of st-DNA (0 – 19.5 μM) in 10 mM phosphate buffer, at pH 7.*

The wedged compound **94**, did not possess as well defined an emission spectrum as its linear analogue. This was attributed to reduced interaction between the diquat and the 1,8-naphthalimide components in **94**, which gave rise to an emission spectrum with features attributable to both. The titration of **94** with st-DNA, upon excitation at 319 nm, also gave smaller changes in emission intensity compared to **93**, with an overall decrease of 31%, Figure 5.20.

In contrast to these results, the titration of **95** with st-DNA caused a significant quenching of emission from the 550 nm band of 55%, upon excitation at 436 nm, as shown in Figure 5.21. A similar change occurred upon excitation at 311 nm (see appendix). These changes were considerably greater than those recorded for the nitro analogue **94**. The observation that a greater overall decrease occurred upon excitation at 436 nm, than at 311 nm, is reflective of the greater absorption hypochromicity at the former wavelength upon titration with DNA. Hence, diminished absorption contributes somewhat to the overall emission decrease.

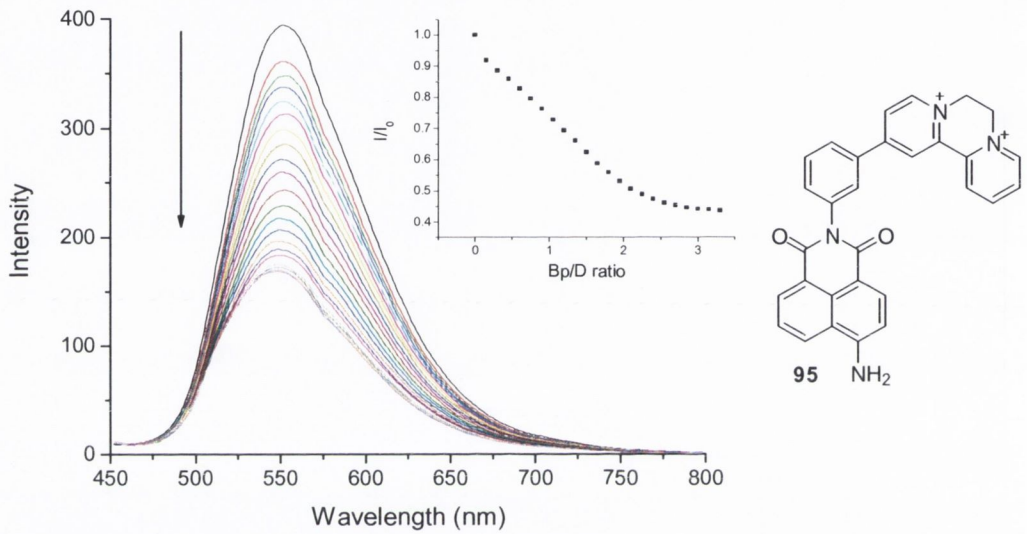

Figure 5.21 *Changes in the emission spectrum of* ***95*** *(6.5 μM) (excitation at 436 nm) upon addition of st-DNA (0 – 21.45 μM) in 10 mM phosphate buffer, at pH 7.*

5.5.2.2 Studies with [poly(dG-dC)]$_2$ and [poly(dA-dT)]$_2$

Similar to their UV/Visible behaviour, **93** – **95** in general did not display any marked differences in their fluorescence spectra upon binding to AT or GC rich DNA. The titration profiles resulting from the addition of [poly(dG-dC)]$_2$ and [poly(dA-dT)]$_2$ to these compounds are shown in appendix 5. The one exception was **95**, which upon titration with [poly(dG-dC)]$_2$ displayed similar behaviour as seen for st-DNA, while titration with [poly(dA-dT)]$_2$, gave rise to a decrease in emission intensity to a Bp/D ratio of *ca.* 1.5, followed by an increase in emission intensity, to a Bp/D ratio of 3.5. It was expected that the decrease was due to electron transfer quenching of the excited state, and that the subsequent changes were due to a redistribution of the compound to a different DNA binding mode, resulting in an enhancement of the emission. This proposed redistribution must remove the compound from an optimal binding mode for electron transfer.

5.5.2.3 Summary

Compounds **93** – **96** displayed quite interesting and variable emission responses upon binding to DNA. Addition of DNA to reference **96** resulted in a substantial decrease in emission intensity of 61%. In conjunction with the binding affinity determined for this system from UV/Visible absorption, it seems that **96** is intimately associated with the DNA, in a manner largely involving electrostatic association. This is in contrast to the mode of interaction of the diquat components of the bifunctional compounds **93** – **95**. Compound **93** was shown to possess the greatest affinity for DNA from UV/Visible absorption studies, in addition to displaying the largest decrease in the emission intensity of 90%. These properties were proposed to be due to binding of the 1,8-naphthalimide *via* intercalation, while the diquat moieties remained externally bound to the phosphate backbone or associated within the grooves. The linear arrangement of these components around the connecting ring allowed the 1,8-naphthalimide to be inserted more effectively, in a manner that is not inhibited by the diquat moiety, as it points in the opposite direction. This results in greater affinity and more pronounced quenching, due to the more intimate association with the DNA bases.

Compound **94**, was shown to possess reduced affinity for DNA in comparison to **93**, based on analysis of the changes in its UV/Visible absorption spectrum. Smaller changes were also seen in the emission intensity upon addition of DNA to **94**, which was again proposed to be due to the molecular arrangement. The wedged or meta arrangement around the connecting ring precludes as efficient insertion of the 1,8-naphthalimide into the DNA helix, due to its closer positioning to the diquat moiety. System **94** also possessed a less well defined emission spectrum, displaying broad, structure-less emission in the range 400 – 960 nm. The different nature of the emissive state, was attributed to a lessened excited state interaction between the 1,8-naphthalimide and diquat moieties.

The 4-amino compound **95**, despite comprising a wedged arrangement of the chromophores, displayed significant interaction between the two units in the excited state, with a single emission band centred at 550 nm. The UV/Visible absorption studies showed that **95** possessed slightly reduced affinity for DNA than **94**, which was attributed to the diminished intercalating ability of the more electron rich 1,8-naphthalimide. Nevertheless, a pronounced decrease of 55% in the luminescence was observed, suggesting that the excited state was more easily quenched by ET. However, the quenching was not as pronounced as observed for **93**, emphasising that a linear arrangement with nitro substitution allowed for more efficient quenching.

5.5.3 DNA Thermal Denaturation Studies of 93 – 96

Thermal denaturation studies were carried out to further investigate the interaction of **93** – **96** with DNA. Some stabilisation of the DNA was observed with addition of the reference compound **96**, with T_m values of 73.4 and 75.4 °C being obtained at a Bp/D ratio of 10 and 5, respectively. The melting profiles obtained with addition of the nitro substituted conjugates **93** and **94** are shown in Figure 5.22. It is worth mentioning that both of these caused a dramatic shift in the T_m value of DNA, to such a degree that it was not possible to determine an exact value. None of the profiles had reached a plateau at 90 °C. Both systems resulted in a similar degree of stabilisation, although at higher loading of the compounds on DNA it seems that the wedged derivative **94** gives a slightly greater shift to higher temperature.

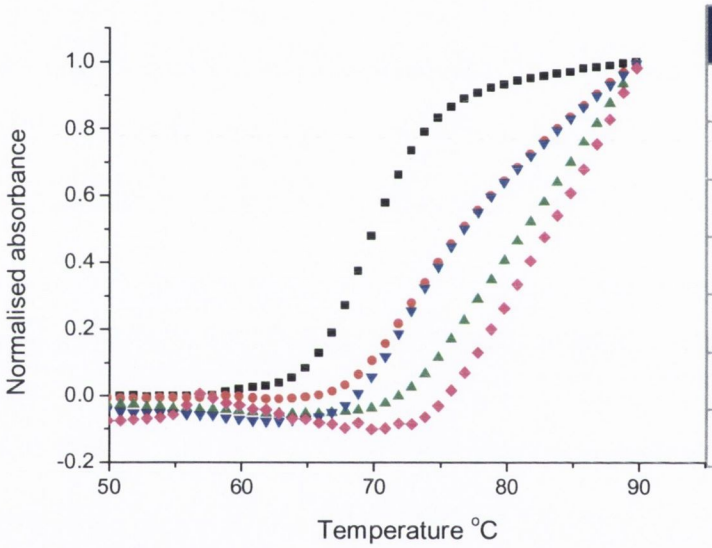

Sample	T_m
DNA	69 °C (± 10%)
93 (Bp/D 10)	> 75 °C (± 10%)
93 (Bp/D 5)	> 75 °C (± 10%)
94 (Bp/D 10)	> 75 °C (± 10%)
94 (Bp/D 5)	> 75 °C (± 10%)
96 (Bp/D 10)	73.4 °C (± 10%)
96 (Bp/D 5)	75.4 °C (± 10%)

Figure 5.22 *Thermal denaturation curves of ct-DNA (150 μM) in 10 mM phosphate buffer, at pH 7, in the absence (■) and presence of* ***93*** *at a Bp/D ratio of 10 (●) and 5 (▲), and* ***94*** *at a Bp/D ratio of 10 (▼) and 5 (♦).*

The amino substituted system **95** resulted in markedly different changes in the melting profile of DNA, as is clear from examination of Figure 5.23. Upon heating an initial decrease in absorbance was observed, followed by the usual sigmoidal increase, which is characteristic of the DNA melting transition. The T_m value for this system was calculated by differentiating the profile from 65 to 90 °C. From this, a T_m of 71.1 °C was estimated, suggesting the stabilisation due to binding of this system to DNA to be significantly less than that of the nitro derivatives. It is not clear why this phenomenon occurs with this system in the presence of ct-DNA, several repeat measurements having given the same result each time.

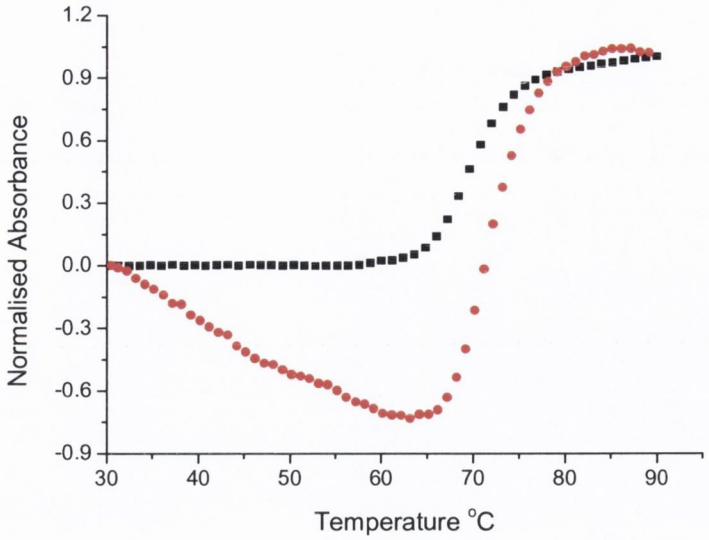

Figure 5.23 *Thermal denaturation curves of ct-DNA (150 μM) in 10 mM phosphate buffer, at pH 7, in the absence (■) and presence of* ***95*** *(●) at a Bp/D ratio of 10.*

Due to the large stabilisation of DNA caused by binding of **93** and **94**, studies were also carried out in the presence of $[poly(dA\text{-}dT)]_2$. This nucleic acid polymer melts at a significantly lower temperature than random sequence DNA, or $[poly(dG\text{-}dC)]_2$ due to diminished nearest neighbour stacking interactions. Each of the systems **93**, **94** and **95** gave very large shifts in T_m, Figure 5.24, being approximately 16.5 °C for **93**, and 23.2 °C for **94** (both at a Bp/D ratio of 5). This would suggest that **94** was binding to DNA more strongly, or in a manner that stabilises the helix to a greater entent. Additionally, the profile with added **93** followed a regular sigmoidal shape, whereas two regions of change could be identified in the profile for **94**. It is possible that the first changes are due to disruption of electrostatic interactions, whereas that at higher temperature corresponds to disruption of intercalative binding.

The amino substituted system **95** gave a shift in T_m of 10.4 °C, considerably less than its nitro analogue, due to the diminished intercalating ability of the 4-amino-1,8-naphthalimide. Interestingly, the melting profile followed a more regular path in this case (in comparison to that with ct-DNA), and two regions could be identified in the profile similar to that observed for **94**.

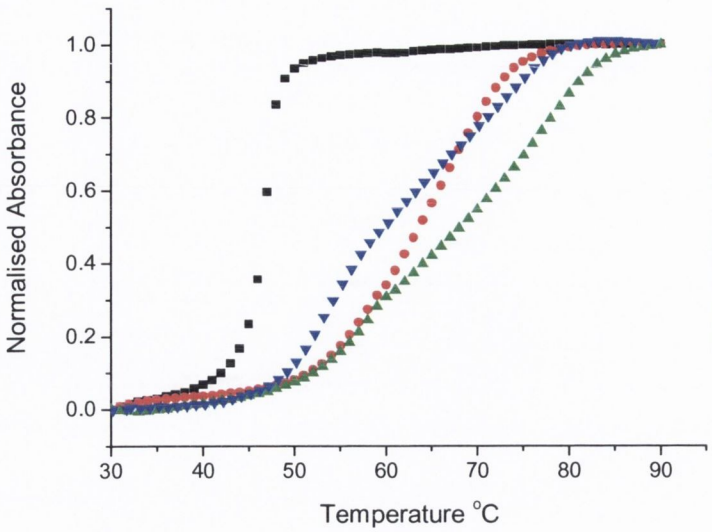

Sample	T_m
[poly(dA-dT)]$_2$	47.2 °C (± 10%)
93	63.7 °C (± 10%)
94	70.4 °C (± 10%)
95	57.6 °C (± 10%)

Figure 5.24 *Thermal denaturation curves of [poly(dA-dT)]$_2$ (150 μM) in 10 mM phosphate buffer, at pH 7, in the absence (■) and presence of* ***93*** *(●),* ***94*** *(▲) and* ***95*** *(▼) all at a Bp/D ratio of 5.*

The above experiments were also carried out at a higher salt concentration. In the presence of 50 mM NaCl (in 10 mM phosphate buffer), Figure 5.25, compound **93** gave a shift in T_m of 6.6 °C, while addition of its wedged analogue resulted in a shift of 10.3 °C. Addition of the wedged amino compound **95** gave a shift of 7.9 °C. Both wedged systems displayed mono-phasic melting profiles implying the loss of one of the binding modes.

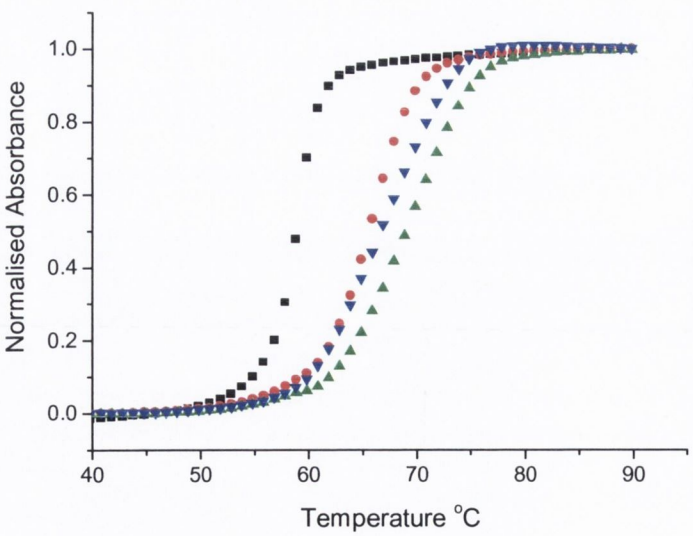

Sample	T_m
[poly(dA-dT)]$_2$	59.4 °C (± 10%)
93	66.0 °C (± 10%)
94	69.7 °C (± 10%)
95	67.3 °C (± 10%)

Figure 5.25 *Thermal denaturation curves of [poly(dA-dT)]$_2$ (150 μM) in 10 mM phosphate buffer + 50 mM NaCl, at pH 7, in the absence (■) and presence of* ***93*** *(●),* ***94*** *(▲) and 95 (▼) all at a Bp/D ratio of 5.*

The melting studies of **93** – **96**, illustrated the high affinity of all of the conjugate systems for DNA, with significant shifts in T_m values, of the order expected for intercalative binding. By comparing **93** with **94**, it was interesting to note that **94** resulted in a more pronounced stabilisation of the helix, which was in contrast to the proposed higher affinity of **93**, calculated from UV/Visible changes. This could indicate that although **93** displays superior intercalating ability, the diquat component is not bound to the helix as tightly as for that of **94,** which allows for more cooperative overall binding of the constituent 1,8-naphthalimide and diquat moieties, by virtue of their orientation. This is similar to the behaviour exhibited by the rigid complexes discussed in *Chapter 4*.

5.5.4 Circular Dichroism Studies of 93 – 96

Circular dichroism titrations were also carried out on **93** – **96**, where the concentration of DNA was kept constant, and that of the compounds was varied. Only minor changes were seen upon addition of the reference compound **96** to DNA, appendix 5. The noticeable absence of an ICD in the region of achiral absorbance at *ca.* 330 nm indicated that this system was not associated within the grooves. In contrast, the addition of the linear nitro compound **93** to DNA resulted in an ICD at *ca.* 350 nm, Figure 5.26.

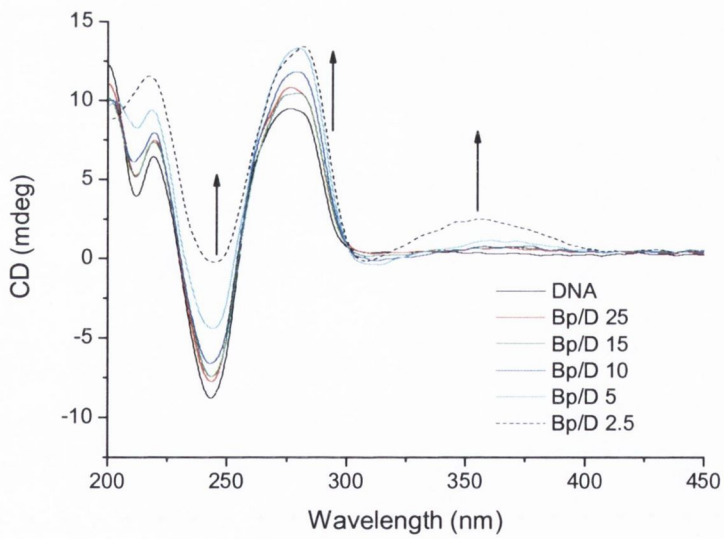

Figure 5.26 *Circular dichroism curves of ct-DNA (150 μM) in 10 mM phosphate buffer, at pH 7, in the absence and presence of* ***93*** *at varying ratios.*

Furthermore, large changes were observed below 300 nm, which may be regarded as being due to a combination of induced CD of the compound, and changes in the intrinsic CD signal of the DNA polymer. Whether the induced CD signal at longer wavelength is

due to the 1,8-naphthalimide or diquat portion of the molecule is unclear. Nevertheless, these results emphasise the high affinity for DNA, and the intimate mode of association possessed by **93**. CD changes of such a magnitude were not observed for the Ru(II) complexes discussed in the previous chapters, and as such it was decided to investigate the CD behaviour of **93** further at varying ionic strengths. The ICD spectra for **93** at varying salt concentration are contained in appendix 5. An ICD still occurred even at high salt concentration, which indicates that **93** remained bound in the chiral environment of the DNA.

Next, CD experiments were carried out in the presence of the alternating co-polymers $[poly(dA\text{-}dT)]_2$ and $[poly(dG\text{-}dC)]_2$. The resulting ICD are depicted in Figure 5.27, in which they are compared to that in the presence of random sequence ct-DNA. Large ICD was observed in both cases, particularly in the region above 300 nm. One notable feature was that the ICD in the presence of both alternating co-polymers was greater than that seen upon binding to ct-DNA. The ICD in the presence of the alternating co-polymers were also much broader, and were more closely in agreement with the absorption spectrum of the compound. It is possible that the fit in binding to these polymers is quite different to that in binding to ct-DNA, the result being that ICD corresponding to both parts of the compound appear.

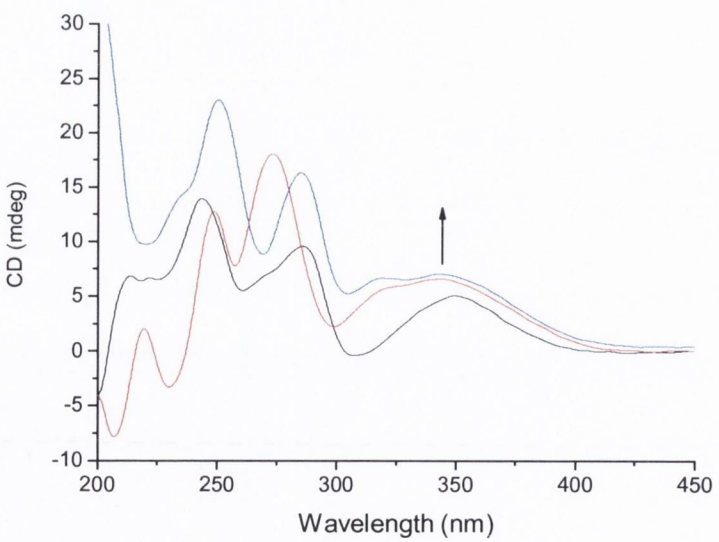

Figure 5.27 *Induced CD spectra of* ***93*** *in the presence of ct-DNA (——), $[poly(dA\text{-}dT)]_2$ (——) and $[poly(dG\text{-}dC)]_2$ (——), all in 10 mM phosphate buffer, at pH 7, at a Bp/D ratio of 2.5.*

The addition of DNA to **94** resulted in more pronounced ICD than seen for **93,** Figure 5.28. Here, a significant CD signal appeared at 350 nm, which corresponds to absorption by the compound itself. Very large changes were also observed in the region of absorption of the DNA. The fact that a greater ICD occured for the wedged derivative over the linear analogue may be related to the orientation of the two chromophores of this compound with respect to each other. We propose that the observed ICD is due to the diquat part of the molecule, which experiences the helicity of the DNA, when bound within the grooves, and that the orientation of the components in this system creates a cleft of similar nature to that discussed in the previous Chapter.

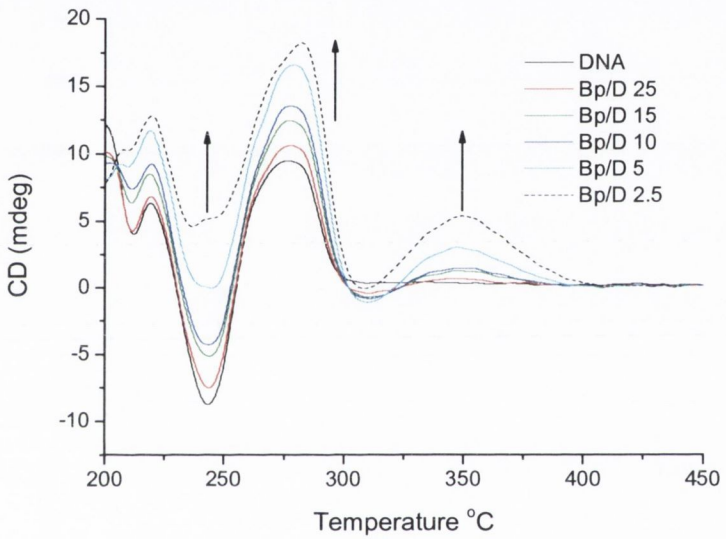

Figure 5.28 *Circular dichroism curves of ct-DNA (150 μM) in 10 mM phosphate buffer, at pH 7, in the absence and presence of* ***94*** *at varying ratios.*

The closer association of the wedged derivative **94** does not correlate with the affinities calculated from the UV/Visible titrations above. These results suggested that the linear system **93** bound to DNA with considerably greater affinity, where the 1,8-naphthalimide moiety interacted efficiently with DNA, while the diquat pointed in the opposite direction, by virtue of the linker used. However, interaction of the 1,8-naphthalimide in **94** may be somewhat inhibited by the diquat due to the closer arrangement of the two components in space. These results again emphasise the sensitivity of such rigid bichromophore molecules to the nature of the linker, and the resulting orientation of the components with respect to each other.

The CD spectrum for **94** bound to DNA was also determined at varying salt concentration. The results of this study are shown in appendix 5, and again showed the

presence of significant ICD at high salt concentration. Moreover, the binding of **94** to $[poly(dA\text{-}dT)]_2$ and $[poly(dG\text{-}dC)]_2$ was investigated the results of which are presented in appendix 5, being very similar to those for the linear nitro conjugate **93**.

In the case of **95** distinct absorption bands associated with both the 1,8-naphthalimide and the diquat chromophores were observed. The CD changes resulting for this compound are depicted in Figure 5.29.

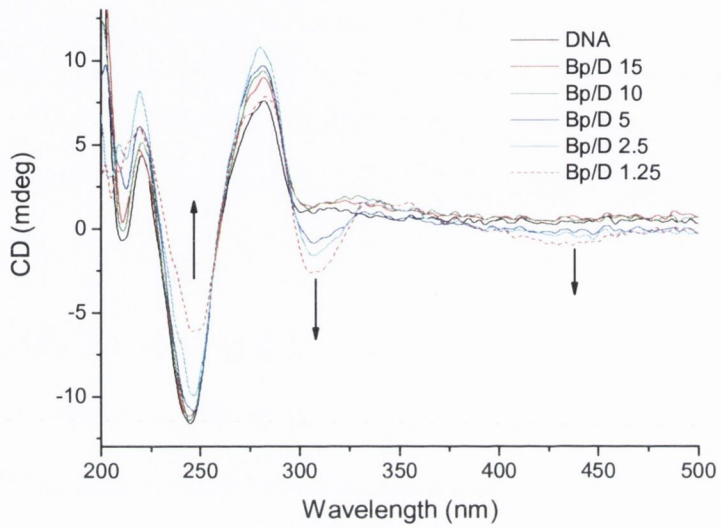

Figure 5.29 *Circular dichroism curves of ct-DNA (150 μM) in 10 mM phosphate buffer, at pH 7, in the absence and presence of* ***95*** *at varying ratios.*

Here, a band was shown to grow in at *ca.* 311 nm, which was assigned to the diquat part of the molecule, and a less significant band at *ca.* 440 nm, assigned to the 1,8-naphthalimide. It would seem therefore that for this system, the diquat moiety remains in the grooves when bound to DNA, while the 1,8-naphthalimide is intercalated, thereby displaying a smaller ICD. The molar absortivity of the 1,8-naphthalimide part of the molecule is also less that than that of the diquat, which will also contribute to some extent to the reduced CD changes. It is thus reasonable to assume, that the nitro derivatives will bind to DNA in a similar manner, and that the majority of the absorption change may be attributed to intercalation of the 1,8-naphthalimide, and the CD changes to groove association of the diquat. It is not clear why a negative ICD is observed for **95**, whereas positive signals were observed for the other two derivatives studied.

The systems described in this chapter displayed quite significant CD changes, which were of considerable use in assigning the nature of their interaction with DNA. Through the use of the amino compound **95**, the CD changes were assigned as being most

likely due to association of the diquat portion of the molecules within the grooves, while the 1,8-naphthalimide was bound by intercalation.

5.5.5 Ethidium Bromide Displacement Assay of 93 and 94

In order to make another comparison of the relative affinities of **93** and **94** for DNA ethidium bromide displacement assays were carried out. From this study binding constants of 1.7 x 10^7 M^{-1} and 2.4 x 10^7 M^{-1} were determined for **93** and **94**, respectively. The binding constant for **93** is in agreement with that calculated from UV/Visible titration in Section 5.5.1. However, the value for **94** is considerably removed from that determined by UV/Visible study, being almost an order of magnitude different.

It has already been indicated that the UV/Visible changes displayed by these compounds are due primarily to interaction of the 1,8-naphthalimide moiety. Compound **93** was determined to bind DNA with higher affinity, as the 1,8-naphthalimide may intercalate in a manner that is not restricted by the diquat, which point in the opposite direction. Binding of **94** to DNA involves both intercalative interaction of the 1,8-naphthalimide, but also a considerable degree of groove association of the diquat part of the molecule, permitted by the wedged arrangement. In such a mode both parts of the molecule may effectively displace DNA bound ethidium bromide and thus the apparent affinity from the displacement assay is higher.

The charged diquat moiety in **93** – **95** may be regarded as having a similar function, and behaving in a similar manner to the Ru(II) centre in complexes **68** – **71**. The diquat contributes to the overall DNA interaction, through electrostatic attraction to the phosphates and association in the grooves.

5.5.6 Isothermal Titration Calorimetry Study of 93 and 94

ITC experiments were firstly conducted on the reference compound **96**. The heat changes and resulting binding profile for **96** are shown in Figure 5.30a and 5.30b repectively. The binding of **96** to DNA appears to be entropically driven as positive heat changes are observed at all points in the ITC experiment.[182,183] Bearing this in mind, it is possible to envisage a binding mode, which involves non-specific surface binding in the grooves and electrostatic interaction with the phosphate backbone. Such binding will result in the displacement of ordered water molecules and ions from the DNA polymer, and hence result in an increase in the disorder of the system.

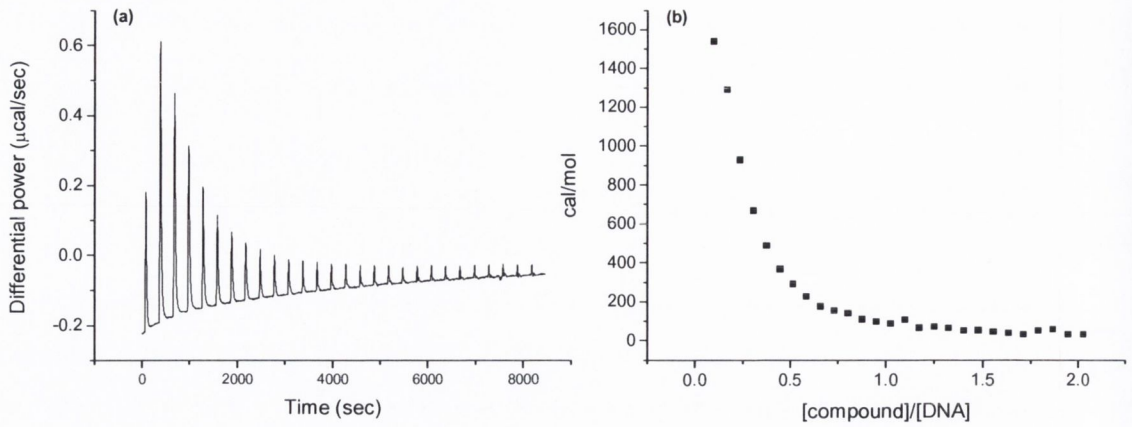

Figure 5.30 *(a) Raw ITC data for titration of* ***96*** *(2 mM) into a solution of st-DNA (0.2 mM), both solutions in 10 mM phosphate buffer, at pH 7, (b) Integrated ITC profile of* ***96*** *binding to st-DNA.*

The bifunctional compounds **93** and **94** display significantly different calorimetric behaviour to that observed for **96**, when added to a solution of DNA. The heat changes and resulting binding profile for **93** are shown in Figure 5.31a and 5.31b respectively.

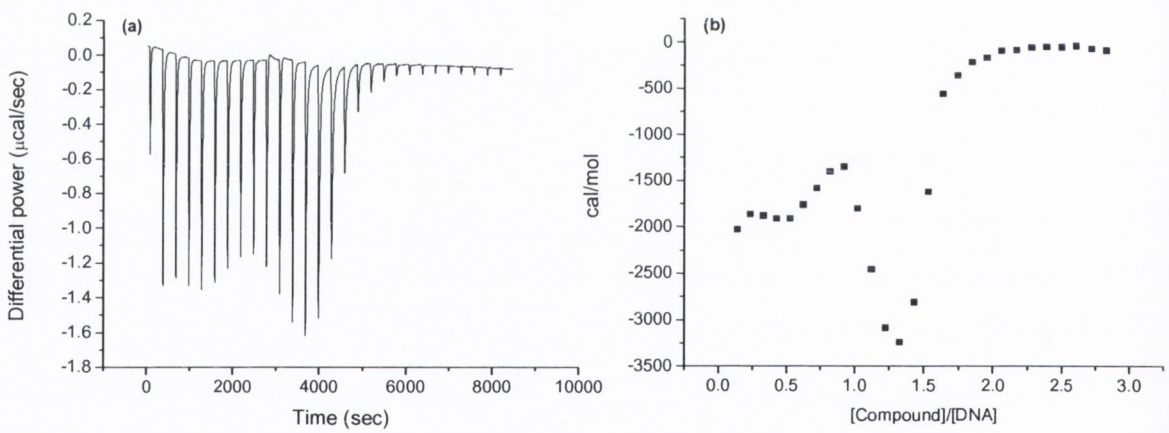

Figure 5.31 *(a) Raw ITC data for titration of* ***93*** *(2 mM) into a solution of st-DNA (0.2 mM), both solutions in 10 mM phosphate buffer, at pH 7,(b) Integrated ITC profile of* ***93*** *binding to st-DNA.*

The first point to note is that negative heat changes occur at all points in the titration, and as such it can be concluded that enthalpy plays an important role in the binding process. The profile displays quite typical behaviour up to a 1:1 ratio of compound to DNA, with several large heat changes occurring up to a ratio of approximately 0.5. Larger changes occur initially as there are more free sites available for

binding of **93** to DNA. The fact that the binding is enthalpically driven, suggests that modes of binding that increase the interactions between atoms, such as electrostatic binding and π-π intercalative stacking, govern the interaction of **93** with DNA. The profile at ratios higher than 1:1 is characterised by a large negative enthalpic dip, which returns quite rapidly to a plateau close to zero.We propose that the dip in the profile in Figure 5.31b, is due to condensation and aggregation of the DNA, which is induced when sufficient amount of **93** has been added. The subsequent changes are suggested to be due to stacking of the compounds, induced by the presence of DNA.

Concerning the first feature, the large negative enthalpic dip that is attributed to condensation and aggregation of the DNA, large dips such as this have previously been observed with polycations such as cobalt hexamine or spermidine.[184,185] It was shown in these publications that the DNA chain collapses after some fraction of the negative charges on the phosphate backbone is neutralised by cationic ligands, such as cobalt hexamine or spermidine. The critical value of charge neutralisation, or the amount of the DNA charge neutralised by a cation, is determined by the valence of the cation. The values in the presence of monovalent, divalent and trivalent cations are 0.76, 0.88 and 0.92, respectively.[186] It was proposed in the same publication that DNA retains its conformation until the degree of charge neutralisation has reached 0.90, this suggesting that cationic species with valences of three or higher are necessary to induce condensation of the helix. The condensation in the case of cobalt hexamine and spermidine is endothermic and so the process is entropically driven.[185]

These features seem at odds with the proposed condensation induced by **93**, as the heat changes resulting from binding of this compound are exothermic at all points, and the compound bears two positive charges. Any observed heat changes are representative of all the processes that are occurring in solution, both binding of the ligand to DNA and condensation of the DNA helix. Thus the initial changes up to a ratio of one, correspond to binding of the ligand to DNA. Between approximately 1 and 1.3 the negative dip occurs. Normally a positive heat change would be expected for such a process. However, it is possible that accompanying the condensation process is self association of **93** on the collapsing helix, and this process gives rise to negative heat changes. These changes mask the positive heat changes that would result otherwise from the condensation process. Concerning the second point, **93** is di-cationic, and as such, from counterion condensation theory would not be expected to induce condensation of the helix. **93** bears an intercalating 1,8-naphthalimide moiety attached to the positively charged diquat, which

will bind to DNA with high affinity. This consequently places the positive centre in close proximity to the negatively charged backbone of DNA.

A similar shaped profile was also observed for the addition of **94** to DNA, as shown in Figures 5.32a and 5.32b. In this case the system displays regular behaviour up to a ratio of approximately 1.25, after which a large exothermic dip occurred. The ITC behaviour of both **93** and **94** in the presence of DNA is complex, but thought to arise from multiple processes including regular DNA binding, DNA condensation and DNA induced stacking. To the best of our knowledge such behaviour has not previously been reported in the literature.

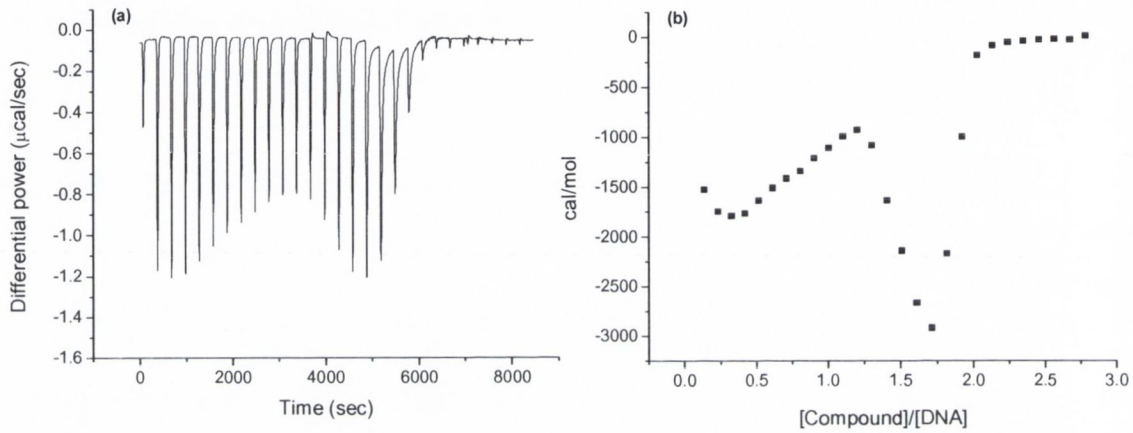

Figure 5.32 *(a) Raw ITC data for titration of* ***94*** *(2 mM) into a solution of st-DNA (0.2 mM), both solutions in 10 mM phosphate buffer, at pH 7, (b) Integrated ITC profile of* ***94*** *binding to st-DNA.*

It is also interesting to note that greater equivalents of **94** were necessary in order to induce the "dip", which is attributed to condensation of the helix. This may be related to the greater association of **94** within the grooves, in comparison to **93**, where the diquat is moiety expected to point outwards and interact with the phosphates, which may lead to a more efficient condensation process.

Reference compound **96** displayed quite typical ITC behaviour for a cationic species, the results showing that its binding to DNA was entropically driven. This is consistent with association in the grooves or at the phosphate backbone of DNA, as displacement of ordered solvent or counter-ions leads to increased disorder. In contrast, the calorimetric behaviour of **93** and **94** was complex, and suggested to involve a number of different processes. For both systems, initial exothermic events occurred, which were attributed to binding of the conjugates to DNA, followed by a large enthalpic dip in the

profiles, attributed to condensation and aggregation of the DNA, with concomitant stacking of the conjugates on the collapsing helix. Such complex ITC behaviour has not been reported previously, and may have been contributed to by other factors. ITC has therefore not provided further information as to the mode of interaction of **93** and **94** with DNA, but has revealed an interesting and previously unreported type of condensation process.

5.6 Conclusions

Through a series of measurements it has been possible to propose binding modes that account for the observed responses of **93** – **96** to added DNA. Variations in binding behaviour were observed depending on the connectivity of the components of each conjugate and the nature of the substituents on the 1,8-naphthalimide ring system. The overall binding modes of the bifunctional systems were closely related to those of the Ru(II) complexes discussed in *Chapter 4*, in that the 1,8-naphthalimide intercalates, while di-cation was found to bind externally and in the grooves.

Reference **96** was shown to bind st-DNA with high affinity ($K = 2.8 \times 10^6\ M^{-1}$) and displayed quite a significant luminescent quenching in the presence of DNA. Such behaviour would normally indicate high affinity intercalative binding, although further experiments suggested this was not the case. Moderate shifts in the melting temperature of DNA were observed with **96.** The absence of an ICD for **96** bound to DNA, suggested the occurrence of an external mode of association. This was further supported using ITC experiments, which showed binding to be entropically driven, which is consistent with electrostatic binding to the phosphate backbone, and association in the grooves.

The linear nitro system **93** was found to bind st-DNA with high affinity ($K = 1.7 \times 10^7\ M^{-1}$) and displayed the largest emission quenching of any of the systems studied, of 90%. These spectroscopic changes, in addition to large shifts in T_m, indicated an intercalative binding mode for this conjugate, which was further confirmed by ethidium bromide displacement assays. Circular dichroism studies showed the presence of a moderate ICD, suggesting that part of the molecule may be associated in the grooves of the DNA. Through the use of another control, namely **95**, the ICD was assigned as being primarily due to the diquat portion of the molecule.

The wedged nitro system **94** was initially suggested to bind DNA with weaker affinity than its linear analogue (this having been ascribed from the lower binding constant of **94** for st-DNA, calculated from UV/Visible absorption titration, $K = 6.5 \times 10^6\ M^{-1}$).

Furthermore, this system possessed a less well defined emission spectrum, attributed to reduced interaction between the 1,8-naphthalimide and diquat components. Upon binding to DNA a quenching of 31% in intensity was observed. In contrast to that observed for **93**, the results of the EtBr displacement experiment were not in agreement with that from UV/Visible absorption titration. An apparent DNA binding constant of 2.4 x 10^7 M^{-1} was calculated for **94** from EtBr displacement. This suggested that overall this system binds DNA with greater affinity than its linear analogue. Further evidence for tighter binding of **94** to DNA was obtained from thermal denaturation studies, this system resulting in the greatest stabilisation of the helix, while CD studies showed the presence of a more pronounced ICD for this system, indicating a more intimate association with the helix. From these results it was proposed that similar to the complexes described in *Chapter 4*, a wedged arrangement allows for a more cooperative binding of both components of the system, and as a result a greater overall affinity for DNA is observed.

The wedged system **95** proved quite useful, in assigning an overall mode of interaction of the 1,8-naphthalimide-diquat conjugates. Absorption bands corresponding to both the 1,8-naphthalimide and the diquat components could be identified, and monitored independently upon addition of DNA. The absorption band at 434 nm, attributed to the 1,8-naphthalimide, exhibited the greatest change, from which a binding constant of 2.3 x 10^6 M^{-1} was determined. This conjugate also displayed more well defined emission than the nitro analogue, with 55% quenching being observed upon binding to DNA. Compound **95** also caused large shifts in the T_m of DNA, although of a slightly smaller magnitude than its nitro analogue, which was attributed to the greater stacking ability of the nitro derivative, due to its more electron deficient nature. Circular dichroism studies showed the presence of an ICD of greater magnitude in the region of absorption of the diquat portion of the molecule. This confirmed the proposed overall binding mode, which involved high affinity intercalative interaction of the 1,8-naphthalimide and groove association of the diquat.

ITC experiments were also carried out with the nitro conjugates **93** and **94**, the results of which proved quite complex. Exothermic events were first observed as compound was added to DNA, attributed to binding of the compound to the helix, followed, in both cases, by large enthalpic dips in the profiles which were proposed to be due to condensation and aggregation of the helix, and stacking of the conjugates on the collapsing helix.

In summary, the family of conjugates discussed in this chapter represent an interesting group of bifunctional molecules, with excellent affinities and spectroscopic responses to DNA. It has been shown that each of the bichromophore systems binds in a similar manner to their Ru(II) complex counterparts. It was also demonstrated that a wedged arrangement of the constituent chromophores resulted in the most efficient interaction with DNA, most likely due to a more cooperative mode of binding of the components. Although it has not been explored as of yet as part of this research, these conjugates may also display interesting excited state reactivity with nucleic acids. This will be the subject of future research within the Gunnlaugsson group.

Chapter 6

Biological Studies

6.1 Introduction

Cancer is a disease characterised by an uncontrolled rate of cell proliferation. It originates primarily due to damage to the cellular DNA, which results in a breakdown in the mechanisms governing cell growth and replication. DNA, therefore, is an important therapeutic target, and agents which mediate its function by a variety of mechanisms have so far been developed.[187] Chemistry plays a vital role in the development of anticancer drugs, not only in the synthesis of active agents, but also in understanding drug-target interactions, and the structural features of molecules that govern their uptake and metabolism.[187] One important therapeutic strategy is photodynamic therapy (PDT) or the activation of a drug molecule by light at a specific target. PDT involves two non-toxic components; light and a chemical moiety (the photosensitizer), which when combined induce a cytotoxic effect. The strategy employed in PDT is represented schematically in Figure 6.1.

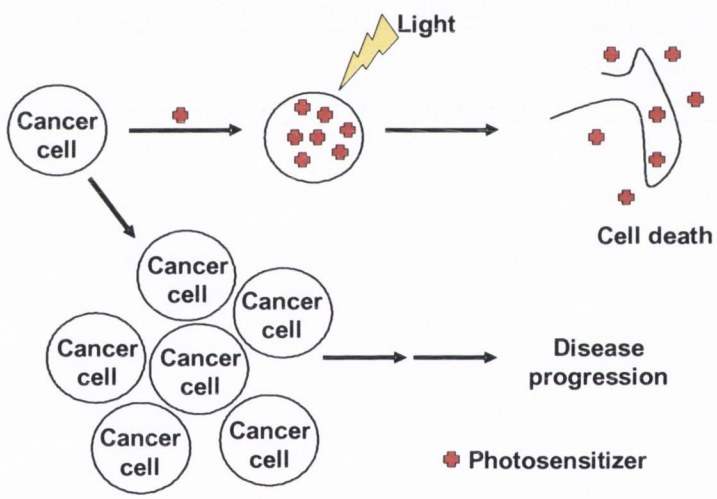

Figure 6.1 *Schematic representation of the strategy used in photodynamic therapy.*

Typically the photosensitizer is administered and allowed to accumulate at the site of the tumour. Subsequently, light of an appropriate wavelength is directed at the tumour, the PDT agent becomes activated in that locality, and cell death results. The advantage of this strategy is that a cytotoxic response is only observed in the region targeted by the light source. The selectivity with PDT is double-fold. Firstly, greater accumulation of the agent in cancer cells will occur, as these cells have greater uptake ability, and the vasculature in tumours is generally more porous.[188] Secondly, by use of a laser light source, cells in a very small region may be targeted and consequently only the agents in these cells become activated. For this reason the therapy is particularly attractive for the treatment of cancer.

The most commonly used agents for PDT are the porphyrins, particularly derivatives of hematoporphyrin. The application of hematoporphyrin derivative (HPD), more commonly knows as Photofrin to PDT has been widely explored.[189] This compound is currently in clinical use in a number of different countries, for the treatment of a variety of cancer types.[190] The mechanism of action of PDT agents such as porphyrins firstly involves absorption of light, to give an excited singlet state. This undergoes intersystem crossing to an excited triplet state, which may then undergo two different types of reaction. **Type II** reactions are the predominant means by which cellular damage is caused, and involve transfer of energy from the triplet state to molecular oxygen forming singlet oxygen, $^1O_2$.[191] The $^1O_2$ formed is referred to as a Reactive Oxygen Species (ROS), and may react with a number of cellular components, leading to damage and ultimately cell death.[190] **Type I** reactions involve direct reaction with cellular substrates that results in the formation of radicals. These radicals then react with oxygen to form oxygenated products, which lead to cellular damage.[190] A schematic representation of **Type I** and **Type II** reactions is given in Figure 6.2.

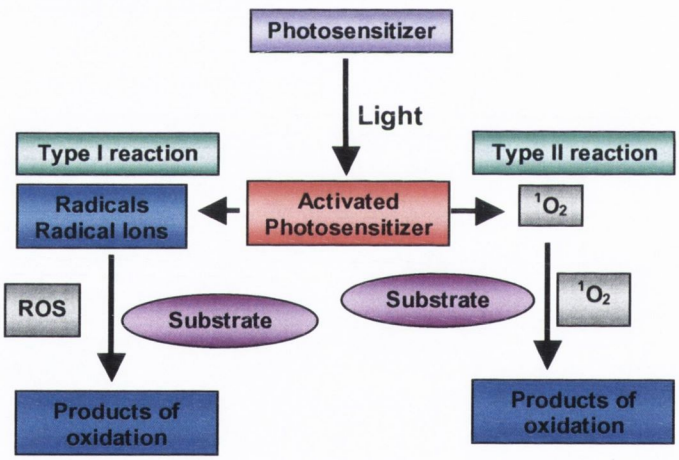

Figure 6.2 *Representation of Type I and II reactions in PDT.*[190]

In the case of Photofrin, the species administered is actually a poorly defined mixture of dimeric and oligomeric compounds, derived from the treatment of hematoporphyrin with acid.[192] As such it is difficult to ascertain which components lead to biological effects and to reproduce the composition of the agent. Many attempts to generate improved agents for PDT have focussed on porphyrin derivatives comprising a single component, with some success having been obtained in this area. Temoporphin, **84** is one such derivative, which has been prepared as a single compound and shown promise for use in PDT.[189]

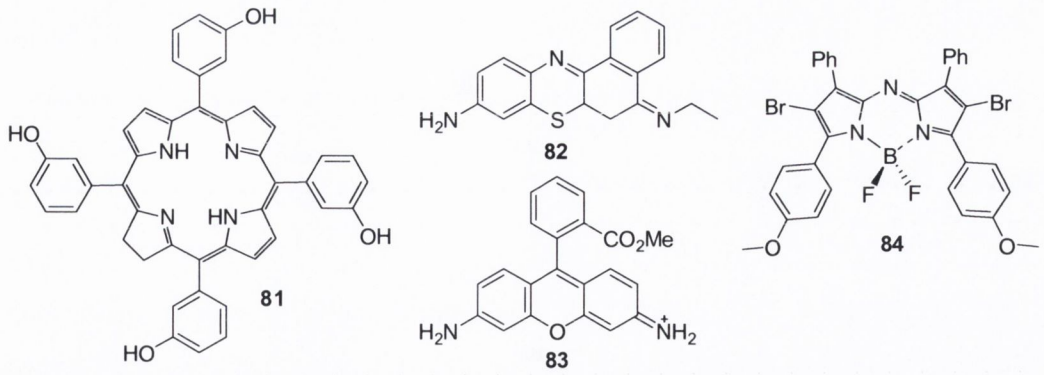

Non-porphyrin based systems have also been explored in attempts to generate more specific and photoactive compounds.[193] Examples of these include the nile blue derivatives such as **82**,[193] rhodamines such as **83**,[193] and BF_2-chelated tetraaryl-azadipyrromethanes such as **84**.[194] Given the useful and well characterised reactivity of Ru(II) complexes with DNA, and their ability to efficiently damage nucleic acids, it may seem surprising that such systems have not been investigated *in vitro* as PDT agents. The reason for this may be related to the charged nature of such complexes. This limits their uptake into cells as they cannot cross the cell membrane, which is hydrophobic at its core. A few publications have appeared which reported studies on the uptake of Ru(II) polypyridyl complexes into cells. One such study by Barton and co-worker investigated the uptake of the series of Ru(II) dppz complexes shown in Figure 6.2 into HeLa cells.[195]

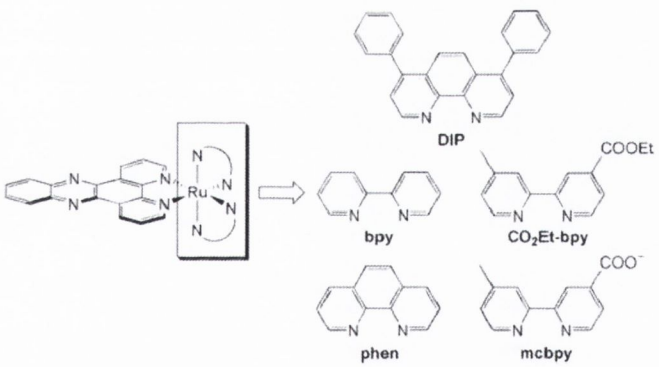

Figure 6.2 *Dipyridophenazine complexes of Ru(II).*[195]

Here, flow cytometry showed that only the complex incorporating hydrophobic DIP ligands entered the cells to any great degree. The entry of this compound into HeLa cells was further confirmed by confocal microscopy. Images were obtained where intense luminescence from the metal complex was observed. The greatest luminescence was observed in the cytoplasm, attributed to association of the complex with the mitochondria and endoplasmic reticulum. Interestingly, quite weak intensity was observed in the

nucleus despite this complex being much more strongly emissive when bound to DNA. As such the complex was proposed to display no preference for nuclear localisation.

Another publication by Nordén and co-workers reported the uptake and toxic effect of complex **13**, discussed in *Chapter 1*, on V79 Chinese hamster cells.[196] Confocal microscope images of cells incubated with the complex for 27 hours showed no accumulation in the nucleus, but did reveal the presence of small "red dots" in the cytoplasm, which the authors stated was an indication of uptake of the complex by pinocytosis, with penetration of the complex into the nucleus facilitated by electroporation.

An interesting application of a Ru(II) polypyridyl complex, which actually relied on the poor uptake of the system into cells was reported by Portolés and co-workers.[197] Complex **100** was investigated for use as a reporter of cell viability. Whereas the charged nature prevented entry into live cells, entry into non-viable cells whose cell membranes were not intact was signalled by large luminescent enhancements, due to binding of the system to DNA. Additionally, it was shown that due to the reasonably long lifetime of the Ru(II) complex, time resolved fluorimetry could be used in the analysis.

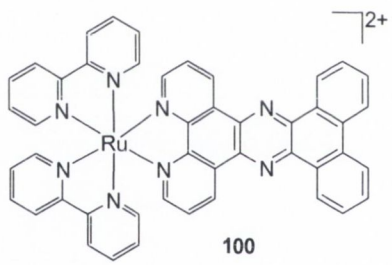

100

Considering the established ability of Ru(II) complexes to photodamage DNA, it was decided to undertake a study of the potential of the complexes discussed in this thesis as PDT agents. Firstly, the ability of each family of complexes from *Chapters 2*, *3*, and *4* to damage DNA was evaluated. Next, the ability of the complexes to accumulate in cells was investigated using flow cytometry and confocal microscopy. Finally, complexes exhibiting both photocleavage ability and cellular accumulation were chosen for study as PDT agents. These steps will be discussed in the following sections.

6.2 Photocleavage of Nucleic Acids

A variety of small molecules have been explored for use as DNA photocleavage agents. Research has focussed on both organic and inorganic compounds for such application.[6] The 1,8-naphthalimides (organic) and Ru(II) polypyridyl complexes (inorganic) represent two important class of potential photocleavers. The cleavage of a

nucleic acid target leads to nicking, or fragmentation of the DNA strand.[6] The most commonly used technique for analysis of such processes is electrophoresis, in which the products of cleavage are separated according to their ability to migrate through an agarose or polyacrylamide gel. The simplest of these techniques and the one used here involves circular segments of DNA from bacteria known as plasmids. In its normal undamaged state, the plasmid DNA is supercoiled and referred to as **Form I**. If single strand cleavage of the plasmid occurs it is converted to the open circular form also known as **Form II**, whereas if double strand cleavage occurs it is converted to the linear form, also known as **Form III**. These cleavage processes are represented schematically in Figure 6.3.

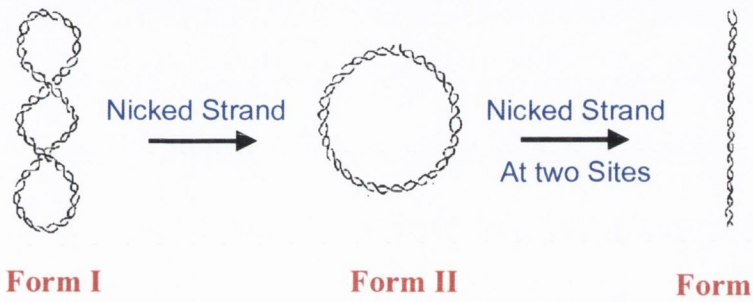

Figure 6.3 *Single and double strand cleavage of plasmid DNA yielding circular* ***(Form II)*** *and linear* ***(Form III)*** *forms.*

The products of plasmid DNA cleavage may be detected by electrophoresis, as the different forms migrate at different rates through the gel. **Form I** is the most compact, and will migrate through the gel to the greatest extent. This is followed by **Form III**, and finally, **Form II**, which due to its bulky circular nature, migrates to the least extent. The differences in migration of the different forms of plasmid DNA are represented schematically in Figure 6.4. Visualisation of the bands is achieved by staining of the gel with ethidium bromide. Such analysis and comparison of the relative amount of each form gives an indication of the efficiency of DNA cleavage, and whether single or double strand breaks have occurred.

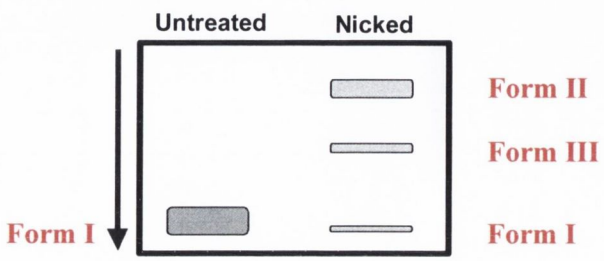

Figure 6.4 *Analysis of nicked plasmid DNA by gel electrophoresis.*

6.2.1 DNA Photocleavage by Complexes 37 – 40

The ability of the Ru(II)-4-nitro-1,8-naphthalimide conjugates **37** – **40** discussed in *Chapter 2*, to cleavage pBR322 plasmid DNA was first investigated. These systems were proposed to bind DNA through intercalation of the 1,8-naphthalimide moiety into the DNA helix and partial insertion of the Ru(II) centre into the grooves.

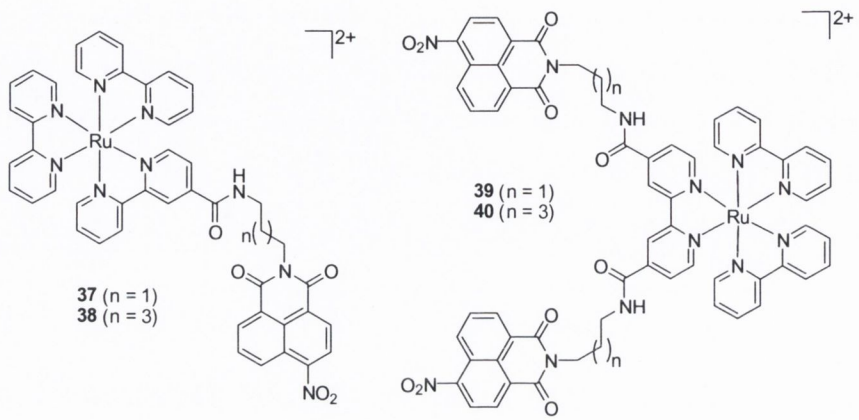

These complexes were expected to damage DNA by the generation of singlet oxygen, as they were not sufficiently oxidizing to undergo charge transfer reactions with the DNA.[29] However, the presence of the 1,8-naphthalimides (that anchor the Ru(II) centre tightly in place) may additionally result in improved efficiency of cleavage over sysyems such as $Ru(bpy)_3^{2+}$. The results of the cleavage experiments for this family of complexes are presented in Figure 6.5.

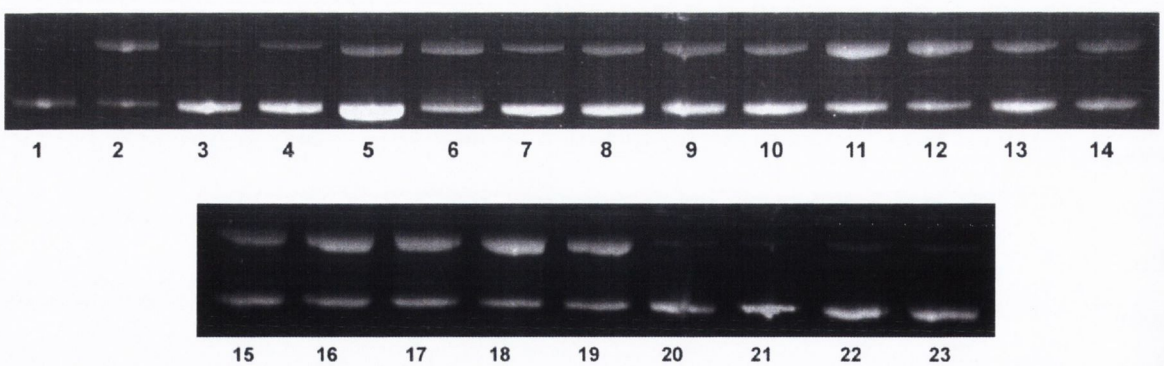

Figure 6.5 *Agarose gel electrophoresis of pBR322 DNA (1mg/ml) after 5 min irradiation at λ > 400 nm in 10 mM phosphate buffer, pH 7. Lane 1: Plasmid DNA control; Lane 2: $Ru(bpy)_3^{2+}$ (Bp/D 25); Lane 3: 10 mM Histidine; Lanes 4-6:* ***40*** *(Bp/D 25, 15, 5); Lanes 7-9:* ***39*** *(Bp/D 25, 15, 5); Lanes 10-12:* ***38*** *(Bp/D 25, 15, 5); Lanes 13-15:* ***37*** *(Bp/D 25, 15, 5); Lanes 16-19: Histidine +* ***40, 39, 38, 37*** *respectively (Bp/D 25, 15, 5); Lanes 20-23:* ***40, 39, 38, 37*** *respectively (Bp/D 5) in the dark.*

All of the complexes were shown to cleave DNA, however, with rather poor efficiency, of approximately the same order as $Ru(bpy)_3^{2+}$. This we attribute to the low quantum yield of MLCT emission determined for these systems. The small amount of populated excited state here leads to an inefficient production of $^1O_2$, and therefore poor efficiency of cleavage of the DNA. **Lane 1** represents intact plasmid which was directly loaded onto the gel, the presence of mostly **Form I** indicating that the stock DNA was undamaged. **Lanes 20 – 23** represent plasmid with added complexes in the dark, the absence of cleavage confirms that **37 – 40** do not damage DNA without irradiation. **Lane 2** represents the control photocleaver $Ru(bpy)_3^{2+}$, which was used to evaluate the relative efficiency of cleavage of the conjugate systems **37 – 40**.

6.2.2 Photocleavage of DNA by Complexes 68 and 69

The photocleavage capabilities of **68** and **69** were next investigated in the same manner as above. These strongly emissive systems, displayed excellent affinity for DNA, and therefore were regarded as improved candidates for use as nucleic acid photocleavage agents.

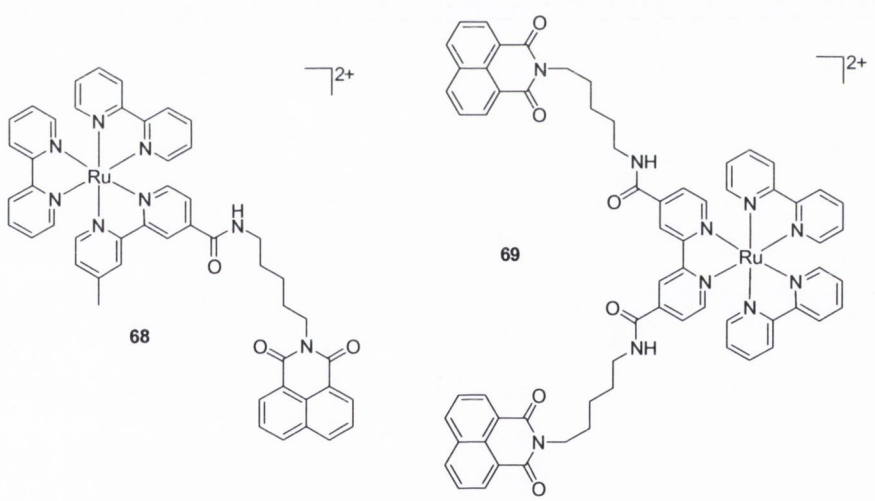

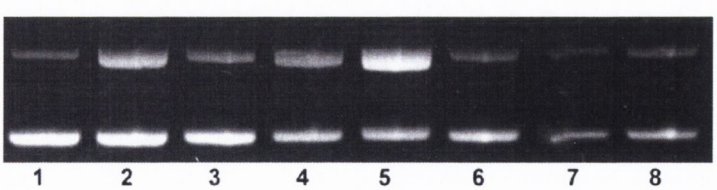

***Figure 6.6**. Agarose gel electrophoresis of pBR322 DNA (1mg/ml) after irradiation at λ > 390 nm in 10 mM phosphate buffer, pH 7. Lane 1: Plasmid DNA control; Lane 2: $Ru(bpy)_3^{2+}$ (Bp/D 5) 5 min irradiation; Lanes 3-5: **68** (Bp/D 5) 1, 3, 5 min respectively; Lanes 6-8: **69** (Bp/D 5) 1, 3, 5 min respectively.*

Shown in Figure 6.6 is the result of these DNA cleavage studies. The relative amounts of **Form I** *vs* **Form II** present are detailed in Table 6.1, as determined from densiometry measurements of the relative fluorescence intensity of the resulting bands.

Table 6.1 *Percentage of Form I vs II pBR322 plasmid DNA from the cleavage study in Figure 6.7.*

Lane	% Form I	% Form II
1	73	27
2	57	43
3	65	35
4	52	48
5	39	61
6	60	40
7	66	34
8	65	35

Determination of the relative intensity of the bands showed that DNA was somewhat damaged to begin with, being comprised of 73% **Form I** and 27% **Form II**. The presence of $Ru(bpy)_3^{2+}$ resulted in an increase in **Form II**, after 5 minutes irradiation. In the presence of **68** (**Lane 3**) a small amount of damage was also apparent after only 1 min of irradiation, the percentage of **Form II** having increased to 35%. After 3 minutes irradiation, this had increased to 49% **Form II**, and at the longest irradiation time of 5 minutes had increased to 61% **Form II**. From these results, it can be concluded that **68** displayed a reasonably efficient photocleavage of DNA, leading to more pronounced changes than the reference $Ru(bpy)_3^{2+}$. In contrast, complex **69** resulted in only a minor cleavage of the nucleic acid, with **Form I** being the predominant DNA species present, even after 5 minutes irradiation.

The fact that **69** displays very little cleavage of DNA may reflect the extremely tight association of the metal centre with the nucleic acid, where access by molecular oxygen is restricted, limiting the amount of $^1O_2$ generated, thereby resulting in a low efficiency of DNA cleavage.

6.2.3 Photocleavage of DNA by Complexes 76 – 79

Finally, the efficiency of sensitised DNA cleavage by the rigid complexes (**76** – **79**) was investigated. The orientation of the components within these systems was shown to have interesting consequences on the DNA binding behaviour (*Chapter 4*), and it was hoped that this would also be reflected in the cleavage studies. Complexes **78** and **79** were reasonably strongly emissive in solution, bound DNA with high affinity, and also displayed emission enhancements in the presence of DNA. In contrast, the nitro substituted complexes **76** and **77** were only weakly emissive in solution, and displayed moderate emission enhancements. However, they did display high affinity for DNA, of the same order as their amino analogues, and as such, represented a useful comparison for DNA cleavage experiments. The results of the cleavage studies with these systems are presented below, along with some initial mechanistic investigation into the nature of the process.

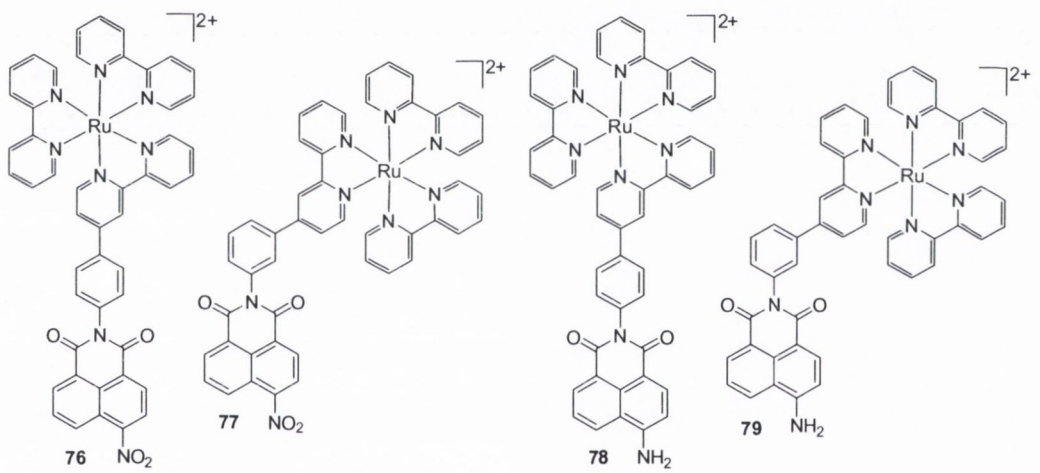

6.2.3.1 Irradiation for Varying Time

The first study conducted on **76** – **79**, involved irradiation of DNA in the absence and presence of each of the complexes, in 10 mM phosphate buffer solution, for varying time periods. A summary of the results are given in Figure 6.7, the complete Figures and corresponding tables are contained in Appendix 6. A number of notable trends were observed in Figure 6.7. Firstly (at all irradiation times), the nitro substituted conjugates **76** and **77** display poorer photocleavage efficiency than their amino substituted analogues **78** and **79**. Some minor differences were also apparent between corresponding linear and wedged derivatives. A slightly greater efficiency was observed in both cases for complexes comprising a linear arrangement of the 1,8-naphthalimide and Ru(II) components (**76** and **78**).

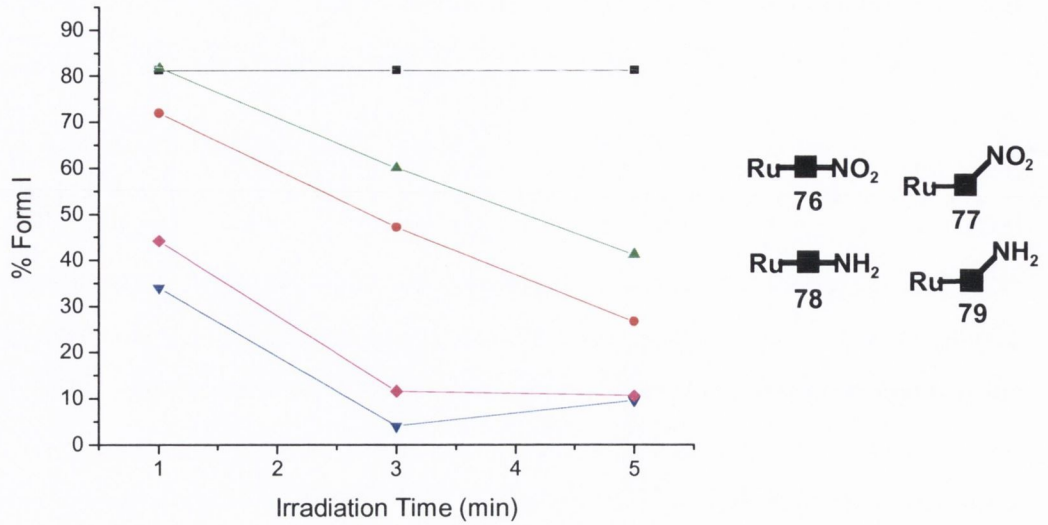

Figure 6.7 *The % of form I pBR322 plasmid DNA remaining after irradiation in the absence (■) and presence of* ***76*** *(●),* ***77*** *(▲),* ***78*** *(▼) and* ***79*** *(♦).*

It is worth noting that in Figure A6.1 (Appendix 6), **Lanes 7** and **8**, that some streaking on the gel is observed. This type of behaviour has previously been suggested to be due to the formation of adducts with DNA.[29] This was somewhat unexpected, considering the structure of the metal complex core, which should not be expected to be very oxidizing in the excited state. The possible formation of adducts by these complexes will be investigated in the future using dialysis experiments. However, the most important property to establish initially was the ability of the complexes to cleave DNA, and the relativity sensitivity of this process to the presence of molecular oxygen.

As the amino complexes demonstrated significantly improved photocleavage efficiency over $Ru(bpy)_3^{2+}$, more extensive studies as to the nature of the photocleavage process by **76 – 79** were conducted, as detailed in the following sections.

6.2.3.2 Irradiation in the Presence of Sodium Azide

As $^1O_2$ was expected to play an important role in the sensitized damage of DNA, studies were carried out in the presence of the $^1O_2$ scavenger sodium azide (NaN_3). A summary of the results is presented in Figure 6.8. The sensitivity of reference $Ru(bpy)_3^{2+}$ to added NaN_3 is clearly visible from Figure 6.8, as in the absence of NaN_3 just under 30% of **Form I** plasmid DNA remained, the rest having been converted to **Form II**. However, in the presence of NaN_3 the efficiency of cleavage was very much reduced, with just under 80% of **Form I** present under these conditions. This result indicates that the

photocleavage efficiency of $Ru(bpy)_3^{2+}$ is almost completely inhibited by the presence of the $^1O_2$ scavenger.

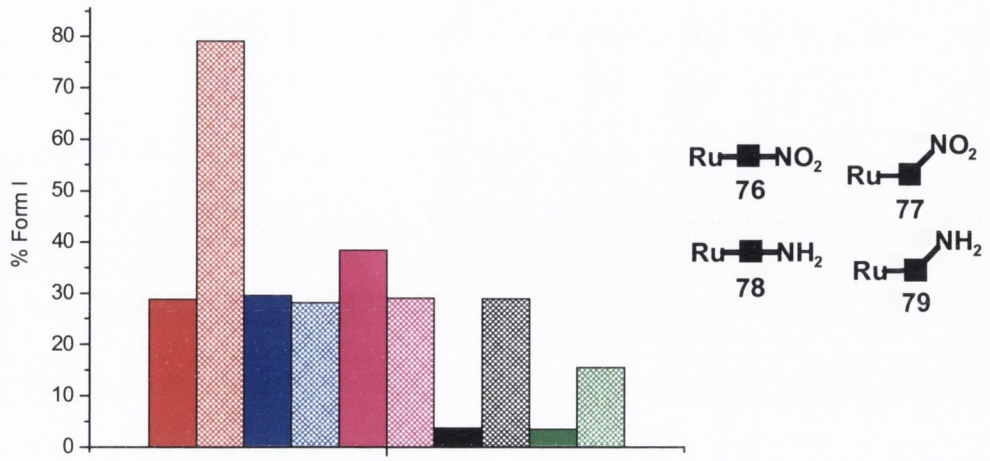

Figure 6.8 *Effect of added NaN_3 on the photocleavage efficiency of $Ru(bpy)_3^{2+}$ (■), **76** (■), **77** (■), **78** (■) and **79** (■). Solid bars represent cleavage in the absence of NaN_3 and hatched bars cleavage in the presence of NaN_3.*

The efficiency of the nitro substituted complexes **76** or **77** appeared insensitive to the presence of NaN_3, suggesting that damage mediated by singlet oxygen was not important for these derivatives. A process involving electron transfer to the DNA, or the formation of another reactive oxygen species may occur for these derivatives, although the presence of such a mechanism has not been investigated as of yet. The amino substituted conjugates **78** and **79** were also shown to be moderately sensitive to the presence of the singlet oxygen scavenger, with both inducing approximately the same amount of DNA damage in the absence of NaN_3, though it was reduced, with the change apparently being slightly greater for the linear complex. Nevertheless, in the presence of NaN_3, both **78** and **79** still displayed substantially improved cleavage efficiency over the reference $Ru(bpy)_3^{2+}$.

6.2.3.3 Irradiation in D_2O Solution

The lifetime of $^1O_2$ is known to be extended in D_2O. Therefore, to further investigate the involvement of $^1O_2$ in the DNA photocleavage process, studies were carried out in D_2O solution. A longer lifetime will result in greater persistence of the $^1O_2$, and consequently more efficient damage of the DNA. The differences in this medium may easily be identified in Figure 6.9, where the results for each system are compared. The complete figures and corresponding tables are contained in Appendix 6.

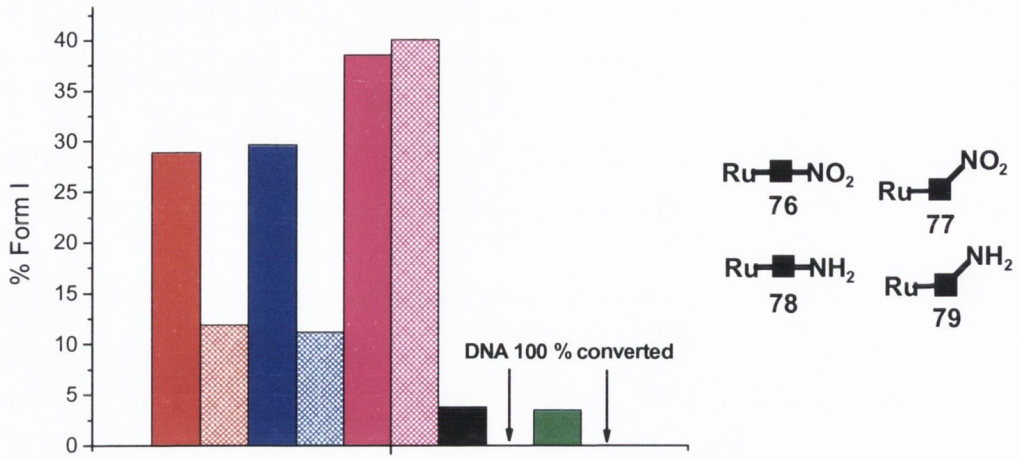

Figure 6.9 *Effect of irradiation in D_2O solution on the photocleavage efficiency of $Ru(bpy)_3^{2+}$ (■), **76** (■), **77** (■), **78** (■) and **79** (■). Solid bars represent cleavage in H_2O solution and hatched bars cleavage in D_2O solution.*

In the case of $Ru(bpy)_3^{2+}$, cleavage was observed to be more efficient in D_2O solution than in H_2O solution. Similarly complex **76** displayed an enhancement in photocleavage efficiency in the presence of D_2O, implicating $^1O_2$ in the mechanism of damage induced by this system. This was in contrast to the results obtained with addition of NaN_3 to this system, where no sensitivity to the added $^1O_2$ scavenger was observed. Complex **77** displayed, however, no enhancement in cleavage efficiency in D_2O solution. The mechanism of DNA damage by this system may involve direct oxidation of the bases or another reactive oxygen species.

Both **78** and **79** displayed improved photocleavage efficiency of the DNA in D_2O solution, giving a quantitative conversion. This in conjunction with the results in the presence of NaN_3, implicates $^1O_2$ as an important reactive species in the damage induced to DNA, by these complexes. **78** and **79** displayed significantly greater cleavage efficiency compared to the reference $Ru(bpy)_3^{2+}$, emphasising the importance of the 1,8-naphthalimide unit in these systems.

6.2.3.4 Irradiation upon Degassing

The final set of electrophoresis experiments carried out, involving degassing of the medium before irradiation. These experiments showed that all the complexes studied displayed a requirement for the presence of O_2 in order to photocleave DNA. This result is not that surprising, as oxygen is involved at some stage in photoinduced damage of DNA, regardless of the mechanism, the formation of reactive oxygen species being dependent on

the presence of oxygen.[190] However, damage to DNA resulting from direct electron transfer to the bases is also oxygen dependent, as it is the products that form after reaction with oxygen, subsequent to the electron transfer event that cause the observed damage to the helix.[190] It is not appropriate to make a direct comparison of the cleavage efficiencies displayed by corresponding complexes under degassing conditions, as the method employed in degassing was to purge the samples with argon for 10 minutes. Such a method of degassing of small samples (~ 10 μL) leads to the possibility for a considerable amount of error. Full details on this experiment are given in Appendix 6.

6.2.3.5 Summary (Irradiation Studies)

In conclusion, complexes **76** – **79** display useful photocleavage properties, whose efficiency depends on the substitution of the 1,8-naphthalimide moiety of the complex. The nitro substituted complexes **76** and **77** displayed cleavage efficiencies of the same order as $Ru(bpy)_3^{2+}$. The linear derivative **76** seemed to display some dependence on $^1O_2$ formation to exert damage, whereas its wedged analogue **77** did not.

Both of the amino substituted complexes **78** and **79** showed improved cleavage efficiency over the reference $Ru(bpy)_3^{2+}$. It was expected that this was due to the high binding affinity of these systems for DNA, which places the metal centre in close proximity to the helix, whereby it may effectively induce damage. The damage to DNA caused by **78** and **79** was shown to involve $^1O_2$ formation and possibly other reactive oxygen species. The next step was to establish the cellular uptake properties of these systems, as their application as diagnostic or therapeutic agents would require localisation within the target cells.

6.3 Flow Cytometry Study of Cell Uptake of Ru(II)-1,8-naphthalimide Conjugates

The first method used to evaluate the uptake of the complexes into cells was flow cytometry, the basic operation of which is shown in Figure 6.10. The technique of flow cytometry is based on the detection of fluorescence from cells in which a dye has accumulated.[198] The cells, which have been incubated with dye, are hydrodynamically focussed in a flow chamber into a continuous stream of single cells. Incident light from a laser hits the cells as they pass a particular point, and the emitted or scattered light is detected as appropriate. The FSC detector picks up forward scattered light and the SSC detector picks up side scattered light. The amount of light picked up by these two detectors is important in identifying different cell populations, or different sized particles

within the mixture. The remainder of the optics comprises a series of filters and detectors for different wavelength light. An appropriate channel can therefore be chosen to identify a particular dye, when a number of dyes emitting at different wavelengths are present. Up to 10,000 cells are read in about 30 seconds, and thus the experiment gives a very good average representation of the uptake event into the cells. The uptake of each of the families of Ru(II) complexes discussed in *Chapters 2*, *3*, and *4* will be discussed separately in the following sections. The uptake studies were carried out in collaboration with Mr. Daniel Frimannsson in the research group of Prof. Mark Lawlor at St. James Hospital.

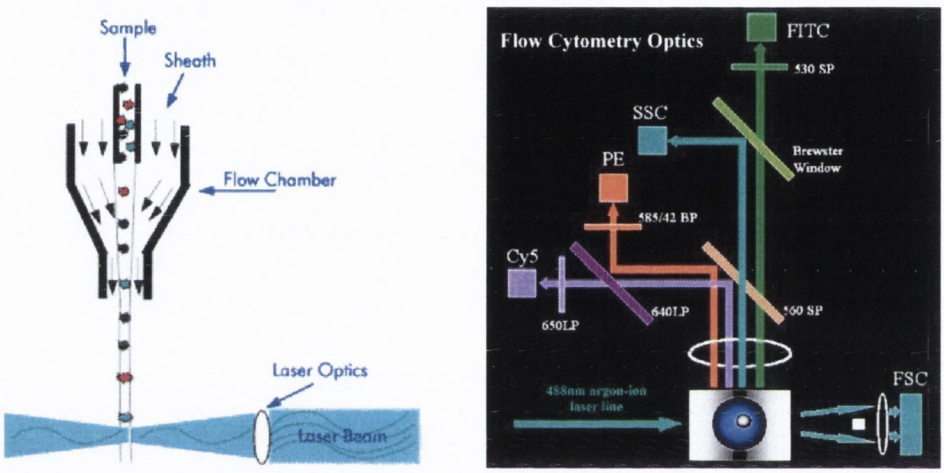

Figure 6.10 *Schematic representation of the operation of a flow cytometer. Shown on the left is the focussing of cells in the flow chamber and on the right the optical set-up of the instrument.*

6.3.1 Flexible Ru(II)-4-nitro-1,8-naphthalimide Conjugates from Chapter 2

The first series of complexes to be studied were the flexible Ru(II)-4-nitro-1,8-naphthalimide conjugates **37** – **40**. Shown in Figure 6.11 is the experimental read-out from the flow cytommetry analysis of HeLa cells, after incubation with complex **40** for 3 hours. The plot of side scatter *vs* forward scatter is used to identify the live cell population, and gate the emission so that only cells in this region are counted. In any biological study a percentage of the cells will not be viable, and it is necessary to exclude these in order to gain a more accurate reading. The live cell population corresponds to the dense grouping of dots in the bottom right corner in the scatter diagram in Figure 6.11.

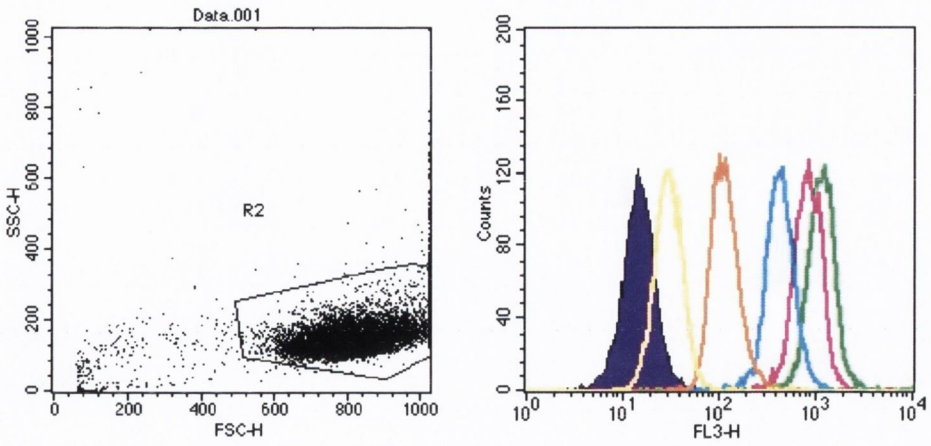

Figure 6.11 *Flow cytometry analysis of the uptake of* ***40*** *into HeLa cells after 3 hours. On the left is shown the plot of side scatter vs forward scatter and the gate chosen to select the live cell population. On the right is shown the fluorescence intensity from HeLa cells in the absence (—) and presence of* ***40*** *at 1 μM (—), 5 μM (—), 12.5 μM (—), 25 μM (—) and 50 μM (—) concentration.*

On the right is the intensity of emitted light as detected in the FL-3 channel. By means of a long pass filter this detector only detects light with a wavelength greater than 650 nm. The solid purple peak represents background fluorescence from the cell. As increasing amounts of complex are added the maximum fluorescence shifts to higher intensity, reaching a value approximately two orders of magnitude greater at the highest concentration used. For each of the complexes studied, data such as that presented in Figure 6.11 was generated for three different periods of incubation; 3, 6, and 24 hours, respectively. The results obtained for each of the systems **37** – **40** is summarised in Appendix 6.

In all cases large shifts in detected fluorescence intensity were observed, increasing with longer incubation times, and greater concentration of complex. However, quite a large amount of data is represented in the Figures in Appendix 6 and would take a considerable length of time to discuss individually. Consequently, the material will be summarised here. For ease of comparison the results at the intermediate concentration of complex used (12.5 μM) are plotted on the same graph, as shown in Figure 6.12. After 3 hours incubation, emission corresponding to each of the complexes was observed. The order of intensity is broadly what would be expected, the bis-1,8-naphthalimide conjugates **39** and **40** displaying greater emission intensity than their mono-analogues **37** and **38**. As cellular uptake is favoured for hydrophobic species, the presence of the second

1,8-naphthalimide moiety leads to accumulation in the cells to a greater extent. The same general trend was observed after incubation for 6 hours. However, after incubation for 24 hours a somewhat different trend was observed. Here, the greatest intensity was observed for the bis-complex **40**, which contains a pentyl linker, followed by the mono-complex **37**, which contains a propyl linker, followed by its bis-analogue. In contrast, on all occasions, the mono-pentyl linked complex **38** displayed the smallest intensity change. The fact that **37**, comprising a single 1,8-naphthalimide, accumulates to a greater extent after 24 hours than its bis-analogue **39** is in contrast to what would be expected. However, the value does give a true representation of the uptake process, as the events in 10,000 different cells are counted. As the factors governing the uptake of such complexes are currently poorly understood, it is not possible to propose an explanation for this phenomenon at this time.

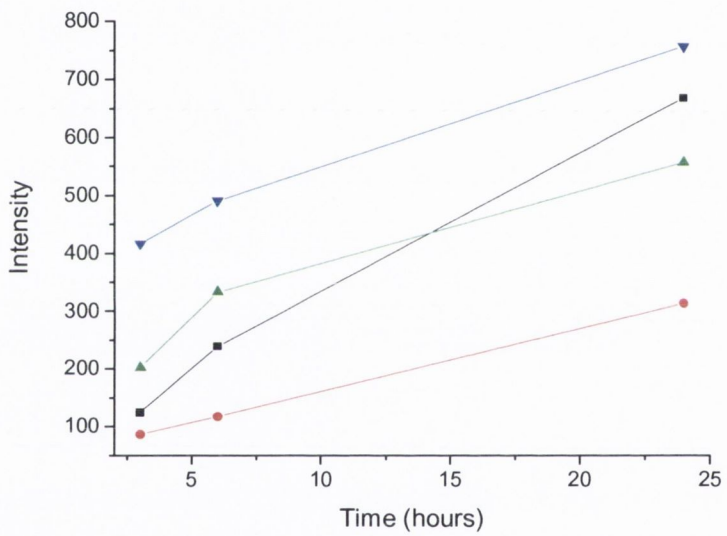

Figure 6.12 *Observed fluorescence intensity from HeLa cells upon incubation with* ***37*** *(—■—),* ***38*** *(—●—),* ***39*** *(—▲—) and* ***40*** *(—▼—), all at a concentration of 12.5 μM.*

These flow cytometry studies represent an important milestone in the development of Ru(II) polypyridyl complexes based probes for use as diagnostic agents, both *in vitro* and *in vivo*. It has been successfully demonstrated that each of the flexibly linked Ru(II)-4-nitro-1,8-naphthalimide conjugates could effectively enter HeLa cells, resulting in large shifts in fluorescence intensity in flow cytometry experiments. It is expected that the useful cell penetration properties are a function of the bifunctional nature of the complexes, which contain both charged and hydrophobic centres. Considering the very promising results from studies on **37** – **40** it was decided to conduct similar studies on the complexes described in *Chapter 3* and *4*.

6.3.2 Flexible Ru(II)-1,8-naphthalimide Conjugates from Chapter 3

The fluorescence intensity from HeLa cells resulting from the addition of **68** and **69** at varying concentrations is shown in Appendix 6. The changes resulting from the addition of an intermediate concentration of complex (12.5 μM) are shown in Figure 6.13.

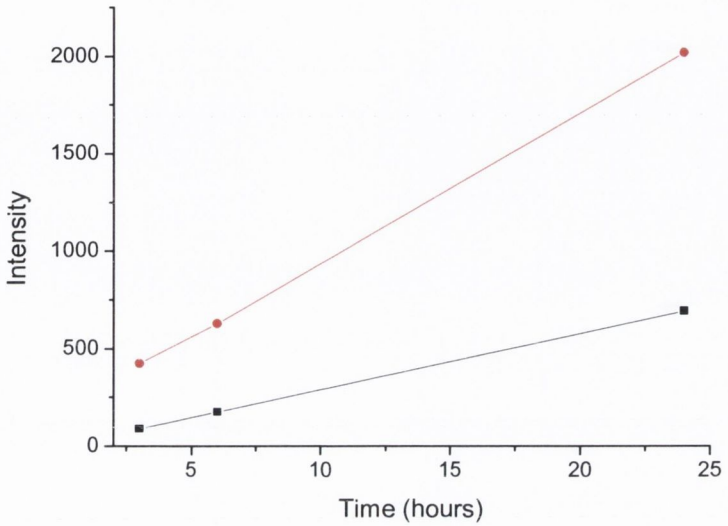

Figure 6.13 *Observed fluorescence intensity from HeLa cells upon incubation with* ***68*** *(—■—) and* ***69*** *(—●—), all at a concentration of 12.5 μM.*

At all time points greater intensity was observed for incubation with complex **69**, which was attributed to the more hydrophobic nature of this complex in comparison to **68**, due to the presence of the second 1,8-naphthalimide. In fact accumulation of this complex was so efficient that at the higher concentrations used the intensity went off the scale on the detector of the flow cytometer. Furthermore, the uptake of these derivatives seems to be more efficient than that of their nitro-1,8-naphthalimide analogues discussed in the previous section. However, as mentioned before **68** and **69** were strongly emissive in solution, and therefore, a similar concentration of compound within the cell would give rise to a greater fluorescence intensity than complexes **37** – **40**. It is expected that both families of complexes should possess similar uptake properties, due to their closely related structures.

In conclusion, the results from the study of **68** and **69**, are again of considerable significance in providing evidence for our assertion that the use of bifunctional complexes, comprising separate hydrophilic and hydrophobic centres is the best means of effecting cellular accumulation of Ru(II) based probes and reactive agents within cells.

6.3.3 Rigid Ru(II)-1,8-naphthalimide Conjugates from Chapter 4

The final complexes studied in this programme were the rigid complexes **76** – **79**, discussed in *Chapter 4*. These had been shown to photocleave DNA; the efficiency of which was found to be dependent on the 1,8-naphthalimide ring functionality. The uptake of each of the complexes into HeLa cells was verified by flow cytometry studies, and the results for each complex are shown in Appendix 6. Again, for ease of comparison the results at the intermediate concentration (12.5 μM) are shown in Figure 6.14.

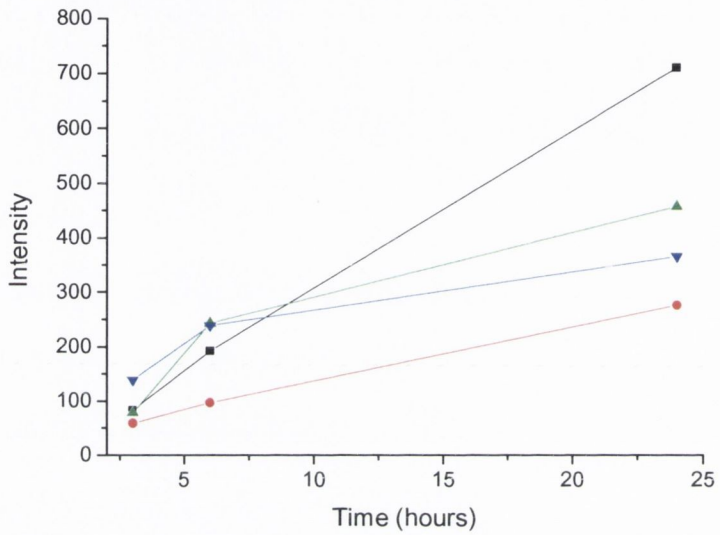

Figure 6.14 *Observed fluorescence intensity from HeLa cells upon incubation with* ***76*** *(—■—),* ***77*** *(—●—),* ***78*** *(—▲—) and* ***79*** *(—▼—), all at a concentration of 12.5 μM.*

From analysis of the results in Figure 6.14, a number of important points may be identified. Firstly, at all time points the amino substituted complexes **78** and **79** displayed similar intensities, suggesting that the uptake properties of these two derivatives are quite similar in nature. Secondly, the nitro substituted complexes **76** and **77** display quite contrasting uptake properties to each other, where the linear derivative **76** was observed to enter cells much more effectively. Complex **76** was in fact found to be the most easily taken up by the HeLa cells after 24 hours incubation. Complex **76**, was weakly emissive in solution, possessing a Φ_F of 0.004 in water, in comparison to the amino complexes **78** and **79** which possessed Φ_F of 0.019 and 0.018, respectively. Furthermore, **76** displayed a smaller luminescent enhancement in the presence of DNA than did **78** and **79**. For complex **76** to give rise to a larger shift in the fluorescence intensity than **78** or **79** it must have been present in the cells at a much higher concentration. The reduced intensity displayed by HeLa cells incubated with **77** may also be reflective of the emission properties of the system. This complex possessed the lowest quantum yield at 0.001.

Therefore, the amount of this complex that accumulates in the cells will be approximately the same as for **76**, the difference in intensities resulting from the differing quantum yields of emission possessed by the complexes.

Overall it seems that the nitro complexes **76** and **77** can more effectively enter the HeLa cells than their amino analogues **78** and **79**. The reasons for this are not clear at present, as no literature precedents exist for comparison. Nevertheless, the studies importantly showed that each of **76** – **79** could enter cells, which in conjunction with their photocleavage ability, make these compounds excellent leads for use in PDT.

6.4 Confocal Microscopy Study of Complexes 76 – 79 in HeLa cells

As the results discussed in the previous section represent one of the first comprehensive studies of the uptake ability of a series of Ru(II) complexes, confocal microscopy was also carried out to provide visual confirmation of the metal complexes in cells. This was particularly important for complexes **76** – **79**, as it was intended to investigate the ability of these compounds to selectively kill cells upon irradiation. Shown in Figure 6.15 is the confocal image obtained of HeLa cells with complex **76**. The change is in agreement with the flow cytometry discussed above as the complex is observed to be within the cell interior. However, and of even greater significance, is the observation that the complex also seems to be localised within the nucleus. This can be concluded from comparison to the nuclear co-stain HOECHST 3342, where the red emission from the complex perfectly overlays with the blue emission from the HOECHST 3342. To the best of our knowledge this is the first example of the accumulation of a Ru(II) polypyridyl complex in the nucleus of a cell without electroporation.[196] This result is therefore extremely significant and promising in light of the requirements we set for use of these agents in PDT.

Similar nuclear localisation was observed for the corresponding amino complex **70**. One of the images obtained with this derivative is shown in Figure 6.16, from which it is clear that the complex is also in the cell interior, and more specifically localised in the nucleus. Similar images were obtained for the wedged complexes **77** and **79**, and are contained in the appendix.

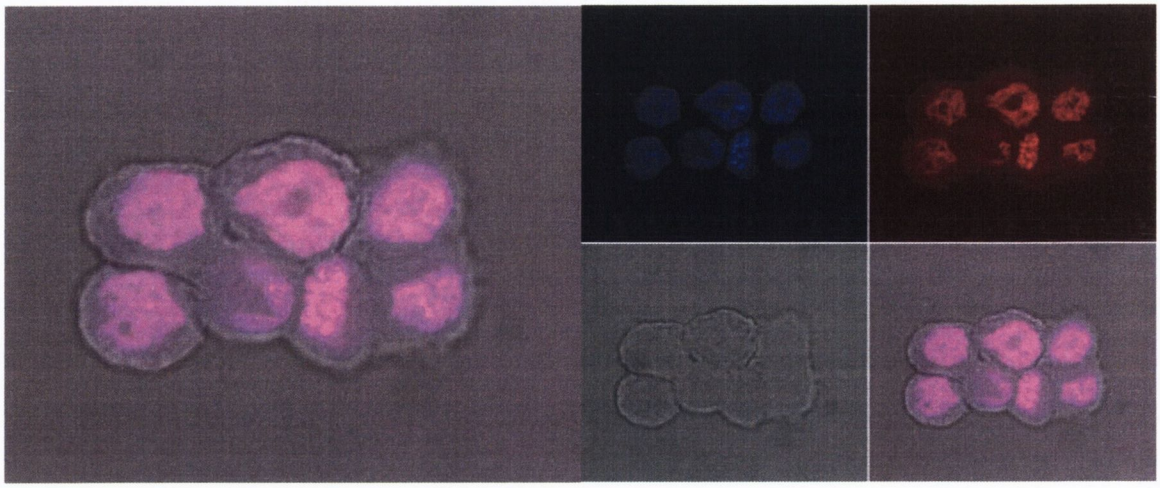

Figure 6.15 *Confocal laser scanning microscopy image of* ***76*** *in HeLa cells. On the right is shown the image obtained of HOESCHT nuclear co-stain (blue),* ***76*** *(red), optical image of the cells (grey) and the overlay of these three. On the left is an enlarged version of the overlayed image.*

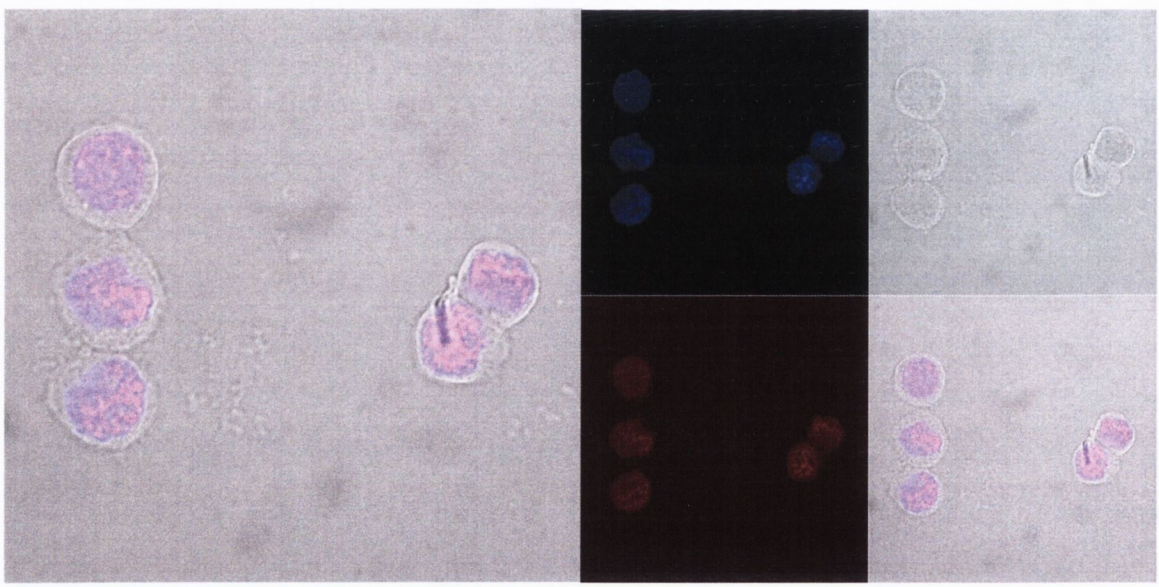

F***igure 6.16*** *Confocal laser scanning microscopy image of* ***78*** *in HeLa cells. On the right is shown the image obtained of HOESCHT nuclear co-stain (blue),* ***78*** *(red), optical image of the cells (grey) and the overlay of these three. On the left is an enlarged version of the overlayed image.*

At this point all of the criteria that were specified for a PDT agent were fulfilled. The complexes could effectively damage DNA upon excitation and were shown using flow cytometry and confocal microscopy to enter cells. The next step in the research was therefore to assess the cytotoxicity of complexes **76** – **79** in the dark and with irradiation,

to establish if they displayed potential for use as PDT agents. These studies have been carried out by Mr. Daniel Frimannsson at St. James Hospital and have shown that certain derivatives of the family of complexes display promising PDT activity. Most importantly, all of the complexes were poorly cytotoxic in the dark, which was one of the criteria for a useful PDT agent. However, they became activated upon irradiation, with **78** and **79** proving particularly good. The order of activities was the same as that for the efficiency of photodamage to DNA. Full details of these experiments will be provided in the PhD thesis of Mr. Daniel Frimannsson.

6.5 Conclusions

The work presented in this chapter has demonstrated that in addition to displaying varying spectroscopic responses to DNA, Ru(II)-1,8-naphthalimide conjugates may also possess varying abilities to photocleave DNA. Both families of flexibly linked complexes were shown to be relatively inefficient photocleavers. This was in contrast to the rigid complexes, which displayed promising photocleavage efficiency, comparable or greater than that of $Ru(bpy)_3^{2+}$. Each family of complexes were found to enter cells and localise within the nucleus, ascribed from flow cytometry experiments, and confocal microscopy experiments for **77** – **79**. The research was therefore one step further towards the development of Ru(II) based complexes for use in PDT.

Chapter 7

Conclusions and Future Work

7.1 Conclusions

The work described in this thesis represents a systematic study of a series of related bifunctional DNA binding molecules. In each chapter a different modification to the overall design is considered, and the effect that this has on the solution photophysical properties and the DNA binding behaviour established.

In *Chapter 2*, a series of flexibly linked Ru(II)-nitro-1,8-naphthalimide conjugates were investigated. These systems were shown to be weakly emissive in aqueous solution, and as such displayed chromophore-quencher behaviour. Upon titration with DNA each complex displayed a substantial luminescent enhancement, the magnitude of which was shown to be sensitive to the length of the linker moiety, and the presence of one or two 1,8-naphthalimide chromophores. Greater enhancements were observed for the C_5 linked complexes than the C_3 linked complexes, most likely due to greater separation of the chromophore and quencher upon DNA binding. Slight structural modification of the 1,8-naphthalimide moiety, involving a change in the substitution pattern from 4-nitro to 3-nitro had a significant effect on the binding properties of the resulting complex, where the latter resulted in improved DNA binding ability and emission response. It was therefore demonstrated in this Chapter that the DNA binding properties and emission response of Ru(II)-1,8-naphthalimide conjugates were dependent on both the substitution pattern of the attached quencher and the length of the linker moiety.

In *Chapter 3*, a slight structural modification to the basic design was considered in which an un-substituted 1,8-naphthalimide was incorporated into the bichromophore complexes. In this case the 1,8-naphthalimide was shown to sensitize the Ru(II) MLCT emission, and the complexes were shown to be strongly emissive in solution, due to the absence of a quenching pathway. Both mono and bis-1,8-naphthalimide complexes were studied, both of which were shown to strongly bind DNA. Furthermore, each complex displayed substantial quenching of emission upon titration with DNA, attributed to both decreased absorbance and electron transfer quenching of the 1,8-naphthalimide. Of particular significance with these derivatives were the varying emission changes in the presence of different DNA sequences. More pronounced quenching was observed in the presence of GC rich DNA, attributed to enhanced electron transfer quenching of the 1,8-naphthalimide excited state by the guanine nucleotides. Similar to the complexes in *Chapter 2*, the flexible linkers allowed for independent movement of the constituent chromophores, and a large number of possible binding modes.

In *Chapter 4*, a more rigid arrangement of the Ru(II) and 1,8-naphthalimide subunits was investigated, in which their orientation was more precisely controlled. A wedged or meta arrangement around a central aromatic ring was shown to result in greater affinity for DNA, and greater changes in spectroscopic properties, due to greater complementarity in the shape of the complex to that of the DNA. The substituents on the 1,8-naphthalimide were again shown to have significant effects on the DNA binding properties. Complexes containing nitro substituents displayed emission quenching at low ratios of DNA due to an induced stacking conformation, followed by enhancement at higher ratios. In contrast, those containing amino substituents displayed emission enhancement at all DNA ratios. From a series of spectroscopic studies it was possible to propose a binding mode for these conjugates involving intercalation of the 1,8-naphthalimide and groove association of the Ru(II) centre.

In *Chapter 5*, a different set of conjugates were studied comprising 1,8-naphthalimide and diquat functionality. The arrangement of the components around a central aromatic ring was again shown to have substantial effects on the DNA binding behaviour, with a wedged arrangement resulting in the most efficient interaction. The study of these conjugates demonstrated that a charged organic unit could perform the same function as a Ru(II) complex in terms of DNA binding, in providing both electrostatic attraction to the helix and associating in the grooves. However, the emission response of these organic systems were not as pronounced, emphasising the utility of the Ru(II) complex core in probing DNA.

In *Chapter 6*, the ability of the complexes discussed in *Chapters 2 – 4* to photocleave DNA was described. Here, it was demonstrated that the complexes from *Chapter 2* and *3* were relatively inefficient DNA photocleavers, but those described in *Chapter 4* displayed promising photocleavage efficiency, comparable or greater than that of $Ru(bpy)_3^{2+}$. Two systems proved particularly efficient, a more detailed study of which showed their cleavage to involve singlet oxygen as a reactive intermediate. Flow cytometry studies showed each of the families of complexes from *Chapters 2 – 4* to enter HeLa cells effectively. This was an extremely important result as the cellular uptake properties of Ru(II) complexes has not been widely described in the literature. We propose that the bifunctional nature of the complexes, which contain both hydrophobic and hydrophilic components is responsible for the excellent uptake. Significantly, the complexes from *Chapter 4* were also shown using cofocal microscopy to accumulate in the

nucleus. As such, they were chosen as potential PDT agents, the study of which will be described in the thesis of Mr. Daniel Frimannsson.

Overall the work described in this thesis has emphasised the utility of Ru(II)-1,8-naphthalimide conjugates as DNA probes and photoreagents. Systematic variation of the components of each complex has allowed us to establish the important structural features for efficient DNA interaction and response. If a probe for DNA is required a flexible chromophore-quencher arrangement of the type discussed in *Chapter 2* seems the best strategy, as large spectroscopic responses to DNA are observed. However, if a photocleaver is required a more rigid arrangement, in which a non-quenching amino substituted 1,8-naphthalimide is incorporated results in the most efficient reaction. It has been demonstrated that the different components of the complex – Ru(II) complex, linker, and 1,8-naphthalimide may be regarded as modules, that can be combined in different ways depending on the properties that are required.

7.2 Future work

Future work in this research programme will primarily focus on exploiting the cellular uptake properties of the complexes described in this thesis. Complexes such as **101** are currently being prepared, whose binding to DNA will firstly be established. Their ability to photocleave DNA will then be investigated, which is expected to be extremely efficient due to the presence of the TAP ligands. These complexes are expected to enter cells and will therefore be investigated as PDT agents.

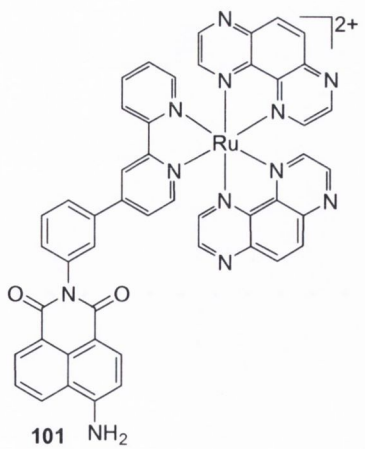

101

More extensive photophysical studies involving flash photolysis experiments will also be conducted on the complexes described in *Chapter 3*, to establish if electron transfer to the 1,8-naphthalimide, from the DNA bases, is responsible for the observed quenching of emission.

Chapter 8

Experimental

8.1 General Experimental Techniques

All NMR spectra were recorded using a Brüker DPX-400 Avance spectrometer, operating at 400.13 MHz for ^{1}H NMR and 100.6 MHz for ^{13}C NMR, or a Brüker AV-600 spectrometer, operating at 600.1 MHz for ^{1}H NMR and 150.2 MHz for ^{13}C NMR. Shifts are referenced relative to the internal solvent signals. Electrospray mass spectra were recorded on a Micromass LCT spectrometer, running Mass Lynx NT V 3.4 on a Waters 600 controller connected to a 996 photodiode array detector with HPLC-grade methanol or acetonitrile. High resolution mass spectra were determined by a peak matching method, using leucine Enkephalin, (Tyr-Gly-Gly-Phe-Leu), as the standard reference (m/z = 556.2771). Melting points were determined using an IA9000 digital melting point apparatus. Infrared spectra were recorded on a Perkin Elmer Spectrum One FT-IR spectrometer fitted with a Universal ATR Sampling Accessory. X-Ray diffraction studies were carried out by Dr. Thomas McCabe (School of Chemistry, Trinity College Dublin) using a Brüker SMART APEX single crystal CD diffractometer. Elemental analysis was conducted at the Microanalytical Laboratory, School of Chemistry and Chemical Biology, University College Dublin.

UV-visible absorption spectra were recorded on a Varian Cary 50 spectrometer. Emission spectra were recorded on a Cary Eclipse Luminescence spectrometer. The luminescence quantum yields were calculated by comparison with $[Ru(bpy)_3]^{2+}$. Circular dichroism (CD) spectra were recorded at a concentration corresponding to an optical density of approximately 1.0, in buffered solutions, on a Jasco J-810-150S spectropolarimeter. Thermal denaturation experiments were performed on a thermoelectrically coupled Varian Cary 50 Spectrometer. The temperature in the cell was ramped from 20 to 90 °C, at a rate of 1 °C min^{-1} and the absorbance at 260 nm was measured every 0.2 °C. Isothermal titration calorimetry was carried out using a MicroCal VP-ITC instrument using a cell temperature of 25 °C. The experiment was carried out by making small injections of a 2 mM solution of compound into a 0.2 mM solution of DNA contained in the sample cell. Control experiments were also carried out in which buffer was injected into a solution of DNA and compound injected into a solution of buffer. The results of these were subtracted from the actual experimental profile.

The HeLa cell line, which was derived from cervical cancer cells was used for the flow cytometry studies, as the cells are adherent and grow on a surface, and are therefore easy to work with. In preparation for a typical experiment the growth medium was removed from the culture flask, in which the cells were growing, and trypsin added to

detach the cells from the surface. After incubation for ~ 10 minutes the sample was centrifuged and the trypsin decanted off. The cells were then re-suspended in growth medium and placed in a six well plate. The cells were left for 24 hours to adhere to the surface. The growth medium was replaced and varying concentrations of the compound being studied added to the well. After the desired period of incubation, the medium was removed and trypsin added. The sample was centrifuged and PBS buffer added to re-suspend the cells. The centrifugation and re-suspension procedure was repeated, and the samples then analysed using the flow cytometer.

Samples for confocal microscopy were prepared in a similar manner to those for flow cytometry. Rather than using a six well plate a chamber slide consisting of a glass slide divided into 6 wells by means of a plastic overlay was used. Complex was added to the cells in the chamber slide and incubated for the desired period of time. A co-stain was then added and incubated for a further 10 minutes. The medium was removed from the chamber slide and replaced with PBS buffer.

Electrochemical measurements were preformed by Mr. Gareth Keeley on a CH Instruments Model 440 Potentiostat. Experiments were conducted in a cell consisting of a glass working vessel (maximum capacity *ca.* 15 cm^3), three electrodes and an electrolyte solution. Solutions were purged with nitrogen for a minimum of 15 minutes prior to measurements in order to remove dissolved oxygen. The working electrode was a glassy carbon macroelectrode (IJ Cambria, model CHI104), the reference a Ag / AgCl reference (IJ Cambria, model CHI111), and the counter electrode a platinum wire (IJ Cambria, model CHI115).

8.2 Materials

cis-$[Ru(bpy)_2Cl_2].2H_2O$,[199] 4,4'-dicarboxy-2,2'-bipyridine[136], and 4-carboxy-4'-methyl-2,2'-bipyridine[135] were prepared by the literature routes. All other reagents and solvents were purchased commercially and used without further purification unless otherwise stated. Anhydrous solvents were prepared using standard procedures, according to Vögel, with distillation under argon prior to each use.[200] Chromatographic columns were run using Silica gel 60 (230 – 400 mesh ATSM) or Aluminium Oxide (activated, neutral, Brockmann I STD grade 150 mesh). Analytical TLC was performed using Merck Kieselgel 60 F_{254} silica gel plates or Polygram Alox N/UV_{254} aluminium oxide plates. Solutions of DNA in 10mM phosphate buffer (pH 7) gave a ratio of UV absorbance at 260 and 280 nm of 1.86:1, indicating that the DNA was sufficiently free of protein. Its

concentration was determined spectrophotometrically using the molar absortivity of 6600 M^{-1} cm^{-1} (260nm). Poly(dAdT)poly(dAdT) and poly(dGdC)poly(dGdC) were purchased from Amersham Biosciences and their concentration determined spectrophotometrically using the molar absortivities of 6600 M^{-1} cm^{-1} (262nm) and 8400 M^{-1} cm^{-1} (254nm), respectively.

8.3 General Synthetic Procedures

8.3.1 Procedure 1: Condensation Reaction with 1,8-naphthalic anhydrides

To a mixture of the relevant amine (1.1 eq.) and 1,8-naphthalic anhydride (1 eq.) in anhydrous toluene was added triethylamine (3 eq.). The reaction mixture was heated at reflux under an argon atmosphere for 24 hours. The mixture was filtered while hot through celite, and the solvent removed under reduced pressure. Chloroform was added to the residue and the solution washed twice with 0.1 M HCl and once with water. The organic layer was dried over $MgSO_4$, filtered and the solvent removed under reduced pressure. Purification of the product by recrystallisation was carried out where necessary, details of which are provided later.

7.3.2 Procedure 2: Deprotection of Boc Protecting Group using Trifluoroacetic Acid

A solution of the Boc protected compound in trifluoroacetic acid (TFA) CH_2Cl_2 (1:1 v/v) was stirred at room temperature for 1 hour. The solvent was removed under reduced pressure and co-evaporated several times with CH_2Cl_2 to remove traces of TFA. The resulting product was dried under high vacuum. Further purification was not necessary.

8.3.3 Procedure 3: Coupling of 1,8-naphthalimide to bipyridine

The relevant 1,8-naphthalimide (1.1 or 2.1 eq.) and Et_3N (3 or 5 eq.) were dissolved in dry CH_2Cl_2, and 4,4'-bis(carbonylchloride)-2,2'-bipyridine or 4-(carbonylchloride)-4'-methyl-2,2'-bipyridine (1 eq.), dissolved in dry CH_2Cl_2 was added dropwise. The resulting suspension was stirred at room temperature for 16 hours. The solvent was removed under reduced pressure. The resulting residue was stirred with 0.1 M HCl, filtered and washed with water. Purification was carried out as described for each compound.

8.3.4 Procedure 4: Complexation of 1,8-naphthalimide-bipyridine ligands with $Ru(bpy)_2Cl_2$

The appropriate ligand (1 eq.) was dissolved in DMF and water added until it began to precipitate. A few drops of DMF were added to fully dissolve the ligand and $Ru(bpy)_2Cl_2.2H_2O$ added. The solution was saturated with argon by bubbling for 10 minutes. The reaction mixture was heated at reflux under an argon atmosphere for 24 hours. The solvent was removed under reduced pressure, and the resulting residue re-dissolved in water and filtered. The filtrate was reduced in volume and to it was added a concentrated aqueous solution of NH_4PF_6. The resulting precipitate was extracted with CH_2Cl_2, dried over $MgSO_4$ and the solvent removed under reduced pressure. The product was purified by silica flash column chromatography eluting with CH_3CN/H_2O/Aqueous $NaNO_{3(sat)}$ 40:4:1. The chloride form of the complex was reformed by stirring a solution of the PF_6 salt in methanol with Amberlite ion exchange resin (Cl^- form) for 1 hour.

8.3.5 Procedure 5: Reduction of 4-nitro-1,8-naphthalimide-Ru(II) Complexes

The complex was dissolved in HPLC grade MeOH and 10% Pd/C added. The reaction mixture was subjected to 3 Atm H_2 for 24 hours. The reaction mixture was filtered through a celite plug and the solvent removed under reduced pressure.

8.3.6 Procedure 6: Chalcone Formation

The nitro-benzaldehyde (1 eq.) was added to EtOH and the mixture heated to 70 °C until the solid dissolved. Sodium pyruvate (1.1 eq.) dissolved in water was added, and the mixture cooled to 0 °C in an ice bath. NaOH solution (2M) (30 ml) was added dropwise and the mixture stirred at 0 °C for 2.5 hours. The mixture was then neutralised with 2M HCl (~30 ml), filtered, the solid washed with EtOH (2 x 10 ml) and dried.

8.3.7 Procedure 7: 4-(Nitrophenyl)-2,2'-bipyridine Formation

The appropriate chalcone (1 eq.), 2-pyridacyl pyridinium iodide (1 eq.) and ammonium acetate (8 eq.) were added to H_2O and the mixture heated at reflux for 5 hours. The solid was filtered, and washed with water (2 x 10 ml) and acetone (2 x 5 ml) to give the ammonium salt of the 4-(nitrophenyl)-6-carboxylate-2,2'-bipyridine. The ammonium salt was heated under vacuum with a heat gun until evolution of CO_2 ceased. The resulting black solid was dissolved in EtOAc (150 ml), activated charcoal added and the mixture

refluxed for 15 min. The mixture was filtered through a pad of celite and the solvent removed under reduced pressure.

8.3.8 Procedure 8: 4-(Nitrophenyl)-2,2'-bipyridine Reduction

The relevant ligand and 10% Pd/C were added to EtOH (30 ml) and the mixture heated at reflux for 1 hour. Hydrazine monohydrate (98%) was added and the mixture heated at reflux for 1 hour. The mixture was filtered through a pad of celite and the solid washed with CH_2Cl_2 (40 ml). The filtrate was washed with water, dried over $MgSO_4$, and the solvent removed under reduced pressure.

8.3.9 Procedure 9: 4-[*N*-Phenyl-4-nitro-1,8-napthalimide]-2,2'-bipyridine Formation

The appropriate aromatic amine (1 eq.) and 4-nitro-1,8-naphthalic anhydride (1 eq.) were suspended in HPLC grade ethanol and the mixture refluxed under an argon atmosphere for 48 hours. The reaction mixture was cooled to room temperature and ether added to further precipitate product, which was collected by suction filtration.

8.3.10 Procedure 10: Bipyridine Quaternization

The appropriate bipyridine was suspended in dibromoethane and the mixture heated at reflux for 48 hours. The reaction mixture was cooled to room temperature, the resulting precipitate collected by filtration and washed with acetone (5 ml) and hexane (5 ml). The product was dried under high vacuum. The product was dissolved in MeOH and stirred for 1 hour with Amberlite Ion exchange resin (Cl^-). The suspension was filtered and the solvent removed under reduced pressure.

8.4 Synthesis and Characterisation of Compounds Described in Chapter 2

Ru(53)(bpy)$_2$Cl$_2$ (37)

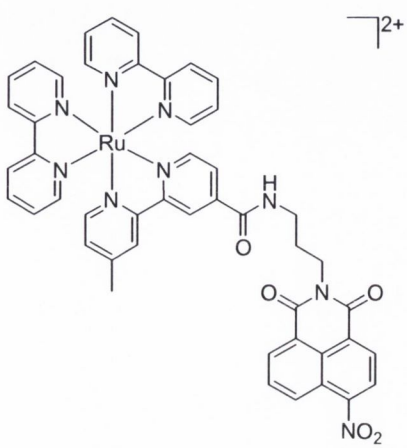

Compound **37** was synthesised according to **Procedure 4** using **53** (0.20 g, 0.41 mmol, 1 eq.) and $Ru(bpy)_2Cl_2.2H_2O$ (0.24 g, 0.45 mmol, 1.1 eq.) giving the product as a red/brown solid (0.240 g, 60%). Calculated for $C_{47}H_{37}F_{12}N_9O_5P_2Ru.CH_3OH$: C, 46.39; H, 3.23; N, 10.36. Found: C, 46.12; H, 3.02; N, 9.90; Accurate MS (m/z) Calculated for $C_{47}H_{37}N_9O_5Ru$ (M^{2+}): 909.1961.

Found: 909.1982; ^{1}H NMR δ_H (CD_3CN, 600 MHz): 8.79 (1H, s, NH), 8.66 (1H, d, J = 8.6 Hz, Ar-H), 8.58 (1H, d, J = 7.1 Hz, Ar-H), 8.55 (1H, d, J = 8.1 Hz, Ar-H), 8.51 (5H, m, 5 x Ar-H), 8.36 (1H, d, J = 8.0 Hz, Ar-H), 8.05 (4H, m, 4 x Ar-H), 7.94 (1H, m, Ar-H), 7.86 (1H, d, J = 5.9 Hz, Ar-H), 7.73 (5H, m, 5 x Ar-H), 7.63 (1H, d, J = 5.9 Hz, Ar-H), 7.56 (1H, d, J = 5.7 Hz, Ar-H), 7.40 (4H, m, 4 x Ar-H), 7.27 (1H, d, J = 5.7 Hz, Ar-H), 4.17 (2H, t, J = 7.2 Hz, CH_2), 3.48 (2H, m, CH_2), 2.54 (3H, s, CH_3), 2.02 (2H, m, CH_2); ^{13}C NMR δ_C (CD_3OD, 150 MHz): 164.1, 163.1, 162.2, 157.9, 157.0, 156.9, 156.8, 156.0, 151.9, 151.2, 151.0, 150.8, 150.3, 149.2, 142.2, 137.9, 137.7, 131.5, 129.4, 128.7, 128.5, 128.3, 127.6, 127.4, 126.2, 125.6, 124.8, 124.3, 124.2, 123.6, 122.9, 122.4, 121.5, 37.9, 37.5, 27.2, 19.9; IR ν_{max} (cm^{-1}): 1704 (w, -CO-N-CO-), 1659 (m, -CONH-), 1525 (m, C-NO_2), 1342 (m, C-NO_2).

Ru(54)(bpy)$_2$Cl$_2$ (38)

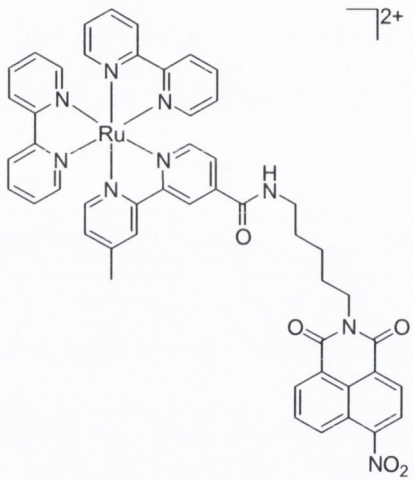

Compound **38** was synthesised according to **Procedure 4** using **54** (0.38 g, 0.72 mmol, 1 eq.) and $Ru(bpy)_2Cl_2.2H_2O$ (0.37 g, 0.72 mmol, 1 eq.) giving the product as a red/brown solid (0.56 g, 65%). Calculated for $C_{50}H_{44}F_{12}N_9O_5P_2Ru$: C, 47.53; H, 3.24; N, 10.39. Found C, 47.57; H, 3.36; N, 9.98; Accurate MS (m/z) Calculated for $C_{48}H_{34}NN_8O_2Ru$ (M^{2+}): 937.2274. Found: 937.2228; ^{1}H NMR δ_H (CD_3CN, 400 MHz): 9.08 (1H, s, NH), 8.66 (3H, m, Ar-H), 8.56 (6H, m, Ar-H), 8.35 (1H, d, J = 8.2 Hz, Ar-H), 8.08 (4H, m, Ar-H), 7.93 (1H, dd, J = 8.8, 7.6 Hz, Ar-H), 7.82 (1H, d, J = 5.8 Hz, Ar-H), 7.75 (4H, m, Ar-H), 7.68 (1H, d, J = 5.2 Hz, Ar-H), 7.58 (1H, d, J = 5.8 Hz, Ar-H), 7.42 (4H, m, Ar-H), 7.28 (1H, d, J = 5.8 Hz, Ar-H), 4.09 (2H, m, CH_2), 3.41 (2H, dd, J = 12.3, 6.4 Hz, CH_2), 2.54 (3H, s, CH_3), 1.71 (4H, m, 2CH_2), 1.46 (2H, m, CH_2); ^{13}C NMR δ_C (CD_3CN, 100 MHz): 162.9, 162.6, 162.1, 157.4, 156.6, 156.5, 156.4, 155.8, 151.7, 151.3, 151.2, 150.3, 150.2, 150.0, 142.3, 137.4, 137.3, 131.2, 129.4, 128.9, 128.4, 128.3, 128.1, 127.1, 126.8, 125.3, 124.5, 123.8, 123.6, 122.8, 121.0, 39.8, 39.2, 28.2, 26.8, 23.6, 19.8; IR ν_{max} (cm^{-1}): 1703 (m, -CO-N-CO-), 1657 (s, -CONH-), 1526 (m, C-NO_2), 1340 (m, C-NO_2).

Ru(57)(bpy)$_2$Cl$_2$ (39)

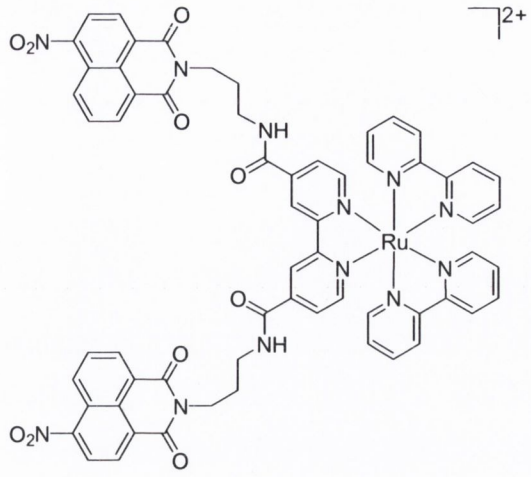

Compound **39** was synthesised according to **Procedure 4** using **57** (0.080 g, 0.099 mmol, 1.1 eq.) and Ru(bpy)$_2$Cl$_2$.2H$_2$O (0.047 g, 0.090 mmol, 1 eq.) giving the product as a red/brown solid (0.060 g, 52%). Calculated for $C_{62}H_{46}Cl_2N_{12}O_{14}Ru.H_2O.CH_3CN.CH_2Cl_2$: C, 54.40; H, 3.72; N, 12.69. Found: C, 54.00; H, 3.82; N, 12.92; Accurate MS (m/z) Calculated for $C_{62}H_{46}N_{12}O_{10}Ru$ (M^{2+}): 1220.2503. Found 1220.2505; ^{1}H NMR δ_H (CD_3CN, 400 MHz): 9.25 (2H, s, Ar-H), 8.85 (2H, m, NH), 8.56 (4H, m, Ar-H), 8.51 (2H, d, J = 8.5 Hz, Ar-H), 8.39 (4H, m, Ar-H), 8.23 (2H, d, J = 8.0 Hz, Ar-H), 8.11 (6H, m, Ar-H), 7.90 (2H, d, J = 6.0 Hz, Ar-H), 7.82 – 7.76 (10H, m, Ar-H), 7.46 (6H, m, Ar-H), 4.20 (4H, m, CH$_2$), 3.52 (4H, m, CH$_2$), 2.01 (4H, m, CH$_2$); ^{13}C NMR δ_C (CD_3CN, 100 MHz): 163.1, 162.9, 162.3, 157.4, 156.7, 152.2, 151.8, 151.5, 149.2, 142.5, 137.9, 131.6, 129.6, 129.3, 128.7, 128.4, 127.6, 127.5, 126.7, 125.5, 124.2, 123.9, 122.9, 122.7, 121.7, 38.3, 37.8, 27.5; IR ν_{max} (cm^{-1}): 1704 (m, -CO-N-CO-), 1659 (m, -CONH-), 1527 (s, C-NO$_2$), 1332 (s, C-NO$_2$).

Ru(58)(bpy)$_2$Cl$_2$ (40)

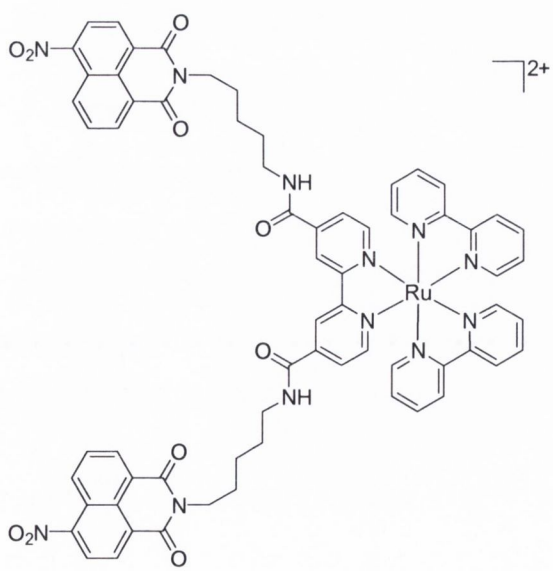

Compound **40** was synthesised according to **Procedure 4** using **58** (0.078 g, 0.009 mmol, 1 eq.) and Ru(bpy)$_2$Cl$_2$.2H$_2$O (0.049 g, 0.0095 mmol, 1.05 eq.) giving the product as a red/brown solid (0.06 g, 49%). Calculated for $C_{66}H_{54}Cl_2N_{12}O_{14}Ru.2.5CH_2Cl_2$: C, 52.76; H, 3.81; N, 10.78. Found C, 52.49; H, 4.02; N, 10.95; Accurate MS (m/z) Calculated for $C_{66}H_{54}N_{12}O_{10}Ru$ (M^{2+}): 1276.3129. Found 1276.3088; ^{1}H NMR δ_H (CD_3OD, 400 MHz): 9.29 (2H, s, Ar-H), 8.80 (2H, m, NH), 8.55 (4H, dd, J = 3.5, 8.0 Hz, Ar-H), 8.51 (2H, d, J = 7.5 Hz, Ar-H), 8.42 (2H, m, Ar-H), 8.40 (2H, d, J = 8.0 Hz, Ar-H), 8.22 (2H, d, J = 7.6 Hz, Ar-H), 8.09 (4H, m, Ar-H), 7.86 (2H, d, J = 6.0 Hz, Ar-H), 7.80 (2H, m, Ar-H), 7.76 (6H, m, Ar-H), 7.43 (4H, m, Ar-H), 3.97 (4H,

m, C<u>H</u>$_2$), 3.42 (4H, m, C<u>H</u>$_2$), 1.70 (8H, m, C<u>H</u>$_2$), 1.46 (4H, m, C<u>H</u>$_2$); ^{13}C NMR (CD_3CN, 150 MHz): 164.2, 164.0, 163.4, 158.5, 157.8, 153.2, 152.8, 152.6, 150.3, 143.9, 139.0, 132.6, 130.7, 130.3, 129.7, 129.6, 128.7, 127.8, 126.5, 125.3, 124.9, 124.0, 123.9, 122.7, 41.2, 40.8, 29.5, 28.2, 25.1; IR ν_{max} (cm^{-1}): 1704 (w, -CO-N-CO-), 1657 (s, -CONH-), 1526 (m, C-NO_2), 1341 (C-NO_2).

Ru(64)(bpy)$_2$Cl$_2$ (41)

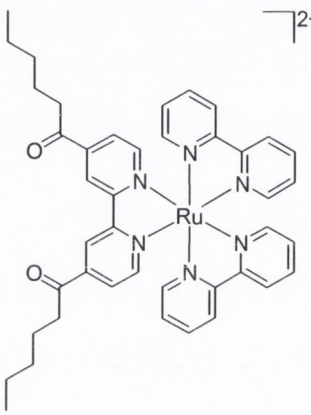

Compound **41** was synthesised according to **Procedure 4** using **64** (0.12 g, 0.34 mmol, 1.1 eq.) and Ru(bpy)$_2$Cl$_2$.2H$_2$O (0.16 g, 0.31 mmol, 1 eq.) giving the product as a red/brown solid (0.17 g, 70%). Calculated for $C_{40}H_{42}F_{12}N_8O_2P_2Ru.0.66CH_2Cl_2$: C, 43.83; H, 3.92; N, 10.05. Found: C, 43.61; H, 3.85; N, 9.86; Accurate MS (m/z) Calculated for $C_{42}H_{44}N_6O_2Ru$ (M^{2+}): 766.2569. Found 766.2440; ^{1}H NMR δ_H (CD_3CN, 400 MHz): 8.94 (2H, s, Bpy-<u>H</u>), 8.53 (4H, d, J = 7.5 Hz), 8.09 (4H, dd, J = 13.1, 7.0 Hz), 7.89 (2H, d, J = 6.0 Hz, Bpy-<u>H</u>), 7.72 (6H, m, Bpy-<u>H</u>), 7.53 (2H, br s, N<u>H</u>), 7.42 (4H, m, Bpy-<u>H</u>), 3.42 (4H, q, J = 6.5 Hz, C<u>H</u>$_2$), 1.61 (4H, m, C<u>H</u>$_2$), 1.41 (4H, h, J = 7.5 Hz, C<u>H</u>$_2$), 0.96 (6H, t, J = 7.5 Hz, C<u>H</u>$_3$); ^{13}C NMR δ_C (CD_3CN, 100 MHz): 163.9, 158.4, 157.8, 157.7, 153.4, 152.7, 152.5, 143.7, 139.0, 128.64, 128.58, 125.8, 125.3, 122.9, 40.5, 32.0, 20.7, 14.0; IR ν_{max} (cm^{-1}): 1644 (s, -CONH-).

***N*-(*tert*-Butoxycarbonyl)-1,3-diaminopropane (44)**

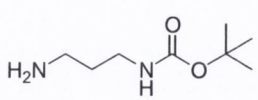

Compound **44** was synthesised by dropwise addition of a solution of Boc_2O (0.75 g, 3.45 mol, 1 eq.) in $CHCl_3$ to a solution of 1,3-diaminopropane (1.28 g, 1.44 ml, 5 eq.) in $CHCl_3$ cooled to 0 °C. The reaction mixture was stirred at room temperature overnight. The solvent was removed under reduced pressure and the residue dissolved in water and filtered. The product was extracted into CH_2Cl_2, which was then dried over $MgSO_4$, filtered and the solvent removed under reduced pressure. This yielded the product as a yellow oil (0.48 g, 80%). ^{1}H NMR δ_H ($CDCl_3$, 400 MHz): 4.94 (1H, br, s, N<u>H</u>), 3.22 (2H, m, C<u>H</u>$_2$), 2.77 (2H, m, C<u>H</u>$_2$), 1.62 (2H, m, C<u>H</u>$_2$), 1.45 (12H, s, (C<u>H</u>$_3$)$_3$); ^{13}C NMR δ_C ($CDCl_3$, 100 MHz): 155.8, 78.7, 38.5, 37.6, 36.8, 27.6; ESI-MS m/z 175.1 (M+H).

N-(*tert*-Butoxycarbonyl)-1,5-diaminopentane (45)

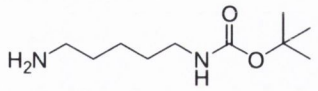

Compound **45** was synthesised by dropwise addition of Boc_2O (0.80 g, 3.67 mmol, 1 eq.) in 1,4-dioxane (20 ml) to a solution of 1,5-diaminopentane (1.50 g, 14.68 mmol, 4 eq.) in 1,4-dioxane (60 ml). The solution was stirred overnight. The solvent was removed under reduced pressure. The residue was dissolved in CH_2Cl_2 (50 ml), washed with water, dried over $MgSO_4$ and the solvent removed under reduced pressure. The product was obtained as a yellow oil (0.57 g, 82%). Accurate MS m/z Calculated for $C_{10}H_{23}N_2O_2$ (M+H): 202.1700. Found 203.1681; ^{1}H NMR δ_H ($CDCl_3$, 400 MHz): 4.63 (1H, br s, NH), 3.11 (2H, d, J = 6.0 Hz, CH_2), 2.68 (2H, m, CH_2), 1.53 – 1.30 (18H, m, 3 x CH_2 + $C(CH_3)_3$); ^{13}C NMR δ_C ($CDCl_3$, 100 MHz): 155.7, 78.5, 40.4, 39.8, 30.3, 29.8, 29.2, 28.0, 23.4.

***N*-[(*tert*-Butoxycarbonyl)-3-aminopropyl]-4-nitro-1,8-naphthalimide (47)**

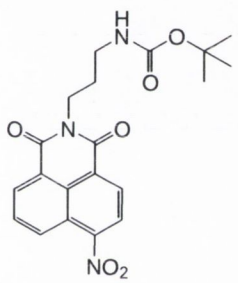

Compound **47** was synthesized according to **Procedure 1** using 4-nitro-1,8-naphthalic anhydride (0.59 g, 2.41 mmol, 1 eq.), **44** (0.46 g, 2.65 mmol, 1.1 eq.) and Et_3N (0.73 g, 1.01 ml, 3 eq.). After purification by recrystallisation from acetone/ether the product was obtained as a pale brown solid (0.89 g, 93%). m.p. 120-121 °C; Accurate MS (m/z) Calculated for $C_{20}H_{21}N_3NaO_4$ (M+Na): 422.1328. Found 422.1320; ^{1}H NMR δ_H ($CDCl_3$, 400 MHz): 8.85 (1H, d, J = 8.5 Hz, Naph-H), 8.74 (1H, d, J = 7.0 Hz, Naph-H), 8.70 (1H, d, J = 8.0 Hz, Naph-H), 8.42 (1H, d, J = 8.0 Hz, Naph-H), 8.00 (1H, m, Naph-H), 5.16 (1H, br s, NH), 4.28 (2H, m, CH_2), 3.19 (2H, d, J = 5.5 Hz, CH_2), 1.96 (2H, m, CH_2), 1.46 (9H, s, $(CH_3)_3$); ^{13}C NMR δ_C ($CDCl_3$, 400 MHz): 163.1, 162.3, 155.5, 149.2, 132.2, 129.5, 129.0, 128.6, 126.3, 123.5, 123.2, 122.3, 78.7, 37.7, 37.1, 30.0.

***N*-[(*tert*-Butoxycarbonyl)-5-aminopentyl]-4-nitro-1,8-naphthalimide (48)**

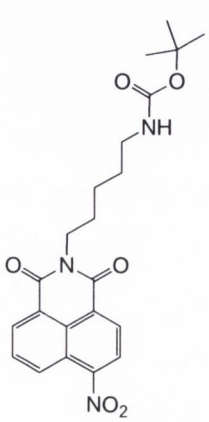

Compound **48** was synthesised according to **Procedure 1** using 4-nitro-1,8-naphthalic anhydride (0.50 g, 2.87 mmol, 1 eq.), **45** (0.60 g, 3.15 mmol, 1.1 eq.), and Et_3N (0.87 g, 1.2 ml, 8.61 mmol, 3 eq.). The product was obtained as an orange solid (1.12 g, 91%). m.p. 109 – 110 °C; ^{1}H NMR δ_H ($CDCl_3$, 400 MHz): 8.85 (1H, d, J = 8.6 Hz, Naph-H), 8.74 (1H, d, J = 7.0 Hz, Naph-H), 8.70 (1H, d, J = 8.0 Hz, Naph-H), 8.42 (1H, d, J = 7.5 Hz, Naph-H), 8.00 (1H, m, Naph-H), 4.60 (1H, br s, NH), 4.20 (2H, t,

J = 7.5 Hz, C$\underline{H}_2$), 3.14 (2H, m, C$\underline{H}_2$), 1.78 (2H, p, J = 7.5 Hz, C$\underline{H}_2$), 1.60 – 1.44 (17H, m, 2C$\underline{H}_2$, 3C$\underline{H}_3$, solvent); ^{13}C NMR δ_C ($CDCl_3$, 100 MHz): 162.9, 162.0, 155.5, 149.1, 132.0, 129.5, 128.6, 127.8, 126.5, 123.5, 123.3, 122.5, 78.6, 40.1, 40.0, 29.2, 28.0, 27.2.

N-(propylammonium)-4-nitro-1,8-naphthalimide trifluoroacetate (49)

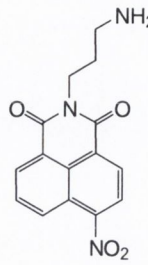

Compound **49** was synthesised according to **Procedure 2** using **47** (0.8 g, 2 mmol, 1 eq.) in TFA/CH_2Cl_2 (10 ml). The product was obtained as an orange oil, which later became an orange solid (0.83 g, 100%). m.p. 120 °C decomp.; ^{1}H NMR δ_H ([D_6]DMSO, 400 MHz): 8.67 (1H, d, J = 8.5 Hz, Naph-$\underline{H}$), 8.61 – 8.51 (3H, m, 3 x Naph-$\underline{H}$), 8.07 (1H, t, J = 8.0 Hz, Naph-$\underline{H}$), 7.85 (3H, br s, N$\underline{H}_3^+$), 4.11 (2H, m, C$\underline{H}_2$), 2.92 (2H, m, C$\underline{H}_2$), 1.98 (2H, m, C$\underline{H}_2$); ^{13}C NMR δ_C ([D_6]DMSO, 100 MHz): 163.3, 162.5, 149.1, 149.0, 131.7, 130.1, 129.6, 128.8, 128.4, 126.7, 124.2, 122.8, 122.7, 37.4, 37.0, 25.8.

N-(pentylammonium)-4-nitro-1,8-naphthalimide trifluoroacetate (50)

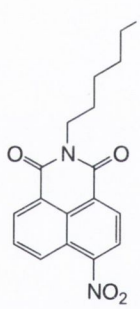

Compound **50** was synthesised according to **Procedure 2** using **48** (1.05 g, 2.46 mmol, 1 eq.). The product was obtained as an orange/brown hygroscopic solid (1.09 g, 100%). ^{1}H NMR δ_H ([D_6]DMSO, 400 MHz): 8.68 (1H, d, J = 8.5 Hz, Naph-$\underline{H}$), 8.56 (3H, m, Naph-$\underline{H}$), 8.07 (1H, dd, J = 8.5, 7.5 Hz, Naph-$\underline{H}$), 7.77 (3H, br s, N$\underline{H}_3^+$), 4.04 (2H, m, C$\underline{H}_2$), 2.80 (2H, m, C$\underline{H}_2$), 1.69 – 1.53 (4H, m, 2C$\underline{H}_2$), 1.38 (2H, m, C$\underline{H}_2$); ^{13}C NMR δ_C ([D_6]DMSO, 100 MHz): 162.9, 162.1, 158.6, 158.2, 149.1, 131.7, 130.1, 129.6, 128.7, 128.3, 126.6, 124.2, 122.7, 51.9, 40.3, 39.2, 26.9, 26.8, 23.3; ES-MS (m/z) 328.13 $(M)^+$; IR ν_{max} (cm^{-1}): 1707 (w, -CO-N-CO-), 1532 (m, C-NO_2), 1342 (m, C-NO_2).

4-[*N*-(propylcarboxamide)-4-nitro-1,8-naphthalimide]-4'-methyl-2,2'-bipyridine (53)

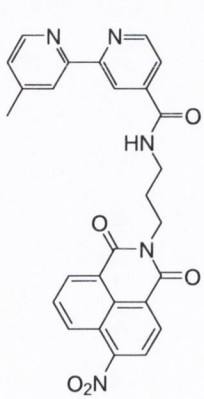

Compound **53** was synthesised according to **Procedure 3** using **49** (0.90 g, 2.18 mmol, 1.1 eq.), Et_3N (0.60 g, 0.83 ml, 5.94 mmol, 3 eq.) and 4-(carbonylchloride)-4'-methyl-2,2'-bipyridine (0.46 g, 1.98 mmol, 1 eq.). After purification by silica flash column chromatography eluting with CH_2Cl_2/MeOH 10% the product was obtained as an orange solid (0.73 g, 74%). Calculated for $C_{27}H_{21}N_5O_5.0.2CH_2Cl_2$: C, 63.75; H, 4.21; N, 13.67. Found C, 63.68; H, 4.10; N, 13.45; Accurate MS (m/z) Calculated

for $C_{27}H_{22}N_5O_5$ (M+H): 496.1621. Found 496.1602; ^{1}H NMR δ_H ($CDCl_3$, 400 MHz): 8.86 (1H, d, J = 8.5 Hz, Ar-H), 8.83 (1H, d, J = 5.0 Hz, Ar-H), 8.80 (1H, s, Ar-H), 8.78 (1H, d, J = 6.5 Hz, Ar-H), 8.74 (1H, d, J = 8.0 Hz, Ar-H), 8.60 (1H, d, J = 5.0 Hz, Ar-H), 8.41 (1H, d, J = 8.0 Hz, Ar-H), 8.30 (1H, s, Ar-H), 8.03 (2H, m, 2 x Ar-H), 8.00 (1H, m, Ar-H), 7.83 (1H, m, Ar-H), 7.53 (1H, br m, NH), 7.23 (1H, d, J = 4.5 Hz, Ar-H), 4.38 (2H, t, J = 6.5 Hz, CH_2), 3.57 (2H, dd, J = 6.0, 12.5 Hz, CH_2), 2.30 (3H, s, CH_3), 2.16 (2H, m, CH_2), ^{13}C NMR δ_C ($CDCl_3$, 100 MHz): 165.0, 163.4, 162.5, 162.1, 156.3, 154.6, 149.6, 149.3, 148.3, 142.3, 132.4, 129.8, 129.5, 129.2, 128.6, 126.1, 124.8, 123.5, 123.2, 122.2, 121.9, 121.2, 117.5, 37.8, 36.6, 27.2, 20.8,; IR ν_{max} (cm^{-1}): 1705 (w, -CO-N-CO-), 1660 (m, -CONH-), 1526 (m, C-NO_2), 1340 (m, C-NO_2).

4-[N-(pentylcarboxamide)-4-nitro-1,8-naphthalimide]-4'-methyl-2,2'-bipyridine (54)

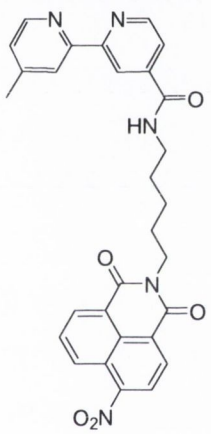

Compound **54** was synthesised according to **Procedure 3** using **50** (0.69 g, 1.56 mmol, 1.1 eq.), 4-(carbonylchloride)-4'-methyl-2,2'-bipyridine (0.33 g, 1.42 mmol, 1 eq.) and Et_3N (0.43 g, 0.60 ml, 4.26 mmol, 3 eq.). After purification by silica flash column chromatography eluting with CH_2Cl_2/MeOH 10% the product was obtained as an orange solid (0.43g, 53%). ^{1}H NMR δ_H ($CDCl_3$, 400 MHz): 8.79 (2H, m, 2 x Ar-H), 8.68 (2H, d, J = 8.6 Hz, Ar-H), 8.62 (1H, d, J = 8.0 Hz, Ar-H), 8.50 (1H, d, J = 5.0 Hz, Ar-H), 8.31 (2H, d, J = 8.5 Hz, Ar-H), 7.92 (1H, m, Ar-H), 7.76 (1H, dd, J = 5.0, 1.52 Hz, Ar-H), 7.21 (1H, d, J = 4.5 Hz, Ar-H), 6.84 (1H, br s, NH), 4.24 (2H, m, CH_2), 3.54 (2H, m, CH_2), 2.50 (3H, s, CH_3), 1.82 (4H, m, $2CH_2$), 1.54 (2H, m, CH_2); ^{13}C NMR δ_C ($CDCl_3$, 100 MHz): 165.2, 163.0, 162.2, 154.3, 149.6, 149.0, 148.4, 148.1, 142.4, 132.0, 129.4, 129.3, 128.8, 128.7, 128.5, 126.4, 124.8, 123.4, 123.1, 122.4, 121.8, 121.6, 117.0, 39.8, 28.4, 27.1, 23.7, 20.8; IR ν_{max} (cm^{-1}): 1666 (s, -CONH-), 1531 (m, C-NO_2), 1344 (m, C-NO_2).

4,4'-bis-{[*N*-propylcarboxamide]-4-nitro-1,8-naphthalimide}-2,2'-bipyridine (57)

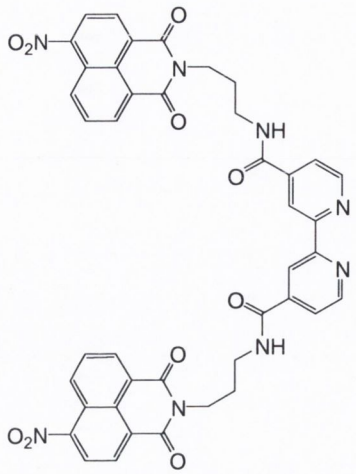

Compound **57** was synthesised according to **Procedure 3** using **49** (0.300 g, 0.73 mmol, 2.1 eq.), Et_3N (0.175 g, 0.24 ml, 1.73 mmol, 5 eq.) and 4,4'-bis(carbonylchloride)-2,2'-bipyridine (0.097 g, 0.35 mmol, 1 eq.). After purification by trituration with MeOH the product was obtained as a brown solid (0.15 g, 55%). m.p. 230 °C; Calculated for $C_{42}H_{30}N_8O_{10}.CH_3OH$: C, 61.57; H, 4.09; N, 13.36. Found: C, 61.57; H, 3.87; N, 13.39; ^{1}H NMR δ_H ([D$_6$]DMSO, 400 MHz): 9.02 (2H, t, J = 5.5 Hz, NH), 8.81 (2H, d, J = 5.0 Hz, Bpy-H$_6$), 8.71 (2H, s, Bpy-H$_3$), 8.67 (2H, d, J = 9.6 Hz, Naph-H), 8.59 (4H, m, 2 x Naph-H), 8.52 (2H, d, J = 8.0 Hz, Naph-H), 8.06 (2H, m, Naph-H), 7.81 (2H, dd, J = 1.5, 5.0 Hz, Bpy-H$_5$), 4.15 (4H, m, CH$_2$), 3.40 (4H, m, CH$_2$), 2.00 (4H, m, CH$_2$); ^{13}C NMR δ_C ([D$_6$]DMSO, 100 MHz): 164.5, 163.0, 162.2, 155.4, 150.0, 149.1, 142.8, 131.7, 130.1, 129.6, 128.7, 128.4, 126.7, 124.2, 122.8, 122.7, 121.8, 118.1, 38.3, 37.5, 27.3; IR ν_{max} (cm^{-1}): 1707 (m, -CO-N-CO-), 1658 (s, -CONH-), 1526 (s, C-NO$_2$), 1347 (s, C-NO$_2$).

4,4'-bis-[(*N*-pentylcarboxamide)-4-nitro-1,8-naphthalimide]-2,2'-bipyridine (58)

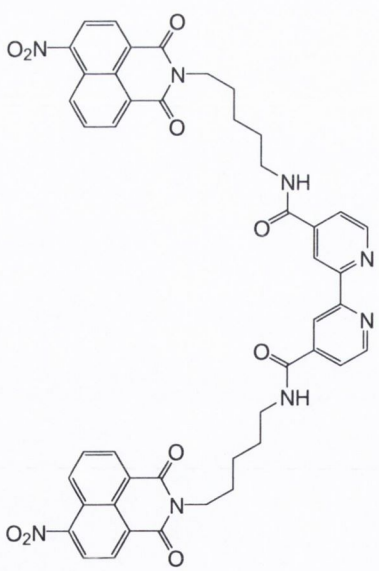

Compound **58** was synthesised according to **Procedure 3** using **50** (0.250 g, 0.565 mmol, 2.1 eq.), 4,4'-bis(carbonylchloride)-2,2'-bipyridine (0.076 g, 0.269 mmol, 1 eq.), and Et_3N (0.136 g, 0.19 ml, 1.345 mmol, 5 eq.). After purification by trituration with MeOH the product was obtained as an orange/brown solid (0.113 g, 49%). Calculated for $C_{46}H_{38}N_8O_{10}.H_20$: C, 62.72; H, 4.58; N, 12.72. Found: C, 63.05; H, 4.60; N, 13.09; ^{1}H NMR δ_H (DMSO[D$_6$], 400 MHz): 8.90 (2H, m, NH), 8.77 (2H, d, J = 5.0 Hz, Bpy-H$_6$), 8.67 (2H, s, Bpy-H$_3$), 8.64 (2H, d, J = 8.6 Hz, Naph-H), 8.56 (4H, m, Naph-H), 8.49 (2H, d, J = 7.5 Hz, Naph-H), 8.03 (2H, m, Naph-H), 7.74 (2H, d, J = 2.5 Hz, Bpy-H$_5$), 4.07 (2H, m, CH$_2$), 3.47 (2H, m, CH$_2$), 1.72 (2H, m, CH$_2$), 1.63 (2H, m, CH$_2$), 1.42 (2H, m, CH$_2$); IR ν_{max} (cm^{-1}): 1706 (m, -CO-N-CO-), 1662 (s, -CONH-), 1527 (s, C-NO$_2$), 1342 (s, C-NO$_2$).

Ru(63)(bpy)$_2$Cl$_2$ (60)

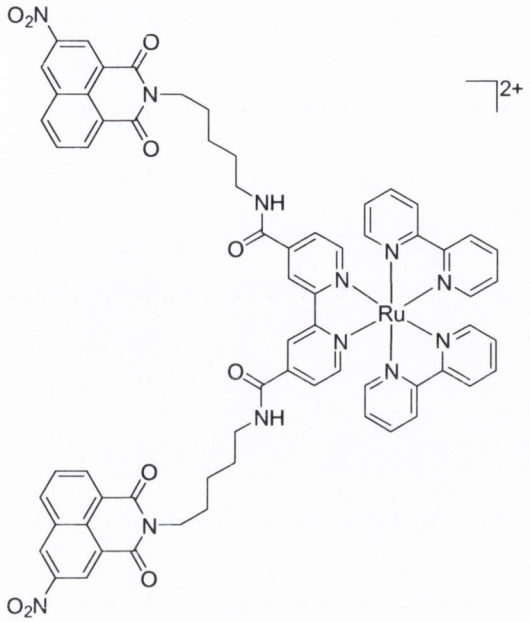

Compound **60** was synthesised according to **Procedure 5** using **63** (0.13 g, 0.15 mmol, 1 eq.) and Ru(bpy)$_2$Cl$_2$.2H$_2$O (0.08 g, 0.15 mmol, 1 eq.). The product was obtained as a red/brown solid (0.093 g, 46%). Accurate MS (m/z) Calculated for $C_{66}H_{54}N_{12}O_{10}Ru$ (M^{2+}): 1276.3129. Found 1276.3110; ^{1}H NMR δ_H (CD_3CN, 400 MHz): 9.09 (1H, d, J = 2.0 Hz, Ar-H), 9.00 (1H, s, Ar-H), 8.88 (1H, d, J = 2.0 Hz, Ar-H), 8.56 (2H, m, Ar-H), 8.53 (1H, d, J = 3.5 Hz, Ar-H), 8.43 (1H, d, J = 8.0 Hz, Ar-H), 8.11 (2H, m, Ar-H), 7.91 (1H, d, J = 6.0 Hz, Ar-H), 7.86 (1H, m, Ar-H), 7.73 (3H, m, Ar-H), 7.63 (1H, br m, NH), 7.46 (1H, m, Ar-H), 7.40 (1H, m, Ar-H), 4.09 (2H, t, J = 7.5 Hz, CH$_2$), 3.45 (2H, m, CH$_2$), 1.74 (4H, m, 2 x CH$_2$), 1.54 (2H, m, CH$_2$), ^{13}C NMR δ_C (CD_3CN, 100 MHz): 164.2, 164.0, 163.4, 158.5, 157.8, 153.2, 152.8, 152.6, 150.3, 143.9, 139.0, 132.6, 130.7, 130.3, 129.7, 129.6, 128.6, 127.8, 126.5, 125.3, 124.9, 124.0, 123.9, 122.7, 41.2, 40.7, 29.5, 28.2, 25.1; IR ν_{max} (cm^{-1}): 1704 (w, -CO-N-CO-), 1660 (s, -CONH-), 1538 (m, C-NO$_2$), 1345 (m, C-NO$_2$).

***N*-[(*tert*-Butoxycarbonyl)-5-aminopentyl]-3-nitro-1,8-naphthalimide (61)**

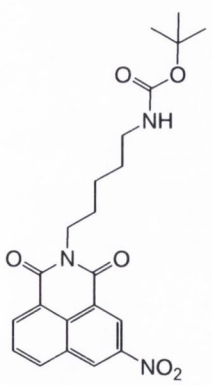

Compound **61** was synthesised according to *procedure 1* using 3-nitro-1,8-naphthalic anhydride (0.14 g, 0.81 mmol, 1 eq.), **45** (0.17 g, 0.89 mmol, 1.1 eq.), and Et$_3$N (0.25 g, 0.34 ml, 2.43 mmol, 3 eq.). After purification by recrystallisation from methanol the product was obtained as an orange solid (0.31 g, 90%). ^{1}H NMR δ_H ($CDCl_3$, 400 MHz): 9.27 (1H, d, J = 2.0 Hz, Ar-H), 9.13 (1H, d, J = 2.0 Hz, Ar-H), 8.77 (1H, dd, J = 1.0, 7.5 Hz, Ar-H), 8.44 (1H ,d, J = 8.0 Hz, Ar-H), 7.95 (1H, m, Ar-H), 4.64 (1H, br s, NH), 4.19 (2H, t, J = 7.5 Hz, CH$_2$), 3.14 (2H, dd, J = 6.5, 12.6 Hz, CH$_2$), 1.77 (2H, pent, J = 7.5 Hz, CH$_2$), 1.58 (2H, m, CH$_2$), 1.50 – 1.42 (11H, m, CH$_2$ + (CH$_3$)$_3$), ^{13}C NMR δ_C ($CDCl_3$, 100 MHz): 162.6, 162.0, 155.5, 145.9, 135.1, 134.0, 130.5, 129.7, 128.7, 128.5, 124.2, 123.7, 122.7, 78.6, 40.1, 40.0, 29.3, 28.0, 27.2, 23.8.

_N_-(pentylammonium)-3-nitro-1,8-naphthalimide trifluoroacetate (62)

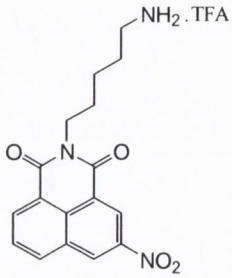

Compound **62** was synthesised according to *procedure 4* using **61** (0.26 g, 0.61 mmol, 1 eq.). The product was obtained as an orange / brown hydroscopic solid (0.26 g, 97%). Accurate MS (m/z) Calculated for $C_{17}H_{18}N_3O_4$ (M+H): 328.1297. Found 328.1295; ^{1}H NMR δ_H (CD_3OD, 400 MHz): 8.95 (1H, d, J = 2.0 Hz, Ar-H), 8.71 (1H, d, J = 2.0 Hz, Ar-H), 8.48 (1H, d, J = 7.0 Hz, Ar-H), 8.35 (1H, d, J = 8.5 Hz, Ar-H), 7.83 (1H, m, Ar-H), 4.04 (2H, m, CH_2), 3.00 (2H, m, CH_2), 1.78 (4H, m, 2 x CH_2), 1.53 (2H, m, CH_2).

4,4'-bis-[(_N_-pentylcarboxamide)-3-nitro-1,8-naphthalimide]-2,2'-bipyridine (63)

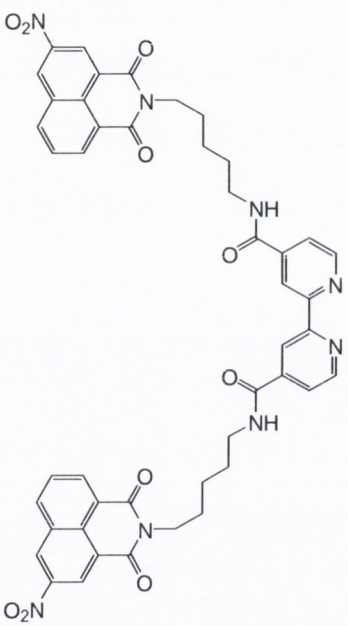

Compound **63** was synthesised according to *procedure 3* using **62** (0.20 g, 0.45 mmol, 2 eq.), 4,4'-bis(carbonylchloride)-2,2'-bipyridine (0.06 g, 0.23 mmol, 1 eq.), and Et_3N (0.12 g, 0.16 ml, 1.15 mmol, 5 eq.). The product was purified by trituration with methanol and was obtained as an orange/brown solid (0.16 g, 80%). Calculated for $C_{46}H_{38}N_8O_{10}$.1.33MeOH: C, 62.78; H, 4.82; N, 12.37. Found: C, 62.43; H, 4.54; N, 12.64; ^{1}H NMR δ_H (DMSO[D_6], 400 MHz): 9.36 (1H, d, J = 2.5 Hz, Ar-H), 8.89 (2H, m, Ar-H), 8.74 (1H, d, J = 5.0 Hz, Ar-H), 8.68 (1H, d, J = 8.6 Hz, Ar-H), 8.63 (2H, m, 2 x Ar-H), 7.99 (1H, m, Ar-H), 7.73 (1H, d, J = 5.0 Hz, Ar-H), 4.09 (2H, t, J = 7.0 Hz, CH_2), peak under solvent, 1.72 (2H, m, CH_2), 1.63 (2H, m, CH_2), 1.43 (2H, m, CH_2); IR ν_{max} (cm^{-1}): 1707 (w, -CO-N-CO-), 1662 (m, -CONH-), 1536 (m, C-NO_2), 1347 (m, C-NO_2).

4,4'-bis(propylcarboxamide)-2,2'-bipyridine (64)

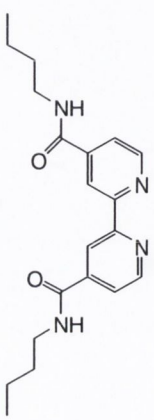

Compound **64** was synthesised according to **Procedure 3** using propylamine (0.095 g, 1.30 mmol, 2 eq.), Et_3N (0.329 g, 0.45 ml, 3.25 mmol, 5 eq.) and 4,4'-bis(carbonylchloride)-2,2'-bipyridine (0.183 g, 0.65 mmol, 1 eq.). The product was obtained as a white solid (0.139 g, 60%). m.p. >250 °C decomp.; Calculated for $C_{20}H_{26}N_4O_2$: C, 67.77; H, 7.39; N, 15.81. Found: C, 67.48; H, 7.41; N, 15.64; ^{1}H NMR δ_H ([D_6]DMSO, 400 MHz): 8.94 (1H, m, NH), 8.87 (1H, d, J = 5.0 Hz, Bpy-H_6), 8.78 (1H, s, Bpy-H_3), 7.85 (1H, dd, J

= 5.0, 1.5 Hz, Bpy-H5), 3.31 (2H, m, CH2), 1.55 (2H, m, CH2), 1.35 (2H, m, CH2), 0.92 (3H, m, CH3); ^{13}C NMR δ_C ([D6]DMSO, 100 MHz): 164.5, 155.5, 150.0, 143.1, 121.9, 118.2, 39.1, 31.0, 19.6, 13.7; IR ν_{max} (cm^{-1}): 1632 (s, -CONH-).

7.5 Synthesis and Characterisation of Compounds Described in Chapter 3

Ru(73)(bpy)$_2$Cl$_2$ (68)

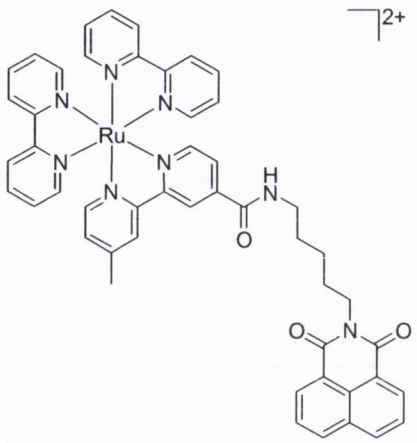

Compound **68** was synthesised according to **Procedure 4** using **73** (0.09 g, 0.19 mmol, 1 eq.) and Ru(bpy)$_2$Cl$_2$.2H$_2$O (0.12 g, 0.23 mmol, 1.2 eq.) giving the product as a red/brown solid (0.16 g, 86%). Calculated for $C_{49}H_{42}F_{12}N_8O_3P_2Ru.CH_3CN$: C, 50.09; H, 3.71; N, 10.31. Found: C, 50.38; H, 3.43; N, 10.39; Accurate MS (m/z) Calculated for $C_{49}H_{42}N_8O_3Ru$ (M^{2+}): 892.2423. Found 892.2420; ^{1}H NMR δ_H (CD_3CN, 400 MHz): 8.90 (1H, d, *J* = 1.5 Hz, Ar-H), 8.60 (1H, s, Ar-H), 8.51 (6H, m, Ar-H), 8.34 (2H, d, *J* = 7.5 Hz, Ar-H), 8.11 – 8.05 (4H, m, Ar-H), 7.82 (2H, m, Ar-H), 7.79 – 7.73 (6H, m, Ar-H + NH), 7.63 (1H, dd, *J* = 1.5, 6.0 Hz, Ar-H), 7.57 (2H, d, *J* = 6.0 Hz, Ar-H), 7.44 – 7.37 (4H, m, Ar-H), 7.29 (1H, d, *J* = 5.5 Hz, Ar-H), 4.13 (2H, t, *J* = 7.5 Hz, CH2), 3.43 (2H, m, CH2), 2.56 (3H, s, CH3), 1.80 – 1.68 (4H, m, 2CH2), 1.49 (2H, m, CH2); ^{13}C NMR δ_C (CD_3CN, 150 MHz): 163.9, 162.9, 157.8, 156.9, 156.84, 156.80, 156.7, 156.0, 152.1, 151.6, 151.5, 151.4, 150.6, 142.7, 137.7, 133.9, 131.6, 130.5, 128.5, 127.9, 127.5, 126.9, 125.5, 124.4, 124.2, 124.1, 122.7, 121.5, 39.7, 39.6, 28.5, 27.3, 24.0, 20.1; IR ν_{max} (cm^{-1}): 1698 (m, -CO-N-CO-), 1658 (m, -CONH-).

Ru(74)(bpy)$_2$Cl$_2$ (69)

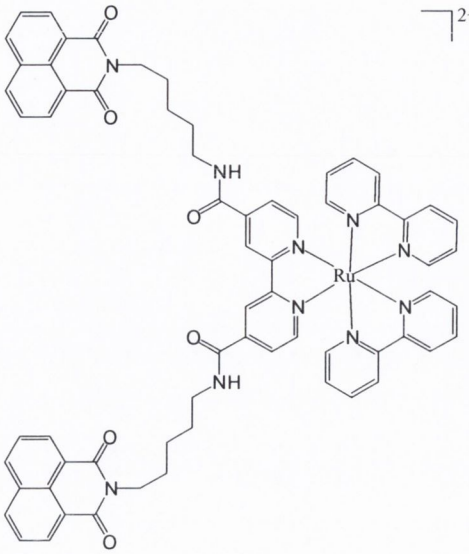

Compound **69** was synthesised according to **Procedure 4** using **74** (0.115 g, 0.15 mmol, 1 eq.) and Ru(bpy)$_2$Cl$_2$.2H$_2$O (0.085 g, 0.16 mmol, 1.1 eq.) giving the product as a red/brown solid (0.142 g, 76%). Calculated for $C_{66}H_{56}F_{12}N_{10}O_6P_2Ru.3H_2O$: C, 51.80; H, 4.08; N, 9.15. Found: C, 51.94; H, 3.81; N, 8.92; Accurate MS (m/z) Calculated for $C_{66}H_{56}N_{10}O_6Ru$ (M^{2+}): 1186.3428. Found 1186.3412; ^{1}H NMR δ_H (CD_3OD, 400 MHz): 9.34 (1H, s, Ar-H), 8.76 (2H, dd, J = 3.0, 8.0 Hz, 2Ar-H), 8.33 (2H, d, J = 7.0 Hz, 2 x Ar-H), 8.18 (4H, m, 4Ar-H), 8.02 (1H, d, J = 5.5 Hz, Ar-H), 7.86 (3H, m, 3Ar-H), 7.64 (2H, m, 2Ar-H), 7.54 (2H, pent, J = 6.5 Hz, 2Ar-H), 4.06 (2H, t, J = 7.6 Hz, CH_2), 3.45 (2H, m, CH_2), 1.73 (4H, m, 2CH_2), 1.49 (2H, m, CH_2); ^{13}C NMR δ_C (CD_3OD, 100 MHz): 164.4, 158.0, 157.4, 152.4, 151.8, 151.6, 143.2, 138.6, 134.4, 131.9, 130.9, 128.1, 128.0, 127.0, 125.8, 124.8, 122.5, 122.4, 40.2, 40.1, 28.9, 27.7, 24.5; IR ν_{max} (cm^{-1}): 1695 (m, -CO-N-CO-), 1652 (s, -CONH-).

***N*-[(*tert*-Butoxycarbonyl)-5-aminopentyl]-1,8-naphthalmide (71)**

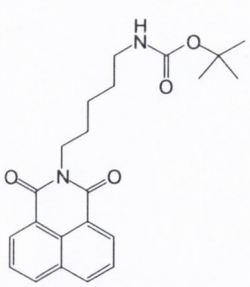

Compound **71** was synthesised according to **Procedure 1** using 1,8-naphthalic anhydride (0.80 g, 4.04 mmol, 1 eq.), **45** (0.90 g, 4.45 mmol, 1.1 eq.), and Et_3N (1.23 g, 1.69 ml, 12.12 mmol, 3 eq.). The product was obtained as an orange oily solid without need for further purification (0.57 g, 82%). Accurate MS (m/s) Calculated for $C_{22}H_{26}N_2O_4Na$ (M+Na): 405.1790. Found 405.1809; ^{1}H NMR δ_H (DMSO[D_6], 400 MHz): 8.53 (2H, d, *J* = 7.6 Hz, Naph-H), 8.49 (2H, d, *J* = 8.5 Hz, Naph-H), 7.91 (2H, m, Naph-H), 6.82 (1H, s, NH), 4.07 (2H, t, *J* = 7.0 Hz, CH_2), 2.94 (2H, d, *J* = 6.0 Hz, CH_2), 1.65 (2H, m, CH_2), 1.45 – 1.36 (13H, m, 2CH_2 + C(CH_3)$_3$); ^{13}C NMR δ_C (DMSO[D_6], 100 MHz): 163.4, 155.6, 134.3, 131.3, 130.7, 127.4, 127.2, 122.1, 77.3, 54.9, 50.8, 29.2, 28.2, 27.3, 23.8; IR ν_{max} (cm^{-1}): 1698 (m, -CO-N-CO-), 1656 (s, -CONH-).

_N_-(pentylammonium)-1,8-naphthalimide trifluoroacetate (72)

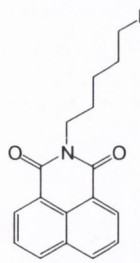

Compound **72** was synthesised according to **Procedure 2** using **71** (0.88 g, 2.29 mmol, 1 eq.). The product was obtained as a pale brown solid (0.90 g, 99%). m.p 151 – 152 °C; Accurate MS (m/z) Calculated for $C_{17}H_{19}N_2O_2$ (M^+): 283.1447. Found 283.1456; ^{1}H NMR δ_H (CD_3OD, 400 MHz): 8.30 (2H, d, J = 7.6 Hz, Naph-H), 8.11 (2H, d, J = 8.0 Hz, Naph-H), 7.62 (2H, t, J = 7.5 Hz, Naph-H), 4.04 (2H, m, CH_2), 2.97 (2H, m, CH_2), 1.74 (4H, m, 2 x CH_2), 1.48 (2H, m, CH_2), ^{13}C NMR δ_C (CD_3OD, 100 MHz): 163.8, 133.8, 313.2 130.3, 127.2, 126.3, 121.5, 39.0, 38.8, 26.6, 26.3, 23.0; IR ν_{max} (cm^{-1}): 3179 (w, -NH_2), 1694 (m, -CO-N-CO-).

4-[N-(pentylcarboxamide)-1,8-naphthalimide]-4'-methyl-2,2'-bipyridine (73)

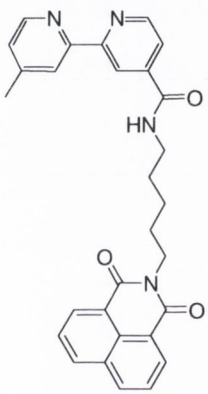

Compound **73** was synthesised according to **Procedure 3** using **72** (0.15 g, 0.38 mmol, 1.1 eq.), **52** (0.08 g, 0.34 mmol, 1 eq.) and Et_3N (0.10 g, 0.14 ml, 1.02 mmol, 3 eq.). After purification by silica column chromatography eluting with CH_2Cl_2/MeOH 10% the product was obtained as a pale brown solid (0.14 g, 83%). m.p. 162 – 164 °C; Calculated for $C_{29}H_{26}N_4O_3.0.25CH_2Cl_2$: C, 70.29; H, 5.34; N, 11.21. Found: C, 70.62; H, 5.48; N, 10.84; ^{1}H NMR δ_H (DMSO[D_6], 400 MHz): 8.90 (1H, m, NH), 8.76 (1H, d, J = 5.0 Hz, Bpy-H), 8.71 (1H, s, Bpy-H), 8.57 (1H, d, J = 5.0 Hz, Bpy-H), 8.48 (2H, d, J = 7.0 Hz, Naph-H), 8.44 (2H, d, J = 8.0 Hz, Naph-H), 8.26 (1H, s, Bpy-H), 7.85 (2H, m, Naph-H), 7.73 (1H, dd, J = 1.5, 5.0 Hz, Bpy-H), 7.33 (1H, d, J = 4.5 Hz, Bpy-H), 4.07 (2H, t, J = 7.6 Hz, CH_2), 3.29 (2H, m, CH_2), 2.44 (3H, s, CH_3), 1.71 (2H, m, CH_2), 1.63 (2H, m, CH_2), 1.41 (2H, m, CH_2); IR ν_{max} (cm^{-1}): 1698 (m, -CO-N-CO-), 1658 (s, -CONH-).

4,4'-bis-[(*N*-pentylcarboxamide)-1,8-naphthalimide]-2,2'-bipyridine (3)

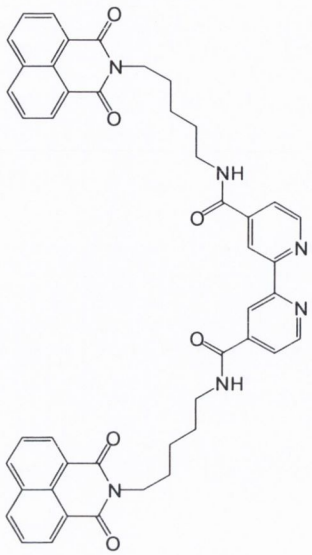

Compound **74** was synthesised according to **Procedure 3** using **72** (0.40 g, 1.01 mmol, 2.1 eq.), 4,4'-bis(carbonylchloride)-2,2'-bipyridine (0.14 g, 0.48 mmol, 1 eq.) and Et_3N (0.24 g, 0.33 ml, 2.40 mmol, 5 eq.) added. After purification by trituration with MeOH the product was obtained as a purple solid (0.35 g, 95%). m.p. 210 – 211 °C; Calculated for $C_{46}H_{40}N_6O_6$ .0.33CH_2Cl_2.0.33DMF: C, 68.87; H, 5.25; N, 10.75. Found: C, 68.60; H, 5.16; N, 11.01; Accurate MS (m/z) Calculated for $C_{46}H_{40}N_6O_6Na$ (M+Na): 795.2907. Found 795.2898; ^{1}H NMR δ_H (DMSO[D_6], 400 MHz): 8.97 (1H, br s, NH), 8.80 (1H, m, Bpy-H), 8.75 (1H, m, Bpy-H), 8.46 (2H, d, J = 7.0 Hz, Naph-H), 8.42 (2H, d, J = 8.0 Hz, Naph-H), 7.83 (2H, m, Naph-H), 7.77 (1H, m, Bpy-H), 4.06 (2H, m, CH_2), ~3.30 (CH_2, under solvent peak – from CH COSY), 1.69 (2H, m, CH_2), 1.63 (2H, m, CH_2), 1.41 (2H, m, CH_2); ^{13}C NMR δ_C (DMSO[D_6], 150 MHz): 164.8, 163.7, 155.8, 150.2, 143.3, 134.5, 131.6, 131.0, 127.7, 127.5, 122.4, 122.2, 118.5, 40.1, 39.7, 28.9, 27.6, 24.3; IR ν_{max} (cm^{-1}): 1698 (w, -CO-N-CO-), 1658 (m, -CONH-).

7.6 Synthesis and Characterisation of Compounds Described in Chapter 4

Ru(4-[*N*-(p-phenyl)-4-nitro-1,8-naphthalimide]-2,2'-bipyridine)(bipyridine)$_2$$Cl_2$ (76)

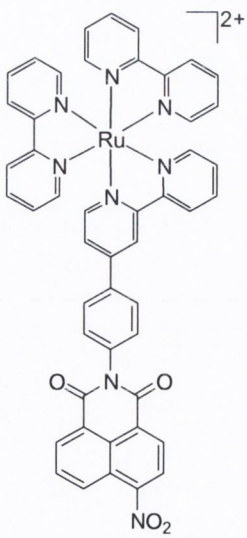

Compound **76** was synthesised according to **Procedure 4** using **88** (0.12 g, 0.25 mmol, 1 eq.) and and Ru(bpy)$_2$$Cl_2$.2$H_2O$ (0.13 g, 0.25 mmol, 1 eq.) giving the product as a red/brown solid (0.16 g, 69%). Calculated for $C_{48}H_{32}F_{12}N_8O_4P_2Ru$.1.33EtOH: C, 49.19; H, 3.26; N, 9.06. Found: C, 49.43; H, 2.92; N, 8.66; Accurate MS (m/z) Calculated for $C_{48}H_{32}N_8O_4Ru$ (M^{2+}): 886.1590. Found 886.1572; ^{1}H NMR δ_H (CD_3CN, 400 MHz): 8.91 (1H, s, Ar-H), 8.87 (1H, d, J = 8.6 Hz, Ar-H), 8.79 (1H, d, J = 8.3 Hz, Ar-H), 8.73 (1H, d, J = 7.1 Hz, Ar-H), 8.69 (1H, d, J = 7.9 Hz, Ar-H), 8.60 (4H, m, 4 x Ar-H), 8.51 (1H, d, J = 7.9 Hz, Ar-H), 8.11 (8H, m, 8 x Ar-H), 7.85 (3H, m, 3 x Ar-H), 7.81 (3H, m, 3 x Ar-H), 7.77 (1H, d, J = 4.9 Hz, Ar-H), 7.63 (2H, d, J = 8.3 Hz, Ar-H), 7.46 (5H, m, 5 x Ar-H); ^{13}C NMR δ_C (CD_3CN, 150 MHz): 163.6, 162.8, 157.4, 157.0, 156.9, 156.8, 151.7, 151.6, 151.5, 151.4, 149.8, 148.6, 137.7, 137.6, 137.5, 136.2, 132.3,

132.0, 129.9, 129.8, 129.7, 129.4, 129.2, 128.3, 127.6, 127.5, 127.4, 127.2, 125.0, 124.4, 124.3, 124.2, 124.1, 123.4, 123.3, 122.2; IR ν_{max} (cm^{-1}): 1716 (m, -CO-N-CO-), 1521 (m, C-NO_2), 1348 (m, C-NO_2).

Ru(4-[N-(m-phenyl)-4-nitro-1,8-naphthalimide]-2,2'-bipyridine)(bipyridine)$_2$Cl$_2$ (77)

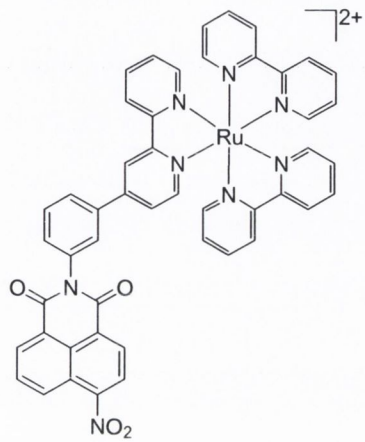

Compound **77** was synthesised according to **Procedure 4** using **89** (0.29 g, 0.62 mmol, 1 eq.) and and $Ru(bpy)_2Cl_2.2H_2O$ (0.32 g, 0.62 mmol, 1 eq.) giving the product as a red/brown solid (0.45 g, 75%). Calculated for $C_{48}H_{32}F_{12}N_8O_4P_2Ru$: C, 49.03; H, 2.74; N, 9.53. Found: C, 48.87; H, 2.90; N, 9.25; Accurate MS (m/z) Calculated for $C_{48}H_{32}N_8O_4Ru$ (M^{2+}): 886.1590. Found 886.1614; ^{1}H NMR δ_H (CD_3CN, 600 MHz): 8.87 (1H, dd, J = 1.0, 8.8 Hz, Ar-H), 8.83 (1H, d, J = 1.9 Hz, Ar-H), 8.73 (1H, dd, J = 0.9, 7.3 Hz, Ar-H), 8.72 (1H, d, J = 8.2 Hz, Ar-H), 8.70 (1H, d, J = 8.0 Hz, Ar-H), 8.57 (1H, d, J = 3.4 Hz, Ar-H), 8.56 (3H, m, 3 x Ar-H), 8.51 (1H, d, J = 7.9 Hz, Ar-H), 8.13 – 8.05 (7H, m, 7 x Ar-H), 7.95 (1H, t, J = 1.9 Hz, Ar-H), 7.84 – 7.77 (7H, m, 7 x Ar-H), 7.69 (1H, dd, J = 2.0, 6.1 Hz, Ar-H), 7.60 (1H, m, Ar-H), 7.46 – 7.42 (7H, m, 7 x Ar-H); ^{13}C NMR δ_C (CD_3CN, 150 MHz): 164.7, 163.9, 158.6, 158.0, 152.8, 152.70, 152.67, 152.6, 151.0, 149.3, 138.8, 138.7, 138.0, 137.9, 133.1, 131.8, 131.5, 131.0, 130.9, 130.5, 130.3, 128.9, 128.7, 128.6, 128.5, 128.2, 125.7, 125.6, 125.3, 125.2, 124.6, 124.3, 122.9; IR ν_{max} (cm^{-1}): 1715 (w, -CO-N-CO), 1528 (m, C-NO_2), 1349 (m, C-NO_2).

Ru(4-[*N*-(p-phenyl)-4-amino-1,8-naphthalimide]-2,2'-bipyridine)(bipyridine)$_2$Cl$_2$ (78)

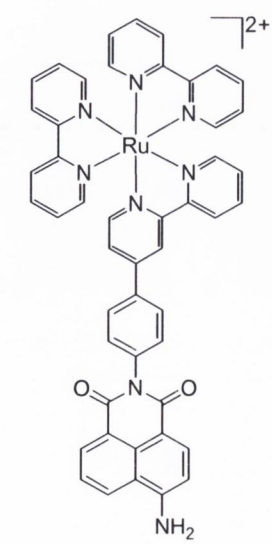

Compound **78** was synthesised according to **Procedure 5** using **76** (0.075 g, 0.078 mmol, 1 eq.) giving the product as an orange solid (0.07 g, 98%). Calculated for $C_{48}H_{34}F_{12}N_8O_2P_2Ru.2CH_3CN.EtOH$ C, 50.91; H, 3.64; N, 10.99. Found C, 51.11; H, 3.33; N, 10.76; Accurate MS (m/z) Calculated for $C_{48}H_{34}N_8O_2Ru$ (M^{2+}): 856.1848. Found 856.1822; ^{1}H NMR δ_H (CD_3CN, 400 MHz): 8.90 (1H, s, Ar-H), 8.78 (1H, d, J = 8.0 Hz, Ar-H), 8.57 (5H, m, 5 x Ar-H), 8.51 (1H, d, J = 8.6 Hz, Ar-H), 8.32 (1H, d, J = 8.0 Hz, Ar-H), 8.10 (5H, m, 5 x Ar-H), 8.05 (2H, d, J = 8.5 Hz, 2 x Ar-H), 7.78 (8H, m, 8 x Ar-H), 7.57 (2H, d, J = 8.6 Hz, 2 x Ar-H), 7.46 (5H, m, 5 x Ar-H),

7.00 (1H, d, J = 8.6 Hz, Ar-H), 6.24 (2H, s, NH_2); ^{13}C NMR δ_C (CD_3CN, 150 MHz): 165.6, 164.8, 158.4, 158.1, 158.0, 157.9, 152.9, 152.8, 152.7, 152.6, 152.5, 150.0, 140.2, 138.8, 138.7, 136.5, 134.9, 132.2, 131.4, 131.3, 129.7, 129.1, 128.6, 128.5, 126.0, 125.6, 125.5, 125.3, 124.0, 123.2, 121.0, 117.5, 111.0, 109.7; IR ν_{max} (cm^{-1}): 1684 (w, -CO-N-CO-), 1635 (m, NH_2).

Ru(4-[N-(m-phenyl)-4-amino-1,8-naphthalimide]-2,2'-bipyridine)(bipyridine)$_2$Cl$_2$ (79)

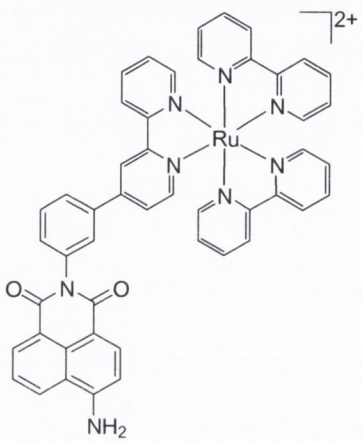

Compound **79** was synthesised according to **Procedure 5** using **77** (0.14 g, 0.12 mmol, 1 eq.) giving the product as an orange solid (0.13 g, 98%). Calculated for $C_{48}H_{34}F_{12}N_8O_2P_2Ru.2.5CH_3CN$: C, 50.99; H, 3.35; N, 11.78. Found: C, 51.14; H, 3.65; N, 11.54; Accurate MS (m/z) Calculated for $C_{48}H_{43}N_8O_2Ru$ (M^{2+}): 856.1848. Found 856.1818; ^1H NMR δ_H (CD_3CN, 600 MHz): 8.71 (1H, s, Ar-H), 8.54 (6H, m, 6 x Ar-H), 8.35 (1H, d, J = 7.1 Hz, Ar-H), 8.23 (1H, d, J = 8.3 Hz, Ar-H), 8.09 (6H, m, 6 x Ar-H), 7.97 (1H, t, J = 7.9 Hz, Ar-H), 7.80 (1H, d, J = 4.9 Hz, Ar-H), 7.75 (5H, m, 5 x Ar-H), 7.66 (1H, d, J = 6.0 Hz, Ar-H), 7.63 (1H, d, J = 7.6 Hz, Ar-H), 7.54 (1H, t, J = 7.6 Hz, Ar-H), 7.50 – 7.38 (7H, m, 7 x Ar-H), 6.70 (1H, br d, J = 6.8 Hz, NH_2); ^{13}C NMR δ_C (CH_3CN, 150 MHz): 164.6, 163.9, 157.4, 156.9, 156.8, 156.78, 156.77, 151.8, 151.6, 151.5, 151.4, 151.3, 147.4, 138.2, 137.8, 137.7, 137.6, 135.8, 133.6, 131.3, 131.1, 129.9, 128.6, 128.2, 127.5, 127.49, 127.48, 126.1, 124.5, 124.3, 124.2, 124.1, 123.9, 122.0, 121.1, 119.4, 109.1, 108.5; IR ν_{max} (cm^{-1}): 3354 (w, -NH_2), 1684 (m, -CO-N-CO-), 1634 (s, -NH_2).

(*E*)-4-(4-nitrophenyl)-2-oxo-3-butenoic acid (82)

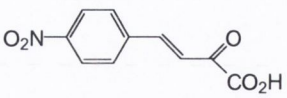

Compound **82** was synthesised according to **Procedure 6** using 4-nitrobenzaldehyde (2.0 g, 13.2 mmol, 1 eq.) and sodium pyruvate (1.5 g, 13.6 mmol, 1.03 eq.) giving the product as a yellow solid (1.58 g, 54%). m.p. 94 – 95 °C (lit. 95 °C); ^1H NMR δ_H ([D_6]DMSO, 400 MHz): 8.24 (2H, d, J = 8.5 Hz, Ar-H), 7.96 (2H, d, J = 8.52 Hz, Ar-H), 7.53 (1H, d, J = 16.6 Hz, CH), 7.01 (1H, d, J = 16.6 Hz, CH); ^{13}C NMR δ_C ([D_6]DMSO, 100 MHz): 196.8, 168.4, 147.8, 141.5, 140.2, 129.1, 129.0, 124.4.

(*E*)-4-(3-nitrophenyl)-2-oxo-3-butenoic acid (83)

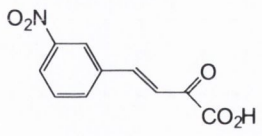

Compound **83** was synthesised according to **Procedure 6** using 3-nitrobenzaldehyde (7.7 g, 51.1 mmol, 1 eq.) and sodium pyruvate (6.2 g, 56.2 mmol, 1.1 eq.) giving the product as a yellow solid (7.11 g, 63%). m.p. 250 °C decomposition; ^{1}H NMR δ_H (DMSO[D_6], 400 MHz): 8.45 (1H, s, Ar-H), 8.22 (1H, dd, J = 2.0, 8.0 Hz, Ar-H), 8.16 (1H, d, J = 8.0 Hz, Ar-H), 7.70 (1H, t, J = 8.0 Hz, Ar-H), 7.62 (1H, d, J = 16.6 Hz, CH), 7.14 (1H, d, J = 16.6 Hz, CH); ^{13}C NMR δ_C (DMSO[D_6], 100 MHz): 196.1, 168.5, 148.3, 140.9, 136.6, 134.1, 130.4, 127.2, 124.4, 122.6; IR ν_{max} (cm^{-1}): 1683 (w, -CO-), 1536 (m, C-NO_2), 1348 (m, C-NO_2).

4-(4-nitrophenyl)-2,2'-bipyridine (84)

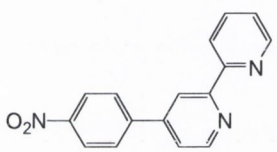

Compound **84** was synthesized according to **Procedure 7** using **82** (1.27 g, 5.75 mmol, 1 eq.), 2-pyridacyl pyridinium iodide (1.89 g, 5.75 mmol, 1 eq.), and ammonium acetate (3.55 g, 46.00 mmol, 8 eq.) giving the product as a pale yellow solid (0.98 g, 87%). m.p. 156 °C; Accurate MS (m/z) Calculated for $C_{16}H_{11}N_3O_2$ (M+H): 277.0851. Found 278.0932; ^{1}H NMR δ_H ($CDCl_3$, 400 MHz): 8.83 (1H, d, J = 5.0 Hz, Bpy-H), 8.75 (2H, m, Bpy-H), 8.52 (1H, d, J = 8.0 Hz, Bpy-H), 8.39 (2H, m, Ar-H), 7.96 (2H, m, Ar-H), 7.91 (1H, m, Bpy-H), 7.59 (1H, m, Bpy-H), 7.40 (1H, m, Bpy-H); ^{13}C NMR δ_C ($CDCl_3$, 100 MHz): 156.7, 155.1, 149.6, 148.8, 147.7, 146.5, 144.3, 136.7, 127.7, 123.9, 123.8, 121.2, 120.9, 118.7.

4-(3-nitrophenyl)-2,2'-bipyridine (85)

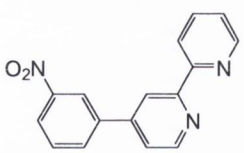

Compound **85** was synthesised according to **Procedure 7** using **83** (2.13 g, 9.64 mmol, 1 eq.), 2-pyridacyl pyridinium iodide (3.14 g, 9.64 mmol, 1 eq.), and ammonium acetate (5.95 g, 77.12 mmol, 8 eq.) giving the product as a pale yellow solid (0.92 g, 37%). m.p. 107 – 109 °C; Accurate MS (m/z) Calculated for $C_{16}H_{12}N_3O_2$ (M+H): 278.0930. Found 278.0925; ^{1}H NMR δ_H ($CDCl_3$, 400 MHz): 8.78 (1H, d, J = 5.2 Hz, Ar-H), 8.71 (2H, m, 2 x Ar-H), 8.59 (1H, m, Ar-H), 8.47 (1H, d, J = 7.6 Hz, Ar-H), 8.29 (1H, dd, J = 1.2, 8.2 Hz, Ar-H), 7.86 (1H, dt, J = 1.8, 8.2 Hz, Ar-H), 7.68 (1H, t, J = 7.6 Hz, Ar-H), 7.56 (1H, dd, J = 1.7, 5.3 Hz, Ar-H), 7.36 (1H, m, Ar-H); ^{13}C NMR δ_C ($CDCl_3$, 100 MHz): 156.6, 155.1, 149.6, 148.8, 148.3, 146.3, 139.6, 136.6, 132.6, 129.7, 123.7, 121.6, 121.0, 120.9, 118.4; IR ν_{max} (cm^{-1}): 1525 (s, C-NO_2), 1343 (s, C-NO_2).

4-(4-aminophenyl)-2,2'-bipyridine (86)

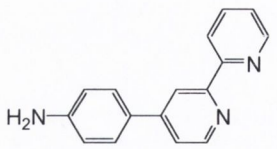

Compound **86** was synthesised according to **Procedure 8** using **84** (0.95 g, 3.51 mmol, 1 eq.) and hydrazine monohydrate (98%) (2.19 g, 2.12 ml 68.23 mmol, 20 eq.) giving the product as an off white solid (0.73 g, 86%). Accurate MS (m/z) Calculated for $C_{16}H_{14}H_3$ (M+H): 248.1188. Found 248.1191; ^{1}H NMR δ_H ($CDCl_3$, 400 MHz): 8.74 (1H, d, J = 4.0 Hz, Bpy-H), 8.68 (1H, d, J = 5.2 Hz, Bpy-H), 8.64 (1H, d, J = 1.8 Hz, Bpy-H), 8.48 (1H, d, J = 7.6 Hz, Bpy-H), 7.86 (1H, dt, J = 1.8, 7.6 Hz, Bpy-H), 7.66 (2H, d, J = 8.8 Hz, Ar-H), 7.53 (1H, m, Bpy-H), 7.35 (1H, dd, J = 7.0, 4.6 Hz, Bpy-H), 6.80 (2H, d, J = 8.2 Hz, Ar-H); ^{13}C NMR δ_C ($CDCl_3$, 100 MHz): 156.3, 149.4, 149.1, 149.0, 148.9, 147.6, 136.8, 128.1, 127.7, 123.6, 121.2, 120.5, 117.8, 115.2.

4-(3-aminophenyl)-2,2'-bipyridine (87)

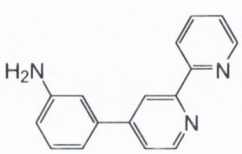

Compound **87** was synthesised according to **Procedure 8** using **85** (0.87 g, 3.14 mmol, 1 eq.) and hydrazine monohydrate (98%) (2.01 g, 1.95 ml, 62.75 mmol, 20 eq.) giving the product as an off white solid (0.75 g, 97%). m.p. 131 – 133 °C; Accurate MS (m/z) Calculated for $C_{16}H_{14}N_3$ (M+H): 248.1188. Found 248.1193; ^{1}H NMR δ_H ($CDCl_3$, 400 MHz): 8.70 (1H, d, J = 3.5 Hz, Ar-H), 8.67 (1H, d, J = 15.1 Hz, Ar-H), 8.46 (1H, d, J = 8.0 Hz, Ar-H), 7.82 (1H, m, Ar-H), 7.48 (1H, dd, J = 1.5, 5.0 Hz, Ar-H), 7.31 (1H, m, Ar-H), 7.25 (1H, m, Ar-H), 7.13 (1H, d, J = 7.5 Hz, Ar-H), 7.05 (1H, d, J = 2.0 Hz, Ar-H), 6.74 (1H, dd, J = 1.5, 8.0 Hz, Ar-H), 3.89 (2H, br s, NH_2); ^{13}C NMR δ_C ($CDCl_3$, 100 MHz): 156.0, 155.7, 149.1, 148.7, 146.7, 138.9, 136.5, 129.5, 123.4, 121.2, 120.8, 118.5, 116.9, 115.3, 113.1; IR ν_{max} (cm^{-1}): 3422 (w, -NH_2 stretch), 1626 (w, -NH_2 bending).

4-[*N*-(p-phenyl)-4-nitro-1,8-napthalimide]-2,2'-bipyridine (88)

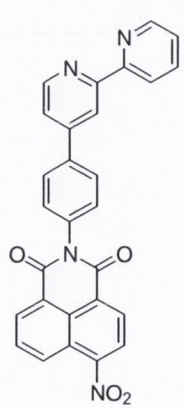

Compound **88** was synthesised according to **Procedure 9** using **86** (0.48 g, 1.95 mmol, 1 eq.) and 4-nitro-1,8-naphthalic anhydride (0.47 g, 1.95 mmol, 1 eq.) giving the product as a pale yellow solid (0.77 g, 84%). m.p. 199 – 200 °C; Calculated for $C_{28}H_{16}N_4O_4.H_2O$: C, 68.57; H, 3.70; N, 11.42. Found: C, 68.75; H, 3.37; N, 11.16; Accurate MS (m/z) Calculated for $C_{28}H_{17}N_4O_4$ (M+H): 473.1250. Found 473.1250; ^{1}H NMR δ_H ([D_6]DMSO, 400 MHz): 8.82 (1H, d, J = 5.0 Hz, Ar-H), 8.78 (1H, d, J = 8.5 Hz, Ar-H), 8.76 (2H, m, 2 x Ar-H), 8.69 (1H, d, J = 7.5 Hz, Ar-H), 8.66 (1H, d, J = 8.0

Hz, Ar-H), 8.61 (1H, d, J = 8.0 Hz, Ar-H), 8.48 (1H, d, J = 8.0 Hz, Ar-H), 8.16 (1H, m, Ar-H), 8.07 (2H, d, J = 8.6 Hz, Ar-H), 8.01 (1H, dt, J = 1.5, 7.5 Hz, Ar-H), 7.90 (1H, dd, J = 1.5, 5.0 Hz, Ar-H), 7.52 (1H, m, Ar-H); ^{13}C NMR δ_C ([D_6]DMSO, 100 MHz): 163.3, 162.5, 155.7, 154.7, 150.0, 149.3, 149.2, 147.9, 137.7, 137.4, 136.7, 131.8, 130.2, 130.0, 129.7, 129.0, 128.8, 127.6, 127.3, 124.6, 124.3, 123.4, 122.9, 121.9, 120.9, 117.9; IR ν_{max} (cm^{-1}): 1714 (w, -CO-N-CO-), 1520 (w, C-NO_2), 1346 (w, C-NO_2).

4-[*N*-(m-phenyl)-4-nitro-1,8-napthalimide]-2,2'-bipyridine (89)

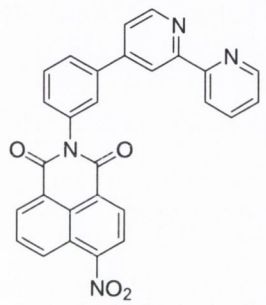

Compound **89** was synthesised according to **Procedure 9** using **87** (0.50 g, 2.04 mmol, 1 eq.) and 4-nitro-1,8-naphthalic anhydride (0.50 g, 2.04 mmol, 1 eq.) giving the product as a pale brown solid (0.81 g, 84%). Calculated for $C_{28}H_{16}N_4O_4.0.4H_2O$: C, 70.11; H, 3.53; N, 11.68. Found: C, 70.27; H, 3.35; N, 11.40; Accurate MS (m/z) Calculated for $C_{28}H_{17}N_4O_4$ (M+H): 473.1250. Found 473.1268; ^1H NMR δ_H ($CDCl_3$, 400 MHz): 8.81 (1H, s, Ar-H), 8.79 (1H, d, *J* = 4.5 Hz, Ar-H), 8.69 (4H, m, 4 x Ar-H), 8.62 (1H, d, *J* = 8.0 Hz, Ar-H), 8.46 (1H, d, *J* = 7.5 Hz, Ar-H), 8.17 (1H, m, Ar-H), 8.07 (1H, s, Ar-H), 8.04 (1H, d, *J* = 8.0 HZ, Ar-H), 7.98 (1H, dt, *J* = 1.5, 8.0 Hz, Ar-H), 7.86 (1H, m, Ar-H), 7.76 (1H, m, Ar-H), 7.59 (1H, d, *J* = 8.0 Hz, Ar-H), 7.49 (1H, m, Ar-H); ^{13}C NMR δ_C ($CDCl_3$, 100 MHz): 163.3, 162.5, 156.1, 155.0, 150.2, 149.3, 149.2, 147.2, 138.0, 137.4, 136.6, 131.7, 130.1, 130.0, 129.9, 129.6, 128.9, 128.8, 127.4, 127.3, 126.8, 124.4, 124.2, 123.4, 122.9, 121.4, 120.6, 117.4; IR ν_{max} (cm^{-1}): 1718 (w, -CO-N-CO-), 1524 (m, C-NO_2), 1350 (m, C-NO_2).

7.6 Synthesis and Characterisation of Compounds Described in Chapter 5

4-[N-(p-phenyl)-4-nitro-1,8-naphthalimide]-2,2'-ethylenebipyridyldiylium dichloride (93)

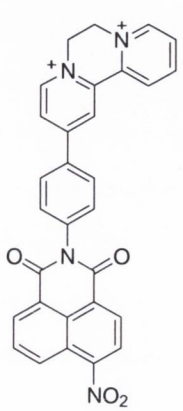

Compound **93** was synthesised according to **Procedure 10** using **88** (0.33 g, 0.70 mmol, 1 eq.) and dibromoethane (30 ml) giving the product as a brown solid (0.32 g, 80%). Calculated for $C_{30}H_{20}F_{12}N_4O_4P_2$: C, 45.59; H, 2.55; N, 7.09. Found: C, 45.37; H, 2.46; N, 6.88; Accurate MS (m/z) Calculated for $C_{30}H_{20}N_4O_4$ (M^{2+}): 500.1485. Found 500.1478; ^1H NMR δ_H (D_2O, 400 MHz): 9.23 (1H, s, Ar-H), 9.17 (2H, m, 2 x Ar-H), 9.06 (1H, d, *J* = 8.0 Hz, Ar-H), 8.87 (1H, m, Ar-H), 8.63 (1H, d, *J* = 6.0 Hz, Ar-H), 8.53

(1H, d, J = 9.0 Hz, Ar-H), 8.49 (1H, d, J = 7.5 Hz, Ar-H), 8.44 (1H, d, J = 8.0 Hz, Ar-H), 8.32 (1H, t, J = 7.0 Hz, Ar-H), 8.23 (3H, m, 3 x Ar-H), 7.83 (1H, t, J = 7.6 Hz, Ar-H), 7.65 (2H, d, J = 8.0 Hz, Ar-H), 5.30 (4H, d, J = 7.0 Hz, 2 x CH_2); ^{13}C NMR δ_C (D_2O, 100 MHz): 165.4, 164.4, 157.5, 149.8, 148.2, 147.1, 146.9, 139.6, 135.8, 134.8, 133.0, 132.7, 131.4, 130.7, 130.3, 130.0, 129.6, 128.6, 128.4, 128.2, 127.1, 125.7, 125.4, 124.3, 122.9, 121.5, 52.8, 51.7; IR ν_{max} (cm^{-1}): 1712 (m, -CO-N-CO-), 1523 (m, C-NO_2), 1347 (m, C-NO_2).

4-[*N*-(m-phenyl)-4-nitro-1,8-naphthalimide]-2,2'-ethylenebipyridyldiylium dichloride (94)

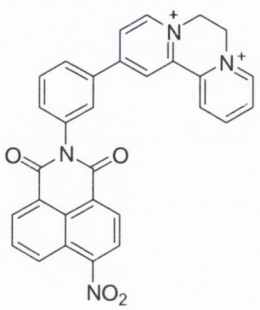

Compound **94** was synthesised according to **Procedure 10** using **89** (0.25 g, 0.53 mmol, 1 eq.) and dibromoethane (30 ml) giving the product as a brown solid (0.25 g, 82%). Calculated for $C_{30}H_{20}F_{12}N_4O_4P_2$: C, 45.59; H, 2.55; N, 7.09. Found: C, 45.82; H, 2.42; N, 7.08; Accurate MS (m/z) Calculated for $C_{30}H_{19}N_4O_4$ (M^{2+}): 499.1406. Found 499.1411; ^1H NMR δ_H (D_2O, 400 MHz): 9.14 (1H, d, J = 6.0 Hz, Ar-H), 9.11 (1H, d, J = 6.5 Hz, Ar-H), 9.07 (1H, s, Ar-H), 8.95 (1H, d, J = 8.0 Hz, Ar-H), 8.79 (1H, t, J = 8.0 Hz, Ar-H), 8.54 (1H, d, J = 8.6 Hz, Ar-H), 8.46 (3H, m, 3 x Ar-H), 8.28 (1H, m, Ar-H), 8.23 (1H, d, J = 8.0 Hz, Ar-H), 8.11 (1H, d, J = 8.0 Hz, Ar-H), 8.02 (1H, s, Ar-H), 7.76 (2H, m, 2 x Ar-H), 7.62 (1H, d, J = 7.5 Hz, Ar-H), 5.26 (4H, d, J = 8.0 Hz, 2 x CH_2); ^{13}C NMR δ_C (D_2O, 100 MHz): 165.4, 164.4, 157.5, 149.7, 148.2, 147.1, 146.9, 139.6, 139.5, 135.8, 134.8, 133.0, 132.7, 131.4, 130.7, 130.3, 130.0, 129.5, 128.5, 128.4, 128.2, 127.1, 125.8, 125.7, 125.4, 122.9, 121.5, 52.5, 51.6; IR ν_{max} (cm^{-1}): 1715 (m, -CO-N-CO-), 1523 (m, C-NO_2), 1345 (m, C-NO_2).

4-[*N*-(m-phenyl)-4-amino-1,8-napthalimide]-2,2'- ethylenebipyridyldiylium dichloride (95)

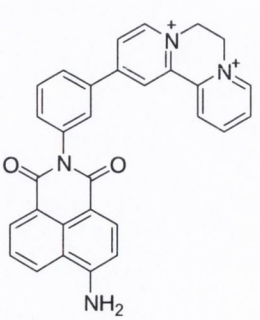

Compound **99** (0.15 g, 0.34 mmol, 1.eq.) was suspended in dibromoethane (30 ml) and the mixture heated at reflux for 4.5 hours. The reaction mixture was cooled to room temperature, the resulting precipitate collected by filtration and washed with acetone (5 ml) and hexane (5 ml). The product was adsorbed onto a short pad of silica and purified using MeOH-$NH_{3(sat)}$. The silica was stirred with $CH_3CN/H_2O/NaNO_{3(sat)}$ 40:4:1, filtered and the CH_3CN removed under vacuum. A

concentrated solution of NH_4PF_6 was added which gave a precipitate that could not be isolated by filtration. The product was extracted into DMF/CH_2Cl_2 and the solution concentrated under vacuum. The product was precipitated out by dropping into toluene and isolated by filtration. After drying under vacuum the product was obtained as an orange solid (0.003 g, 1.6%). Accurate MS (m/z) Calculated for $C_{30}H_{23}N_4O_2$ (M^{2+}): 471.1821. Found 471.1806; ^{1}H NMR δ_H (D_2O, 400 MHz): 9.11 (1H, d, J = 6.0 Hz, Ar-H), 9.00 (1H, d, J = 6.5, Ar-H), 8.93 (1H, s, Ar-H), 8.81 (1H, d, J = 8.5, Ar-H), 8.69 (1H, m, Ar-H), 8.35 (1H, d, J = 5.5 Hz, Ar-H), 8.23 (1H, m, Ar-H), 8.17 (1H, d, J = 8.0 Hz, Ar-H), 8.07 (1H, d, J = 8.0 Hz, Ar-H), 8.03 (1H, s, Ar-H), 7.96 (1H, d, J = 8.6 Hz, Ar-H), 7.90 (1H, d, J = 8.5 Hz, At-H), 7.58 (2H, m, Ar-H), 7.35 (1H, m, Ar-H), 6.54 (1H, d, J = 8.5 Hz, Ar-H), 5.21 (4H, m, 2CH2); ^{13}C NMR δ_C (D_20, 150 MHz): 166.3, 165.2, 157.3, 153.6, 148.1, 147.2, 146.8, 139.45, 139.38, 137.1, 135.0, 134.3, 133.2, 123.4, 131.2, 130.7, 130.2, 129.7, 128.8, 128.7, 128.2, 126.7, 125.0, 124.4, 120.0, 118.9, 109.4, 106.7, 52.5, 51.5.

4-(4-methylphenyl)-2,2'-ethylenebipyridyldiylium dibromide (96)

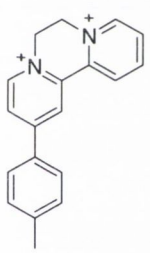

4-(4-methylphenyl)-2,2'-bipyridne (0.13 g, 0.53 mmol, 1.eq.) was suspended in dibromoethane (5 ml) and the mixture heated at reflux for 4 hours. The reaction mixture was cooled to room temperature, the resulting precipitate collected by filtration and washed with acetone (5 ml) and ether (5 ml). After drying under high vacuum the product was obtained as a yellow solid (0.21 g, 92%). Calculated for $C_{19}H_{18}Br_2N_2.1.25H_2O$: C, 49.81; H, 4.55; N, 6.11. Found: C, 49.94; H, 4.22; N, 6.07; Accurate MS (m/z) Calculated for $C_{19}H_{19}N_2$ (M^{2+}): 275.1548. Found 275.1555; ^{1}H NMR δ_H (D_2O, 400 MHz): 9.13 (1H, dd, *J* = 0.8, 6.0 Hz, Ar-H), 9.05 (1H, d, *J* = 2.3 Hz, Ar-H), 8.99 (1H, dd, *J* = 1.0, 8.2 Hz, Ar-H), 8.98 (1H, d, *J* = 6.52 Hz, Ar-H), 8.83 (1H, dt, *J* = 1.3, 8.0 Hz, Ar-H), 8.46 (1H, dd, *J* = 2.0, 6.5 Hz, Ar-H), 8.8 (1H, m, Ar-H), 7.91 (2H, d, *J* = 8.5 Hz, Ar-H), 7.22 (2H, d, *J* = 8.5 Hz, Ar-H), 5.25 (2H, m, CH_2), 5.18 (2H, m, CH_2), 2.37 (3H, s, CH_3); ^{13}C NMR δ_C (D_2O, 100 MHz): 159.0, 148.2, 147.0, 146.3, 145.0, 140.1, 139.3, 130.6, 130.5, 130.1, 128.4, 128.2, 126.2, 124.8, 52.7, 51.3, 20.7.

4-[*N*-(m-phenyl)-4-amino-1,8-napthalimide]-2,2'-bipyridine (99)

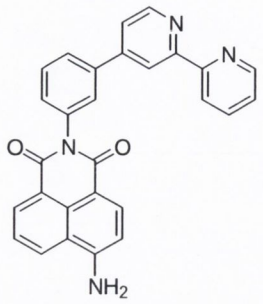

Compound **89** (0.30 g, 0.64 mmol, 1.eq.) was dissolved in DMF (30 ml) and MeOH (30 ml) added. To this was added 10% Pd/C (0.05 g) and the mixture heated at 65 °C for 1 hour. Hydrazine monohydrate (0.41 g, 0.40 ml, 12.74 mmol, 20 eq.) was added and the mixture heated at 65 °C for a further 16 hours. The reaction mixture was filtered through celite and the solvent removed under vacuum. The resulting residue was triturated with water to remove unreacted hydrazine and the solid isolated by filtration to give the product as an orange solid (0.27 g, 94%). Accurate MS (m/z) Calculated for $C_{28}H_{19}N_4O_2$ (M^{2+}): 443.1508. Found 443.1495; ^{1}H NMR δ_H (DMSO[D_6], 400 MHz) 8.78 (1H, d, J = 5.5 Hz, Ar-H), 8.69 (3H, m, Ar-H), 8.45 (2H, m, Ar-H), 8.23 (1H, d, J = 8.5 Hz, Ar-H), 8.00 – 7.92 (2H, m, Ar-H), 7.84 (1H, d, J = 5.0 Hz, Ar-H), 7.71 (2H, m, Ar-H), 7.53 – 7.47 (4H, m, Ar-H + NH2), 6.90 (1H, d, J = 8.5 Hz, Ar-H); ^{13}C NMR δ_C (DMSO[D_6], 100 MHz): 164.5, 163.6, 156.4, 155.4, 153.2, 150.5, 149.6, 147.8, 138.2, 138.0, 137.7, 134.3, 131.5, 130.7, 130.6, 130.1, 129.9, 128.1, 126.6, 124.7, 124.3, 122.7, 121.9, 121.0, 119.9, 117.9, 108.6, 108.2.

Chapter 9

References

1. Jenkins, T. C. *Curr. Med. Chem.* **2000,** *7*, 99-115.
2. Dervan, P. B.; Burli, R. W. *Curr. Opin. Chem. Biol.* **1999,** *3*, 688-693.
3. Chaires, J. B. *Curr. Opin. Struc. Biol.* **1998,** *8*, 314-320.
4. Hannon, M. J. *Chem. Soc. Rev.* **2007,** *36*, 280-295.
5. Erkkila, K. E.; Odom, D. T.; Barton, J. K. *Chem. Rev.* **1999,** *99*, 2777-2795.
6. Armitage, B. *Chem. Rev.* **1998,** *98*, 1171-1200.
7. Doonan, S. *Nucleic acids*, 1st ed.; RSC, 2004.
8. Weaver, R. F. *Molecular Biology*, 3rd ed.; Mc-Graw Hill, 2005.
9. Voet, D.; Voet, J. G. *Biochemistry*, 2nd ed.; Wiley, 1995.
10. Watson, J. D.; Crick, F. H. C. *Nature* **1953,** *171*, 737.
11. Bloomfield, V. A.; Crothers, D. M.; Tinoco, I. *Nucleic Acids. Structures, Properties and Functions.*, 1st ed.; University Science Books, 2000.
12. Rich, A.; Zhang, S. *Nat. Rev. Genetics* **2003,** *4*, 566-572.
13. Demeunynck, M.; Bailly, C.; Wilson, W. D. *DNA and RNA Binders. From Small Molecules to Drugs.*, 1st ed.; Wiley, 2003; Vol. 2.
14. Dervan, P. B.; Poulin-Kerstien, A. T.; Fechter, E. J.; Edelson, B. S. *Top. Curr. Chem.* **2005,** *253*, 1-31.
15. Dervan, P. B.; Edelson, B. S. *Curr. Opin. Struc. Biol.* **2003,** *13*, 284-299.
16. Mergny, J. L.; Duval-Valentin, G.; Nguyen, C. H.; Perrouault, L.; Faucon, B.; Rougee, T.; Montenay-Garestier, T.; Bisagni, E.; Helene, C. *Science* **1992,** *256*, 1681-1684.
17. Lee, J. S.; Latimer, L. J. P.; Hampel, K. J. *Biochem.* **1993,** *32*, 5591-5597.
18. Wakelin, L. P. G.; Waring, M. J. *DNA Intercalating Agents. In Comprehensive Medicinal Chemistry.*; Pergamon: Oxford, 1990; Vol. 2.
19. Bailly, C.; Henichart, J.-P. *Molecular Aspects of Anticancer Drug-DNA Interactions*, 1st ed.; Macmillan, 1993; Vol. 2.
20. Harris, A.; Qu, Y.; Farrell, N. *Inorg. Chem* **2005,** *44*, 1196-1198.
21. *Burgers Medicinal Chemistry and Drug Discovery*, 6th ed.; Wiley; Vol. 5.
22. Zhang, C. X.; Lippard, S. J. *Curr. Opin. Chem. Biol.* **2003,** *7*, 481-489.
23. Moucheron, C.; Kirsch-De Mesmaeker, A.; Kelly, J. M. *J. Photochem. Photobiol. B: Biol.* **1997,** *40*, 91-106.
24. Vos, J. G.; Kelly, J. M. *J. Chem. Soc. Dalton Trans.* **2006**, 4869-4883.
25. Kalyanasundaram, K. *Photochemistry of Polypyridine and Porphyrin Complexes*; Academic Press Ltd.: London, 1992.
26. Kober, E. M.; Meyer, T. J. *Inorg. Chem.* **1984,** *23*, 3877-3886.
27. Chang, Y. J.; Xu, X.; Yabe, T.; Yu, S. C.; Anderson, D. R.; Orman, L. K.; Hopkins, J. B. *J. Phys. Chem.* **1990,** *94*, 729-736.
28. Durham, B.; Caspar, J. V.; Nagle, J. K.; Meyer, T. J. *J. Am. Chem. Soc* **1982,** *104*, 4803-4810.
29. Kelly, J. M.; Tossi, A. B.; McConnell, D. J.; OhUigin, C. *Nucleic Acids Res.* **1985,** *13*, 6017-6034.
30. Tossi, A. B.; Kelly, J. M. *Photochem. Photobiol.* **1989,** *49*, 545-556.
31. Kelly, J. M.; Tossi, A. B.; McConnell, D. J.; O Huigin, C. *Nucleic Acids Res.* **1985,** *13*, 6017.
32. Barton, J. K.; Danishefsky, A. T.; Goldberg, J. M. *J. Am. Chem. Soc* **1984,** *106*, 2172-2176.
33. Kumar, C. V.; Barton, J. K.; Turro, N. J. *J. Am. Chem. Soc.* **1985,** *107*, 5518-5523.
34. Barton, J. K. *Science* **1986,** *233*, 727-734.
35. Yamagishi, A. *J. Chem. Soc., Chem. Comm.* **1983**, 572-573.
36. Barton, J. K.; Goldberg, J. M.; Kumar, C. V.; Turro, N. J. *J. Am. Chem. Soc* **1986,** *108*, 2081-2088.

37. Rehmann, J. P.; Barton, J. K. *Biochem.* **1990,** *29*, 1701-1709.
38. Eriksson, M.; Leijon, M.; Hiort, C.; Norden, B.; Graslund, A. *J. Am. Chem. Soc* **1992,** *114*, 4933-4934.
39. Eriksson, M.; Leijon, M.; Hiort, C.; Norden, B.; Graslund, A. *Biochem.* **1994,** *33*, 5031-5040.
40. Hiort, C.; Norden, B.; Rodger, A. *J. Am. Chem. Soc* **1990,** *112*, 1971-1982.
41. Satyanarayana, S.; Dabrowiak, J. C.; Chaires, J. B. *Biochem.* **1992,** *31*, 9319-9324.
42. Coury, J. E.; Anderson, J. R.; McFail-Isom, L.; Williams, L. D.; Bottomley, L. A. *J. Am. Chem. Soc* **1997,** *119*, 3792-3796.
43. Coggan, D. Z. M.; Haworth, I. S.; Bates, P. J.; Robinson, A.; Rodger, A. *Inorg. Chem.* **1999,** *38*, 4486-4497.
44. Amouyal, E.; Homsi, A.; Chambron, J. C.; Sauvage, J. P. *J. Chem. Soc. Dalton Trans.* **1990,** 1841-1845.
45. Friedman, A. E.; Chambron, J. C.; Sauvage, J. P.; Turro, N. J.; Barton, J. K. *J. Am. Chem. Soc.* **1990,** *112*, 4960-4962.
46. Olson, E. J. C.; Hu, D.; Hormann, A.; Jonkman, A. M.; Arkin, M. R.; Stemp, E. D. A.; Barton, J. K.; Barbara, P. F. *J. Am. Chem. Soc.* **1997,** *119*, 11458-11467.
47. Coates, C. G.; Olofsson, J.; Coletti, M.; McGarvey, J. J.; Onfelt, B.; Lincoln, P.; Norden, B.; Tuite, E.; Matousek, P.; Parker, A. W. *J. Phys. Chem. B* **2001,** *105*, 12653-12664.
48. Coates, C. G.; Callaghan, P.; McGarvey, J. J.; Kelly, J. M.; Jacquet, L.; Kirsch-De Mesmaeker, A. *J. Mol. Struc.* **2001,** *598*, 15-25.
49. Brennanman, M. K.; Alstrum-Acevedo, J. H.; Fleming, C. N.; Jang, P.; Meyer, T. J.; Papanikolas, J. M. *J. Am. Chem. Soc.* **2002,** *124*, 15094-15098.
50. Brennaman, M. K.; Meyer, T. J.; Papanikolas, J. M. *J. Phys. Chem. A* **2004,** *108*, 9938-9944.
51. Onfelt, A.; Olofsson, J.; Lincoln, P.; Norden, B. *J. Phys. Chem. A* **2003,** *107*, 1000-1009.
52. Batista, E. R.; Martin, R. L. *J. Phys. Chem. A* **2005,** *109*, 3128-3133.
53. Olofsson, J.; Onfelt, A.; Lincoln, P. *J. Phys. Chem. A* **2004,** *108*, 4391-4398.
54. Olofsson, J.; Wilhelmsson, L. M.; Lincoln, P. *J. Am. Chem. Soc.* **2004,** *126*, 15458-15465.
55. Hartshorn, R. M.; Barton, J. K. *J. Am. Chem. Soc* **1992,** *114*, 5919-5925.
56. Jenkins, Y.; Friedman, A. E.; Turro, N. J.; Barton, J. K. *Biochem.* **1992,** *31*, 10809-10816.
57. Hiort, C.; Lincoln, P.; Norden, B. *J. Am. Chem. Soc* **1993,** *115*, 3448-3454.
58. Lincoln, P.; Broo, A.; Norden, B. *J. Am. Chem. Soc* **1996,** *118*, 2644-2653.
59. Haq, I.; Lincoln, P.; Suh, D.; Norden, B.; Chowdhry, B. Z.; Chaires, J. B. *J. Am. Chem. Soc* **1995,** *117*, 4788-4796.
60. Dupureur, C. M.; Barton, J. K. *J. Am. Chem. Soc* **1994,** *116*, 10286-10287.
61. Tuite, E.; Lincoln, P.; Norden, B. *J. Am. Chem. Soc.* **1997,** *119*, 239-240.
62. Homlin, R. E.; Stemp, E. D. A.; Barton, J. K. *Inorg. Chem.* **1998,** *37*, 29-34.
63. Blasius, R.; Moucheron, C.; Kirsch-De Mesmaeker, A. *Eur. J. Inorg. Chem.* **2004**, 3971-3979.
64. Fleisher, M. B.; Waterman, K. C.; Turro, N. J.; Barton, J. K. *Inorg. Chem.* **1986,** *25*, 3549-3551.
65. Kirsch-De Mesmaeker, A.; Nasielski-Hinkens, R.; Maetens, D.; Pauwels, D.; Nasielski, J. *Inorg. Chem.* **1984,** *23*, 377.
66. Masschelein, A.; Jacquet, L.; Kirsch-De Mesmaeker, A.; Nasielski, J. *Inorg. Chem.* **1990,** *29*, 855-860.

67. Kelly, J. M.; McConnell, D. J.; OhUigin, C.; Tossi, A. B.; Kirsch-De Mesmaeker, A.; Masschelein, A.; Nasielski, J. *J. Chem. Soc. Chem. Comm.* **1987**, 1821-1822.
68. Tossi, A.; Kelly, J. M. *Photochem. Photobiol.* **1989,** *49*, 545-556.
69. Lecomte, J.-P.; Kirsch-De Mesmaeker, A.; Kelly, J. M.; Tossi, A. B.; Gorner, H. *Photochem. Photobiol.* **1992,** *55*, 681-689.
70. Kelly, J. M.; Feeney, M. M.; Tossi, A. B.; Lecomte, J.-P.; Kirsch-De Mesmaeker, A. *Anti-Cancer Drug Design.* **1990,** *5*, 69-75.
71. Feeney, M. M.; Kelly, J. M.; Tossi, A. B.; Kirsch-De Mesmaeker, A.; Lecomte, J.-P. *J. Photochem. Photobiol. B: Biol.* **1994,** *23*, 69-78.
72. Lecomte, J.-P.; Kirsch-De Mesmaeker, A.; Kelly, J. M. *Bull. Soc. Chim. Belg.* **1994,** *5-6*, 193-200.
73. Jacquet, L.; Kelly, J. M.; Kirsch-De Mesmaeker, A. *J. Chem. Soc. Chem. Comm.* **1995**, 913-914.
74. Jacquet, L.; Davies, R. J. H.; Kirsch-De Mesmaeker, A.; Kelly, J. M. *J. Am. Chem. Soc* **1997,** *119*, 11763-11768.
75. Blasius, R.; Nierengarten, H.; Luhmer, M.; Constant, J.-F.; Defrancq, E.; Dumy, P.; van Dorsselaer, A.; Moucheron, C.; Kirsch-DeMesmaeker, A. *Chem. Eur. J.* **2005,** *11*, 1507-1517.
76. Lecomte, J.-P.; Kirsch-De Mesmaeker, A.; Feeney, M. M.; Kelly, J. M. *Inorg. Chem.* **1995,** *34*, 6481-6491.
77. Moucheron, C.; Kirsch-DeMesmaeker, A.; Choua, S. *Inorg. Chem.* **1997,** *36*, 584-592.
78. Boisdenghien, A.; Moucheron, C.; Kirsch-De Mesmaeker, A. *Inorg. Chem.* **2005,** *44*, 7678-7685.
79. Sentagne, C.; Chambron, J. C.; Sauvage, J. P.; Paillous, N. *J. Photochem. Photobiol. B: Biol.* **1994,** *26*, 165-174.
80. Vicendo, P.; Mouysset, S.; Paillous, N. *Photochem. Photobiol.* **1997,** *65*, 647-655.
81. Gicquel, E.; Paillous, N.; Vicendo, P. *Photochem. Photobiol.* **2000,** *72*, 583-589.
82. Ortmans, I.; Elias, B.; Kelly, J. M.; Moucheron, C.; Kirsch-De Mesmaeker, A. *Dalton Trans.* **2004**, 668-676.
83. Le Pecq, J.-B.; Le Bret, M.; Barbet, J.; Roques, B. *Proc. Natl. Acad. Sci.* **1975,** *72*, 2915-2919.
84. Wakelin, L. P. G.; Romanos, M.; Chen, T. K.; Glaubiger, D.; Canellakis, E. S.; Waring, M. J. *Biochem.* **1978,** *17*, 5057-5063.
85. O' Reilly, F. M.; Kelly, J. M.; Kirsch-De Mesmaeker, A. *J. Chem. Soc. Chem. Comm.* **1996**, 1013-1014.
86. O' Reilly, F. M.; Kelly, J. M. *J. Phys. Chem. B* **2000,** *104*, 7206-7213.
87. O' Reilly, M.; Kelly, J. M. *New J. Chem.* **1998**, 215-217.
88. Lincoln, P.; Norden, B. *J. Chem. Soc. Chem. Comm.* **1996**, 2145-2146.
89. Onfelt, A.; Lincoln, P.; Norden, B. *J. Am. Chem. Soc* **1999,** *121*, 10846-10847.
90. Onfelt, B.; Lincoln, P.; Norden, B. *J. Am. Chem. Soc* **2001,** *123*, 3630-3637.
91. Wilhelmsson, L. M.; Westerlund, F.; Lincoln, P.; Norden, B. *J. Am. Chem. Soc.* **2002,** *124*, 12092-12093.
92. Wilhelmsson, L. M.; Esbjorner, E. K.; Westerlund, F.; Norden, B.; Lincoln, P. *J. Phys. Chem. B* **2003,** *107*, 11784-11793.
93. Westerlund, F.; Wilhelmsson, L. M.; Norden, B.; Lincoln, P. *J. Phys. Chem. B* **2005,** *109*, 21140-21144.
94. Nordell, P.; Westerlund, F.; Wilhelmsson, L. M.; Norden, B.; Lincoln, P. *Angew. Chem. Int. Ed.* **2007,** *46*, 2203-2206.
95. Thornton, N. B.; Schanze, K. S. *Inorg. Chem.* **1993,** *32*, 4994-4995.
96. Thornton, N.; Schanze, K. S. *New J. Chem.* **1996,** *20*, 791-800.

97. Lecomte, J.-P.; Kirsch-De Mesmaeker, A.; Demeunynck, M.; Lhomme, J. *J. Chem. Soc. Faraday Trans.* **1993,** *89*, 3261-3269.
98. Del Guerzo, A.; Kirsch-De Mesmaeker, A.; Demeunynck, M.; Lhomme, J. *J. Phys. Chem. B* **1997,** *101*, 7012-7021.
99. Del Guerzo, A.; Kirsch-De Mesmaeker, A.; Demeunynck, M.; Lhomme, J. *J. Chem. Soc., Dalton Trans.* **2000**, 1173-1179.
100. Del Guerzo, A.; Kirsch-De Mesmaeker, A. *Inorg. Chem.* **2002,** *41*, 938-945.
101. Fu, P. K. L.; Bradley, P. M.; van Loyen, D.; Durr, H.; Bossmann, S. H.; Turro, C. *Inorg. Chem.* **2002,** *41*, 3808-3810.
102. Liu, L. F. *Annu. Rev. Biochem.* **1989,** *58*, 351-375.
103. Brana, M. F., Ramos, A. *Curr. Med. Chem.* **2001,** *1*, 237-255.
104. Veale, E. Ph.D. Thesis, University of Dublin, Trinity College, 2007.
105. Gillespie, L. J. PhD Thesis, University of Dublin, Trinity College, 2007.
106. Hussey, G. M. Ph.D. Thesis, University of Dublin, Trinity College 2003.
107. Phelan, C. Ph.D. Thesis, University of Dublin, Trinity College, 2002.
108. Brana, M. F.; Sanz, A. M.; Castellano, J. M.; Roldan, C. M.; Roldan, C. *Eur. J. Med. Chem. Chim. Ther.* **1981,** *16*, 207.
109. Chen, S. F.; Behrens, D. L.; Behrens, C. H.; Czerniak, P. M.; Dexter, D. L.; Dusak, B. L.; Fredericks, J. R.; Gale, K. C.; Gross, J. L.; Jiang, J. B.; Kirshenbaum, M. R.; McRipley, R. J.; Papp, L. M.; Patten, A. D.; Perrella, F. W.; Seitz, S. P.; Stafford, M. P.; Sun, J. H.; Wuonola, M. A.; Von Hoff, D. D. *Anti-Cancer Drugs* **1993,** *4*, 447-457.
110. Brana, M. F.; Castellano, J. M.; Moran, M.; Perez de Vega, M. J.; Perron, D.; Conlon, D.; Bousquet, P. F.; Romerdahl, C. A.; Robinson, S. P. *Anti-Cancer Drug Des.* **1996,** *11*, 297-309.
111. Kirshenbaum, M. R.; Chen, S. F.; Behrens, C. H.; Papp, L. M.; Stafford, M. M.; Sun, J. H.; Behrens, D. L.; Fredericks, J. R.; Polkus, S. T.; Sipple, P.; Patten, A. D.; Dexter, D.; Seitz, S. P.; Gross, J. L. *Cancer Res.* **1994,** *54*, 2199-2206.
112. Bailly, C.; Brana, M. F.; Waring, M. J. *Eur. J. Biochem.* **1996,** *240*.
113. Gallego, J.; Reid, B. R. *Biochem.* **1999,** *38*, 15104-15115.
114. Lin, P. K. T.; Pavlov, V. A. *Bioorg. Med. Chem. Lett.* **2000,** *10*, 1609-1612.
115. Saito, I., Takayama, M. *J. Am. Chem. Soc.* **1995,** *117*, 5590-5591.
116. Saito, I., Takayama, M, Sugiyama, H, Nakatani, K. *J. Am. Chem. Soc.* **1995,** *117*, 6406-6407.
117. Wintgens, V.; Valat, P.; Kossanyl, J.; Biczok, L.; Demeter, A.; Berces, T. *J. Chem. Soc., Faraday Trans.* **1994,** *90*, 411-421.
118. Aveline, B. M.; Matsugo, S.; Redmond, R. W. *J. Am. Chem. Soc.* **1997,** *119*, 11785-11795.
119. Rogers, J. E.; Kelly, L. A. *J. Am. Chem. Soc.* **1999,** *121*, 3854-3861.
120. Rogers, J. E.; Weiss, S. J.; Kelly, L. A. *J. Am. Chem. Soc.* **2000,** *122*, 427-436.
121. Rogers, J. E.; Abraham, B.; Rostkowski, A.; Kelly, L. A. *Photochem. Photobiol.* **2001,** *74*, 521-531.
122. Pogozelski, W. K.; Tullius, T. D. *Chem. Rev.* **1998,** *98*, 1089-1107.
123. Tao, Z. F.; Qian, X.; Wei, D. *Dyes and Pigments* **1996,** *31*, 245-251.
124. Saito, I.; Takayama, M.; Matsuura, T. *J. Am. Chem. Soc* **1990,** *112*, 883-884.
125. Yao, W.; Qian, X. *Dyes and Pigments* **2001,** *48*, 43-47.
126. Matsugo, S.; Kawanishi, S.; Yamamoto, K.; Sugiyama, H.; Matsuura, T.; Saito, I. *Angew. Chem. Int. Ed. Engl.* **1991,** *30*, 1351-1353.
127. Kuruvilla, E.; Joseph, J.; Ramaiah, D. *J. Phys. Chem. B.* **2005,** *109*, 21997-22002.
128. King, H. D.; Wilson, W. D.; Gabbay, E. J. *Biochem.* **1982,** *21*, 4982-4989.

129. Wright, R. G.; Wakelin, L. P. G.; Fieldes, A.; Acheson, R. M.; Waring, M. J. *Biochem.* **1980,** *19*, 5825-5836.
130. Van Vliet, L. D.; Ellis, T.; Foley, P. J.; Liu, L.; Pfeffer, F. M.; Russell, R. A.; Warrener, R. N.; Hollfelder, F.; Waring, M. J. *J. Med. Chem.* **2007,** *50*, 2326-2340.
131. Chen, L.; McBranch, D.; Wang, R.; Whitten, D. *Chem. Phys. Lett.* **2000,** *330*, 27-33.
132. Kim, H.-B.; Kitamura, N.; Kawanishi, Y.; Tazuki, S. *J. Phys. Chem.* **1989,** *93*, 5757-5764.
133. Glazier, S.; Barron, J. A.; Morales, N.; Ruschak, A. M.; Houston, P. L.; Abruna, H. D. *Macromolecules* **2003,** *36*, 1272-1278.
134. Focsaneanu, K.-S.; Scaiano, J. C. *Photochem. Photobiol. Sci.* **2005,** *4*, 817-821.
135. Launikonis, A.; Lay, P. A.; Mau, A. W.; Sargeson, A. M.; Sesse, W. H. F. *Aust. J. Chem.* **1986,** *39*, 1053-1062.
136. Oki, A. R.; Morgan, R. J. *Synth. Commun.* **1995,** *24*, 4093.
137. Strouse, G. F.; Anderson, P. A.; Schoonover, J. R.; Meyer, T. J.; Keene, F. R. *Inorg. Chem.* **1992,** *31*, 3004-3006.
138. Mehrotra, J., Misra, K, Mishra, R K,. *Indian J. Chem.* **1993,** *32B*, 540-545.
139. Mabrouk, P. A.; Wrighton, M. S. *Inorg. Chem.* **1986,** *25*, 526-531.
140. Parkesh, R.; Lee, T. C.; Gunnlaugsson, T. *Org. Biomol. Chem.* **2007,** *5*, 310-317.
141. Caspar, J. V.; Kober, E. M.; Sullivan, B. P.; Meyer, T. J. *J. Am. Chem. Soc.* **1982,** *104*, 630-632.
142. *Drug-DNA Interaction Protocols*; Humana Press Inc., 1997; Vol. 90.
143. Marmur, J.; Doty, P. *J. Mol. Biol.* **1962,** *5*, 109-118.
144. Tanaka, K.; Okahata, Y. *J. Am. Chem. Soc.* **1996,** *118*, 10679-10683.
145. Yen, S. F.; Gabbay, E. J.; Wilson, W. D. *Biochem.* **1982,** *21*, 2070-2076.
146. Turro, N. J. *Modern Molecular Photochemistry*; University Science Books, 1991.
147. Lewis, F. D.; Wu, T.; Liu, X.; Letsinger, R. L.; Greenfield, S. R.; Miller, S. E.; Wasielewski, M. R. *J. Am. Chem. Soc.* **2000,** *122*, 2889-2902.
148. Lewis, F. D.; Kalgutkar, R. S.; Wu, Y.; Liu, X.; Liu, J.; Hayes, R. T.; Miller, S. E.; Wasielewski, M. R. *J. Am. Chem. Soc.* **2000,** *122*, 12346-12351.
149. Wilson, W. D.; Tanious, F. A.; Fernandez, M. F.; Rigl, C. T. *Methods Mol. Biol.* **1997,** *90*, 219-240.
150. Pilch, D. S.; Poklar, N.; Baird, E. E.; Dervan, P. B.; Breslauer, K. J. *Biochem.* **1999,** *38*, 2143-2151.
151. Ihmels, H.; Otto, D.; Dall 'Acqua, F.; Faccio, A.; Moro, S.; Viola, G. *J. Org. Chem.* **2006,** *71*, 8401-8411.
152. Garbett, N. C.; Ragazzon, P. A.; Chaires, J. B. *Nat. Protocols* **2007,** *2*, 3166-3172.
153. Monnot, M.; Mauffret, O.; Lescot, E.; Fermandjian, S. *Eur. J. Biochem.* **1992,** *204*, 1035-1039.
154. Boger, D. L.; Fink, B. E.; Brunette, S. R.; Tse, W. C.; Hedrick, M. P. *J. Am. Chem. Soc.* **2001,** *123*, 5878-5891.
155. Stevenson, K. A.; Yen, S. F.; Yang, N. C.; Boykin, D. W.; Wilson, W. D. *J. Med. Chem.* **1984,** *27*, 1677-1682.
156. Fairley, T. A.; Tidwell, R. R.; Donkor, I.; Naiman, N. A.; Ohemeng, K. A.; Lombardy, R. J.; Bentley, J. A.; Cory, M. *J. Med. Chem.* **1993,** *36*, 1746-1753.
157. El Hassan, M. A.; Calladine, C. R. *Phil. Trans. R. Soc. Lond. A* **1997,** *355*, 43-100.
158. Ford, W. E.; Rodgers, M. A. *J. Phys. Chem.* **1992,** *96*, 2917.
159. Wilson, G. J.; Sasse, W. H. F.; Mau, A. W.-H. *Chem. Phys. Lett.* **1996,** *250*, 583-588.
160. Wilson, G. J.; Launikonis, A.; Sasse, W. H. F.; Mau, A. W.-H. *J. Phys. Chem. A* **1997,** *101*, 4860-4866.

161. Tyson, D. S.; Castellano, F. N. *J. Phys. Chem.* **1999,** *103*, 10955.
162. McClenaghan, N. D.; Barigelletti, F.; Maubert, B.; S., C. *Chem. Comm.* **2002**, 602-603.
163. McClenaghan, N. D.; Leydet, Y.; Maubert, B.; Indelli, M. T.; Campagna, S. *Coordination Chemistry Reviews* **2005,** *249*, 1336-1350.
164. O' Brien, A. Ph.D Thesis, University of Dublin, 2003.
165. Tyson, D. S., Luman, C R, Zhou, X, Castellano, F N. *Inorg. Chem.* **2001,** *40*, 4063-4071.
166. Kelly, L. A.; Rodgers, M. A. *J. Phys. Chem.* **1995,** *99*, 13132-13140.
167. Selvin, P. R. *Nature Struct. Bio.* **2000,** *7*, 730-734.
168. Mabrouk, P. A.; Wrighton, M. S. *Inorg. Chem.* **1986,** *25*, 526-531.
169. Bacon, J. R.; Demas, J. N. *Anal. Chem.* **1987,** *59*, 2780-2785.
170. Murov, S. L.; Carmichael, J.; Hug, G. L. *Handbook of Photochemistry*; Marcel Dekker, 1993.
171. Johansson, O.; Borgstrom, M.; Lomoth, R.; Palmblad, J.; Hammarstrom, L.; Sun, L.; Akermark, B. *Inorg. Chem.* **2003,** *42*, 2908-2918.
172. Rillema, D. P.; Jones, D. S.; Woods, C.; Levy, H. A. *Inorg. Chem.* **1992,** *31*, 2935-2938.
173. Norden, B.; Tjerneld, F. *Biopolymers* **1982,** *21*, 1713-1734.
174. Cronshey, J. F. H. *Weed Research* **1961,** *1*, 68-77.
175. Braterman, P. S.; Song, J. I. *J. Org. Chem.* **1991,** *56*, 4678-4682.
176. Knapp, C.; Lecomte, J. P.; Kirsch-De Mesmaeker, A.; Orellana, G. *Journal of Photochemistry and Photobiology B: Biology* **1996,** *36*, 67-76.
177. Joseph, J.; Eldho, N.; Ramaiah, D. *Chemistry - A European Journal* **2003,** *9*, 5926-5935.
178. Rogers, J. E.; Le, T. P.; Kelly, L. A. *Photochem. Photobiol.* **2001,** *73*, 223-229.
179. Phillips, T.; Haq, I.; Meijer, A. J. H. M.; Adams, H.; Soutar, I.; Swanson, L.; Sykes, M. J.; Thomas, J. A. *Biochem.* **2004,** *43*, 13657-13665.
180. Phillips, T.; Rajput, C.; Twyman, L.; Haq, I.; Thomas, J. A. *Chem. Comm.* **2005**, 4327-4329.
181. Le, T. P.; Rogers, J. E.; Kelly, L. A. *J. Phys. Chem. A* **2000,** *104*, 6778-6785.
182. Buurma, N. J.; Haq, I. *Methods* **2007,** *42*, 162-172.
183. Rajput, C.; Rutkaite, R.; Swanson, L.; Haq, I.; Thomas, J. A. *Chem. Eur. J.* **2006,** *12*, 4611-4619.
184. Kim, W.; Yamasaki, Y.; Kataoka, K. *J. Phys. Chem. B* **2006,** *110*, 10919-10925.
185. Matulis, D.; Rouzina, I.; Bloomfield, V. A. *J. Mol. Biol.* **2000,** *296*, 1053-1063.
186. Wilson, R. W.; Bloomfield, V. A. *Biochem.* **1979,** *18*, 2192-2196.
187. Neidle, S.; Thurston, D. E. *Nat. Reviews* **2005,** *5*, 285-296.
188. Jain, R. K. *Adv. Drug Deliv. Rev.* **2001,** *46*, 149-168.
189. Bonnett, R. *Chem. Soc. Rev.* **1995**, 19-33.
190. Dolmans, D. E. J. G. J.; Fukumura, D.; Jain, R. *Nat. Rev. Cancer* **2003,** *3*, 380-387.
191. Halliwell, B.; Gutterridge, J. M. C. *Biochem. J.* **1984,** *219*, 1-14.
192. Bonnett, R.; Ridge, R. J.; Scourides, P. A. *J. Chem. Soc. Chem. Commun.* **1982**, 1198-1199.
193. Wainwright, M. *Chem. Soc. Rev.* **1996**, 351-359.
194. Gallagher, W. M.; Allen, L. T.; O' Shea, C.; Kenna, T.; Hall, M.; Gorman, A.; Killoran, J.; O' Shea, D. F. *Br. J. Cancer* **2005**.
195. Puckett, C. A.; Barton, J. K. *J. Am. Chem. Soc.* **2006,** *129*, 46-47.
196. Onfelt, B.; Gostring, L.; Lincoln, P.; Norden, B.; Onfelt, A. *Mutagenesis* **2002,** *17*, 317-320.

197. Jiménez-Hernández, M. E.; Orellana, G.; Montero, F.; Portolés, M. T. *Photochem. Photobiol.* **2000,** *72*, 28-34.
198. Nunez, R. *Flow Cytometry for Research Scientists: Principles and Applications*; Horizon, 2001.
199. Sullivan, B. P.; Salmon, D. J.; Meyer, T. J. *Inorg. Chem.* **1978,** *17*, 3334-3341.
200. Vogel, A. I.; Furniss, B. S.; Tatchell, A. R.; Hannaford, A. J.; Smith, P. W. G. *Vogels' Textbook of Practical Organic Chemistry*, 5th ed.; Longman, 1989.

Appendix

Appendix 1 – Crystallographic data

Identification code	**77**	
Empirical formula	C48 H32 F12N8 O4 P2 Ru	
Formula weight	2735.74	
Temperature	117 (2) K	
Wavelength	0.71070 Å	
Unit cell dimensions	a = 14.065 (9) Å	α = 104.634 (8)°
	b = 14.572 (9) Å	β = 107.989 (8)°
	c = 14.834 (8) Å	γ = 95.848 (3)°
Volume	2744 (3) $Å^3$	
Z	1	
Density (calculated)	1.656 Mg/m^3	
Absorption coefficient	0.487 mm^{-1}	
F(000)	1368	
Theta range for data collection	2.34 to 25.00°	
Index ranges	-16 ≤h ≤16, -17 ≤k ≤17, -17 ≤l ≤17	
Reflections collected	63741	
Independent reflections	9666	
Completeness to theta = 25.00°	99.9%	
Refinement method	Full-matrix least-squares on F^2	
Data / restraints / parameters	9666 / 0 / 776	
Goodness-of-fit on F^2	1.714	
Final R indices [I>2sigma(I)]	R1 = 0.1567, wR2 = 0.3933	
R indices (all data)	R1 = 0.1622, wR2 = 0.3997	

Appendix 2 - Chapter 2

Bard Binding Model:

The intrinsic binding constant **K** and binding site size **n** were determined using the model derived by Bard *et al.*[29] This model is based on the equilibrium shown in equation **2** and assumes non-cooperative, non-specific binding to DNA with the existence of one discreet type of binding site. Multi-component systems such as those under discussion in this chapter may adopt a number of binding modes at different sites and thus the assumption of one type of binding site may be an oversimplification. Nevertheless, it is generally regarded that the spectroscopic data obtained from DNA titrations is not of sufficient quality to allow one to extract multiple binding constants and binding site sizes. A relatively small number of publications have reported this.[30,31]

This model was chosen for fitting of the data as it takes account of all the data obtained from the titration. Data from DNA titrations is commonly represented as a Scatchard plot and fit to the model of McGhee and von Hippel.[32] However, this may necessitate the omission of data from the beginning and end of the titration and for this reason the Bard model was chosen. In addition, a Scatchard plot requires greater manipulation of the titration data, the result being that it is not trivial to understand exactly what is represented on the titration curve and fit. The Bard model simply requires the observed spectroscopic changes to be plotted against the concentration of added DNA and thus is visually clearer and allows for easy comparison of the binding profiles for different systems.

To construct the binding model we consider the binding of the metal complex, **M**, to a binding site, **S**, composed of s base pairs, resulting in a bound species **M-S**,

$$M + S \rightleftharpoons M\text{-}S \quad (2)$$

The equilibrium binding constant for this process is

$$K = C_b/C_fC_s \quad (3)$$

where C_b, C_f and C_s represent the equilibrium concentrations of bound complex, free complex and free binding sites, respectively.

The total concentration of complex, C_t, is

$$C_t = C_b + C_f \qquad (4)$$

and the total concentration of sites along a DNA molecule with an average number of base pairs L, is

$$xC_{DNA} = C_b + C_s \qquad (5)$$

where

$$x = L/s \qquad (6)$$

$$C_{DNA} = [NP]/2L \qquad (7)$$

and [NP] is the concentration of nucleotide phosphate.

Solution of equations **2** – **4** for the concentration of bound complex as a function of [NP] making appropriate substitutions yields,

$$C_b = \frac{\left(b^2 - \frac{2K^2C_t[NP]}{s}\right)^{1/2}}{2K} \qquad (8a)$$

$$\text{where } b = 1 + KC_t + K[NP]/2s \qquad (8b)$$

The expression is divided by C_t to give an expression in terms of the observed spectroscopic change,

$$(\varepsilon_a-\varepsilon_b)/(\varepsilon_b-\varepsilon_f) = \frac{\left(b^2 - \frac{2K^2C_t[NP]}{s}\right)^{1/2}}{2KC_t} \qquad (8)$$

Plots of $(\epsilon_a-\epsilon_f)/(\epsilon_b-\epsilon_f)$ *vs.* [NP] may be directly fitted to Eq. **8** where ϵ_a, ϵ_f and ϵ_b correspond to the apparent extinction coefficient at each point in the titration, the extinction coefficient for the free ruthenium complex, and the extinction coefficient for the ruthenium complex in the fully bound form respectively. The parameters obtained represent an average which results from any number of different binding geometries.

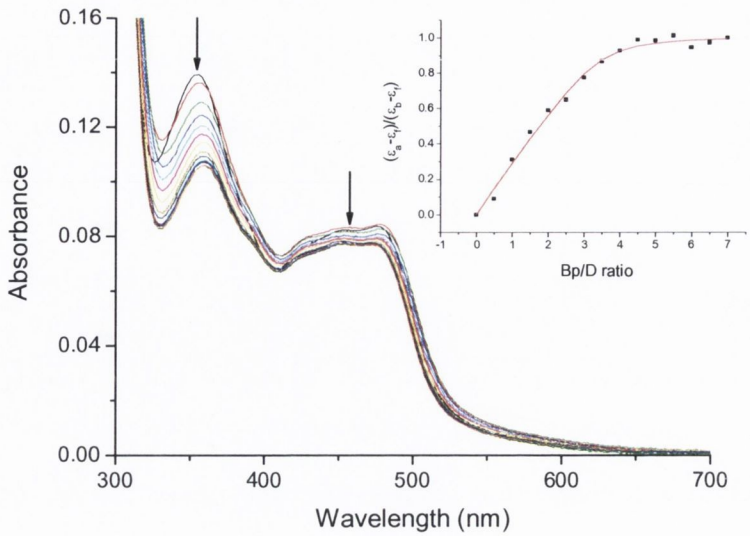

Figure A2.1 *Changes in the UV/Visible spectrum of* ***39*** *(6.5 μM) upon addition of st-DNA (0 – 45.5 μM base pairs) in 10 mM phosphate buffer, at pH 7. Inset: Plot of* $(\epsilon_a-\epsilon_f)/(\epsilon_b-\epsilon_f)$ *at 355 nm vs. [DNA] and the corresponding non-linear fit.*

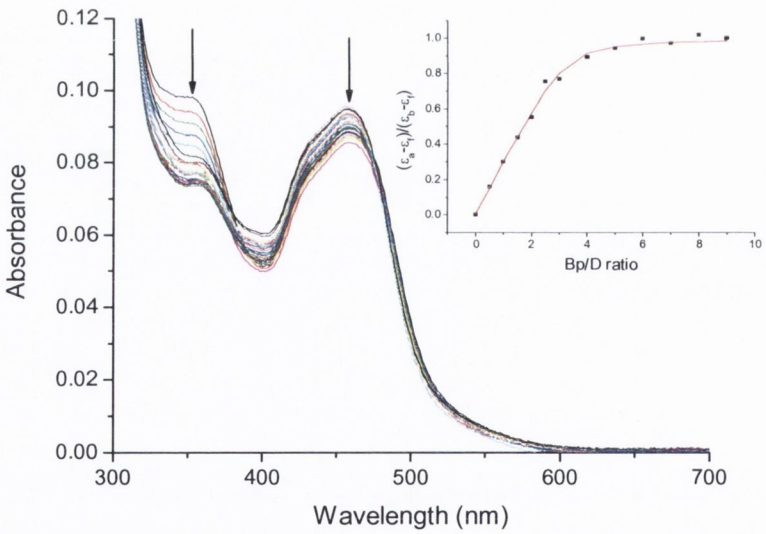

Figure A2.2 *Changes in the UV/Visible spectrum of* ***37*** *(6.5 μM) upon addition of st-DNA (0 – 58.5 μM base pairs) in 10 mM phosphate buffer, at pH 7. Inset: Plot of* $(\epsilon_a-\epsilon_f)/(\epsilon_b-\epsilon_f)$ *at 351 nm vs. [DNA] and the corresponding non-linear fit.*

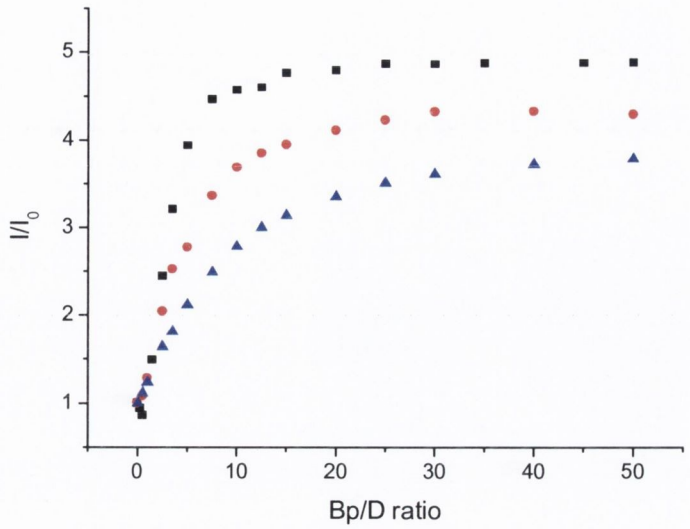

Figure A2.3 *Relative changes in the emission of* ***39*** *(6.5 μM) with increasing concentration of st-DNA (0 – 325 μM base pairs), in 10 mM phosphate buffer (■), 10 mM phosphate buffer + 50 mM NaCl (●) and 10 mM phosphate buffer + 100 mM NaCl (▲).*

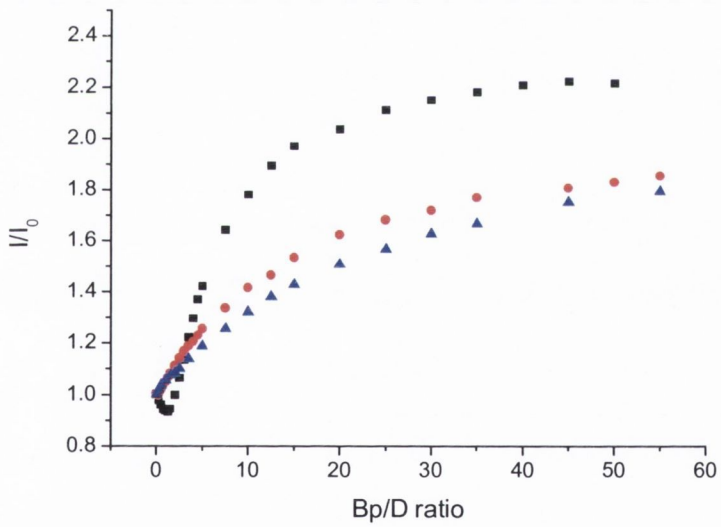

Figure A2.4 *Relative changes in the emission of* ***37*** *(6.5 μM) with increasing concentration of st-DNA (0 – 325 μM), in 10 mM phosphate buffer (■), 10 mM phosphate buffer + 50 mM NaCl (●) and 10 mM phosphate buffer + 100 mM NaCl (▲).*

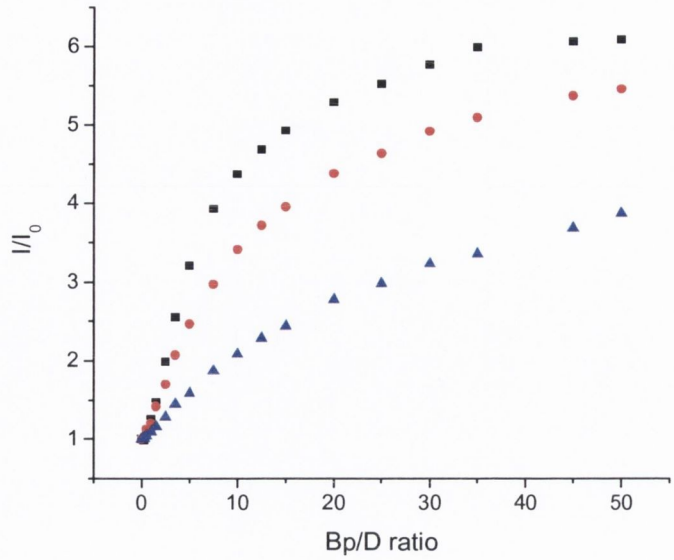

Figure A2.5 *Relative changes in the emission of* ***38*** *(6.5 μM) with increasing concentration of st-DNA (0 – 325 μM), in 10 mM phosphate buffer (■), 10 mM phosphate buffer + 50 mM NaCl (●) and 10 mM phosphate buffer + 100 mM NaCl (▲).*

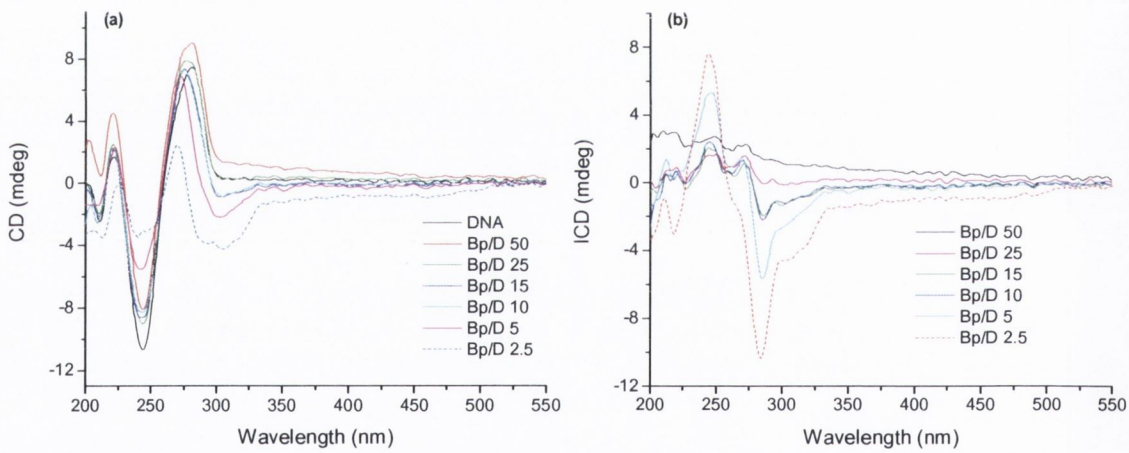

Figure A2.6 *Circular dichroism spectra of (a) st-DNA (150 μM) in 10 mM phosphate buffer, at pH 7, in the absence and presence of* ***37*** *at varying ratios, and (b) the difference spectra obtained.*

Appendix 3 - Chapter 3

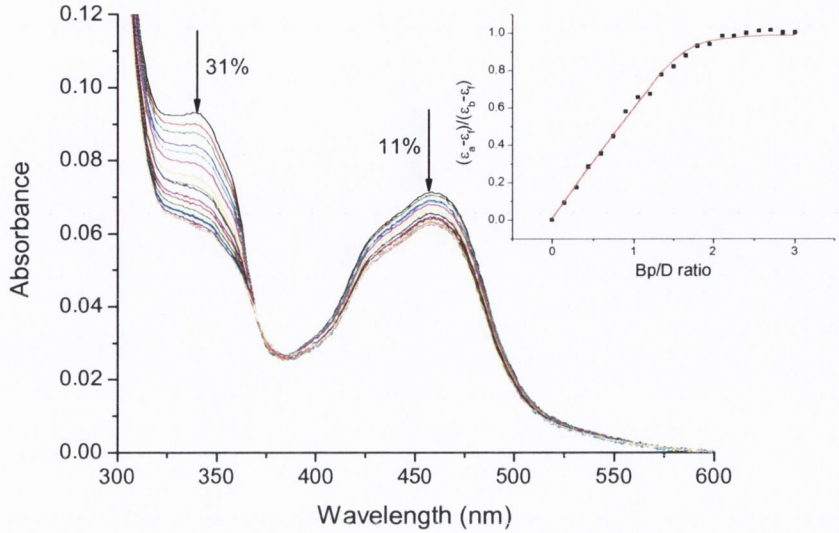

Figure A3.1 *Changes in the UV/Visible spectrum of* ***68*** *(6.5 μM) upon addition of [poly(dG-dC)]$_2$ (0 – 19.5 μM base pairs) in 10 mM phosphate buffer, at pH 7. Inset: Plot of $(\epsilon_a-\epsilon_f)/(\epsilon_b-\epsilon_f)$ at 338 nm vs. equivalents of DNA and the corresponding non-linear fit.*

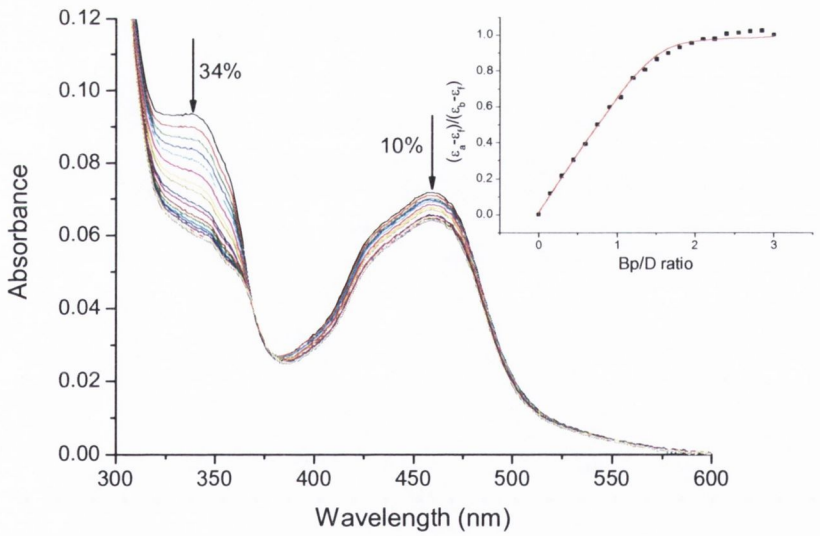

Figure A3.2 *Changes in the UV/Visible spectrum of* ***68*** *(6.5 μM) upon addition of [poly(dA-dT)]$_2$ (0 – 19.5 μM base pairs) in 10 mM phosphate buffer, at pH 7. Inset: Plot of $(\epsilon_a-\epsilon_f)/(\epsilon_b-\epsilon_f)$ at 338 nm vs. equivalents of DNA and the corresponding non-linear fit.*

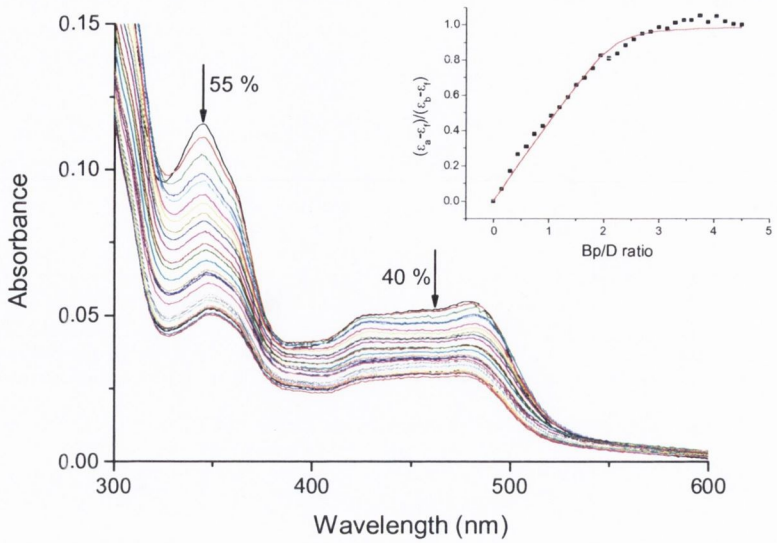

Figure A3.3 *Changes in the UV/Visible spectrum of* ***69*** *(6.5 μM) upon addition of [poly(dG-dC)]$_2$ (0 – 29.25 μM base pairs) in 10 mM phosphate buffer, at pH 7. Inset: Plot of $(\epsilon_a-\epsilon_f)/(\epsilon_b-\epsilon_f)$ at 345 nm vs. equivalents of DNA and the corresponding non-linear fit.*

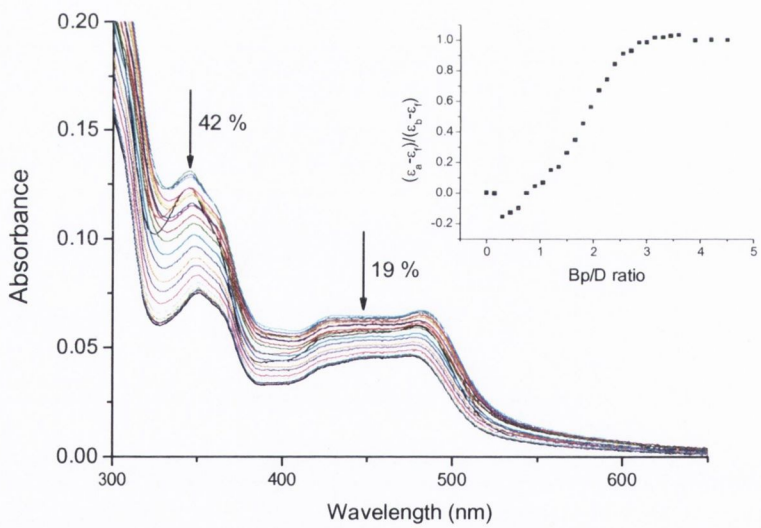

Figure A3.4 *Changes in the UV/Visible spectrum of* ***69*** *(6.5 μM) upon addition of [poly(dA-dT)]$_2$ (0 – 29.25 μM base pairs) in 10 mM phosphate buffer, at pH 7. Inset: Plot of $(\epsilon_a-\epsilon_f)/(\epsilon_b-\epsilon_f)$ at 345 nm vs. equivalents of DNA and the corresponding non-linear fit.*

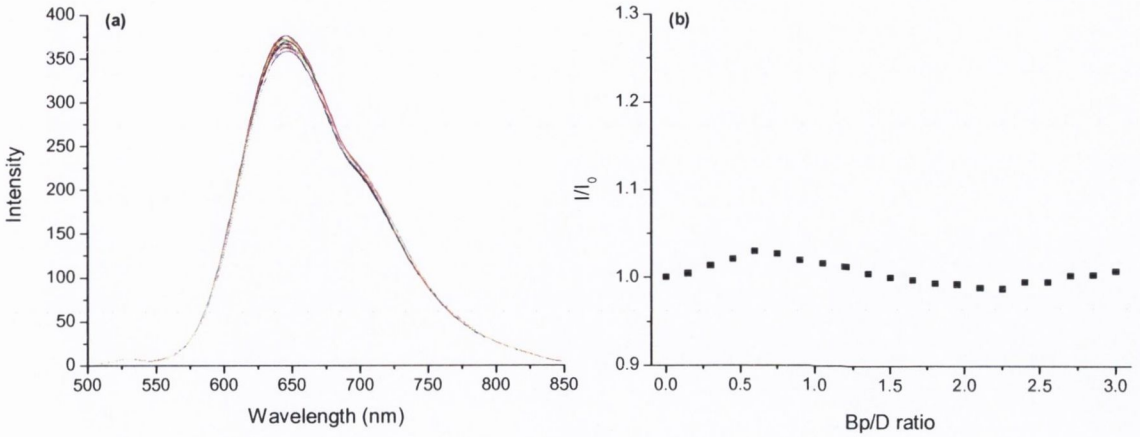

Figure A3.5 *(a) Changes in the emission spectrum of* ***68*** *(6.5 μM) (excitation at 450 nm) upon addition of [poly(dG-dC)]$_2$ (0 – 19.5 μM base pairs) in 10 mM phosphate buffer, at pH 7. (b) The change in the integrated MLCT emission intensity as a function of Bp/D.*

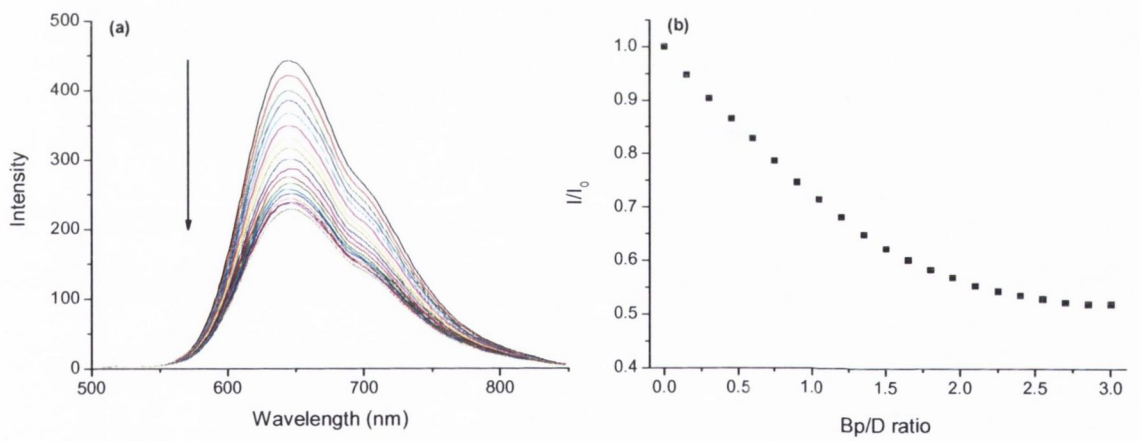

Figure A3.6 *(a) Changes in the emission spectrum of* ***68*** *(6.5 μM) (excitation at 338 nm) upon addition of [poly(dG-dC)]$_2$ (0 – 19.5 μM base pairs) in 10 mM phosphate buffer, at pH 7. (b) The change in the integrated MLCT emission intensity as a function of Bp/D.*

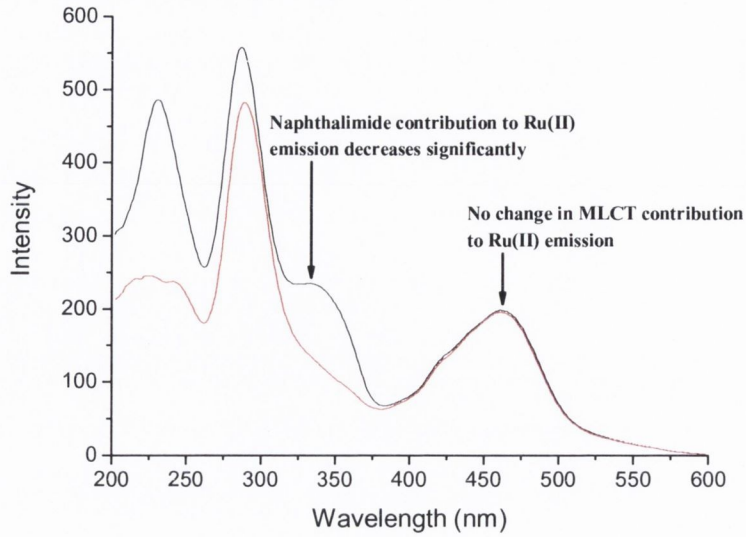

Figure A3.7 *Excitation spectrum of* ***68*** *(6.5 μM) (emission at 645 nm) in 10 mM phosphate buffer, at pH 7 in the absence (——) and presence of [poly(dG-dC)]$_2$ at a Bp/D ratio of 3 (——).*

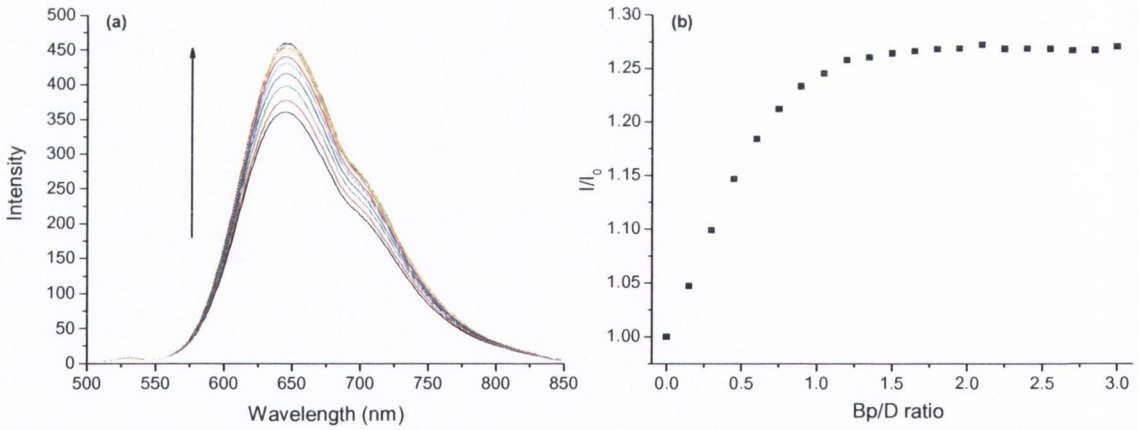

Figure A3.8 *(a) Changes in the emission spectrum of* ***69*** *(6.5 μM) (excitation at 450 nm) upon addition of [poly(dA-dT)]$_2$ (0 – 19.5 μM base pairs) in 10 mM phosphate buffer, at pH 7. (b) The change in the integrated MLCT emission intensity as a function of Bp/D.*

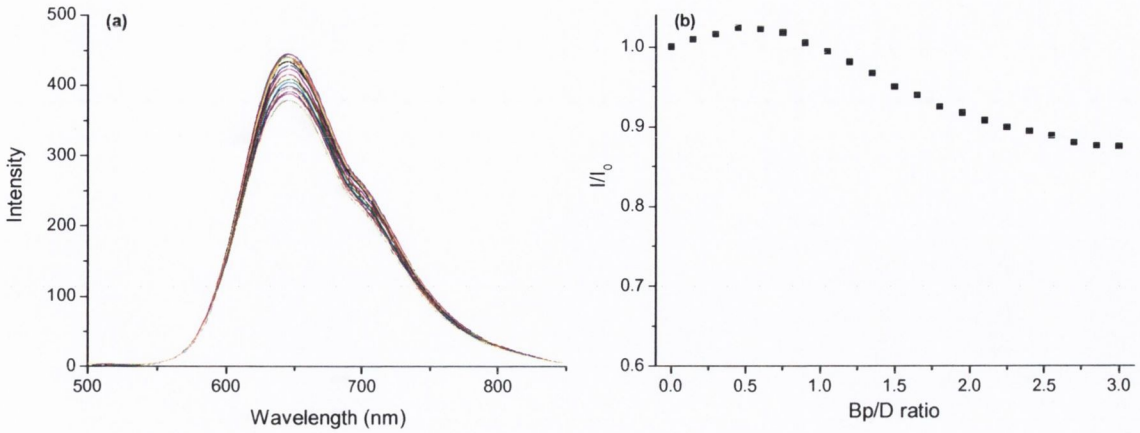

Figure A3.9 *(a) Changes in the emission spectrum of* ***69*** *(6.5 μM) (excitation at 338 nm) upon addition of [poly(dA-dT)]$_2$ (0 – 19.5 μM base pairs) in 10 mM phosphate buffer, at pH 7. (b) The change in the integrated MLCT emission intensity as a function of Bp/D.*

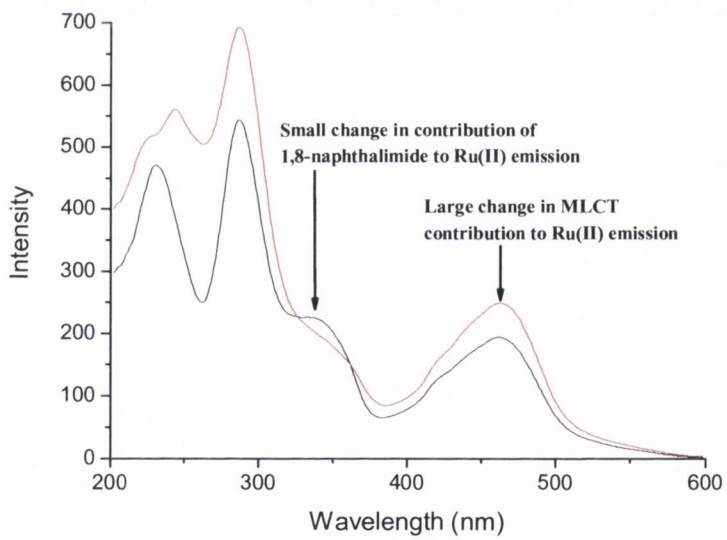

Figure A3.10 *Excitation spectrum of* ***63*** *(6.5 μM) (emission at 645 nm) in 10 mM phosphate buffer, at pH 7, in the absence (——) and presence of [poly(dA-dT)]$_2$ at a Bp/D ratio of 3 (——).*

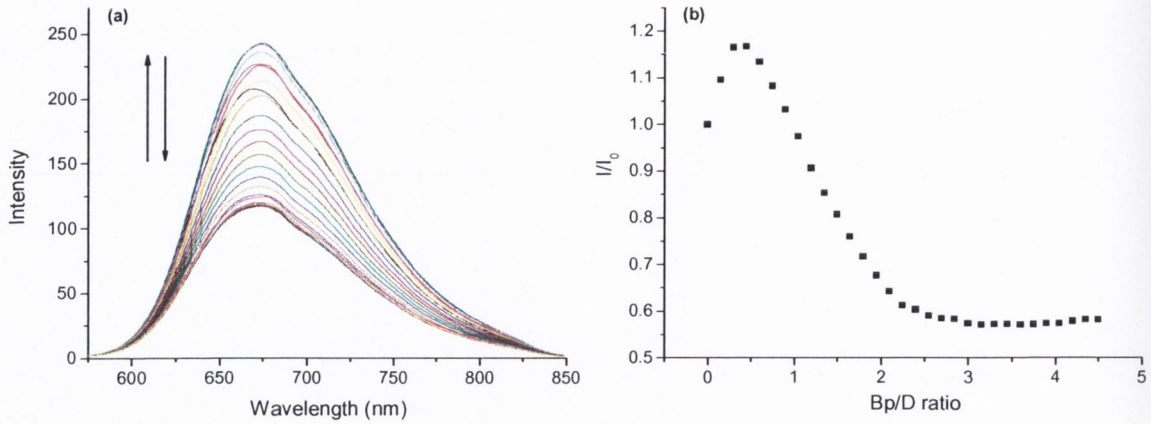

Figure A3.11 *(a) Changes in the emission spectrum of* ***69*** *(6.5 μM) (excitation at 450 nm) upon addition of [poly(dG-dC)]$_2$ (0 – 29.25 μM base pairs) in 10 mM phosphate buffer, at pH 7. (b) The change in the integrated MLCT emission intensity as a function of Bp/D.*

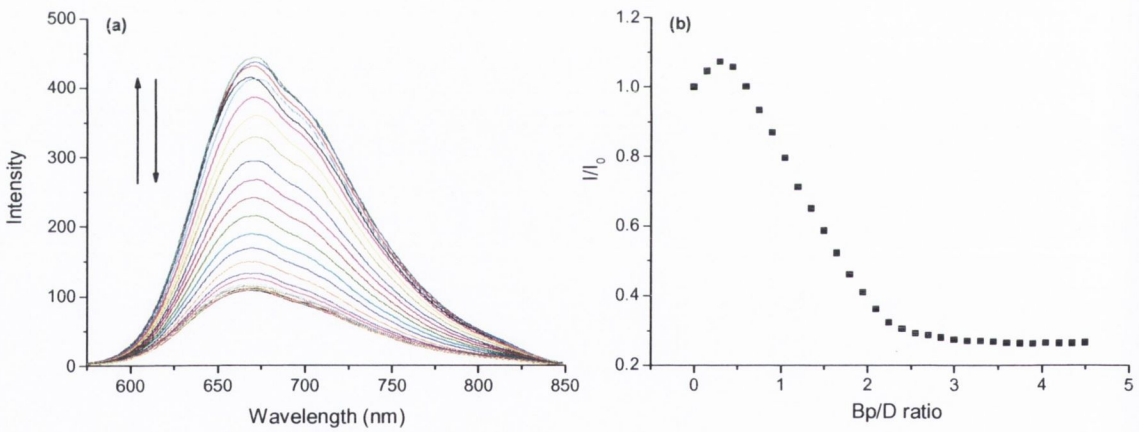

Figure A3.12 *(a) Changes in the emission spectrum of* ***69*** *(6.5 μM) (excitation at 345 nm) upon addition of [poly(dG-dC)]$_2$ (0 – 29.25 μM base pairs) in 10 mM phosphate buffer, at pH 7. (b) The change in the integrated MLCT emission intensity as a function of Bp/D.*

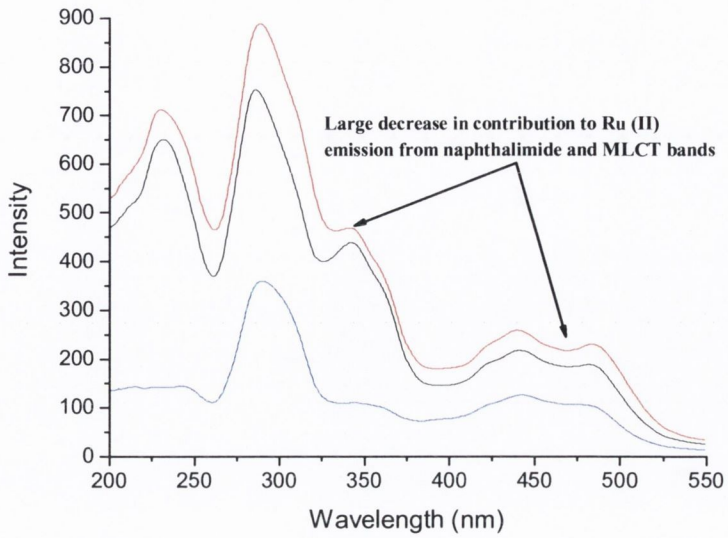

Figure A3.13 *Excitation spectrum of* ***69*** *(6.5 μM) (emission at 670 nm) in 10 mM phosphate buffer, at pH 7 in the absence (——) and presence of [poly(dG-dC)]$_2$ a Bp/D ratio of 0.45 (——) and 4.5 (——).*

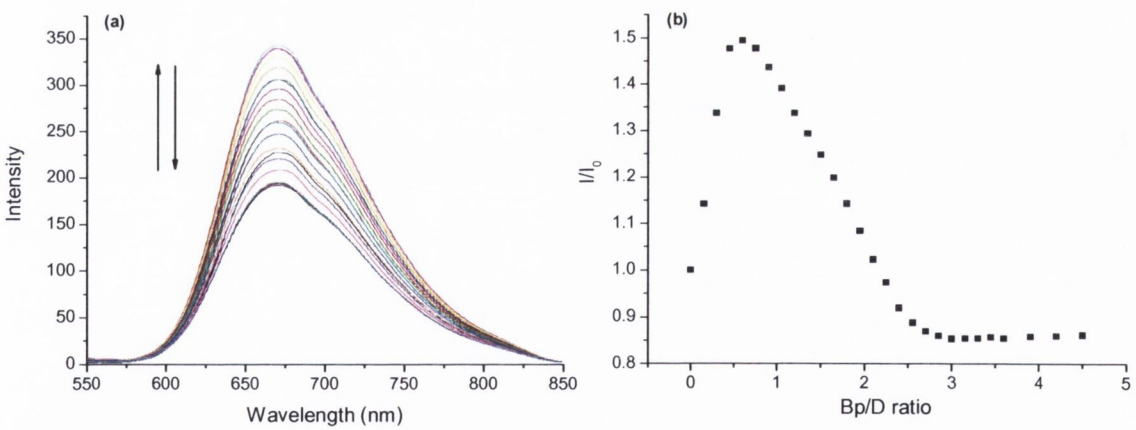

Figure A3.14 *(a) Changes in the emission spectrum of* ***69*** *(6.5 μM) (excitation at 450 nm) upon addition of [poly(dA-dT)]$_2$ (0 – 29.25 μM base pairs) in 10 mM phosphate buffer, at pH 7. (b) The change in the integrated MLCT emission intensity as a function of Bp/D.*

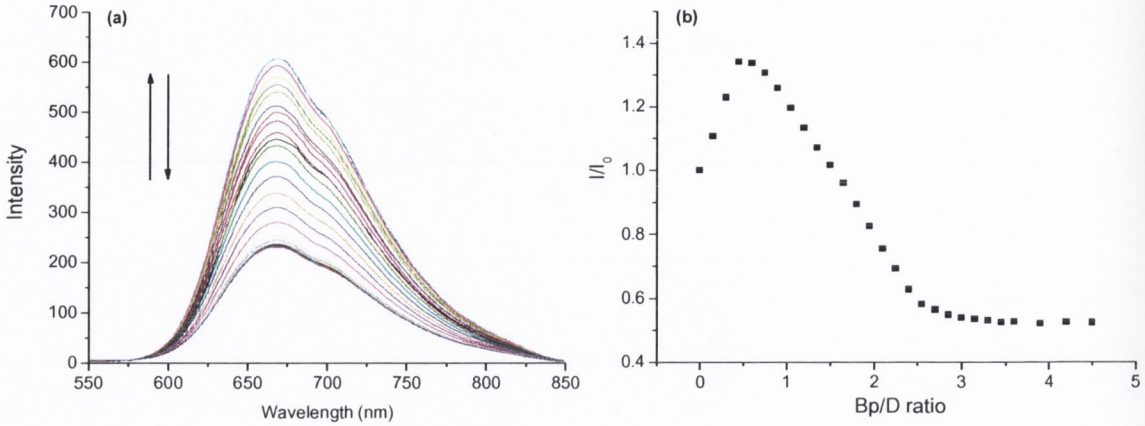

Figure A3.15 *(a) Changes in the emission spectrum of* ***69*** *(6.5 μM) (excitation at 345 nm) upon addition of [poly(dA-dT)]$_2$ (0 – 29.25 μM base pairs) in 10 mM phosphate buffer, at pH 7. (b) The change in the integrated MLCT emission intensity as a function of Bp/D.*

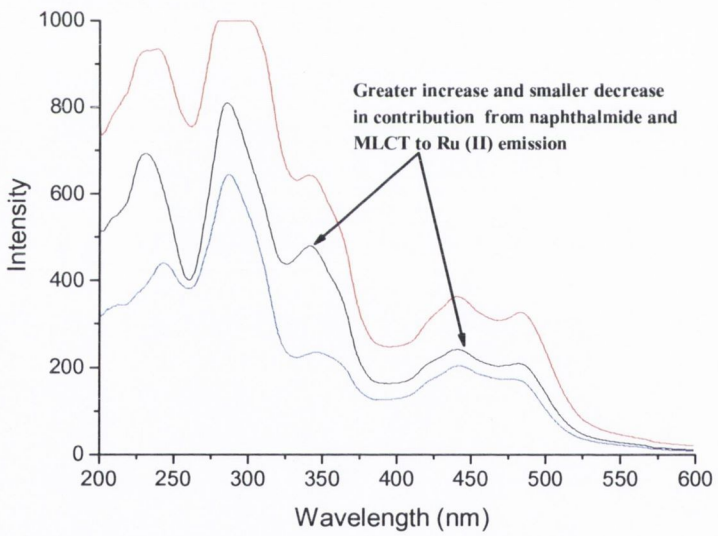

Figure A3.16 *Excitation spectrum of* ***69*** *(6.5 μM) (emission at 670 nm) in 10 mM phosphate buffer, at pH 7 in the absence (——) and presence of [poly(dA-dT)]$_2$ a Bp/D ratio of 0.6 (——) and 4.5 (——).*

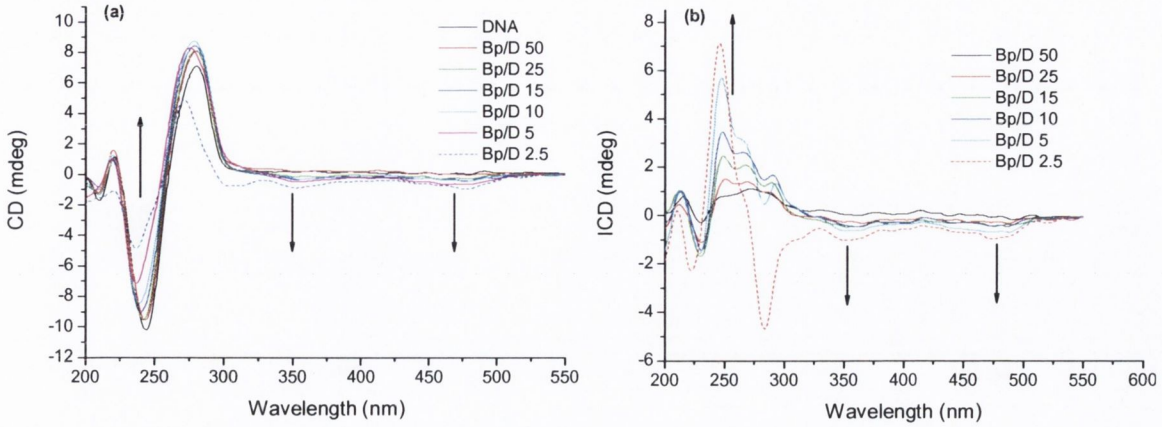

Figure A3.17 *Circular dichroism curves of (a) ct-DNA (150 μM) in 10 mM phosphate buffer, at pH 7 in the absence and presence of* ***69*** *at varying ratios, and (b) the difference spectra obtained.*

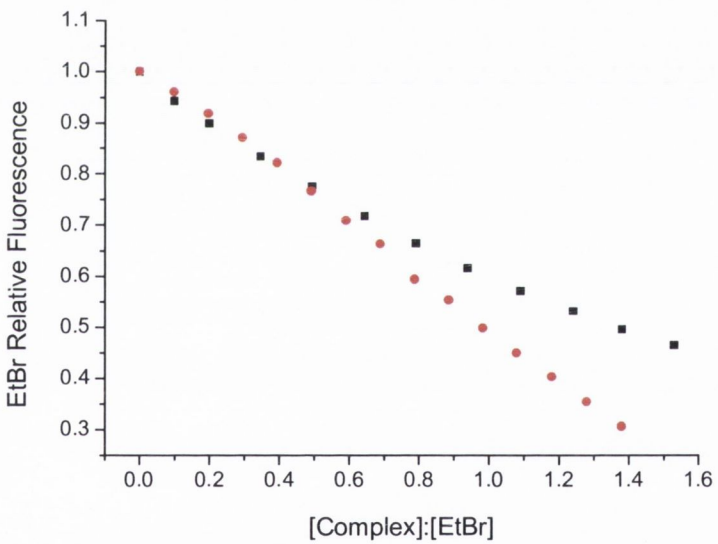

Figure A3.18 *Decrease in fluorescence of DNA bound EtBr upon addition of* ***68*** *(■) and* ***69*** *(●) in 10 mM phosphate buffer, at pH 7.*

Appendix 4 - Chapter 4

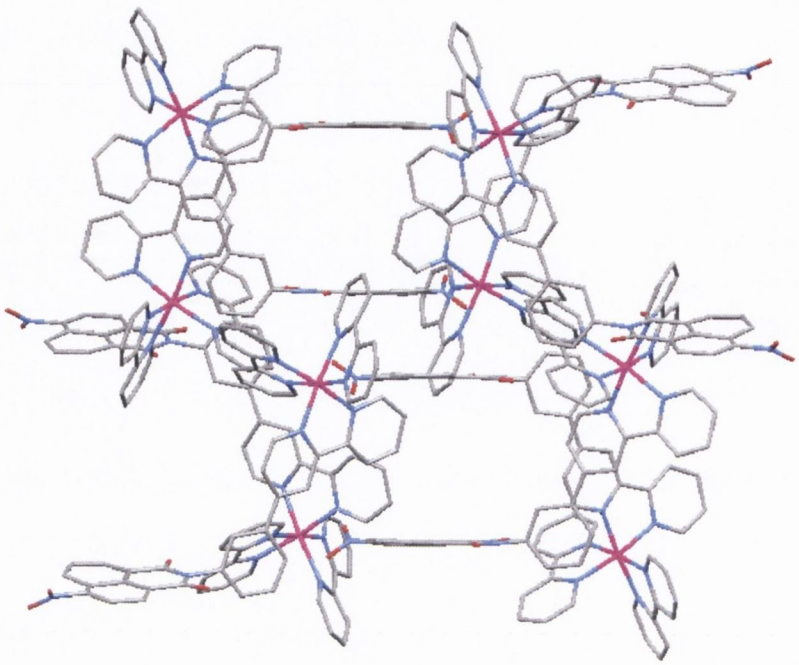

Figure A4.1 *Crystal packing diagram of 77, viewed along the a* axis.*

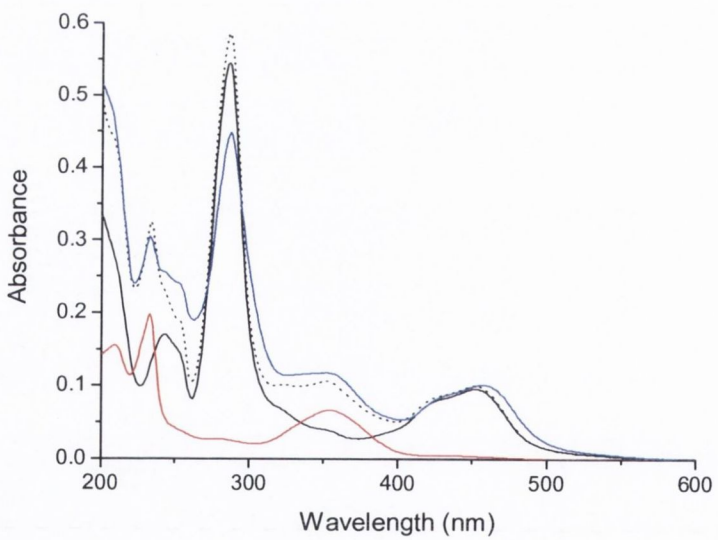

Figure A4.2 *Summed absorption spectra of* ***76****. $Ru(bpy)_3^{2+}$ (——),* ***59*** *(——), $Ru(bpy)_3^{2+}$ + **59** (------) and **76** (——). All solutions at 6.5 μM concentration in 10 mM phosphate buffer, at pH 7.*

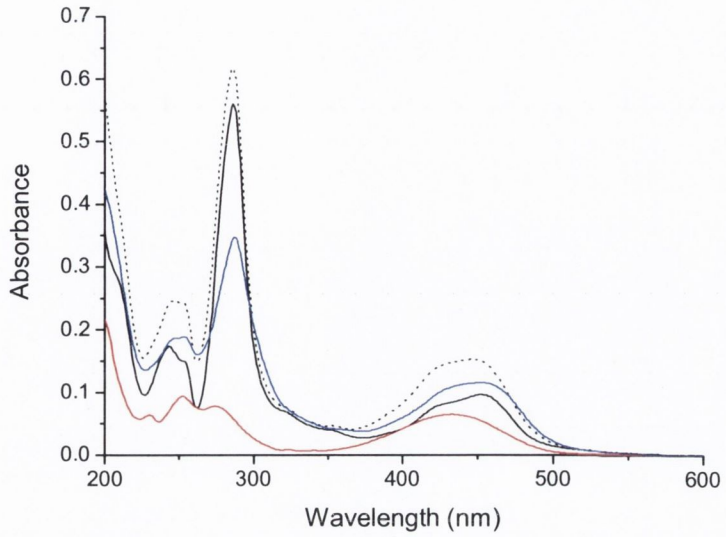

Figure A4.3 *Summed absorption spectra of* ***78****. $Ru(bpy)_3^{2+}$ (——),* ***90*** *(——), $Ru(bpy)_3^{2+}$ +* ***90*** *(------) and* ***78*** *(——). All solutions at 6.5 μM concentration in 10 mM phosphate buffer, at pH 7.*

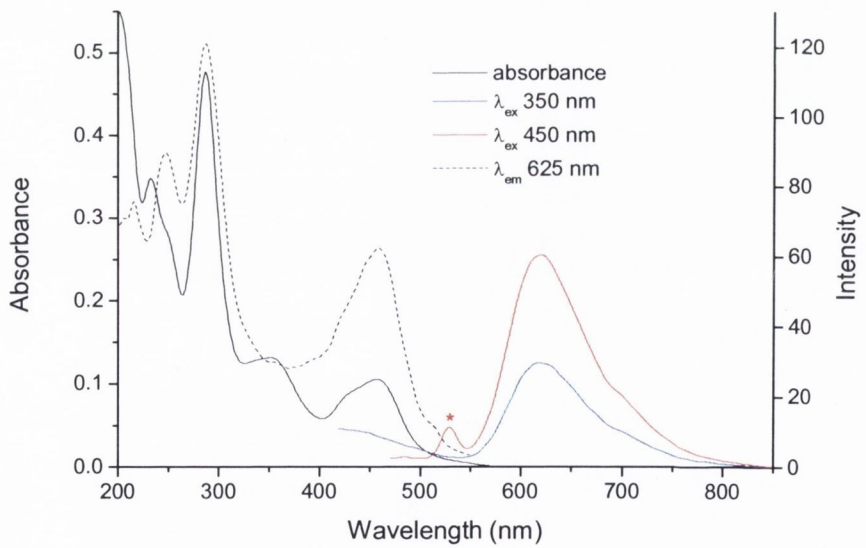

Figure A4.4 *UV/Visible, excitation and emission spectra of 77 (6.5 μM) in 10 mM phosphate buffer, at pH 7. The water Raman band is denoted by *.*

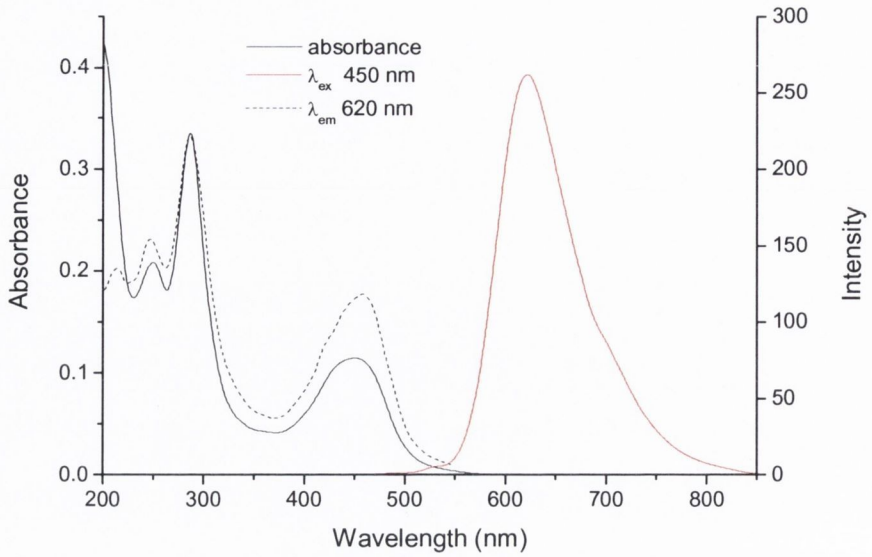

Figure A4.5 *UV/Visible, excitation and emission spectra of* ***79*** *(6.5 μM) in 10 mM phosphate buffer, at pH 7.*

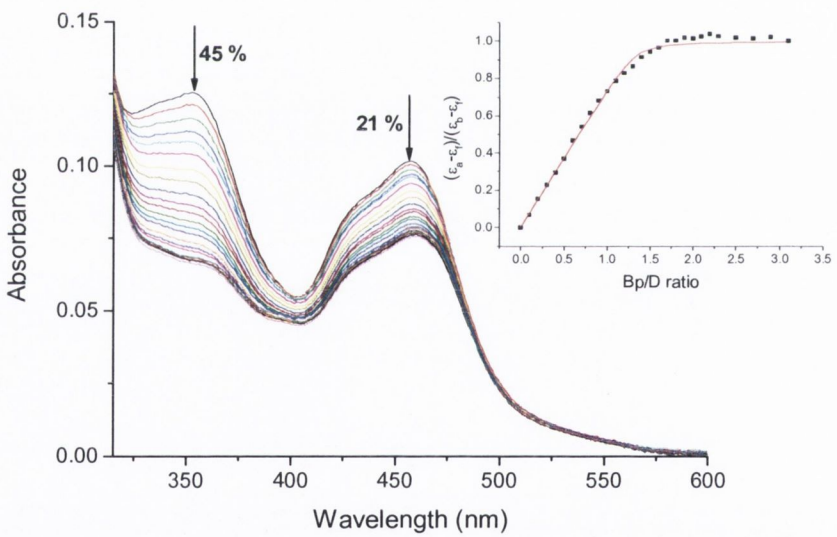

Figure A4.6 *Changes in the UV/Visible spectrum of 77 (6.9 μM) upon addition of st-DNA (0 – 21.39 μM base pairs), in 10 mM phosphate buffer, at pH 7. Inset: Plot of* $(\epsilon_a-\epsilon_f)/(\epsilon_b-\epsilon_f)$ *at 351 nm vs. equivalents of DNA and the corresponding non-linear fit.*

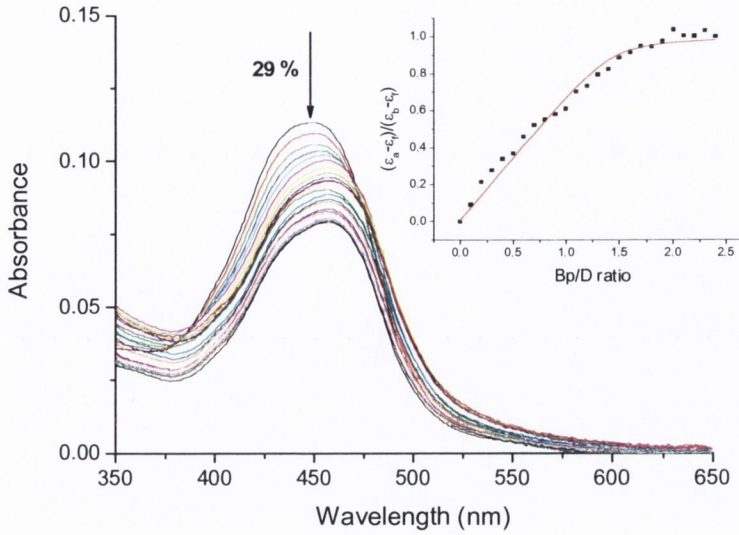

Figure A4.7 *Changes in the UV/Visible spectrum of* ***79*** *(6.5 μM) upon addition of st-DNA (0 – 15.6 μM base pairs), both in 10 mM phosphate buffer, at pH 7. Inset: Plot of* $(\epsilon_a-\epsilon_f)/(\epsilon_b-\epsilon_f)$ *at 451 nm vs. equivalents of DNA and the corresponding non-linear fit.*

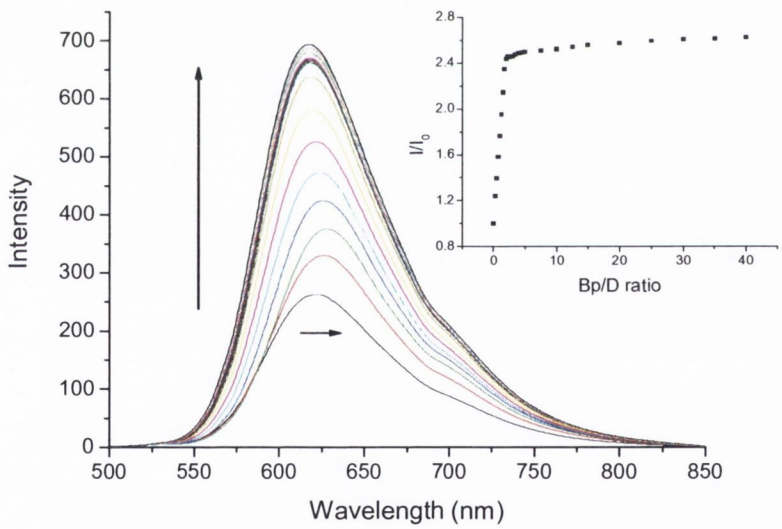

Figure A4.8 *Changes in the emission spectrum of* ***79*** *(6.9 μM) (excitation at 450 nm) upon addition of st-DNA (0 – 345 μM base pairs) in 10 mM phosphate buffer, at pH 7.*

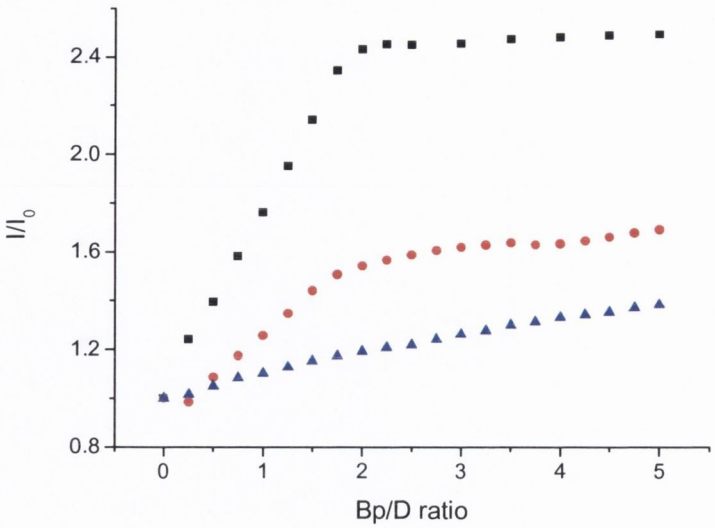

Figure A4.9 *Relative changes in the emission of* ***78*** *(6.5 μM) with increasing concentration of st-DNA (0 – 58.5 μM), in 10 mM phosphate buffer (■), 10 mM phosphate buffer + 50 mM NaCl (●) and 10 mM phosphate buffer + 100 mM NaCl (▲).*

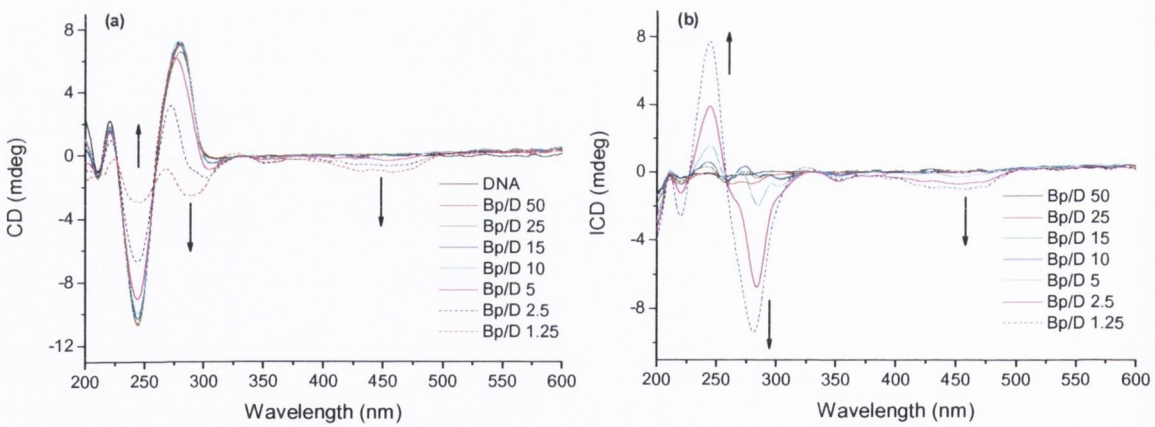

Figure A4.10 *Circular dichroism curves of (a) ct-DNA (150 μM) in 10 mM phosphate buffer, at pH 7, in the absence and presence of* ***78*** *at varying ratios, and (b) the difference spectra obtained.*

Appendix 5 – Chapter 5

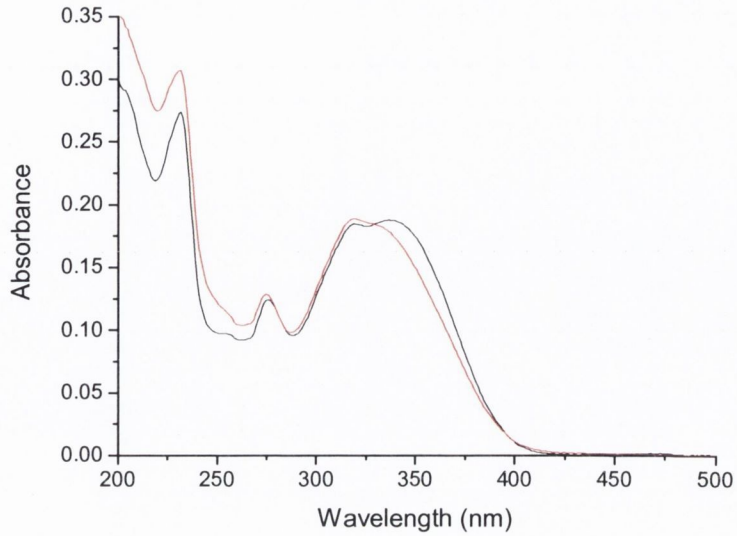

Figure A5.1 *UV/Visible absorption spectra of* ***93*** *(6.5μM) (——) and* ***94*** *(6.5 μM) (——) in 10 mM phosphate buffer, at pH 7.*

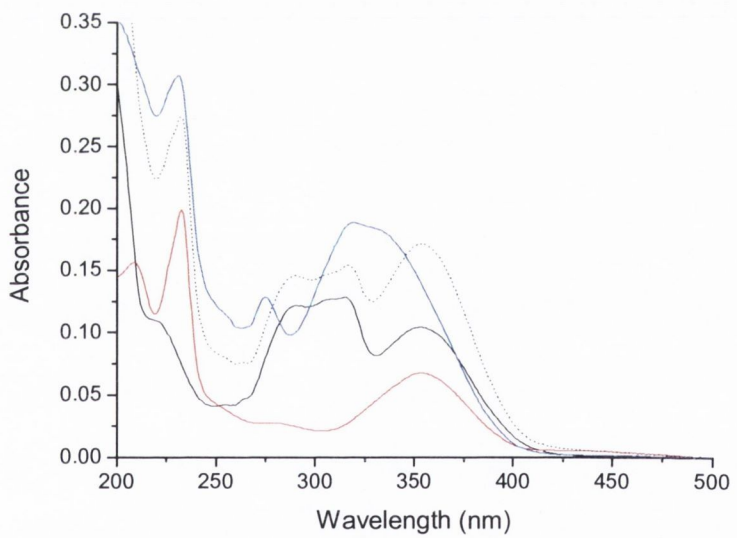

Figure A5.2 *Summed absorption spectra of* ***94****.* ***96*** *(——),* ***59*** *(——),* ***96*** *+* ***59*** *(------) and* ***94*** *(——). All solutions at 6.5 μM concentration in 10 mM phosphate buffer, at pH 7.*

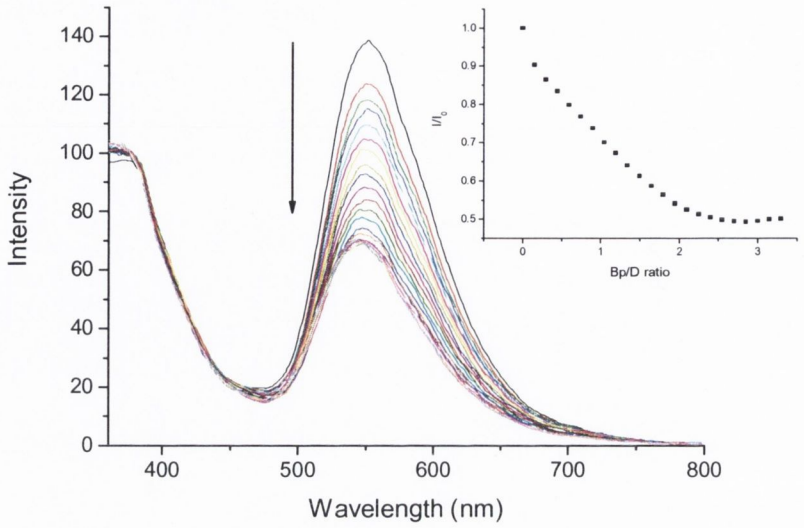

Figure A5.3 *Changes in the emission spectrum of* ***95*** *(6.5 μM) (excitation at 311 nm) upon addition of st-DNA (0 – 21.45 μM) in 10 mM phosphate buffer, at pH 7.*

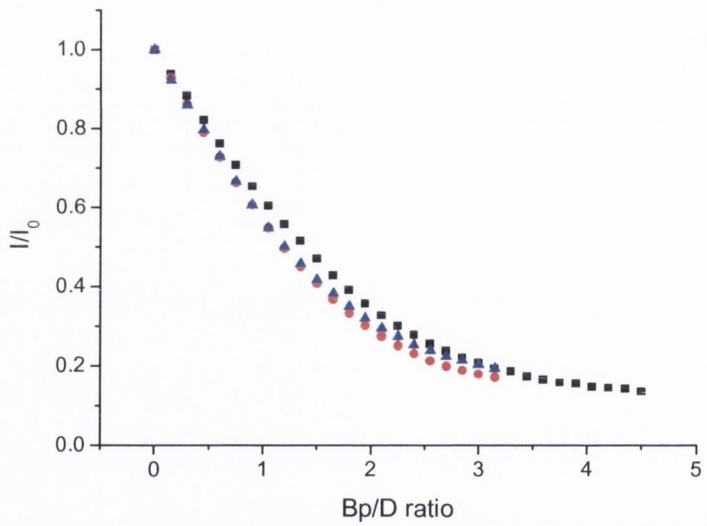

Figure A5.4 *Relative change in the emission of* ***93*** *upon addition of salmon testes DNA (■), [poly(dG-dC)]$_2$ (●) and [poly(dA-dT)]$_2$ (▲) in 10 mM phosphate buffer at, pH 7.*

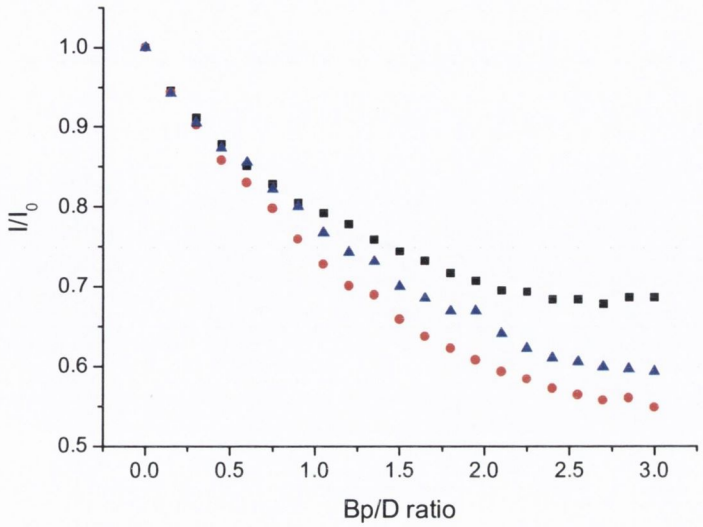

Figure A5.5 *Relative change in the emission of* ***94*** *(6.5 μM) upon addition of st-DNA (■), [poly(dG-dC)]$_2$ (●) and [poly(dA-dT)]$_2$ (▲) in 10 mM phosphate buffer, at pH 7.*

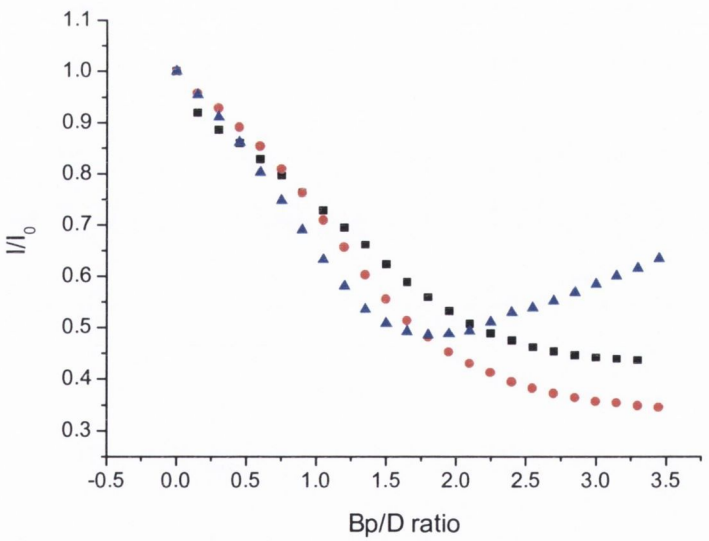

Figure A5.6 *Relative change in the emission of* ***95*** *upon addition of st-DNA (■), [poly(dG-dC)]$_2$ (●) and [poly(dA-dT)]$_2$ (▲) in 10 mM phosphate buffer, at pH 7.*

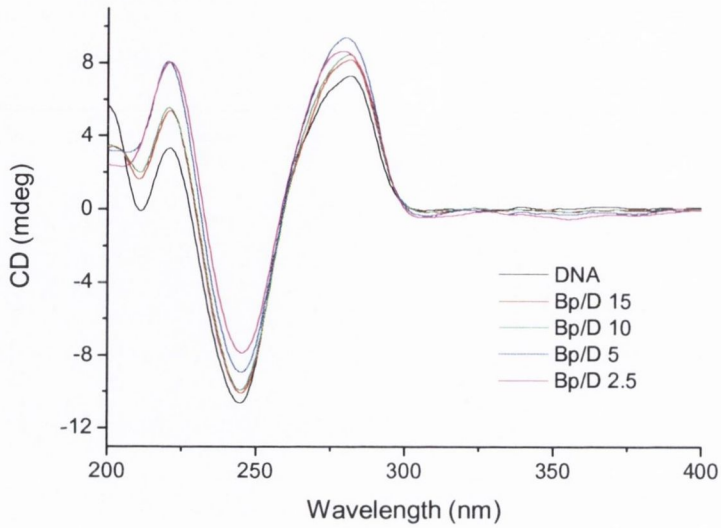

Figure A5.7 *Circular dichroism curves of ct-DNA (150 μM) in 10 mM phosphate buffer, at pH 7, in the absence and presence of* ***96*** *at varying ratios.*

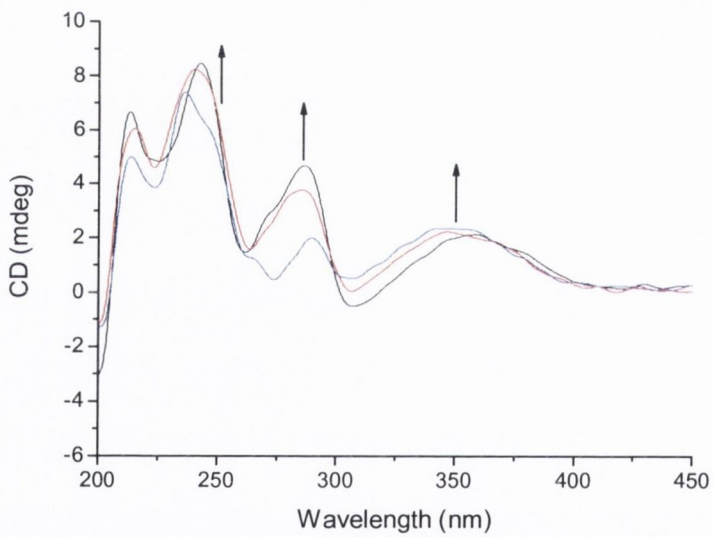

Figure A5.8 *Induced CD spectra of* ***93*** *in the presence of ct-DNA (150 μM) at a Bp/D ratio of 2.5 in 10 mM phosphate buffer (——), 10 mM phosphate buffer + 50 mM NaCl (——) and 10 mM phosphate buffer + 100 mM NaCl (——).*

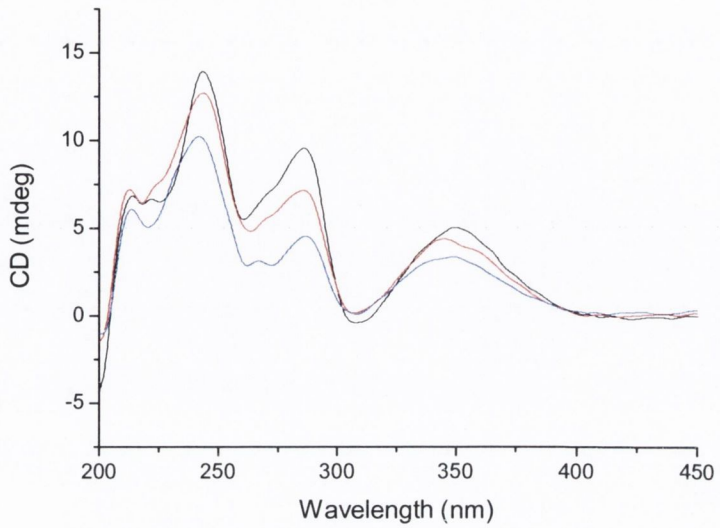

Figure A5.9 *Induced CD spectra of* ***94*** *in the presence of ct-DNA (150 μM) at a Bp/D ratio of 2.5 in 10 mM phosphate buffer (——), 10 mM phosphate buffer + 50 mM NaCl (——) and 10 mM phosphate buffer + 100 mM NaCl (——).*

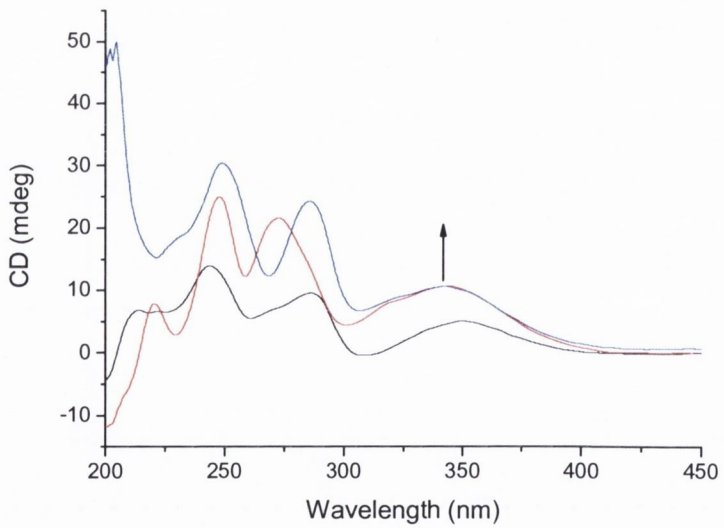

Figure A5.10 *Induced CD spectra of* ***94*** *in the presence of ct-DNA (——), [poly(dA-dT)]$_2$ (——) and [poly(dG-dC)]$_2$ (——), all in 10 mM phosphate buffer, at pH 7, at a Bp/D ratio of 2.5.*

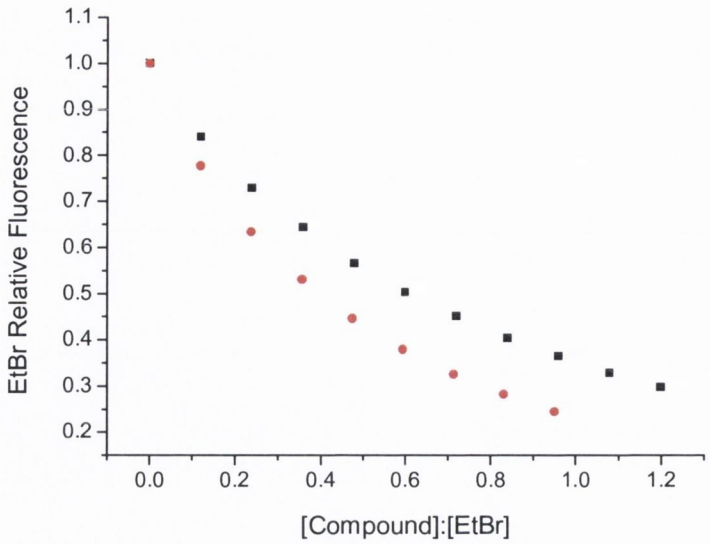

Figure A5.11 *Decrease in fluorescence of DNA bound EtBr upon addition of* ***93*** *(■) and* ***94*** *(●) in 10 mM phosphate buffer, at pH 7.*

Appendix 6 – Chapter 6

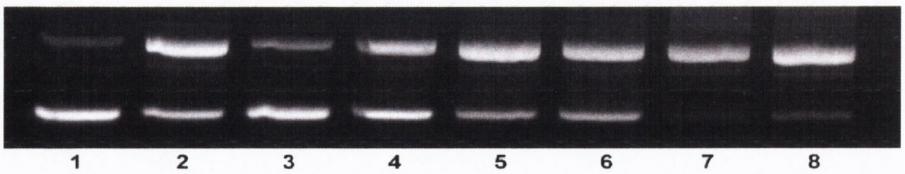

Figure A6.1 *Agarose gel electrophoresis of pBR322 DNA (1mg/ml) after irradiation at λ > 400 nm in 10 mM phosphate buffer, pH 7. Lane 1: Plasmid DNA control; Lane 2: $Ru(bpy)_3^{2+}$ (Bp/D 5) 5 min irradiation; Lanes 3-5:* ***68*** *(Bp/D 5) 1, 3, 5 min respectively; Lanes 6-8:* ***70*** *(Bp/D 5) 1, 3, 5 min respectively.*

Table A6.1 *Percentage of Form I vs II pBR322 plasmid DNA from the cleavage study in Figure 6.8*

Lane	% Form I	% Form II
1	82	18
2	32	68
3	72	28
4	47	53
5	27	73
6	34	66
7	4	96
8	10	90

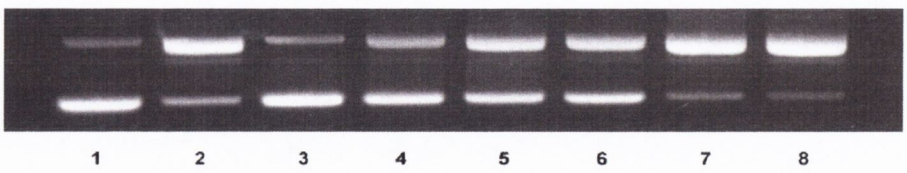

Figure A6.2 *Agarose gel electrophoresis of pBR322 DNA (1mg/ml) after irradiation at λ > 400 nm in 10 mM phosphate buffer, pH 7. Lane 1: Plasmid DNA control; Lane 2: $Ru(bpy)_3^{2+}$ (Bp/D 5) 5 min irradiation; Lanes 3-5:* ***69*** *(Bp/D 5) 1, 3, 5 min respectively; Lanes 6-8:* ***71*** *(Bp/D 5) 1, 3, 5 min respectively.*

Table A6.2 *Percentage of Form I vs II pBR322 plasmid DNA from the cleavage study in Figure 6.9*

Lane	% Form I	% Form II
1	80	20
2	19	81
3	82	18
4	60	40
5	41	59
6	44	56
7	12	88
8	11	89

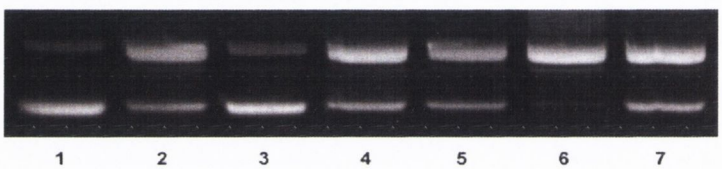

Figure A6.3 *Agarose gel electrophoresis of pBR322 DNA (1mg/ml) after 5 min irradiation at $\lambda > 400$ nm in 10 mM phosphate buffer, pH 7. Lane 1: Plasmid DNA control; Lanes 2-3: $Ru(bpy)_3^{2+}$ (Bp/D 5) without and with 10 mM NaN_3; Lanes 4-5: **68** (Bp/D 5) without and with NaN_3; Lanes 6-7: **70** (Bp/D 5) without and with NaN_3.*

Table A6.3 *Percentage of Form I vs II pBR322 plasmid DNA from the cleavage study in Figure 6.11.*

Lane	% Form I	% Form II
1	84	16
2	29	71
3	79	21
4	30	70
5	28	72
6	4	96
7	29	71

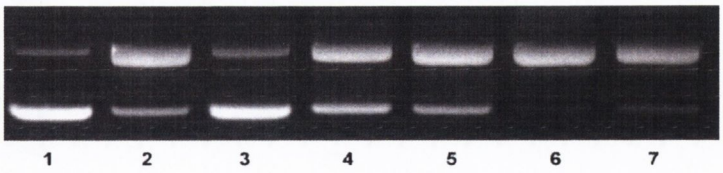

Figure A6.4 *Agarose gel electrophoresis of pBR322 DNA (1mg/ml) after 5 min irradiation at λ > 400 nm in 10 mM phosphate buffer, pH 7. Lane 1: Plasmid DNA control; Lanes 2-3: $Ru(bpy)_3^{2+}$ (P/D 10) without and with 10 mM NaN_3; Lanes 4-5:* ***69*** *(P/D 10) without and with NaN_3; Lanes 6-7:* ***71*** *(P/D 10) without and with NaN_3.*

Table A6.4 *Percentage of Form I vs II pBR322 plasmid DNA from the cleavage study in Figure 6.12.*

Lane	% Form I	% Form II
1	87	13
2	24	76
3	79	21
4	39	61
5	29	71
6	3	97
7	16	84

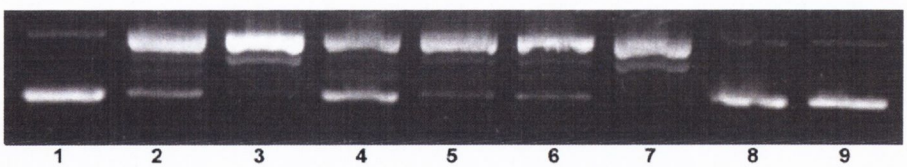

Figure A6.5. *Agarose gel electrophoresis of pBR322 DNA (1mg/ml) after 5 min irradiation at λ > 400 nm in 10 mM phosphate buffer, pH 7. All solutions are in D_2O. Lane 1: Plasmid DNA control; Lanes 2-3: $Ru(bpy)_3^{2+}$ (Bp/D 15, 5); Lanes 4-5:* ***68*** *(Bp/D 15, 5); Lanes 6-7:* ***70*** *(Bp/D 15, 5); Lanes 8-9:* ***68*** *and* ***70*** *(Bp/D 5) in the dark.*

Table A6.5 *Percentage of Form I vs II pBR322 plasmid DNA from the cleavage study in Figure 6.14.*

Lane	% Form I	% Form II
1	86	14
2	14	86
3	12	88
4	39	61
5	11	89
6	15	85
7	0	100
8	100	0
9	85	15

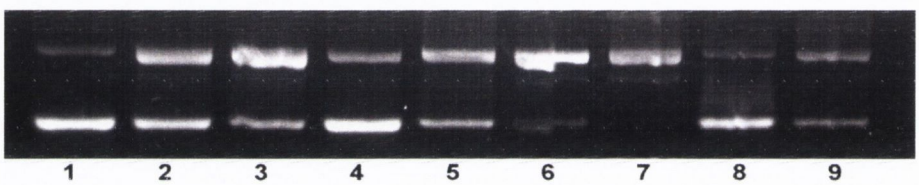

Figure A6.6 *Agarose gel electrophoresis of pBR322 DNA (1mg/ml) after 5 min irradiation at $\lambda > 400$ nm in 10 mM phosphate buffer, pH 7. All solutions are in D_2O. Lane 1: Plasmid DNA control; Lanes 2-3: $Ru(bpy)_3^{2+}$ (Bp/D 15, 5); Lanes 4-5:* ***69*** *(Bp/D 15, 5); Lanes 6-7:* ***71*** *(Bp/D 15, 5); Lanes 8-9:* ***69*** *and* ***71*** *(Bp/D 10) in the dark.*

Table A6.6 *Percentage of Form I vs II pBR322 plasmid DNA from the cleavage study in Figure 6.15.*

Lane	% Form I	% Form II
1	85	15
2	49	51
3	27	73
4	73	27
5	40	60
6	10	90
7	0	100
8	79	21
9	44	56

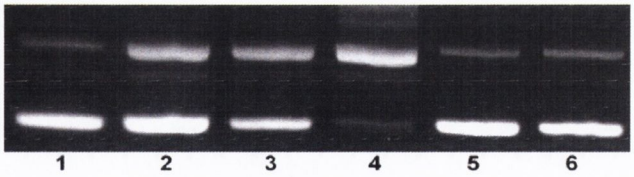

Figure A6.7 *Agarose gel electrophoresis of pBR322 DNA (1mg/ml) after 5 min irradiation at λ > 400 nm in 10 mM phosphate buffer, pH 7. All samples are argon saturated. Lane 1: Plasmid DNA control; Lane 2: $Ru(bpy)_3^{2+}$ (Bp/D 5); Lane 3:* ***68*** *(Bp/D 5); Lane 4:* ***70*** *(Bp/D 5); Lanes 5-6:* ***68*** *and* ***70*** *(Bp/D 5) in the dark.*

Table A6.7 *Percentage of Form I vs II pBR322 plasmid DNA from the cleavage study in Figure 6.17*

Lane	% Form I	% Form II
1	79	21
2	65	35
3	57	43
4	11	89
5	84	16
6	80	20

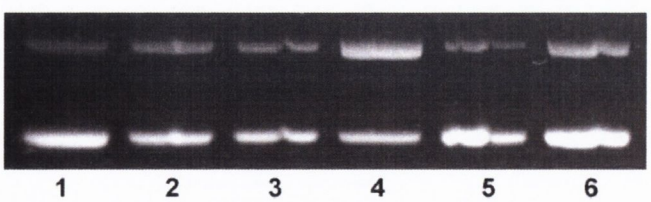

Figure A6.8 *Agarose gel electrophoresis of pBR322 DNA (1mg/ml) after 5 min irradiation at λ > 400 nm in 10 mM phosphate buffer, pH 7. All samples are argon saturated. Lane 1: Plasmid DNA control; Lane 2: $Ru(bpy)_3^{2+}$ (Bp/D 5); Lane 3:* ***69*** *(Bp/D 5); Lane 4:* ***71*** *(Bp/D 5); Lanes 5-6:* ***69*** *and* ***71*** *(Bp/D 5) in the dark.*

Table A6.8 *Percentage of Form I vs II pBR322 plasmid DNA from the cleavage study in Figure 6.18*

Lane	% Form I	% Form II
1	72	28
2	60	40
3	60	40
4	46	54
5	62	38
6	62	38

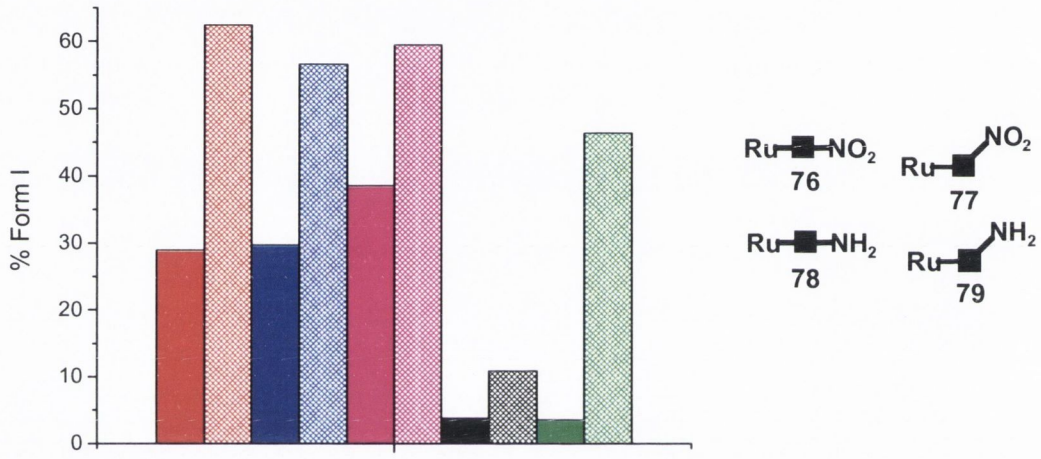

Figure A6.9 *Effect of degassing on the photocleavage efficiency of* $Ru(bpy)_3^{2+}$ *(■),* ***76*** *(■),* ***77*** *(■),* ***78*** *(■) and* ***79*** *(■). Solid bars represent cleavage under oxygen saturated conditions, hatched bars represent cleavage with degassing.*

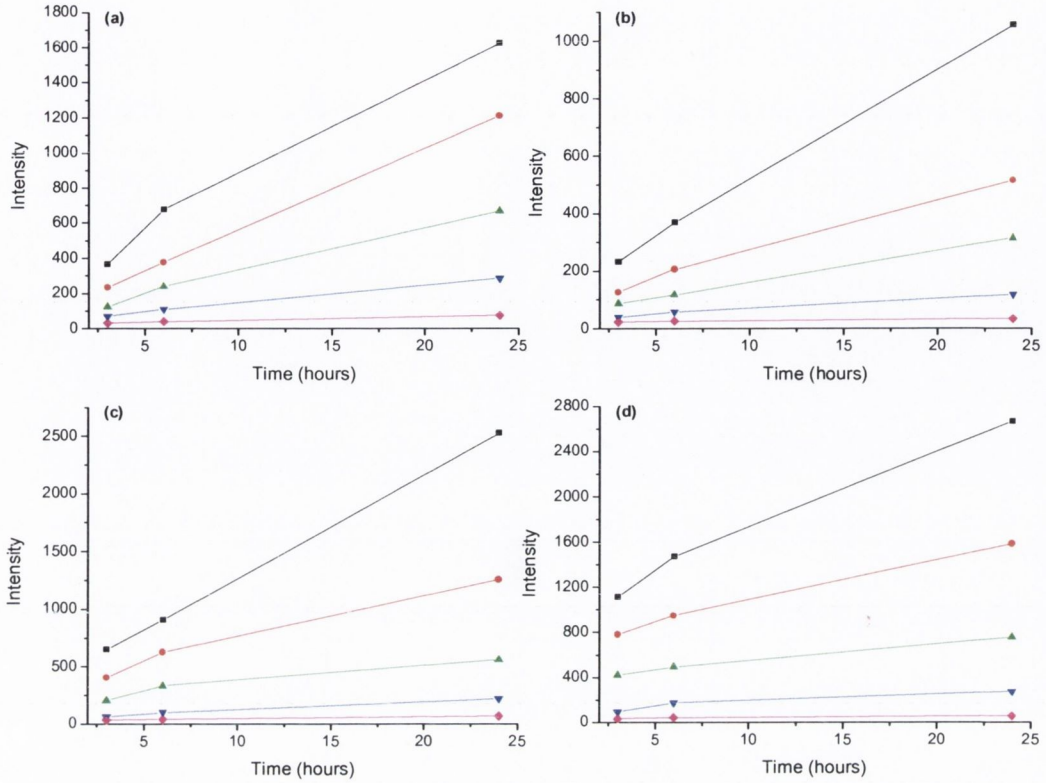

Figure A6.10 *Observed fluorescence intensity from HeLa cells upon incubation with (a)* ***37****, (b)* ***38****, (c)* ***39****, and (d)* ***40****, at a concentration of 1 μM (—♦—), 5 μM (—▼—), 12.5 μM (—▲—), 25 μM (—●—) and 50 μM (—■—). Three time points were studied in all cases; 3, 6, and 24 hours.*

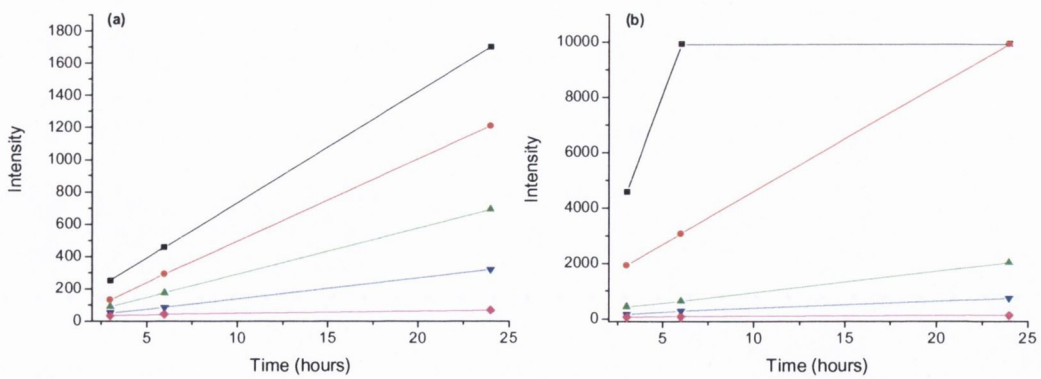

Figure A6.11 *Observed fluorescence intensity from HeLa cells upon incubation with (a)* ***68****, and (b)* ***69****, at a concentration of 1 μM (—♦—), 5 μM (—▼—), 12.5 μM (—▲—), 25 μM (—●—) and 50 μM (—■—). Three time points were studied in all cases; 3, 6, and 24 hours.*

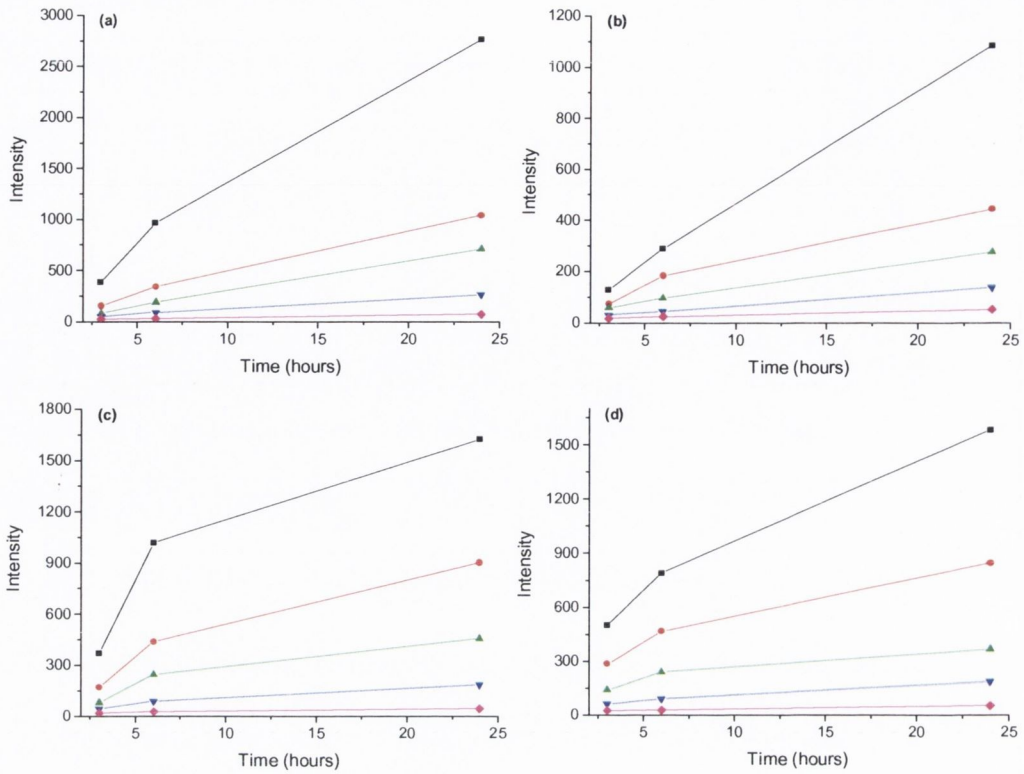

Figure A6.12 *Observed fluorescence intensity from HeLa cells upon incubation with (a)* ***76****, (b) 77, (c)* ***78*** *and (d)* ***79****, at a concentration of 1 μM (—♦—), 5 μM (—▼—), 12.5 μM (—▲—), 25 μM (—●—) and 50 μM (—■—). Three time points were studied in all cases; 3, 6, and 24 hours.*

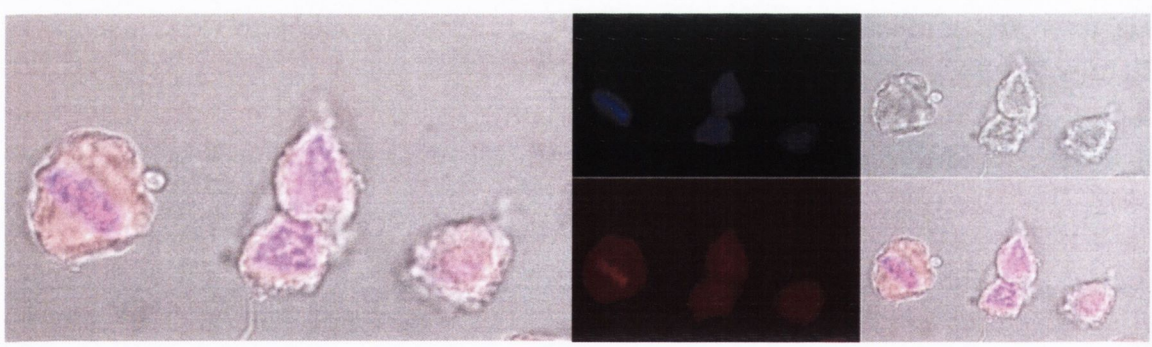

Figure A6.13 *Confocal laser scanning microscopy image of 77 in HeLa cells. On the right is shown the image obtained of HOESCHT nuclear co-stain (blue), 77 (red), optical image of the cells (grey) and the overlay of these three. On the left is an enlarged version of the overlayed image.*

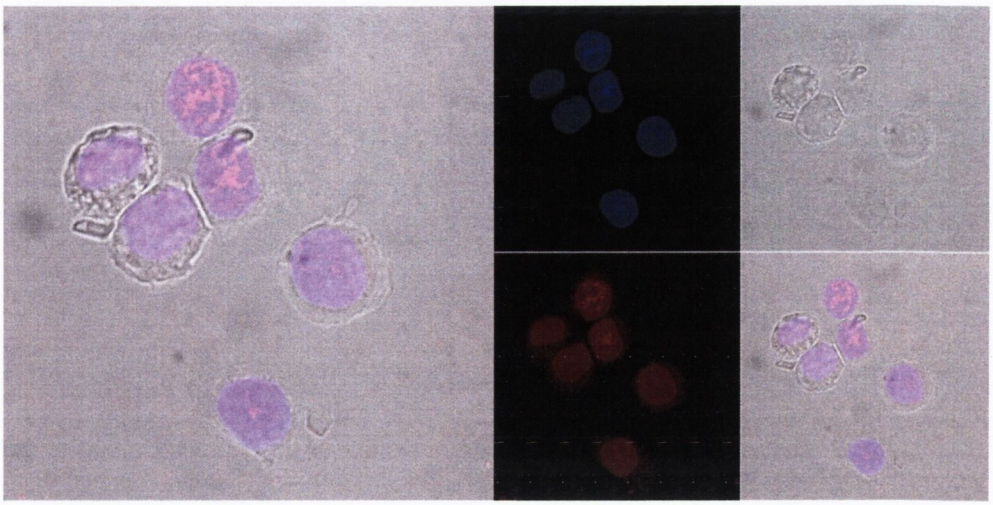

F***igure A6.14*** *Confocal laser scanning microscopy image of* ***79*** *in HeLa cells. On the right is shown the image obtained of HOESCHT nuclear co-stain (blue),* ***79*** *(red), optical image of the cells (grey) and the overlay of these three. On the left is an enlarged version of the overlayed image.*

Inorg. Chem. **2008**, *47*, 401–403

Inorganic Chemistry
Communication

Highly Effective DNA Photocleavage by Novel "Rigid" $Ru(bpy)_3$-4-nitro- and -4-amino-1,8-naphthalimide Conjugates

Gary J. Ryan, Susan Quinn,* and Thorfinnur Gunnlaugsson*

School of Chemistry, Centre for Synthesis and Chemical Biology (CSCB), University of Dublin, Trinity College Dublin, Dublin 2, Ireland

Received May 18, 2007

Redacted

10.1021/ic700967y CCC: $40.75
Published on Web 12/14/2007

Redacted

Redacted